



Reference to Districts.

- A Northern Boundaries
- B Liberty Plains
- C Banks Town
- D Parramatta
- EEEE Ground reserved  
for Govt. purposes
- F Concord
- G Petersham
- H Bulanaming
- I Sydney
- K Hunters Hills
- L Eastern Farms
- M Field of Mars
- N Ponds
- O Toongabbey
- P Prospect
- Q
- R Richmond Hill
- S Green Hills
- T Phillip
- U Nelson
- V Castle Hill
- W Evan

The cover map is a reproduction in part of a map noted as follows:

London: Published by John Booth, Duke Street, Portland Place, July 20th, 1810

Reproduced here by courtesy of The Mitchell Library, Sydney

UNISURV REPORT No. 17

"ACCURACY OF MONOCULAR POINTING TO  
BLURRED PHOTOGRAMMETRIC SIGNALS."

J.C. TRINDER

Received July, 1970.

School of Surveying,  
The University of New South Wales,  
P.O. Box 1,  
Kensington, N.S.W. 2033.      Australia.

ABSTRACT.

The study commences with an introduction of available data on pointing accuracies to artificial sharp and blurred targets, and a discussion of some aspects of the physiology of the visual system which may influence these accuracies. A general description of the visual system, visual acuity and aspects of physical stimuli which may affect acuity are then given. Based on the assumption that the visual system behaves linearly over limited luminance ranges, two estimates of the spread function of the visual system have been derived. Convolutions of these spread functions and target luminance profiles have been carried out to investigate the criteria used by the visual system in pointing to sharp targets. These criteria are similar to those derived in a previous work.

An instrument has been constructed to test pointing accuracies for blurred targets. Observations on this instrument indicate that for target blur above a specific level, which depends on width of annulus of the target, pointing accuracies are primarily dependent on the grade of the density profile of the target and secondly on annulus width. Below this specific level of blur, pointing accuracies are dependent on annulus width alone. Background density has a negligible effect in pointing accuracies.

A technique has been devised for eliminating the systematic errors inherent in the observations. This entailed centering the MM on the target from two mutually opposite directions. A dove prism was used to rotate the image of the measuring mark and target, such that the measuring mask always appeared to move in the same direction. The mean of measurements from mutually opposite directions gave a correct

estimate of the target centre.

Based on results in this study, the optimum size of ground targets to give maximum pointing accuracies has been found to be approximately 2.5 times the scale number of the photograph times the  $\sigma$ -width of the spread function of the photogrammetric system.

PREFACE.

Practical photogrammetry requires the determination of photograph or model coordinates using photogrammetric instruments for a variety of purposes, particularly in aerial triangulation, and numerical relative and absolute orientation. Even with the introduction of automation into some aspects of photogrammetry, coordinates of control points must under normal circumstances, still be carried out by human operators. The capabilities of the human operator may therefore be an important factor in determining the ultimate accuracy of the photogrammetric process.

Very little is known about accuracies which can be obtained in the visual task of coordinate determination, termed pointing. This is despite the fact that considerable research has been carried out on many aspects of vision. Pointing, however, is a task specifically related to photogrammetry, surveying and similar fields of metrology. Its accuracy is a function of the acuity of the visual system, and may vary under different visual conditions.

The purpose of this research is to investigate monocular pointing accuracies (using a black circular measuring mask) of circular targets with blur characteristics and background densities similar to those which occur in photogrammetric practice. Experimental results derived from this study may be related to existing knowledge on the visual system, so that factors affecting pointing accuracies may be better understood. Such investigations should ultimately lead to an improvement in the design of the shape and size of ground signals and hence an increase in accuracies of location of the photographed signals.

Since these investigations involved the use of terms outside the field of photogrammetry, that is, terms related to the physiology of the

visual process, psychophysical testing of visual tasks and optical image transfer theory, a glossary of terms (marked thus<sup>+</sup>) has been given at the conclusion of this work.

The study has been carried out under the supervision and guidance of Professor P.V. Angus-Leppan of the Department of Surveying, and Dr. G. Amigo of the Department of Optometry, to whom the writer is very grateful. The writer would also like to express thanks to fourth year Survey students (1969) and observer A.H. Campbell, who spent many arduous hours observing the artificial targets.

TABLE OF CONTENTS.

Abstract		ii
Preface		iv
1. Experimental Data on Pointing		
1.1 Introduction		1
1.2 Available Data on Pointing		2
1.3 Graphical Presentation of Data		4
1.4 Interpretation		6
1.41 Mach Phenomenon		8
1.5 Outline of Investigations		10
2. The Visual Process and Vernier Acuity		
2.1 The Physiology of the Visual Process		12
2.11 Introduction		12
2.12 The Eye		12
2.13 The Retina		12
2.14 The Neural Passage to the Brain		13
2.15 Processing of the Visual Information		14
2.2 Visual Acuity		16
2.21 Introduction		16
2.22 Detection, Minimum Visible, Absolute and Relative Thresholds		16
2.23 Recognition		18
2.24 Resolution		19
2.25 Localization		19
2.26 Dependence of Acuity on Test Objects		19



2.3	Physical Factors Affecting Visual Acuity	20
2.31	Illumination	20
2.32	Contrast and Blur	20
2.33	Surrounding Conditions	20
2.34	Wavelength of Illumination	21
2.4	Some Theories to Explain Vernier Acuity	21
2.5	The Imaging Capacity of the Visual System	23
2.51	Spread Functions	23
2.52	Determination of a Composite Spread Function for the Visual System	24
2.6	Visual Acuity as a Function of Luminance Discrimination	30
2.7	The Significance of Contour Mechanisms in Vision	33
2.8	Conclusions	35
3.	Convolution of Annulus and Spread Function of the Visual System	
3.1	Introduction	37
3.2	Convolution	37
3.3	Convolution of the Three-Dimensional PSF and Annulus Profiles ("PSF Method")	40
3.4	Maximum Values of the Profiles	45
3.5	Slopes of the Profiles	47
3.6	Widths of Luminance Profiles	49
3.7	Initial Conclusions	53
3.8	Further Computations Involving Different Spread Functions for the Visual System	54
3.9	Shape of Convolved Curves	56

3.10	Maximum Values and Slopes	57
3.11	Widths of the Profiles	62
3.12	Discussion of Results of Convolutions	69
3.13	Conclusions	71
4.	Psychophysical Testing	
4.1	Introduction	72
4.2	Classical Psychophysical Theory	73
	4.21 Weber's Law	74
	4.22 Fechner's Law	75
4.3	Some Aspects of Modern Psychophysics - The Response Matrix	76
4.4	Classical Methods of Psychophysics	78
	4.41 Method of Limits	78
	4.42 Method of Average Error	78
	4.43 Analysis of Errors in Average Error Method	
	4.44 Suitability of Method of Average Error to Psychophysical Testing	80
	4.45 Constant Stimulus Method	81
	4.46 Suitability of the Method	84
4.5	Modern Psychophysical Methods - Scaling Methods	85
4.6	Reliability and Validity of Results obtained by Psychophysical Methods	89
4.7	Recently Developed Psychophysical Laws	90
4.8	Conclusion	91
5.	Experimental Procedures	
5.1	Introduction	92
5.2	Psychophysical Methods Used	93

5.3	Design of Experiments - Statistical Approach	93
5.4	Instrumentation	95
5.5	Observational Technique	98
5.51	Average Error Method	98
5.52	Elimination of Systematic Error	100
5.53	Constant Stimulus Method	102
5.54	Determination of Widths of Targets	102
5.6	Observers	105
5.7	Production of Targets	106
5.71	Sharp Targets and MM	106
5.72	Blurred Targets	106
6.	Standard Deviations of Observations to Sharp and Blurred Targets - Presentation of Results.	
6.1	Introduction	112
6.2	Analysis of Variance	121
6.3	Regression Analysis	127
6.4	The Relationship Between Experimental Results and Psychophysical Formulae	135
6.5	Discussion	143
6.6	Conclusions	148
7.	Systematic Errors	
7.1	Presentation and Discussion of Results	149
7.2	Elimination of Systematic Error	157
7.3	Conclusions	165
8.	Practical Application of Research	
8.1	Introduction	166
8.2	Signalized Targets	167
8.3	Prediction of Pointing Accuracies	168
8.4	Conclusions	174

9. Final Conclusions	175
References	177
Glossary of Terms	182
Appendices	
A Statistical Analysis of Pointing Observations	185
B Experimental Results and Associated Computations	195
C Microdensitometer Traces of Blurred Targets	216
D Profiles of Annuli Derived by Convolution	219
E Visual and Ocular Characteristics of Observers	231

1. EXPERIMENTAL DATA ON POINTING.

1.1 Introduction.

The measurement of photograph or model co-ordinates in aerial triangulation involves pointing to photographic targets with a measuring mark. Pointing is, in effect, the task of centering a dark, circular measuring mark on a bright, roughly circular target. Such targets can be either photographed premarked ground points, or artificial pricked points in the emulsion of the photograph. Under magnification, the edges of these targets appear blurred and ill-defined. Each step in the formation of the photographed images of premarked ground points adds to the degradation in the quality of the images. Some of the causes of degradation are atmospheric effects, image movement, imperfection in the camera lens, blurring effects of the emulsion, and granularity. The edges of pricked points are also ill-defined, mainly due to physical factors in their formation. A full study has been made on pricked points by *Hempenius (1964, 301-314)*. Pointing therefore cannot be considered as simply centering one sharp circular measuring mark on another. The additional factors of unsharp edges, variable contrast around the target, photographic grain and non-circular target shape, all add to difficulties in the pointing task and consequently lower the accuracy.

In photogrammetric practice, an estimate of accuracies in pointing to such targets using photogrammetric instruments with an optical magnification of 10x is about 3 - 4 $\mu$ . In contrast with this figure, some stereocomparators are capable of pointing accuracies of 1 - 2 microns. On the other hand, the accuracy to which we should ultimately aim according to *Schmid (1964)* is 1 micron or better. Investigations aimed at closing the gap between present and desired accuracies must analyse all aspects of aerial photography, measuring equipment and techniques, in order to develop a set of circumstances which will combine most efficiently to produce the best possible pointing accuracies.

Since the human eye is a basic factor in pointing, any research must incorporate investigations into its characteristics and capabilities.

However, the eye is only a part of the visual system. Images projected onto the retina of the eye are transmitted to the brain where processing of size, shape, colour and density is carried out. Psychological, in addition to physiological factors may therefore be involved (*Hempenius, 1968*). Studies on the eye and more generally the visual system have been carried out by physiologists very extensively over the last 30-40 years. However, when it comes to searching for results of experiments on tasks similar to those occurring in photogrammetry, almost no information exists. In addition, since visual performance proves to be strongly dependent on visual conditions, and the actual task involved, little can be drawn from experiments which are unrelated to the pointing task. Generally physiological investigations do not involve the very high accuracies aimed at in photogrammetry. The problem, therefore, is one which is basically peculiar to photogrammetry. It is for this reason, that photogrammetrists must approach the fundamental problem themselves, backed by sufficient knowledge of physics, and the physiology and psychology of the visual process.

#### 1.2 Available Data on Pointing.

Two sets of experiments on pointing will be cited in this paper. *O'Connor (1962)* investigated monocular and stereoscopic pointing to sharp and blurred targets of different sizes, using a number of different measuring marks. These experiments which were made on Wild STK1 and Zeiss Pulfrich Stereocomparators, revealed that monocular pointing accuracies were linearly related to the width of the annulus between the edges of the target and the measuring mark, above a certain width of annulus, and constant below this level. The level of constant pointing accuracies became greater as the image quality deteriorated. *Hempenius (1964, 318)* has given comprehensive graphs of these investigations plotted on logarithmic scales, with the annulus and pointing accuracies expressed in terms of angular subtense at the eye, in radian measure.

Subsequent experiments by *O'Connor (1967)* have been carried out on monocular pointing accuracies using special instrumentation and very sharp targets of high to low contrast. The instrument had no optical elements as did the stereocomparators, except for two reflecting mirrors. This

allowed him to use targets with edges of the utmost sharpness, since the instrument had a minimum effect on the quality of the image viewed. In addition, the least count of this instrument was considerably smaller than that of the stereocomparators used in the first experiment. The second series confirmed his belief that capabilities of the visual system in pointing to sharp targets, were considerably better than the least count of stereocomparators in general use.

Investigations in his second series, were firstly made in terms of one variable - the annulus size or "edge ribbon" between the measuring mark and target, i.e. keeping contrast and image quality constant. Additional experiments were carried out substantiating the conclusions already reached in the first series, that measuring mark (MM) sizes are of minor importance in the determination of pointing accuracies (*O'Connor, 1902, 51*). After the analysis in terms of one variable - annulus width - a second variable, i.e. contrast of the target relative to its background was added. Extension of O'Connor's investigations could introduce additional variables, e.g. edge unsharpness and photographic grain.

The experiments so far, have been carried out using ideal sharp targets which are far superior in quality to those which occur in normal photogrammetric practice. However, investigations have commenced from the simplest situation with a minimum of variables. Based on this work, additional variables may be added, thus bringing the investigations more into line with practical conditions.

A further aspect that requires investigation is the systematic error which occurs when centering the MM on the target. O'Connor has shown in both his studies that systematic errors may be of the order of 3 to 4 times the standard deviation of the observations. They may be due to either an overshoot or an undershoot, but are usually constantly on the same side of the correct position for each coordinate, and increase for increasing annulus size. It is important for photogrammetry, and metrology in general, that these systematic errors be studied and if possible eliminated, particularly considering their magnitude, and their possible effects on coordinate measurement, if targets with varying annulus sizes are being observed.

A summary of results of O'Connor's experiments will be presented in the following section.

### 1.3 Graphical Presentation of Data.

Figure 1.1 represents the results obtained by O'Connor in his two series of experiments. In the first experiment, curves II, III and IV were obtained whilst curve I is a summary of results in the second study. The image quality of the targets corresponding to each curve has been described qualitatively on the figure, as in *Trinder (1965)*. The targets for curve I are of the utmost sharpness. Curve II was obtained using targets which would be described as "excellent" by photogrammetric standards, while curves III and IV were obtained with targets of increasing degrees of blur. The image quality of these targets may be compared with that of photographed images of premarked targets. Cross-section profiles revealing the image quality of these targets have also been presented by *O'Connor (1962)*.

Figure 1.1 represents the pointing accuracies obtained in the x and y-directions, expressed as standard deviations derived from repeated observations, using measuring marks (MM) as indicated. The x-direction is defined as that parallel to the eye-base, and the y-direction at right angles to it.

The curves have been plotted on logarithmic scales with the annulus or "edge ribbon" between MM and target on the abscissa, and pointing accuracy plotted on the ordinate. Each scale is graduated in angular subtense expressed in radians. (1 min. of arc = 0.291 mrad = 291  $\mu$ rad; 1 sec. of arc = 4.85  $\mu$ rad.) The approximate size of the foveola, the most sensitive part of the retina and the minimum width over which all small details are seen by the visual system, the spread function (SF), have been added. The angular subtenses of annulus and pointing error in figure 1.1 have also been converted into a linear measurement, microns, for a specific optical magnification of 10x in a photogrammetric instrument.

The interpolated curves in figure 1.1 are similar to those determined by *Hempenius (1964)*. However, the exact nature of the curves is uncertain. For curve I, *O'Connor (1967)* has computed an exponential curve for annulus



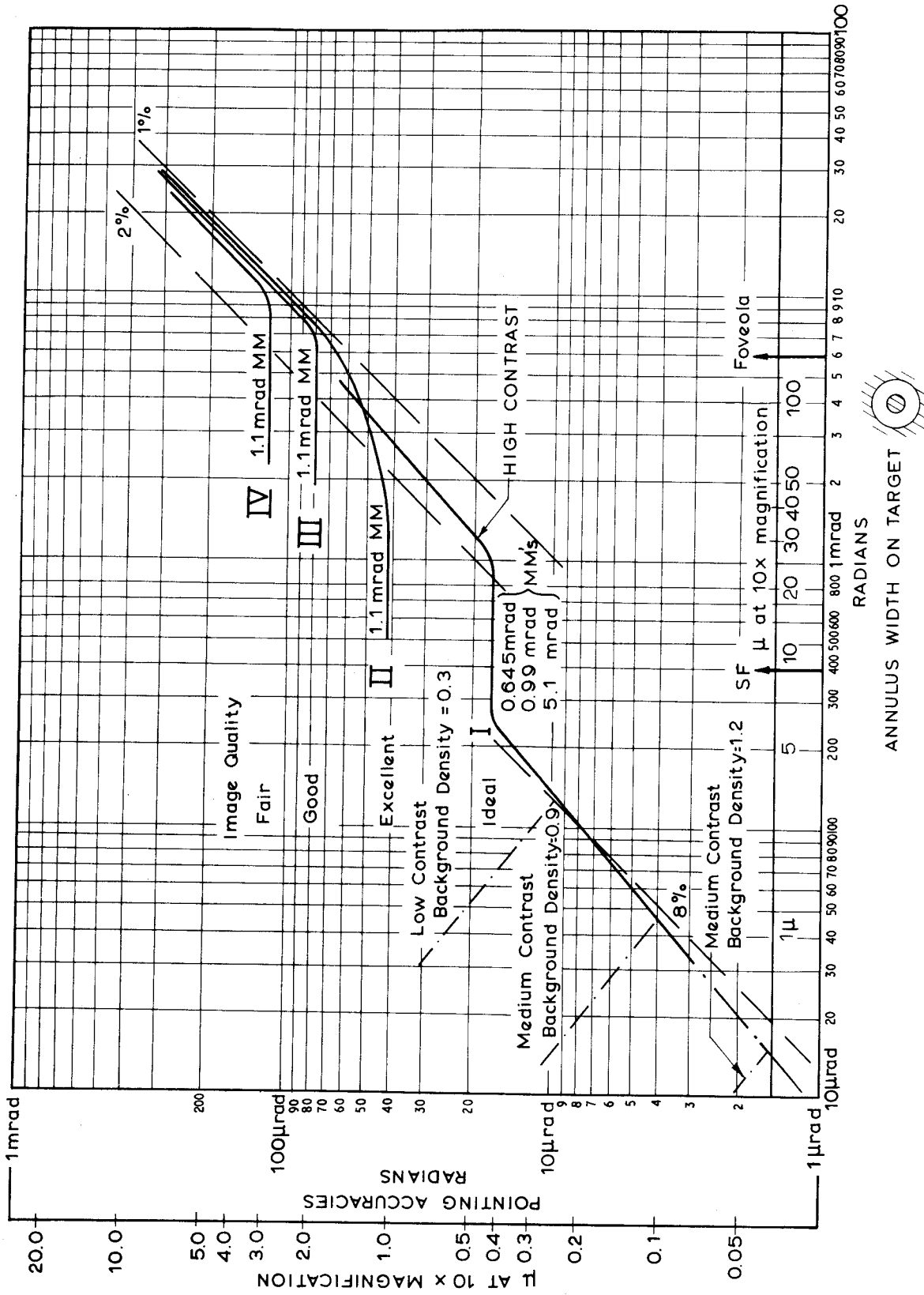


FIG.1.1: Pointing Accuracies for circular targets of varying image qualities using measuring marks (MM) as indicated. They are plotted as a function of annulus width or edge ribbon between the MM and target edge. Both annulus and pointing accuracies have been expressed (a) in radian measure, and (b) as a linear dimension,  $\mu$ , at 10x optical magnification. Curves I, II, III and IV (full lines) have been obtained with high contrast targets. Results obtained with low and medium contrast targets of ideal image quality, agree with curve I, except for annulus widths less than approximately 125  $\mu$ rad, 45  $\mu$ rad and 15  $\mu$ rad on targets with 0.3, 0.9 and 1.2 background density respectively.

widths above 250  $\mu$ rad, and a straight line below this level. In this study the exact path of the interpolated curve is not significant. Nevertheless, there does seem some justification for the curve I given in figure 1.1, since, as will be seen later, separate pointing criteria are involved over each section of this curve.

Figure 1.2 shows the form of systematic errors measured by *O'Connor* (1967), which were only presented graphically. To demonstrate the manner in which the systematic errors may vary with different observers, the results obtained by two other observers have also been given. *O'Connor* has not discussed these errors in detail, as they were not the main object of his study. From the experimental point of view, it should be noted that all targets were approached from the right in x-direction, and from below in the y-direction. In Chapter 7 it will be seen that a constant direction of approach of the MM is important if reliable results are to be obtained.

#### 1.4 Interpretation.

The four curves indicate that for large annuli, pointing accuracies follow a linear relationship - 1 to 2% - with annulus width. For decreasing annulus widths, pointing accuracies reach a constant level, depending on the image quality of the targets. This constant level of pointing accuracies is lower for higher target image qualities.

The relationship of 1 - 2% between annulus width and pointing accuracies has been related to Weber's Law. Weber's Law is used in various aspects of psychophysics, in the study of differential sensitivity of human senses. It states generally that the ratio of

$$\frac{\text{just noticeable stimulus}}{\text{total stimulus}} = \text{constant.}$$
*O'Connor* has indicated that values for the visual system vary from 1 - 2%. He has further proved that it is possible to relate the task of equating areas or widths on each side of the MM to Weber's Law. Stated in terms of pointing, Weber's Law can be rewritten as 
$$\frac{\text{pointing accuracy}}{\text{annulus subtense}} = \text{constant.}$$
Inclined sections of curves I to IV are generally within Weber's Law in figure 1.1

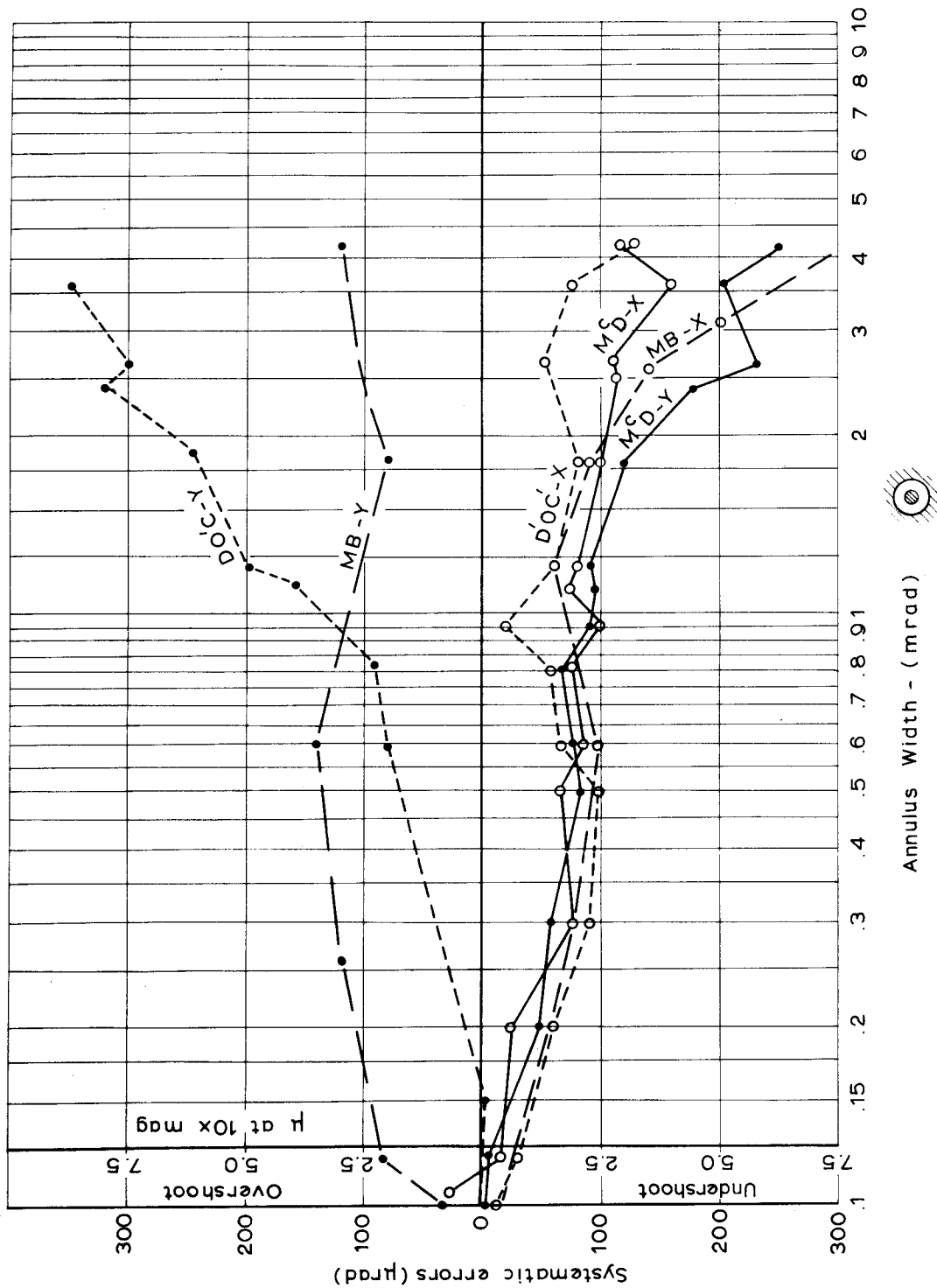


FIG. 1.2: SYSTEMATIC ERRORS DERIVED BY 3 OBSERVERS WITH A MM OF 0.99 mrad, PLOTTED AS A FUNCTION OF ANNULUS WIDTH

The results of pointing to the very high image quality targets in curve I, figure 1.1, are of particular interest in that they reveal the utmost capabilities of the human visual system. Pointing accuracies for these targets reach a constant level, as they did with other targets, but for a further decrease in annulus width, pointing accuracies again improve reaching a final value of approximately 1 sec. of arc (5  $\mu$ rad). This figure is equal to the best results obtained in any acuity test on small well-defined objects. It is worthwhile noting in regard to the efficiency of the human visual system, that the minimum size of receptors in the retina is approximately 20 sec. of arc. Pointing accuracies which are  $1/20$  of the size of the retinal receptors are therefore possible provided the image quality of the targets is very high.

Attempts to explain the complex pattern of pointing accuracies outlined, particularly the constant sections, have so far been concentrated on curve I, since the targets used in its determination contain the least number of variables.

O'Connor in his second study proposed that pointing accuracies for small annuli are dependent to a great extent on the neural activity in the visual system. Such an approach has led to no concrete conclusions. However, because of the importance of the effects of neural activity in vision, the most apparent visual effect, Mach bands will be described in the following section.

#### 1.41 Mach Phenomenon.

As explained by *O'Connor (1967, 41)* when a one dimensional luminance distribution is viewed by an observer (e.g. parallel bright and dark areas separated by a transitional area), a bright band apparently brighter than the original pattern is seen along the edge of the bright region. Also, along the edge of the dark region, a dark band is seen, which itself is darker than the original pattern. These bands are called Mach bands, shown schematically in figure 1.3. A number of investigations have been carried out on the width and intensity of these bands, and are described by *Ratliff (1965)*.

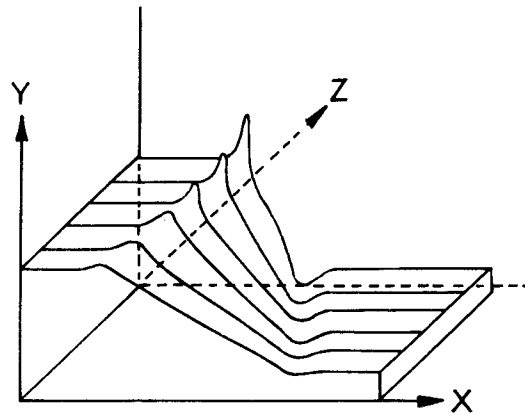


FIG.1.3: Schematic representation of Mach bands, indicating the influence of the gradient of the profile on the appearance of the bands. (Ratliff, 1965, 59)

For small photogrammetric targets the size of the luminance distributions of the annuli are in the order of 1 mrad or less. Experiments on this type of profile have been carried out by *Charman and Watrasiewicz (1964)* and *Watrasiewicz (1966)*. They found similar bright and dark bands, but in addition, at least one smaller secondary dark band adjacent to the luminance intensity change. Also, as the contrast between the light and dark areas decreased, the secondary bands disappeared, but the contrast of the observed pattern became accentuated. According to *Watrasiewicz (1966, 501)* at a contrast similar to that in *O'Connor's (1967)* targets with 0.3 background density, this accentuation was as much as two-fold. Such an accentuation in the apparent contrast was noted by O'Connor in observations of low contrast targets. It is also noteworthy that *Watrasiewicz* found that the Mach bands disappear completely for retinal illuminances<sup>+</sup> below 15 trolands. This is equivalent to a target luminance<sup>+</sup> of approximately 0.7 milliLamberts (mL), for a pupil diameter of 3 mm, ignoring the Stiles-Crawford<sup>+</sup> effect.

#### 1.5 Outline of Investigations.

Theories based on neural effects at the edges of the targets and the Mach phenomenon had resulted in no definite conclusions. *Trinder (1968)* therefore adopted a different approach, whereby the image of the annulus actually seen by the visual system was investigated for the purpose of finding some correlation between this image and pointing accuracies. The spread function,<sup>+</sup> which is the blurring effect of the visual system, was convolved<sup>+</sup> with the luminance profile<sup>+</sup> of the object, to derive the luminance profile seen by the observer. A number of conclusions on the geometry of the visual image resulted from these investigations. In general, the profile of the visual image was analysed in terms of widths, slopes of the flanks and maximum values, and correlations were found between these properties and pointing accuracies.

These investigations did not include the effects of neural activity which may prove significant under certain circumstances. This work in Chapter 3, however, will extend studies on the visual image, to include

some effects of neural activity. Estimates of this activity will be based on the existing limited knowledge of the visual system derived by physiologists and neurophysiologists, as described in Chapter 2.

Extending the experimental work on pointing, a full series of observations has been carried out on blurred targets of varying degrees of blur, background densities and sizes. The effects of these variables on both the standard deviations and systematic errors have been studied in Chapters 6 and 7. Finally, based on the findings on systematic errors an observational procedure, as described in Chapter 5, has been proposed, which will lead to the correct location of the centre of the target and thereby eliminate the systematic error. This procedure entails optically rotating the image seen by the observer, such that movements of the MM against the target are always apparently in the same direction.

## 2. THE VISUAL PROCESS AND VERNIER ACUITY.

### 2.1 The Physiology of the Visual Process.

#### 2.11 Introduction.

A study of the ability of the human visual system to carry out pointing, must include an understanding of the basic visual processes. *O'Connor's (1967)* work contains a very detailed study of the physiology of the visual processes, together with adequate diagrams and references. A duplicate description therefore will not be given in this study. However, for completeness, it is fitting to include a summary of *O'Connor's* work, which in fact has been collected from a large number of papers and texts on the subject.

#### 2.12 The Eye.

The eye is the optical element of the visual image, forming images of objects on the retina at the rear of the eye, via the lens. Normal eye optics follow the refractive laws of light, such that images on the retina are real, inverted and diminished in size.

The aperture of the eye, or diameter of the pupil, is controlled by the iris, and may vary from 1 to 8 millimeters, depending on the intensity of illumination. An approximate relationship between aperture and the level of illumination incident on the eye is given by *Walsh (1953, 55)*. Quality of the image on the retina varies according to the size of pupil. *Gubisch (1967, 408)* gives examples of image qualities of the eye for the different pupil sizes in terms of the point spread functions, indicating that the pupil diameter for best imaging quality is approximately 4 mm.

It is interesting to note the variable nature of the optical performance of the eye, which depends on pupil size, and therefore intensity of incident illumination. This is in contrast to normal optical systems, which perform in exactly the same manner over a wide range of luminances.

#### 2.13 The Retina.

The Retina, composed of discrete minute cells, allows simultaneous reception and transmission of the incident light. In the light receptive



cells, that is, the rods and cones, stimulation by the incident light is carried out by means of a photochemical process. Impulses are then transmitted from the rods and cones to the bipolar cells, which are intermediate cells connected to the ganglion cells. Additional cells, called the association cells, whose function is uncertain, are also found in the retina.

There are two main zones in the retina - the central area, and the extra-areal periphery. For normal fixation, the eyes are turned so that the observed objects are concentrated on the central fovea, within the central area. The central fovea is a small concave depression in the vitreal face of the retina, whose total angular width is approximately  $5^{\circ}$  (90 mrad). The floor of this depression, known as the inner fovea (*Davson, 1963, 85*) or foveola, is the rod-free area of the retina. It is the portion concerned with the highest degree of visual acuity, and therefore of most interest in pointing.

The population of light sensitive rods and cones and the character of the cells themselves vary, depending on their location. Cones are generally characterised by high contrast threshold, colour vision and high acuity. On the other hand rods, which are located away from the centre of the retina are of low acuity, but allow detection of low luminance levels, particularly because of the diffused connections which exist between rods and ganglion cells. This leads to a summation of stimulation of many rods onto the ganglion cells.

#### 2.14 The Neural Passage to the Brain.

Messages from the retina are transmitted to the brain via the optic nerve. A number of different types of nerve fibres constitute the optic nerve, but detailed knowledge is not available. The bulk of the fibres are visual fibres which conduct impulses from the ganglion cells in the retina. The optic nerve tracts from each eye lead through the optic chiasma into the left and right geniculate bodies, known together as the Lateral Geniculate body. O'Connor describes them as the relay stations for transmitting impulses to the brain. In passing through the optic chiasma, the nerve fibres originating from

the nasal part of the retina of each eye cross to the opposite geniculate bodies, while the fibres originating from the temporal part of the retina at each eye remain uncrossed. This process is called semi-decussation. The visual fibres finally pass from the geniculate bodies to the occipital cortex, which is the end of the visual path.

The exact connection between cortical cells and optic fibres is unknown. However, O'Connor indicates that form, contour and space perception are significant features of processing in the cortex. In addition, the cortical image does not represent a precise "image" of the object, because greater emphasis is given to impulses arising from the fovea than from the remainder of the retinal area.

Subsequent processing, involving many psychological processes, as well as connections with other sections of the brain, undoubtedly takes place as a result of the stimulation of the occipital cortex. This subject is outside the scope of the present study.

#### 2.15 Processing the Visual Information.

After the transmission through the optical media, light is incident on the retinal rods and cones, causing a bleaching of the photochemical substance at the surface of the cells, and giving rise to electric impulses within the cones. The neural connections between the retinal cells are extremely complex. Generally speaking, connections between cones or rods with bipolars differ, depending on their location in the retina. Connections of rods with their bipolars, particularly in the periphery of the retina, are diffused and therefore lead to a summation of the rod impulses in the bipolars. Inter-connections between the bipolars may be further diffused by dendrites of the bipolars themselves, such that considerable reciprocal overlapping between cell connections takes place, leading to a much larger group of bipolar cells being affected by the group of rods. Further overlapping may also take place between the ganglion cells.

Couplings of cones onto bipolars, outside the foveal area lead to similar overlapping. For the foveal cones however, couplings between

cones and their bipolars are at a minimum. Pirenne (*Davson, 1962, 177*) indicates that foveal cones have single line connections with the occipital cortex, but also states that the same cones may have connections with other retinal cells as well. This means there may be single-cone and multi-cone units in the fovea. Granit (*Davson, 1962, 547*) states there appears to be one foveal cone to three bipolars and throws doubt on the exact nature of conal couplings. Nevertheless, conal stimuli do appear to be transmitted to the occipital cortex with a near one-to-one relationship between cones and subsequent retinal and geniculate cells (*Polyak, 1948*), (*Davson, 1963, 319*). This point will be referred to in sec. 2.4 with regard to vernier acuity.

Inhibition<sup>+</sup> as defined by *O'Connor (1967, 171)* is the depression of the response to illumination of a given receptor by the stimulation of the neighbouring receptors. The occurrence of inhibition in vision as well as in other senses, and indeed also in the less developed forms of eye, e.g. the compound eye of the crab, *Limulus*, is well known. Theoretical models have been devised to explain inhibition based on knowledge of *Limulus* (*Ratliff, 1965, ch. 3*). Considerable speculation however, exists on the exact manner in which inhibition may occur in the human visual system. It may be through interaction between neighbouring retinal cells. Though it seems possible to explain it in an approximate fashion based on the experiments on *Limulus*, a clear understanding of the neural networks involved is impossible at present. Indeed, it seems clear that the human visual system cannot be described by a simple formula, and in such work there is the danger of attempting to oversimplify the processes involved.

In the lateral geniculate body it seems possible that some compression of information, or even discarding of information may also occur. For instance, *Davson (1963, 320)* indicates that inhibition may be further reinforced in the lateral geniculate body. The neural processes within the six layers of the lateral geniculate body and subsequent passages to and connections in the occipital cortex are extremely complex and diverse. To date, even though considerable knowledge is available on the functions of the various sections of the visual system, the exact manner of

functioning of and detailed intricate interplay between various sections is not known. Tentative proposals only exist on some of these aspects of vision.

As emphasised by O'Connor, preoccupation with the retinal mosaic only must be avoided. The complete visual system must always be considered when carrying out visual studies. Though detailed knowledge is unavailable on some sections of the visual system, the aspects which are well established e.g. interconnections between retinal cells, and their associated effects, such as inhibition must be recognized and included.

The studies in this work will attempt to take cognizance of the various factors in the visual process. Work carried out by a number of visual scientists, which in fact contains some simplifying assumptions will be adopted. In the following sections, the various types of visual acuity tasks will be introduced, together with some physical factors which may affect acuity results. Following this, a theory will be presented to explain vernier acuity, and some aspects of vision which may influence vernier acuity will be discussed.

## 2.2 Visual Acuity.

### 2.21 Introduction.

Visual acuity is the capacity to discriminate fine details of objects in a field of view (*Riggs, 1965, 321*). The clinical procedure for testing visual acuity uses standard test objects of known size for gauging the performance of an observer against the norm. The gap in the Landolt C<sup>+</sup>, for instance, has a known dimension and its recognition is one measure of visual acuity. The minimum recognizable gap determined by repeated observations gives a measure of the visual acuity of the observer. Generally however, acuity will depend on the type of acuity task involved. These tasks are presented in the following sections

### 2.22 Detection, Minimum Visible, Absolute and Relative Thresholds.

Detection requires a statement by the observer that an object is or is not visible. Such a task involves minimum visual effort on the part of the observer.

Absolute Threshold is the minimum light stimulus necessary to evoke the sensation of light (*Davson, 1963, 94*). It must be measured under dark adaptation conditions, and will decrease to a minimum as the duration of adaptation to darkness increases. The minimum value will be approached when the dark adaptation period extends beyond thirty minutes.

The absolute threshold may be given in terms of retinal illuminance derived from target size and luminance. For point sources of light of long duration, it may be expressed as the number of quanta per second required to evoke the sensation of light. When the stimulus is a point source of short duration (less than 0.1 sec) the threshold, termed the "minimum visible threshold" is measured as the total quanta of light entering the eye. Observations carried out in photogrammetry are based on above threshold levels of illumination, and therefore it is unnecessary to consider absolute thresholds.

Relative or differential thresholds involve the measurement of the amount an existing stimulus must be increased for it to produce a change in sensation. In measurements of differential thresholds, a background field is kept at a constant level, while the luminance of a small test object of long or short duration is varied. The threshold depends on luminance of the background, and the size and duration of illumination of the test object. Typical results of differential thresholds are shown in *Davson (1963, 97)*. *Trinder (1968)* proposed that pointing to targets whose annulus widths are less than 250  $\mu$ rad, may involve a task of detection, or discrimination of luminances on each side of the MM, and may therefore depend on the differential threshold of the visual system.

*Riggs (1965, 322)* compares three types of objects which may be used for testing visual acuity, based on absolute and differential thresholds:-

- (i) bright object against a dark background,
- (ii) dark object against a bright background,
- (iii) low contrast object relative to the background.

(i) Bright objects against a dark background prove to be unsuitable for testing acuity, because any very small object with suitable illumination will be visible.

The blurring nature of the visual system can be represented by a spread function, which describes the shape and size of the image of very small objects seen by the visual system. Further discussion on spread functions can be found in section 2.5. Since the image of all small objects will take on the same shape and size, the apparent brightness of the object will decrease as the object size decreases. Any object will therefore be visible, provided the illumination is sufficiently bright. Under dark adaptation conditions, this is equivalent to the absolute threshold.

(ii) Dark objects on a bright background. *Byram (1944)* and *Fry (1955)* have computed the light distribution in the retinal image of a dark line based on the blurring characteristics of the eye. For a thick line, the image is dark in the centre and graded at the edges towards the bright background. For very narrow lines, the line becomes grey against the bright background. The line will become invisible when the intensity of the line appears the same as the background. According to *Byram*, for long lines, only 1% difference in intensity between the image of the line on the retina and its background is needed for visibility. Whether the value of 1% is exactly correct is open to question, particularly considering existing knowledge of the visual system (see Chapter 3). Measurements of widths of dark lines show estimates of acuity of approximately 1 sec. of arc (5  $\mu$ rad) subtended at the eye for long lines, and larger values for objects of smaller dimensions.

(iii) Low contrast test objects. Similar treatment can be given to low contrast targets, as is given in the previous case. The question is whether the image of the target in the visual system of the observer is of sufficient contrast for detection. One would normally expect that for successful detection, low contrast objects would have to be larger than high contrast objects.

### 2.23 Recognition.

Recognition of an object requires more than simply its detection. Some critical aspect of the target must be seen and used by the observer to describe the object. Clinical tests use, for instance, the Landolt

ring or C as a test of acuity. The subject must recognize the orientation of the gap in the ring. Generally figures of 20 to 30 secs. of arc have been obtained with this method, while slightly larger results have been obtained with low contrast objects (*Shlaer et al.*, 1942).

#### 2.24 Resolution.

Resolution requires the subject to state if he can resolve a pattern of parallel lines of a particular separation, e.g. black lines on a white background whose separation equals their width. Tests have shown that widths of black objects on a bright background must be in the order of 1 min. of arc (*Senders*, 1948) to be visible, under favourable conditions.

#### 2.25 Localization.

Localization involves the discrimination of the displacement between two sections of a test object. An example of this type of task is that of vernier acuity, which is measured as the minimum visible displacement between two sections of a line, as in a vernier. Acutities as little as 2 sec. of arc (10  $\mu$ rad) have been found in such tests. *O'Connor* (1962) concluded that photogrammetric pointing is similar to the vernier acuity task and indeed has obtained accuracies (*O'Connor*, 1967) comparable with those of vernier acuity tests.

#### 2.26 Dependence of Acuity on Test Objects.

The four types of visual acuity tests listed above clearly indicate the considerable dependence of results of acuity tests on the type of test object. Though clinical tests normally adopt the recognition task, rendering acuity results of 20 to 30 secs. of arc, detection and localization give results in the order of 1 sec. of arc or less. It therefore seems likely that different mechanisms in the visual system may be involved in each task. Since pointing is a vernier acuity task, discussion in future chapters will concentrate on mechanisms which may affect vernier acuity.

Some of the physical factors which influence acuity will now be discussed briefly, after *O'Connor* (1967). Since these factors are of a general nature, their influence will tend to affect the different acuity tasks similarly.

### 2.3 Physical Factors Affecting Visual Acuity.

#### 2.31 Illumination.

It is generally agreed that visual acuity improves with increased illumination. Conversely, acuity drops significantly for low illumination levels. *O'Connor (1967, 24)* quotes 12 to 18 millilamberts as a suitable range of luminances for observation. This range is comparable with luminance values in photogrammetric equipment, and has therefore been used for observations in this study.

#### 2.32 Contrast and Blur.

Very little research directly applicable to photogrammetry has been carried out in regard to contrast and blur. *O'Connor (1967)* has shown that contrast has no effect on pointing accuracies of sharp targets except for the small annulus widths. He also states (*O'Connor, 1967, 26*) that it is generally considered blur has little or no effect on vernier acuity, but has shown (*O'Connor, 1962*) that it does reduce pointing accuracies for small targets.

#### 2.33 Surrounding Conditions.

Most investigators have found that optimum conditions exist when the background luminance is about the same as that of the target. Further, it seems that disturbing effects around the target can affect results significantly, though little is known on this point.

*Flom et al. (1963)* for instance, found that acuity measurements based on the Landolt C dropped significantly when 4 bars were placed around the C at different distances. The effect was most significant over a distance of approximately five times the gap width in the Landolt C. No suitable explanation was put forward, though it was proposed that the reduction in acuity may be due to:-

- (a) the effects of optical image spread in the visual system,
- (b) interaction between the various objects at the neural level,
- (c) psychological aspects involved in the conflict of tasks,
- (d) eye movements.

Though such measurements cannot be directly related to vernier acuity tasks, it is clear that disturbing influences in the immediate vicinity of the



target may cause a significant drop in pointing accuracies.

#### 2.34 Wavelength of Illumination.

In accordance with spectral sensitivities of rods and cones, acuity is lower under red and blue light than under white, or under the mid-region zone of the spectrum. White light was therefore chosen for the experiments on pointing, and is generally used in most modern photogrammetric instruments.

#### 2.4 Some Theories to Explain Vernier Acuity.

The very high accuracies which can be obtained with vernier acuity type tasks ( $1/10$ th to  $1/20$ th of the interconal distance), were known as early as 1864 by *Hering*. While many attempts were made to explain this phenomenon, it was not until 1923 that a suitable explanation was given (*Andersen and Weymouth, 1923*). Though some modifications may be in order, considering present knowledge on vision, the proposals of Andersen and Weymouth are still basically sound. Their explanation is based on the dynamic theory of vision, which accepts that the involuntary micro-nystagmus<sup>+</sup> of the eye are an integral part of the visual process. As stated by *O'Connor (1967)* modern dynamic theories consider the whole visual system as an integral part, all sections contributing to the whole visual process. The previous theories put forward to explain vernier acuity in general concentrated on the array of receptors on the retina, and ignored the micro-nystagmus of the eye.

*Andersen and Weymouth (1923, 584)* proposed that each cone receptor in the fovea, has its own "local sign" or distinctive influence in the visual system. For cones to have their own local sign, they must have a "one-to-one" nervous connection to the occipital cortex. It is well established that most retinal receptors do not have this one-to-one relationship, but experts agree that for central foveal cones, anatomical arrangement is very close to a one-to-one relationship (see section 2.15)

Firstly, the affects of the micro-nystagmus will be excluded. The image of a straight, very narrow line on the retina will be blurred, because of the imperfections in the optics of the eye. Many cones will

be stimulated across the width of the blurred line, by varying amounts, depending on the intensity of the blurred line at each cone. The local sign of the affected receptors will therefore become related to the local signs of neighbouring cells by virtue of their sharing in the reception of the illumination of the line. Location of the line will be based on the relative stimulation of all cones. In consideration of the fact that the line will have length as well as breadth, considerably more receptors will also be available for the location of the line along its length. Length has been proved to assist in the location of such lines (*Keeseey, 1960, 774*).

The eye, however, is known to move continually, leading to a continual movement of the image over many more receptors on the retina. The line may therefore be located very accurately based on the very large number of cones stimulated during observation. Expressed in terms of local signs, location of the line is based on a mean retinal local sign determined from the local signs of a number of cones.

There is still doubt as to the full effects of eye movements on visual acuity. *Riggs et al. (1953)* investigated the effects of stabilizing the image on the retina. Detection measurements under these conditions showed that visual acuity was improved for short duration targets (less than 0.2 sec.). However for longer durations, the targets faded and disappeared. *Bryndahl (1961, 11)* states that for grid type targets of short duration, eye movements are detrimental to vision. *Keeseey (1960, 774)* states that eye movements do not adversely affect vernier acuity over longer periods of viewing, and claims that vernier acuity tasks are based on the discrimination of the spatial pattern of illumination regardless of any temporal changes of intensity in the receptor cells. The main function of eye movements therefore appears to be in ensuring that light is rapidly distributed over the receptor cells, thus avoiding fading of vision as occurs in the stabilized image. Though some aspects of micro-nystagmus movements are ill-understood, evidence seems to indicate that they are not detrimental to visual tasks occurring in photogrammetry.

The explanation of *Andersen and Weymouth (1923)* is still basically

correct. However, to be in line with modern knowledge of the visual system, it must at least take qualitative account of effects of neural processing of the visual system, particularly inhibition, which may have considerable influence under certain critical circumstances. Accepting the above theory as the basic explanation for pointing accuracies, an attempt will now be made to investigate a satisfactory method for testing the influences of inhibition on pointing results for small annuli.

The visual sensation of inhibition is explained most easily by reference to the Mach phenomenon, as described in section 1.41. Mach bands were not consciously seen by *O'Connor (1967)* in his experiment. *O'Connor* believes however, that the effects of the inhibitory processes were still in action, though subliminally. The pattern of results obtained in the pointing experiments cited, indicate a complex relationship between annulus width and accuracy. Further investigations are necessary on the geometry of the target, and its relation to the visual system. *Trinder (1968)*, using a spread function of the visual system, investigated the shape of the luminance profile of the target seen by the observer. Complex neural processes of inhibition, however, were not included. The following section will investigate a more complete spread function of the visual system than was used previously, to extend these studies.

## 2.5 The Imaging Capacity of the Visual System.

### 2.51 Spread Functions (SF).

The concept of spread functions has been discussed previously (*Trinder, 1968*). It was then stated that the imaging quality of all optical systems could be described by such spread functions. A point spread function (PSF) describes the nature of spreading of an imaging system, for a fine point object, while the line spread function (LSF) describes the nature of spread of an imaging system, for a very narrow linear object. The shape of the image of any other object can be determined using these spread functions.

As expressed in section 2.12, the SF of the optical section of the eye varies with pupil diameter. In the case of the previous study,

the form of the PSF for the visual system adopted was the gaussian function  $f(x, y) = \exp [-(x^2 + y^2)/2\sigma^2]$ , where  $x$  and  $y$  are in  $\mu\text{rad}$  and  $\sigma = 200 \mu\text{rad}$ , as shown in figure 2.2. This spread function clearly did not include any effects due to inhibition. These effects will be investigated in the following section, together with a discussion on the validity of the application of SF's to the visual system.

#### 2.52 Determination of a Composite Spread Function for the Visual System.

The imaging capacity of the visual system depends on two separate sections which may be termed as the optical part, and the neural part. The optical part refers to the system of imaging the light rays from the cornea to the retina, while the neural part concerns the section from the light sensitive cones and rods to the occipital cortex. The characteristics of the optical part can be represented satisfactorily by a spread function, for a given pupil diameter. If the neural part is to be represented in the same manner, a number of assumptions must be made.

Some methods of determining the spread function of the optical part have been summarized by *Fry (1963, 95)*. The earlier methods were based on the observation of images of line objects which were transmitted through the optics of the eye and retina and reflected back. Corrections were made for double transmission in the eye but no corrections were made for the effects of double transmission through the retina, e.g. *Westheimer and Campbell (1962)*. Other determinations of the SF of the optical section of the visual system are cited by *Trinder (1968)*. *Fry (1963, 95)* states that his early determinations of the LSF were based on the response to bar type targets of different widths, but he points out that it is very likely that his LSF's included not only the optical spread, but also the lateral inhibition effects in the retina. He says that subsequent results of LSF's which gave different results for different illuminations seemed to support this fact; some workers called this effect the "neurological spread."

Recent determinations of the optical performance of the visual system have resulted in the determination of the optical response to a sine-wave

target, giving the Modulation Transfer Function. Since the modulation transfer function (MTF) is the Fourier transform of the SF, the SF can be computed by mathematical manipulation. *Gubisch (1967, 408)* found the PSF by this method, for a number of different pupil sizes. The PSF for a pupil size of 4 mm is approximately a gaussian function with a  $\sigma$  of 100  $\mu$ rad. This value is far superior to the values determined by *Westheimer and Campbell (1962)* and *Fry (1963)*, but Gubisch maintains that the inferior values did not agree with high acuity results, and were affected by limitations in experimental procedures.

*Lowry and DePalma (1961)*, *DePalma and Lowry (1962)*, *Bryndahl (1960)* and *Patel (1966)* have investigated the MTF of the whole visual system. *Lowry and DePalma (1961)* computed the MTF from subjective Mach band patterns, based on an analysis of spatial frequencies. *Bryndahl's (1960)* investigations were concentrated on lower spatial frequencies, which are not attenuated by the optical part of the visual system. These tests, therefore, isolated any effects due to the neural section of the eye. *Patel (1966)* measured the threshold response of the visual system to sine-wave targets of different spatial frequencies. This method was also used by *DePalma and Lowry (1962)* who investigated both sine-wave and square wave responses.

*Ratliff (1965, 149)* states that it is obviously impossible to observe the effects of lateral inhibition directly. However, if the physical light distribution, the subjectively observed light distribution and the blurring effects of the eye can be observed, the effects of the neural network can be deduced. In comparing the optical properties with properties of the whole visual system, many researchers have realized that there is apparently a rectification of the optical images, carried out by the neural network, producing the final image as perceived by the brain. In other words the quality of the image actually seen by the observer is apparently better than that which would be obtained by the optical part of the eye alone. This fact has led them to investigate the visual process in more detail.

The interpretation of results of experiments on the whole visual system require Fourier Analysis techniques which are well established in the field of Optics (*Linfoot, 1965*). Before these methods can be applied, it must be assumed that the neural system will react linearly.

As explained by *Lowry and DePalma (1961, 744)* the spread function must be invariant for any type of object pattern, keeping pupil diameter and luminance constant. *Patel (1966, 691)* maintains that the good agreement between his result, and those of *Lowry and DePalma (1961)* - which were obtained by a different procedure - supports the assumption of linearity. However, *Marimot (1963)* points out that this assumption is immediately proved invalid by the asymmetry in the Mach bands. This feature is further supported by the work of *Menzel (1959)*, as quoted by *Ratliff (1965)*, who computed subjective luminance intensities from an observed MTF. The computed profile produced a symmetrical pattern of Mach bands inconsistent with reality. *Ratliff (1965, 130)* recommends that the visual system can at best be assumed only "piece-wise" linear, since its performance will vary, particularly with object luminance. This is generally in line with the assumptions made by *Lowry and DePalma (1961) and Patel (1966)*.

*O'Connor (1967, 50)* speaks of "several prominent non-linear stages" in the visual process. For example:-

- (a) the bleaching of the visual pigments is a non-linear function of intensity at high intensities,
- (b) there seems to be a logarithmic relation between the amount of pigment bleached in the retinal cells and the sensitivity of the visual process,
- (c) saturation occurs in the human rod system.

In view of the adoption of a piece-wise linear system, and the acceptance that the MTF's will vary depending on the retinal illuminance, the effects of these non-linearities tend to be reduced. It is believed therefore that an approximately linear system over restricted

ranges is acceptable, keeping in mind the limited information available about the visual process.

*Ratliff (1965, 155)* states that, although there are difficulties inherent in the application of Fourier methods to the visual system - especially concerning the neural part of it - tentative conclusions may be drawn on the MTF of the whole system. He states that it increases for increasing spatial frequencies, passes through a maximum, and then decreases for the higher spatial frequencies. He also maintains that this is in line with experiences in normal vision, where shallow gradients and greatly rounded curvatures (containing lower spatial frequencies) are seen nearly uniform, since the lower frequencies tend to be attenuated. Moderate curvatures (containing moderate frequencies) are seen distinctly by the visual system, while the very sharp and closely spaced curvatures cannot be resolved. An example of the MTF derived by Lowry and DePalma is shown in figure 2.1. By contrast, the MTF of the optical section of the visual system is a maximum for low frequencies, and decreases for high frequencies. An estimate of this transfer function is also shown in figure 2.1.

Based on these conclusions, *Ratliff* derives a theoretical MTF using a simplified model of the visual system, and obtains a composite spread function of the visual system which is very similar in form to the theoretical models of excitation and inhibition determined by a number of different investigators, e.g. *Fry (1963, 96)*, (see *Ratliff 1965, Ch.3*). *Patel* also maintains that his LSF's for the different retinal illuminances are conceptually similar to the SF's derived by *Fry (1963, 96)*. There is thus agreement on the general form of the SF of the complete visual system, though the relative dimensions vary.

The LSF computed by *Patel* is as shown in figure 2.2. The inhibitory system extends to approximately 8 min. of arc (2.4 mrad) away from the centre of excitation, the maximum inhibition level being - 0.15 times the maximum excitation level. For comparison, the SF used by *Trinder (1968)* is also shown in figure 2.2. *Ratliff's* SF derived by a

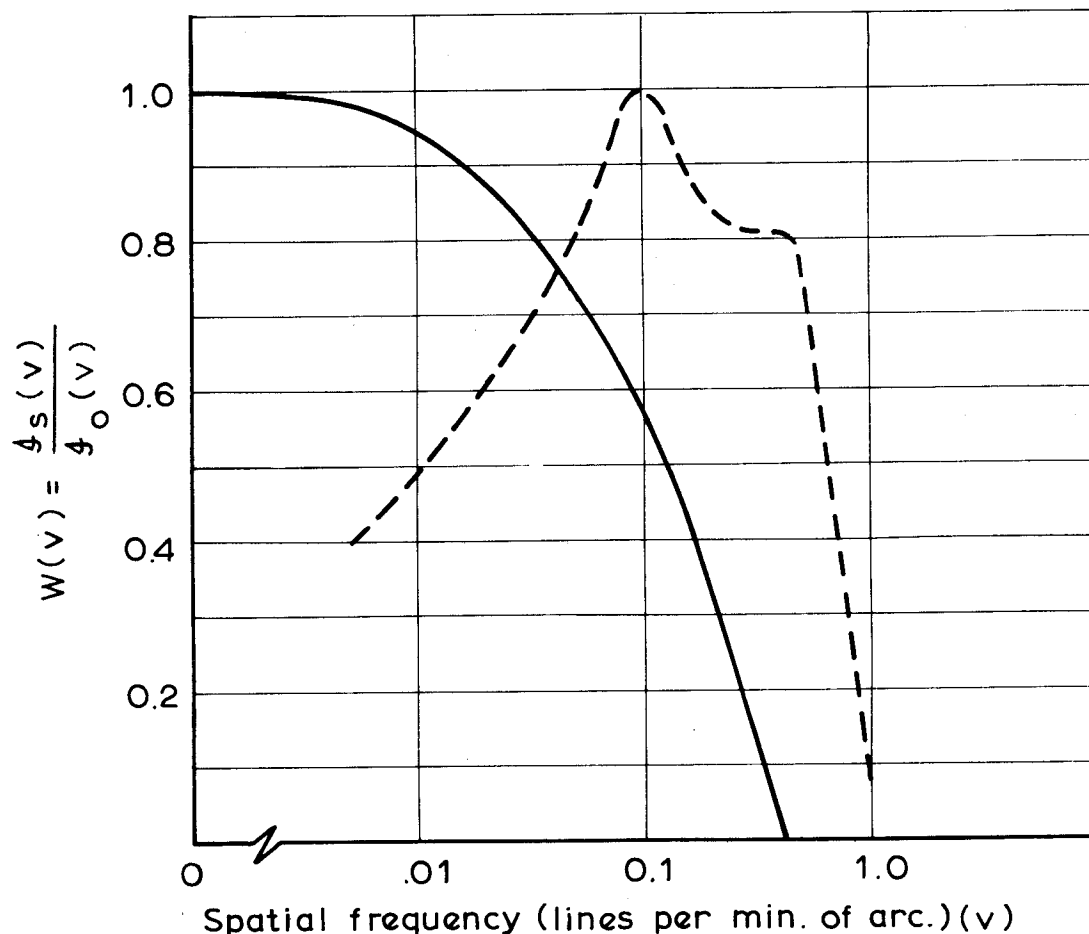


FIG. 2.1: MTF OF OPTICAL SYSTEM OF EYE DERIVED BY KRAUSKOPF (1962), (full line) AND MTF OF COMPLETE VISUAL SYSTEM DERIVED BY LOWRY & DE PALMA (1961) (broken line). Slightly different curves may be obtained by other investigators, but the above curves indicate the form of the two functions.  $\phi_s(v)$  is the Fourier Spectrum of the subjective image distribution  $I_s(x)$ , and  $\phi_o(v)$ , the spectrum of the object intensity distribution  $I_o(x)$  (Ratliff, 1965, 153)



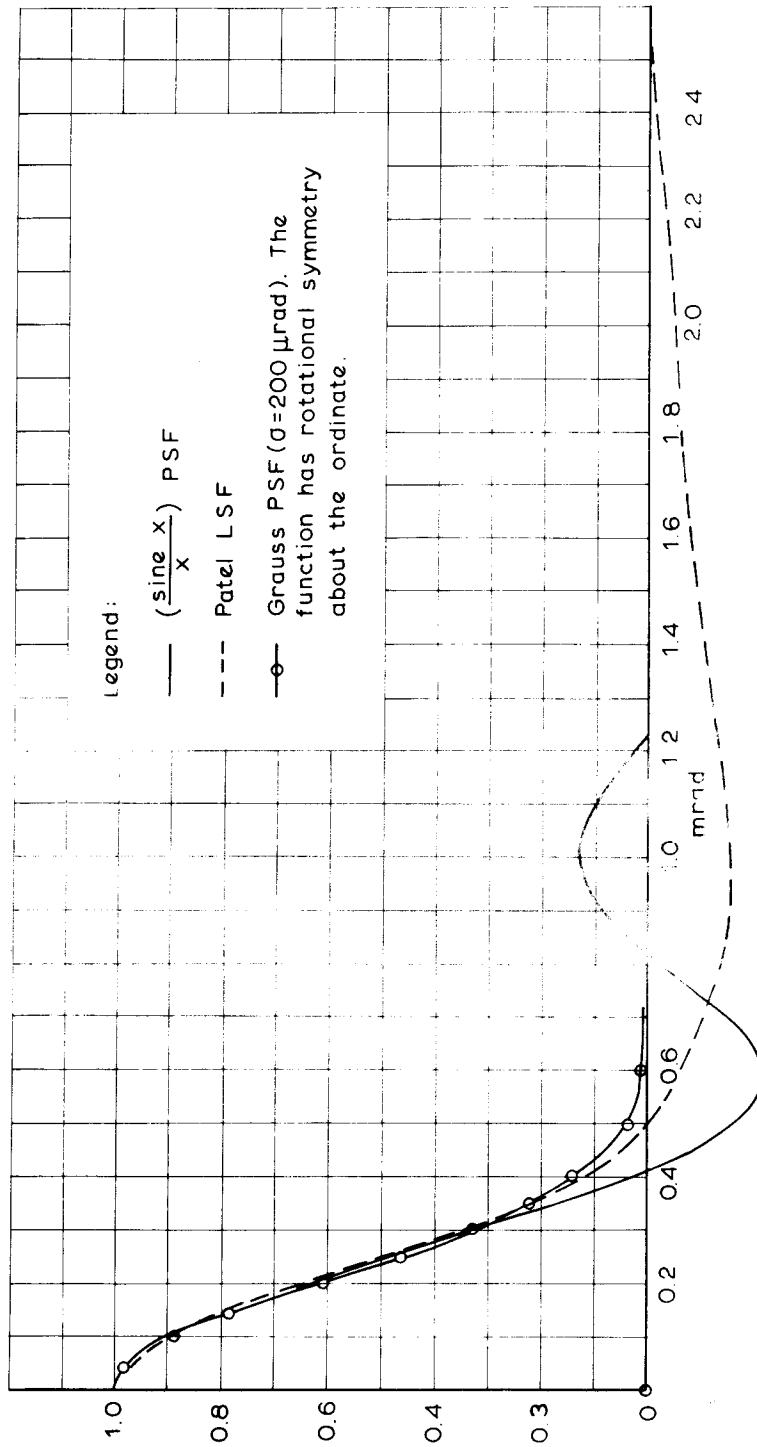


FIG. 2.2: THE SINC PSF AND PATEL'S LSF, AS COMPARED WITH THE GAUSSIAN PSF WITH  $\sigma = 200 \mu\text{rad}$ . ALL FUNCTIONS ARE SYMMETRICAL ABOUT THE ORDINATE.

simplified assumption on the neural networks (*Ratliff, 1965, 132*) follows a form very similar to the  $(\sin x/x)$  function. In figure 2.2, the  $\left(\frac{\sin x}{x}\right)$  function has been computed so that it follows that of Patel over the excitation area, but deviates noticeably from Patel's SF over the inhibition area. In fact, in addition to inhibition, there is also a secondary area of excitation, which according to *Ratliff (1965, 132)* may occur in the visual system.

From the above discussion, it is clear that assumptions on linearity of the visual system are only approximate, and that any conclusions reached using SF's must be guarded. Nevertheless, a number of workers have been able to apply MTF's to the visual system, with some success. At present, the full extent of the effects of non-linearities is unknown. For the treatment of effects of inhibition on circular annuli, the most satisfactory formulation of the excitatory and inhibition effects can be found in the SF's. The technique of convolution of the SF's in figure 2.2 and the target luminance profile, will therefore be adopted as the method of testing the influence of inhibition on small annuli.

Before commencing with the computations, two further aspects of vision which may influence pointing will be discussed. These are luminance discrimination, and contour mechanisms in vision.

#### 2.6 Visual Acuity as a Function of Luminance Discrimination.

The acuity tasks of detection as described in section 2.2 involve the visibility of a target, and depend basically on the intensity of illumination of the object. A number of investigators have analysed detection in terms of the flux or quantity of light reaching the eye. *Lamar et al., (1947, 545)* have made a number of conclusions in respect of the necessary contrast required for the detection of targets. For instance, for targets less than 2 mins. of arc ( $600 \mu\text{rad}$ ), the total flux added to the background by the target for detectability is constant. This simple reciprocal relationship breaks down however, when one dimension of the target is greater than 2 mins. More flux

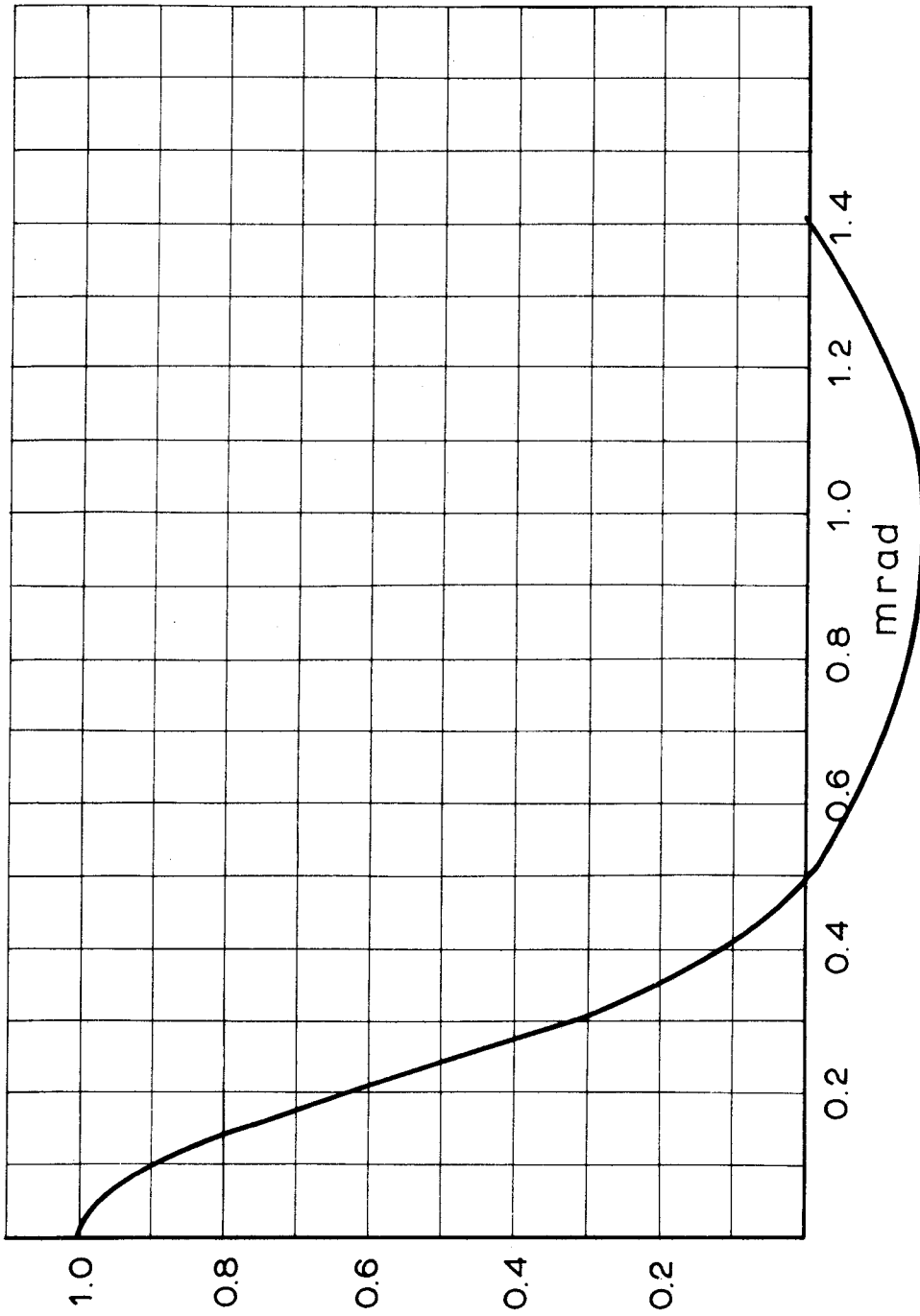


FIG. 2.3: THE MODIFIED PATEL FUNCTION USED IN CONVOLUTIONS IN CHAPTER 3. THE FUNCTION IS SYMMETRICAL ABOUT THE ORDINATE.

is then needed for detection. For targets whose width is less than 2 mins., variations in width can be compensated by inverse variations in contrast. Targets whose dimensions are greater than 2 mins. become increasingly inefficient visually as they increase in size. Lamar et al. proposed that for large areas, the visually critical region of the target is the ribbon inside its perimeter 1 to 1.5 mins. wide. The above conclusions are very complex, and further indicate the intricate nature of the visual system. Similar conclusions were made by *Fry (1947)* who investigated polygons and circles. Fry's investigations were particularly directed to the borders of the targets. He concluded that the border mechanisms of the visual system were better adapted to long straight borders, than the saw-toothed or wavy borders. There is clearly a connection between the work of Lamar et al. and that of Fry, in respect of the significance of the border region. More discussion on the border mechanisms will be given in section 2.7.

A vast amount of work on detection of both short and long duration targets has been made by Blackwell and his colleagues in a number of articles, e.g. *Blackwell (1946)*, *Blackwell (1953)*, and many more. In an article in 1963, *Blackwell (1963)* put forward a number of neural detection theories. In particular, he proposed that the theory of *Kincaid et al. (1960)* was the most recent and complete available. For the present study, it is unnecessary to expound this theory in detail, though simplified models of the neural system have been included. Several conclusions reached by the authors will be given.

Kincaid et al., derived an "element contribution function" which describes the contribution of each element of an object, to the detection of the object. The general form of the equation is\*as follows:-

The total excitation produced by a target,  $E = \Delta B \int_F \int \phi(r) \cdot r \cdot dr \cdot d\theta$  where  $\Delta B$  is the difference in luminance between the object and its background.

$r \cdot dr \cdot d\theta$  gives the area of each element of the object in polar coordinates, the summation being over  $F$ .

$\phi(r)$  describes the element contribution function which is the relative contribution to  $E$  of each element of the object, at the distance  $r$  from the centre of the object. An example of the approximate form of  $\phi(r)$ , for different luminances, after *Kincaid et al.* (1960, 147) given in figure 2.4, shows the functions using circular targets of different diameters. For the very small targets,  $\phi(r) = 1$  over the whole of the target, and  $E = \Delta B \int \int r dr. d\theta = \Delta B. \text{ area of target.}$

Excitation and therefore detectability for small targets is apparently dependent on the light flux of the target, since the excitation  $E$  must reach a constant value  $E_c$  for successful detection. The relationship between these results, (and they are in fact only preliminary) and pointing type tasks is difficult to assess. For the very small annulus sizes encountered by O'Connor, however, i.e. less than 300  $\mu\text{rad}$ , it is held (*Trinder, 1968*) that the criterion for pointing is luminance discrimination. Although it is impossible to relate the element contribution function of circular targets to circular annuli, it does seem that the discrimination of the flux of light is a mechanism which may be used by the visual system for very small annuli. The relationship of this factor to pointing observations will be developed in Chapter 3.

## 2.7 The Significance of Contour Mechanisms in Vision.

*O'Connor (1967)* emphasises his opinion that contour perception, and the associated mechanisms involved in producing Mach bands, in particular lateral inhibition, are of great importance in acuity results. He considers that the preoccupation with the retinal image should be avoided, and that the influences of the whole visual system should be considered in their true perspective. He further states his impression that visibility of details is not simply a matter of brightness discrimination but also involves the perception of contours. These contours are the narrow regions around the edges of the targets where the eye perceives a sharp change in brightness. Such contours are subjective, as is indicated by the Mach phenomenon described in section 1.41, and will vary in nature depending on the luminance of the target, background density, etc.

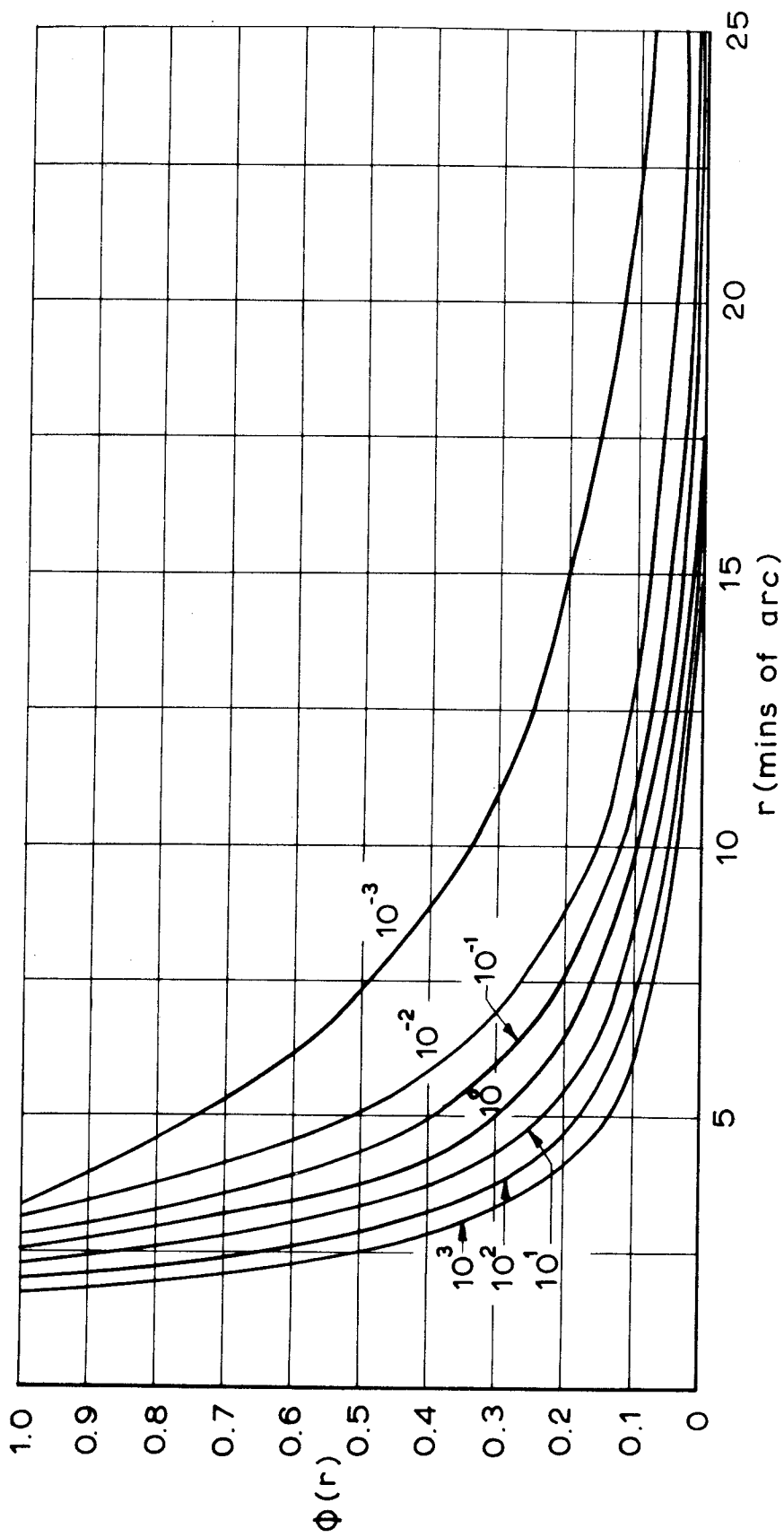


FIG. 2.4: EXPERIMENTALLY DETERMINED ELEMENT CONTRIBUTION FUNCTION FROM KINEAID ET AL., FOR CIRCULAR TARGETS OF DIAMETER  $r$  AGAINST BACKGROUND LUMINANCES INDICATED ON THE INDIVIDUAL CURVES.

O'Connor cites many cases in literature where the Mach phenomenon is observed. Though Mach bands may not be consciously seen in some cases, e.g. sharp targets in O'Connor's experiments, he speculates that the effects may still be present adjacent to the edges, and thereby influence visibility and acuity results. Contour mechanisms and particularly the border areas of targets were also considered important by *Fry (1947)*, in respect of the visibility or detection of targets of various sizes, as indicated in section 2.6.

Contour mechanisms are clearly most significant for the smaller annuli involved in pointing. It is hoped that their influences will be approximated by the SF's which include inhibition effects, given in section 2.5. An indication of their effects should be gained from the convolutions in Chapter 3.

## 2.8 Conclusions.

The information given in this chapter outlines the very complex nature of the visual system. In attempting to derive some explanation for pointing results, it is clear that due consideration must be given to all aspects. The initial explanation for vernier acuity put forward by *Andersen and Weymouth (1923)* included only the influences of eye movements and the image on the retinal mosaic, although some assumptions were made on the neural activity of the foveal cones. This explanation is nevertheless basically correct.

Development of mathematical models to describe inhibition are only in their initial stages. Likewise the development of the Element Contribution Functions by Blackwell and his colleagues is another attempt to include simplified models of the visual system, in this case, for predicting signal detection. Contour sharpening mechanisms undoubtedly play a role in detection type acuity tasks as well as influence vernier acuity tasks. Whether in fact their influence is as important as mentioned in section 2.7 has yet to be proved. It is possible that the influence of such mechanisms will vary according to the visual task,

keeping in mind the likelihood of non-linearity in the neural part of the visual system, and may well be of considerable importance under certain circumstances. This factor however, does not preclude the adoption of simplified linear models which should prove successful in interpreting results of acuity experiments, except those near the threshold of visibility.



### 3. CONVOLUTION OF ANNULUS AND SPREAD FUNCTION OF THE VISUAL SYSTEM.

#### 3.1 Introduction.

The approach of convolving the annulus of the target around the MM and the PSF of the eye was developed by *Trinder (1965)*. The luminance profile of the annulus after convolution was analysed in terms of width and maximum values, to investigate the criteria used by the visual system for pointing. The development of a computer programme to carry out this convolution using a gaussian formula with  $\sigma = 200 \mu\text{rad}$  for the PSF of the visual system, was published by *Trinder (1968)*. The conclusions derived from the subsequent computations were similar in form to those given in *Trinder (1965)* and are similar to those mentioned briefly by *Hempenius (1968, 18)*.

The basis for the development of the computer programme will be repeated as an introduction to this chapter. A summary and discussion of the curves derived by this programme in *Trinder (1968)* will then be given. Following this, the results of further developments using PSF's for the visual system derived in Chapter 2 will be presented in section 3.8 and analysed in a similar manner.

#### 3.2 Convolutions.

When a lens forms an image of a line for instance, with a given intensity profile, the quality of the resulting image will not be as good as that of the object. All imaging systems cause such a loss in quality of the image. This is manifested in an intensity profile of the image, the slopes of which are not as steep as those of the original profile, and maximum intensity probably reduced. When viewing the image of the line, it would be considered as being not as well defined as the object, nor as bright. This process can be formulated as follows: the object intensity profile is affected by the imaging quality of the lens - described by the spread function of the lens - to produce the image intensity profile. The process of combining the object intensity profile and the SF in mathematical terms is called Convolution.

Convolution is described (*Jennison, 1961, 6*) as "the operation whereby a structure under observation is smeared or spread out by the response or resolution of an instrument or mathematical operation." Here, the "structure" is the intensity profile of the object, the "instrument", the lens.

The general formula for the convolution of a two dimensional object and line spread function is:-

$$h(x) = \int_{-\infty}^{+\infty} f(x-z) \cdot g(z) \cdot dz \quad (\text{Jennison, 1961, 47}) \dots\dots\dots(3.1)$$

where  $h(x)$  is the ordinate at point  $x$  after convolution, and  $f(x)$  and  $g(z)$  represent the two functions to be convolved. Each element  $dz$  of the function  $g(z)$ , must be multiplied by the relevant value of  $f(x)$  i.e.  $f(x-z)$ , and the total effects are then added.

Convolution can also be considered as the function  $f(x)$  being scanned mathematically by the function  $g(z)$  (*Hempenius, 1965*), (*Jennison, 1961, 4*), in the same manner as a slit scans the luminance pattern of an object. At each position  $x$  of the scanning function  $g(z)$ , every element of  $g(z)$  is multiplied by the corresponding element of  $f(x)$ . The addition of results after multiplication of corresponding elements, for all coordinates  $z$ , produces the ordinate of  $h(x)$ .

The scanning can be carried out physically as well as mathematically (*Hempenius, 1965, 9*). Figure 3.1 (a) shows the scanning of intensity profiles, with the associated multiplication and addition. Figure 3.1 (b) demonstrates the scanning of a slit in close contact with the luminance pattern. Summation is carried out in this case because the total light passing through the width of the slit is measured at each slit position. Both procedures give identical results.

The physical approach of scanning must be used carefully, because convolution does not only involve addition. Formula (3.1) shows that the relevant values of each function must be multiplied

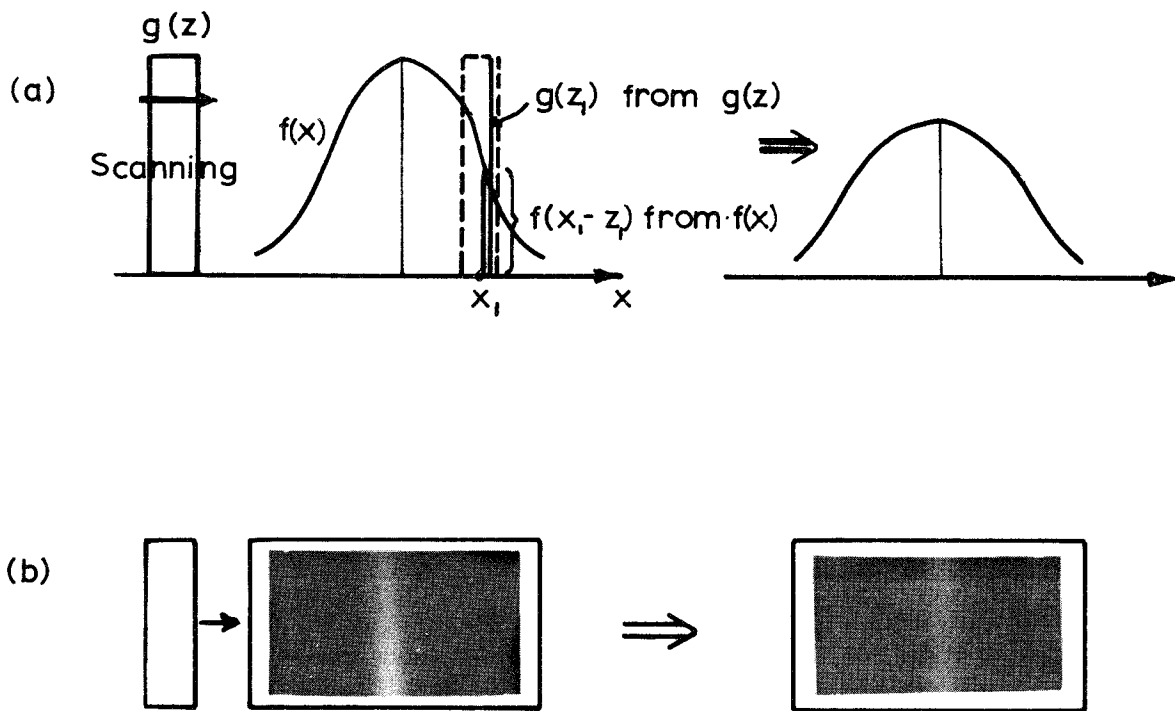


FIG.3.1: CONVOLUTION BY SCANNING

(a) MATHEMATICALLY.

(b) USING LUMINANCE PATTERN AND LIGHT SENSING INSTRUMENT.

before addition is carried out. When one of the functions has a simple intensity profile, as for instance the slit, the multiplication factor of the slit is constant throughout, and therefore is not required if only relative values are needed. If however, the convolution involves two functions similar to  $f(x)$ , the physical scanning must be carried out using a slit of variable transmittance, i.e. a slit with a transmittance profile similar to that of the blurred line. Provided this is done, the convolution will be correct.

One feature that should not be forgotten, is that either function can be used as the scanner. Logically it can be seen from figure 3.1, that the same result must be obtained whether  $g(z)$  or  $f(x)$  is used as the scanning function, (*Hempenius, 1965*) (see also *Trinder, 1965*).

To maintain constant energy before and after convolution, the ordinates  $h(x)$  must be normalized. This is done by dividing  $h(x)$  by the area under the original scanned function  $f(x)$ . In the following discussion, only relative differences are required, and therefore the coordinates have not been normalized.

A number of techniques are available for carrying out convolution in the more complex cases, particularly those which involve the PSF, namely, analogue, graphical and computational methods, (*Trinder, 1965*). Computational methods used in these investigations, based on the scanning concept, will be explained in the following section.

### 3.3 Convolution of the Three-Dimensional PSF and Annulus Profiles. ("PSF method").

Extension of the formula (3.1) to the three-dimensional case gives:-

$$k(x, y) = \int_{-\infty}^{+\infty} \int_{-\infty}^{+\infty} f(x-z, y-w) g(z, w) dz dw \dots\dots\dots (3.2)$$

Mathematical integration of this formula for the functions in hand

proved to be more difficult than the scanning technique adopted, and therefore will not be discussed.

The profiles of annulus and the gaussian PSF are shown in figure 3.2. The intensity profile along the cross-section AA, can be determined by scanning the PSF over AA. At each scanning position of the PSF, the products of the PSF ordinate  $g(x, y)$ , and annulus ordinate  $f(z, w)$  must be computed over the entire annulus. The sum of all products then gives the ordinate for the scanning position on AA.

The annulus was divided into small segments approximately 5 - 10  $\mu$ rad square. Because of the simplicity of  $f(z, w)$ , where the relative ordinate is either 1 or 0, the computation amounted to evaluating the ordinate of the PSF for each small segment, using the distance from scanning point to the segment centre. Summation of these ordinates then gave the required value for each point along AA.

The influence of each element is proportional to its volume, by the law of conservation of energy, i.e. the volume of each element after spreading must equal the volume of the element before spreading. The correct relative influence of each element was therefore obtained by multiplying the evaluated ordinate of the PSF by the volume of the element.

The size of the elements, although finite, proved to be sufficiently small. Investigations were carried out to find a practically sized element. The use of elements approximately 5 - 10  $\mu$ rad square introduced errors of less than 1%, which were acceptably low for these investigations.

In the computer programme, provision was made to introduce small displacements of the MM on the target, along the line AA, so that variations in the intensity profile could be observed as the MM position was varied. Displacements equal to pointing accuracies in curve 1, figure 1.1 were introduced so that just perceptible changes in the luminance profile for varying annulus widths could be determined.

$$g(z,w)=1 \text{ if polar coord } r_1 < r < r_2$$
$$g(z,w)=0 \text{ if polar coord } r_1 > r > r_2$$

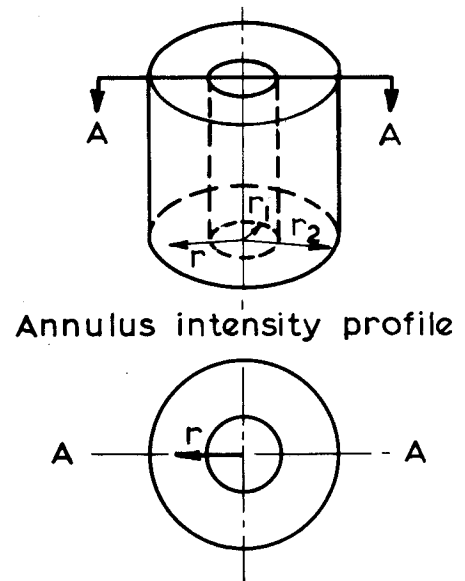
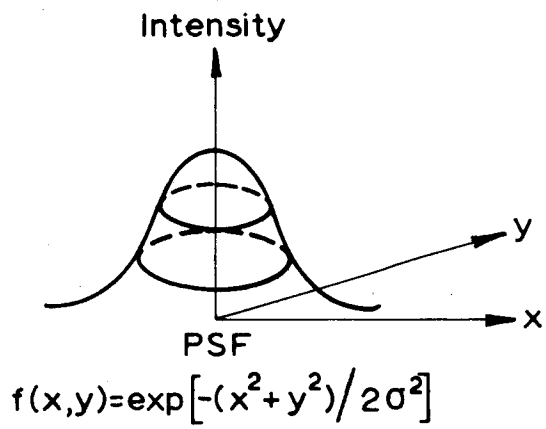
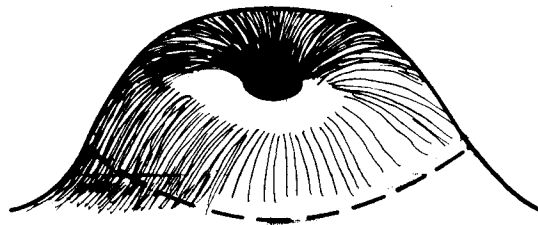


FIG. 3.2: PICTORIAL REPRESENTATION OF PSF,  $f(x,y)$  AND ANNULUS INTENSITY PROFILE  $g(z,w)$  TOGETHER WITH RESULT AFTER CONVOLUTION (AFTER TRINDER, 1965)



Output from the convolution were ordinate values of the convolved curve at intervals of 50  $\mu$ rad along AA. This interval was sufficient for the interpolation of maximum values and widths as mentioned in section 3.4

Convolutions of the targets with background densities of 0.3, 0.9 and 1.2 (*O'Connor, 1967*) were carried out in a similar manner, but the profile had to be divided into two sections, and the effect of one subtracted from the effect of the other (See Appendix D for full details). A similar technique was used by *Gubisch (1967, 412)* to determine the profile of an annulus.

The profile was divided as shown in figure 3.3 The section above the background luminance level was convolved in the usual manner, i.e. as if the annulus had an infinite background density. The MM section below the background level was then convolved. This had a negative effect, that is, an effect which caused a decrease in luminance level. Algebraic addition of the two profiles then gave the profile of the annulus after convolution.

Cross-section profiles obtained by the convolutions have been presented in Appendix D for a number of annulus widths using high, medium and low contrast targets, and MM's sizes as indicated.

In addition to the above convolutions, the more simple convolutions of the LSF and linear elements of different widths were carried out by *Trinder (1968)*, in a similar manner to *Trinder (1965)*. This is particularly applicable to annuli which occur when a MM of 5.1 mrad is used, where annuli tend to be linear over short intervals.

Formula (3.1) was computed for

$$\begin{aligned} f(x) &= \exp \left( -\frac{1}{2} x^2 / \sigma^2 \right) & -\infty < x < +\infty \\ g(z) &= 1 & -c < x < c \\ &= 0 & -c > x > c \end{aligned}$$

where the annulus width was  $2c$ . In *Trinder (1968)*  $\sigma$  equalled 200  $\mu$ rad, while in the original study  $\sigma$  equalled 300  $\mu$ rad.

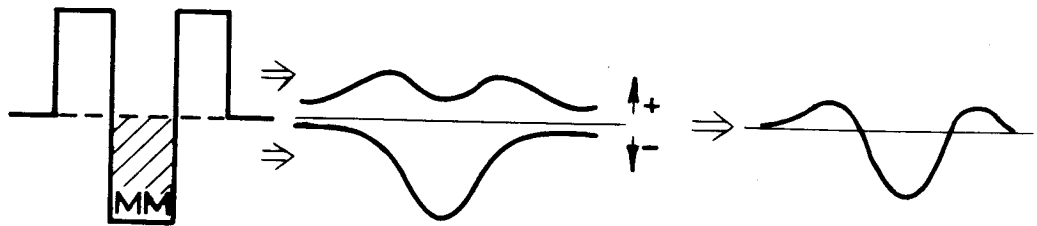


FIG.3.3: DIVISION OF INTENSITY PROFILE INTO 2 SECTIONS EACH OF WHICH WAS CONVOLVED SEPARATELY. ADDITION OF THE TWO PROFILES GAVE THE PROFILE OF THE ANNULUS AFTER CONVOLUTION



Annulus widths were chosen to represent widths when the MM was correctly centered, and when errors in centering of the MM equalled accuracies in curve 1, figure 1.1. The original study (*Trinder, 1965*) analysed the curves derived from formula (3.1) (termed the "LSF method") in terms of maximum values and widths of the profiles. *Trinder (1968)* carried out a similar analysis of the convolved curves derived using the PSF method, in terms of maximum values, widths and also slopes of the profiles. The results of this analysis are presented in the following sections. Values derived by the LSF method with  $\sigma$  equal 200  $\mu$ rad have also been presented purely for comparison.

#### 3.4 Maximum Values of Profiles.

A displacement of the MM on the target (equal to accuracies in curve 1, figure 1.1), causes an increase in the width of the annulus on one side of the MM, and a decrease in the annulus width on the other side. Referred to the images seen by the visual system, the MM displacement will cause an increase in the maximum value of the profile corresponding to the larger annulus width, and a decrease in the maximum value of the profile corresponding to the smaller annulus. The extent to which maximum values increase and decrease depends on the original annulus width as indicated in figure 3.4. Original annulus widths are shown on the abscissa while the percentage differences\* between maximum values of the profiles are shown on the ordinate. From figure 3.4, it can be seen that the relationship is constant at approximately 16 per cent for annulus widths less than approximately 250  $\mu$ rad, but above 250  $\mu$ rad it decreases rapidly and approaches zero as the annulus width approaches 1 mrad.

---

\* The percentage difference between maxima on each side of the MM is computed as the difference between maxima, over the mean of the maximum values of the two profiles.

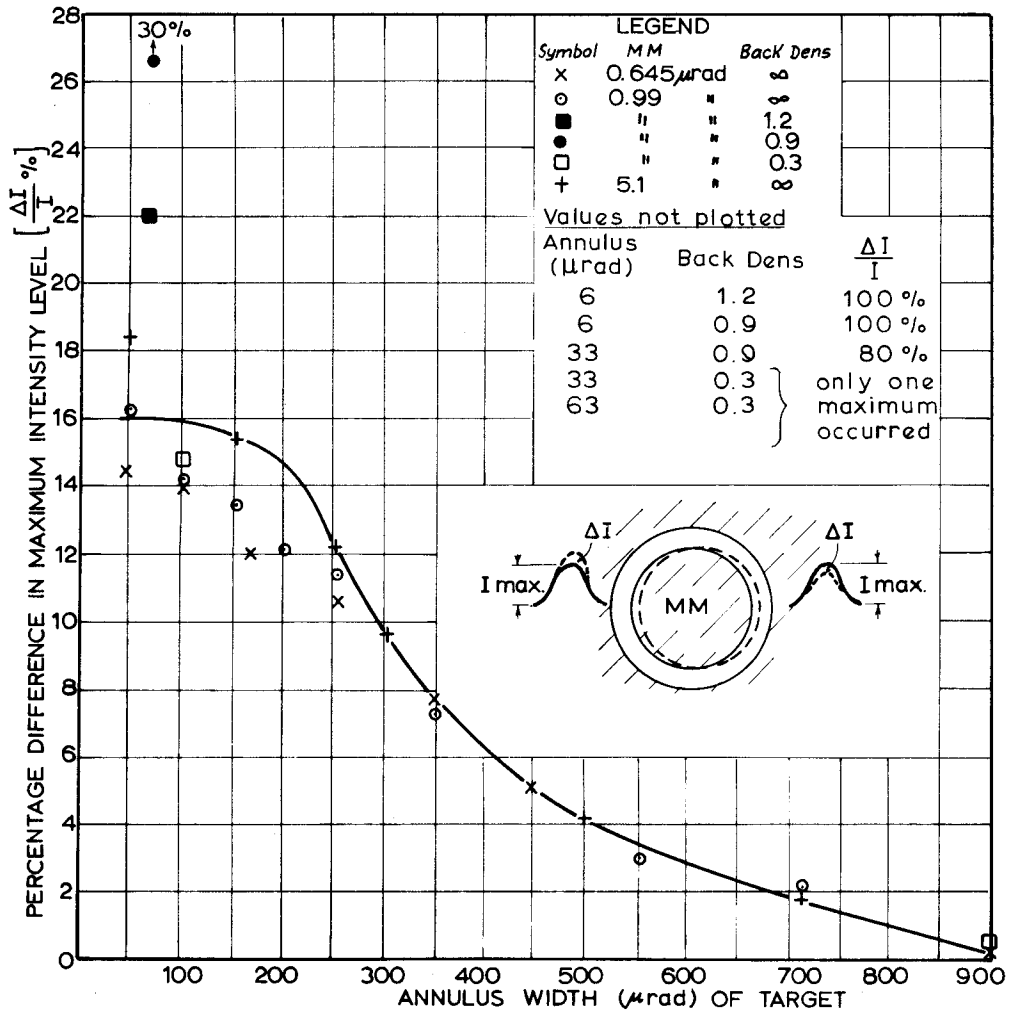


FIG.34:THE RELATION BETWEEN PERCENTAGE CHANGE IN INTENSITIES OF EACH ANNULUS IN THE CONVOLVED PROFILE, AGAINST ANNULUS WIDTH. THE CURVE HAS BEEN COMPUTED BY THE LSF METHOD. THE RESULTS BY THE PSF METHOD HAVE BEEN ADDED ACCORDING TO THE LEGEND.

For the low and medium contrast targets, the results for the very small targets were erratic and did not follow the general relationship. This is apparently because the annuli of these targets approached the threshold of visibility. Values not plotted have been added separately.

### 3.5 Slopes of the Profiles.

Slopes of the intensity profiles were determined from profiles computed by the PSF method. No values were deduced from results computed from the LSF method. The position on the curves at which the slopes were calculated was the straight section on the main slope of the profile, where the rate of change in slope was a minimum. The reason for choosing this section is that if the visual system uses a slope in the intensity profile, it should be one which follows a simple pattern, and is of sufficient length to allow a good comparison of each side of the profile. It is believed that where rapid changes in slope occur on the intensity profile, e.g. near the maximum values of the profile, comparison of slopes by the visual system would be impossible.

Differences in slopes of the profiles when the MM is displaced by amounts equal to pointing accuracies in curve 1, figure 1.1, are presented in figure 3.5, which expresses the percentage change in the slopes of the profile in terms of annulus width. For the larger two measuring marks either side of each annulus profile gave approximately the same result. However, for the smallest MM, the inner flank of the profile was taken, except for annulus widths of 50 and 100  $\mu$ rad. For these two annulus widths the inner slopes are difficult to determine with any degree of accuracy because of their very limited length. In addition, it is felt that their length would be insufficient for accurate discrimination by the visual system. For annulus widths greater than 100  $\mu$ rad, using 0.645 mrad MM, the inner slopes produced higher percentages than the outer slopes, and therefore were included in the graph. When inner slopes were used, the figure has been marked accordingly. The slopes of curves for the low and medium contrast

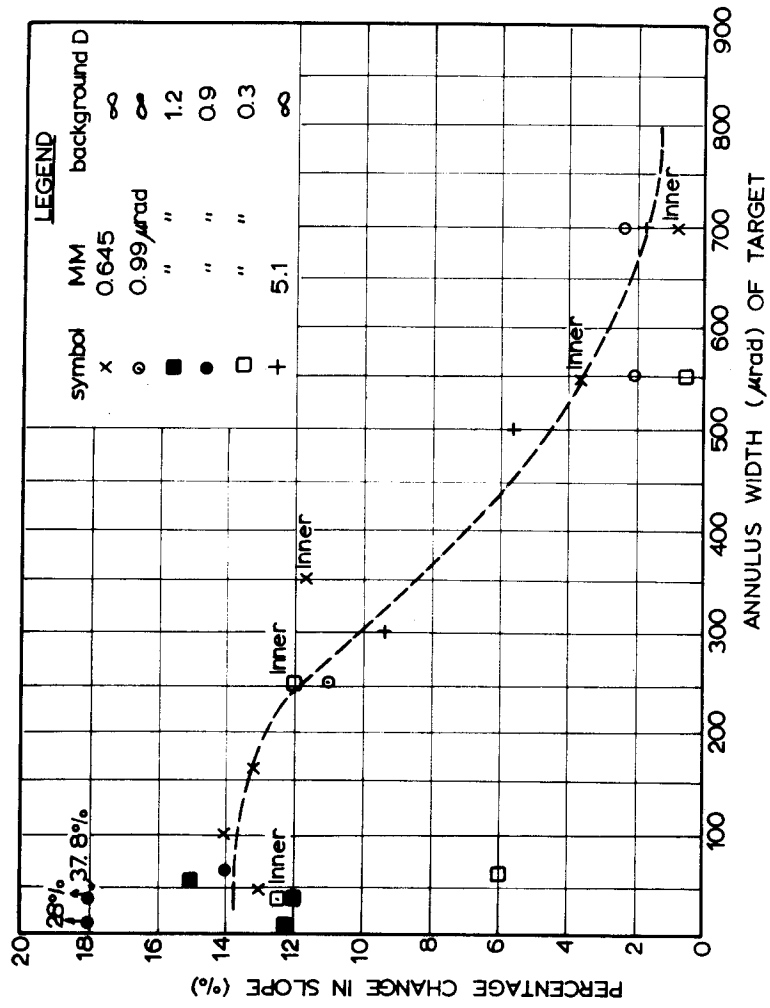


FIG. 3.5: THE RELATION BETWEEN THE VARIATION IN SLOPE OF THE INTENSITY PROFILES DERIVED BY THE PSF METHOD, AND ANNULUS WIDTH COMPUTED FROM POINTING ERRORS IN CURVE 1, FIG. 1.1 (inner refers to the inner slope of the profile)

targets have also been added to figure 3.5

The accuracy of slope determination, which is an average value over the approximately linear section of the curve, is about 1%. Despite slight inaccuracies in slope determinations, however, a general trend in the pattern of the percentage changes in slope is clearly visible in figure 3.5. Except for three values, which do not seem to follow any pattern, maximum values generally are 12 - 16% for the annuli less than 200 - 250  $\mu$ rad, and then gradually decrease, following a pattern similar to that in figure 3.4.

### 3.6 Widths of Luminance Profiles.

The width of the target actually seen by the visual system can only be determined during the observations. Since this has not been done for the data in hand, an estimation of width of the profile derived by the LSF method was made at -

- 1) the 60.6% luminance level, which is the level at which the  $2\sigma$  - width is read on a purely gaussian curve, and
- 2) the point of maximum slope.

Although the latter criterion gave widths at luminance levels of 60.6% for purely gaussian curves, the widths were located at levels gradually decreasing for the non-gaussian curves, and tended towards the 50% level for a purely gaussian integral curve (the edge). (*Trinder, 1965*).

If an error exists in the position of the MM, the annulus width seen by the visual system on one side of the MM will be larger, and on the other, smaller than when the MM is correctly placed. The actual difference in widths of the two annuli is therefore twice the pointing error. Weber's Law which generally states that the ratio of

$\frac{\text{just noticeable stimulus}}{\text{total stimulus}}$  is a constant, when related to the pointing task is as follows:-  $\frac{\text{pointing accuracy}}{\text{annulus width}}$  is a constant (*O'Connor, 1962*).

In terms of the visual image, this law may be expressed as:-

$$\frac{\text{total difference in annulus widths seen by the visual system}}{\text{sum of widths of annuli seen by the visual system on each side of MM}}$$
 is constant. The total difference in profile widths determined by the standard deviations of observations, represents the minimum visible difference in annuli seen by the visual system. The above formula may therefore be expressed as:-

$$\frac{\text{half the minimum visible difference in annulus width}}{\text{mean of annulus widths on each side of the MM}}$$
,  
the annulus widths being those seen in the visual image.

Figure 3.62 shows curves representing this ratio for the two width criteria, based on the LSF method. The ordinate scale is half the minimum visible difference in annulus width in the visual system computed in the convolution, using pointing accuracies in curve 1, figure 1.1 as displacements of the MM. On the abscissa is plotted the annulus width of the target seen by the visual system. The 1% - 2% limits representing the approximate range of Weber's Law for localization tasks in visual acuity, are also shown.

The differences in widths of the profiles determined by the PSF method, using displacements of the MM equal to accuracies in curve 1, figure 1.1, have been added to figure 3.62 for a number of target annulus widths, measured at the 60.6% intensity level only. The actual point at which the maximum slope occurs on each profile is unknown. Because of the curved nature of the annulus for small MM's, the point of maximum slope will not be at the same level on profiles determined by the PSF method, as on profiles derived by the LSF method.

Widths were interpolated linearly from the computed profile. Though this represents an approximation, no significant errors were introduced because the section of the curve at the 60.6% level is approximately linear. In addition, the good agreement obtained between the LSF method and the PSF method in figures 3.61 and 3.62 for a MM of 5.1 mrad, is further proof of this point. For the 0.99 mrad MM, the widths of the profiles were very close to those for the

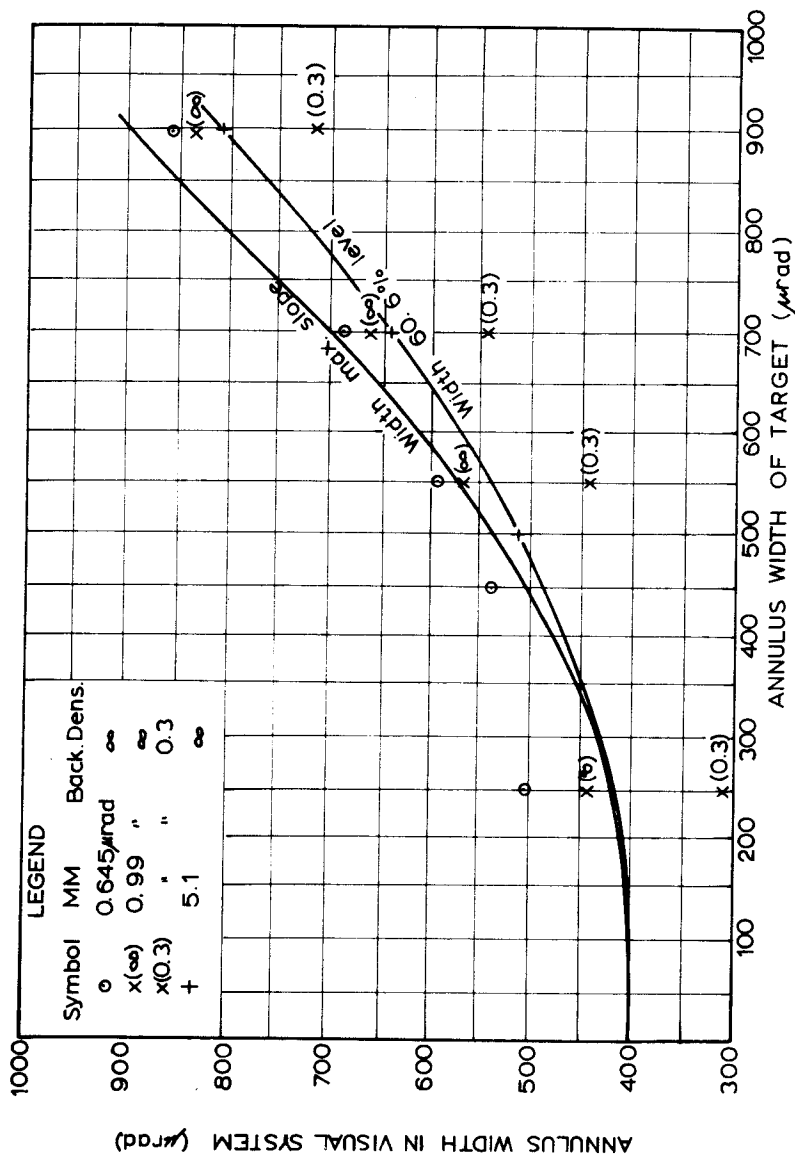


FIG 3.6: RELATIONSHIP BETWEEN WIDTH IN OBJECT SPACE, AND WIDTH AS SEEN BY THE VISUAL, USING THE TWO CRITERIA FOR WIDTH, FOR CURVES DERIVED BY THE LSF METHOD. WIDTHS OF PROFILES AT 60.6% LEVEL, DETERMINED BY THE PSF METHOD HAVE BEEN ADDED, ACCORDING TO THE ABOVE LEGEND.

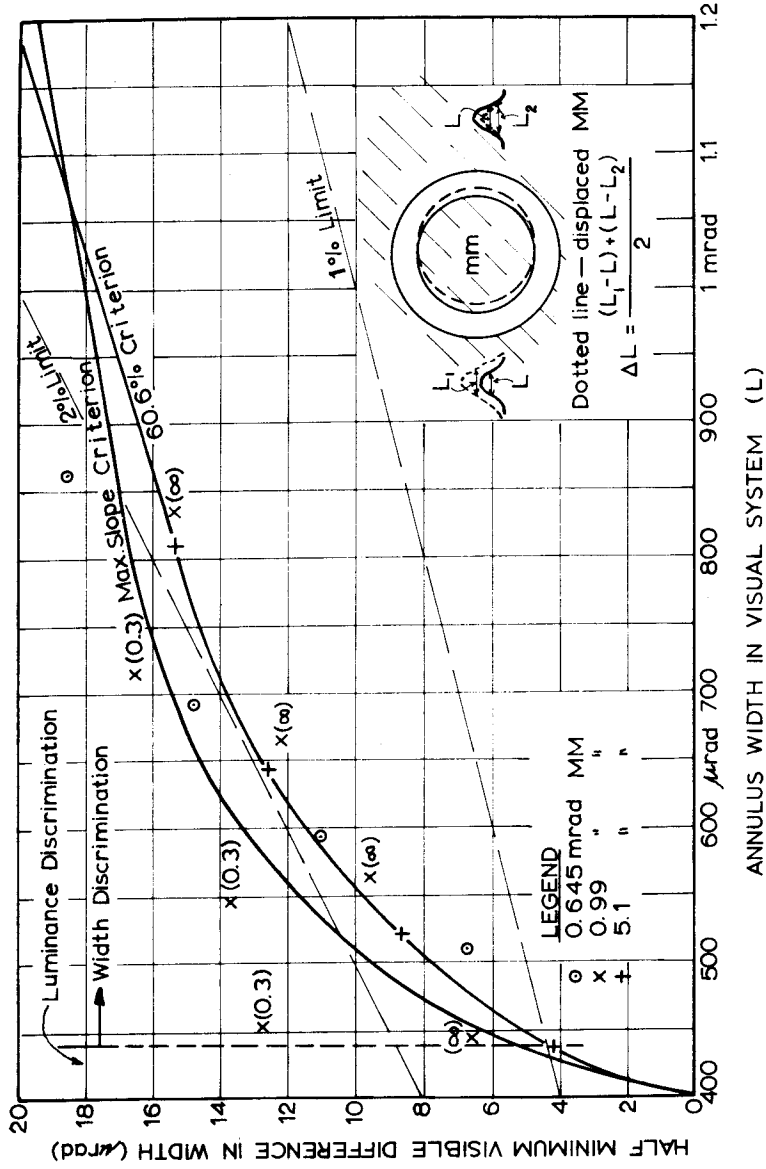


FIG.3.62:THE RELATION, FOR IMAGE IN THE VISUAL SYSTEM, BETWEEN ANNULUS WIDTH L AND HALF THE MINIMUM VISIBLE DIFFERENCE IN ANNULUS WIDTH ΔL, DERIVED FROM POINTING ERRORS IN FIG.1. THE COMPUTATIONS BY THE LSF METHOD GAVE THE TWO CURVES AS MARKED. COMPUTATIONS BASED ON THE PSF METHOD HAVE BEEN ADDED AND ANNOTATED ACCORDING TO THE LEGEND.



5.1 mrad MM in figure 3.61. Widths determined for the .645 mrad MM agreed with those obtained for the other two MM's, for larger annuli, but differed considerably for annuli less than approximately 400  $\mu$ rad. This is mainly due to the tendency for the profiles of the small annuli to overlap.

Widths of the profiles of low contrast targets were less than those of high contrast targets. For instance, at 450  $\mu$ rad, the width of the profile is only 400  $\mu$ rad, and for smaller annuli, the width approaches zero, i.e. no maxima occur. The ratio of half the minimum visible difference in annulus width/width in visual system for low contrast targets, ranges from 2.3% (derived from an annulus of 900  $\mu$ rad) to 5.5% (derived from 250  $\mu$ rad annulus - not plotted in figure 3.62) and approaches infinity as annulus width approaches zero.

In general, the results in figure 3.62 obtained for the LSF method agree well with those obtained by the PSF method for all MM's, for the high and low contrast targets. The conclusions reached based on figures 3.4 to 3.62 are listed in the next section.

### 3.7 Initial Conclusions.

The following conclusions based on the PSF method computations with  $\sigma$  equal 200  $\mu$ rad, are generally in agreement with conclusions made in the original investigation (*Trinder, 1965*).

1. The approach of determining the shape of annulus in the visual system proved successful in explaining pointing accuracies to small targets.
2. Parallel to the findings of O'Connor that MM is of secondary importance in determining pointing accuracies, the shape of the luminance profile is only of minor importance, while the *effect on the profile* of small movements of the MM is the most important factor in determining pointing accuracies.
3. Differences in widths of annuli on opposite sides of the MM for both high and low contrast targets, are visible if they

exceed approximately 1 - 2% of the sum of annulus widths, provided these widths are measured in the visual image. This applies to annulus widths greater than approximately half the  $2\sigma$  - width of the spread function of the visual system.

4. Pointing to targets with annulus widths less than approximately half the  $2\sigma$  - width of the spread function of the visual system, is based on discrimination of slopes and maximum values of the luminance profile. For the experiments described, the minimum visible differences in slopes of approximately 12 - 16% and in maximum values of 14 - 16% resulted in pointing accuracies of approximately 8% of the annulus width, measured on the target.
5. Pointing criteria as outlined in 3 and 4 above depend on the observation conditions, and therefore may vary for different experiments.

Extension of these investigations to include the PSF's derived in Chapter 2 will now follow.

### 3.8 Further Computations Involving Different Spread Functions for the Visual System.

In prescribing a SF for the visual system, *Trinder (1968)* adopted an average value to describe the excitation caused by a point object, but the inhibitory effects were ignored. *Hempenius (1968, 5)* quotes the  $\sigma$  of the gaussian PSF of the optical media of the visual system to be 150  $\mu$ rad and the LSF, 200  $\mu$ rad. In figure 2.2 two SF's which are simplified models of the PSF for the whole visual system, and include estimates of the inhibitory effects are given. The  $\frac{\sin x}{x}$  function (commonly termed "sinc" function) was proposed by *Ratliff (1965)* while the other is the LSF derived by *(Patel, 1966)*. The actual PSF similar to the Patel function which will be used for the convolution, is shown in figure 2.3. For this function, inhibitory effects terminate at 1.4 mrad, instead of 2.4 mrad as shown in the Patel function in figure 2.2. The reason for this is that inhibitory effects extending to 2.4 mrad tend to swamp the excitation associated with large annuli. A SF similar to that of Patel has been adopted to investigate

the influences of functions with larger inhibition areas than those prescribed in the sinc function. Keeping in mind the additional fact that Patel's function is a LSF rather than a PSF, it is considered that the function given in figure 2.3 is satisfactory for this purpose. (In the following discussion, this function will be referred to as the "Patel function") It must be remembered that investigations with functions which include estimates of inhibition are only of an exploratory nature, particularly because of the many unknown factors involved and the somewhat dubious assumptions on the linearity of the visual system.

A fifth degree orthogonal polynomial was computed to represent the Patel function, after *Hildebrand (1956, 288)* as follows:-

$$f(t) = - 0.136916 - 0.021389 t + 0.017335 t^2 + 0.002183 t^3 \\ - 0.000085 t^4 + 0.000045 t^5 \text{ where } t = (x - 700)/100, \\ \text{and 'x' is the distance from the centre of the} \\ \text{function in } \mu\text{rad.}$$

In addition to the Patel and sinc functions, gaussian functions with  $\sigma$ 's equal to 150  $\mu$ rad and 250  $\mu$ rad were also used in the convolutions, to investigate the influences of different gaussian functions.

The results for a MM of 0.99 mrad and high contrast targets only, were computed for the additional convolutions. Since the same conclusions could be applied for all MM's as shown in figures 3.4 to 3.62, it was considered sufficient to compute the further convolutions for one MM only. In respect of the low and medium contrasts, no convolutions have been carried out because the SF's which include inhibition may behave differently for targets of different background densities. The possibility of this fact is indicated in the descriptions of the Mach phenomenon in section 1.41.

On the convolved profiles, widths have been determined at intensity levels of 20% to 60% of the maximum value of each profile in steps of

10% above the background. This has been done to overcome the difficulties encountered in section 3.6, in determining the level on the luminance profile at which the widths should be measured. Experiments described in Chapter 5 indicate that different observers perceive the width of the annulus at different intensity levels. The investigation of widths at a number of levels was therefore considered as the best approach. Widths of the profiles have been determined graphically from the plotted profile. The accuracy of these determinations was 1 - 2  $\mu$ rad for the small annuli, and 5  $\mu$ rad for the large annuli. Slopes of the profiles have been determined over the straight section of the profile. For many profiles these slope determinations are an estimate only, since the flanks of the profiles tend to be curved rather than straight. The results presented in the following, nevertheless, give a good guide as to the shape and size of the profiles. Examples of the profiles may be found in Appendix D.

### 3.9 Shape of Convolved Curves.

Figures D6 to D9 represent profiles for the gaussian SF's with  $\sigma$ 's of 150  $\mu$ rad and 250  $\mu$ rad, the sinc function and the Patel function. These profiles are for a MM of 0.99 mrad as used by *O'Connor (1967)*, and high contrast annuli of 50, 250 and 900  $\mu$ rad. With regard to shape for the three gaussian functions, the profiles are very similar, except that the intensity of the central area of the MM increases as the size of the SF increases. This is particularly noticeable for the small annuli, where the MM becomes almost obscured for the gaussian SF with  $\sigma = 250 \mu$ rad.

In the sinc function results, the inhibitory effects are significant for the smaller annuli but show no effects on the more irregular profile of the largest annulus width of 900  $\mu$ rad. As the annulus width increases further, the profile would presumably take on a pattern similar to a step function with perhaps some influences of the inhibition effects superimposed. It is noticed, however, that the pattern for annulus

widths of 900  $\mu$ rad and presumably larger, show no negative values. This may be due to inaccuracies in the estimation of the PSF, but it nevertheless does agree with observations by *Lowry and DePalma (1961, 742)* that Mach bands apparently do not occur at sharp changes in luminance.

The Patel function has the reverse effect to the sinc function. In this case the inhibition effects are apparent for the small annuli, but become far more significant for the larger annuli, and in fact tend to overwhelm the excitation associated with the 900  $\mu$ rad annulus. Indeed for the larger annuli, the inhibitory effects seem also to introduce a lower artificial background. Movement of the MM from its central position equal to accuracies in curve 1, figure 1.1, has a much more significant effect with the Patel function than with the other functions. This effect is so great on very small annuli, that it becomes ineffectual estimating the profile widths. Differences in slopes and maximum values for the Patel function computations have been derived in the same manner as for the other functions. However, because of the strong artificial background introduced by this function, widths have been estimated at levels referred to the artificial background instead of the true background. Though this technique introduced an unreal estimate of the true widths, it allowed a better comparison between the widths of the profiles on each side of the MM. Since percentage differences in widths only are computed, this technique is considered satisfactory.

### 3.10 Maximum Values and Slopes.

Differences between maximum values and slopes of the profiles on each side of the MM derived from the convolutions using the five SF's, are presented in figures 3.71 to 3.73.\* In all cases, the slope computations refer to the outer flanks of the profiles. The differences in maxima and slopes of the profiles have been presented as percentage differences referred to the mean of values of the two profiles.

---

\* The results of convolutions with  $\sigma$  equal to 200  $\mu$ rad have been repeated, to give a better comparison between the different PSF's.

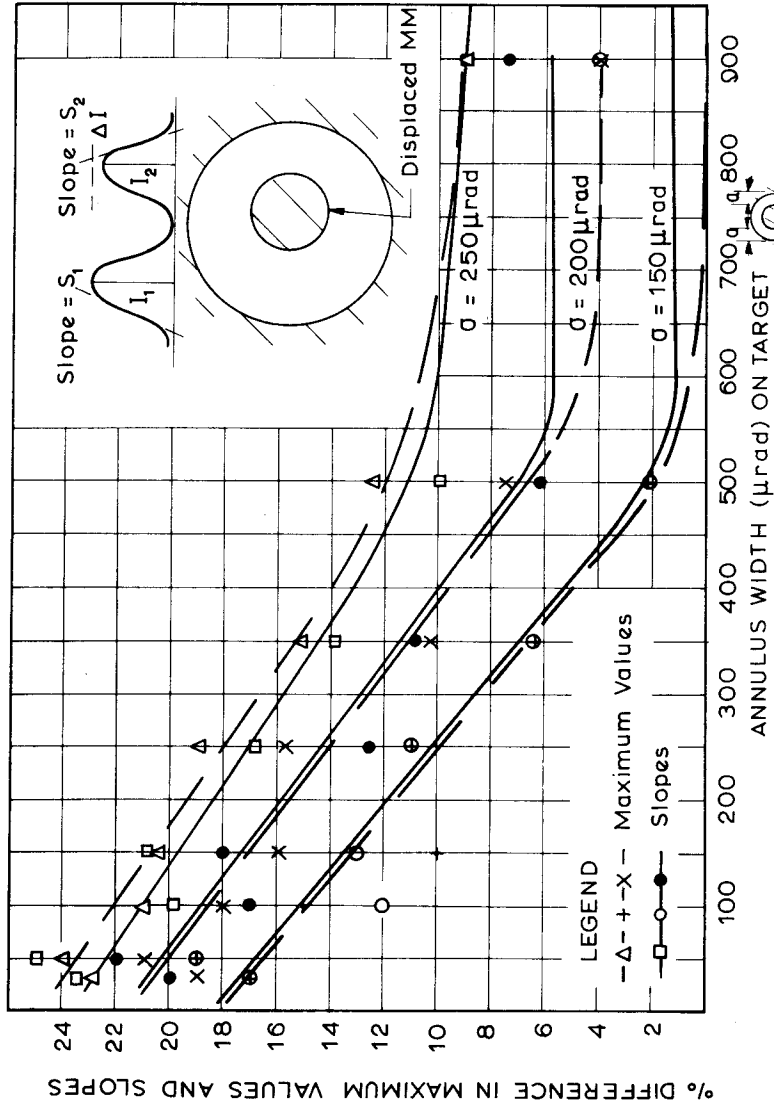


FIG. 3.71: Percentage differences in maximum values and slopes, caused by displacement of the MM equal to curve 1, fig. 1.1 for profiles derived using gaussian PSFS with  $\sigma = 150 \mu\text{rad}$ ,  $200 \mu\text{rad}$  and  $250 \mu\text{rad}$ . Curves for P.S.F.S with  $\sigma$  equal to  $200 \mu\text{rad}$  and  $250 \mu\text{rad}$  have been raised 4 units and 8 units respectively. Values on the ordinate are computed from  $\Delta I / \frac{1}{2} (I_1 + I_2)$  and  $(S_1 - S_2) / \frac{1}{2} (S_1 + S_2)$  for maximum values and slopes respectively.

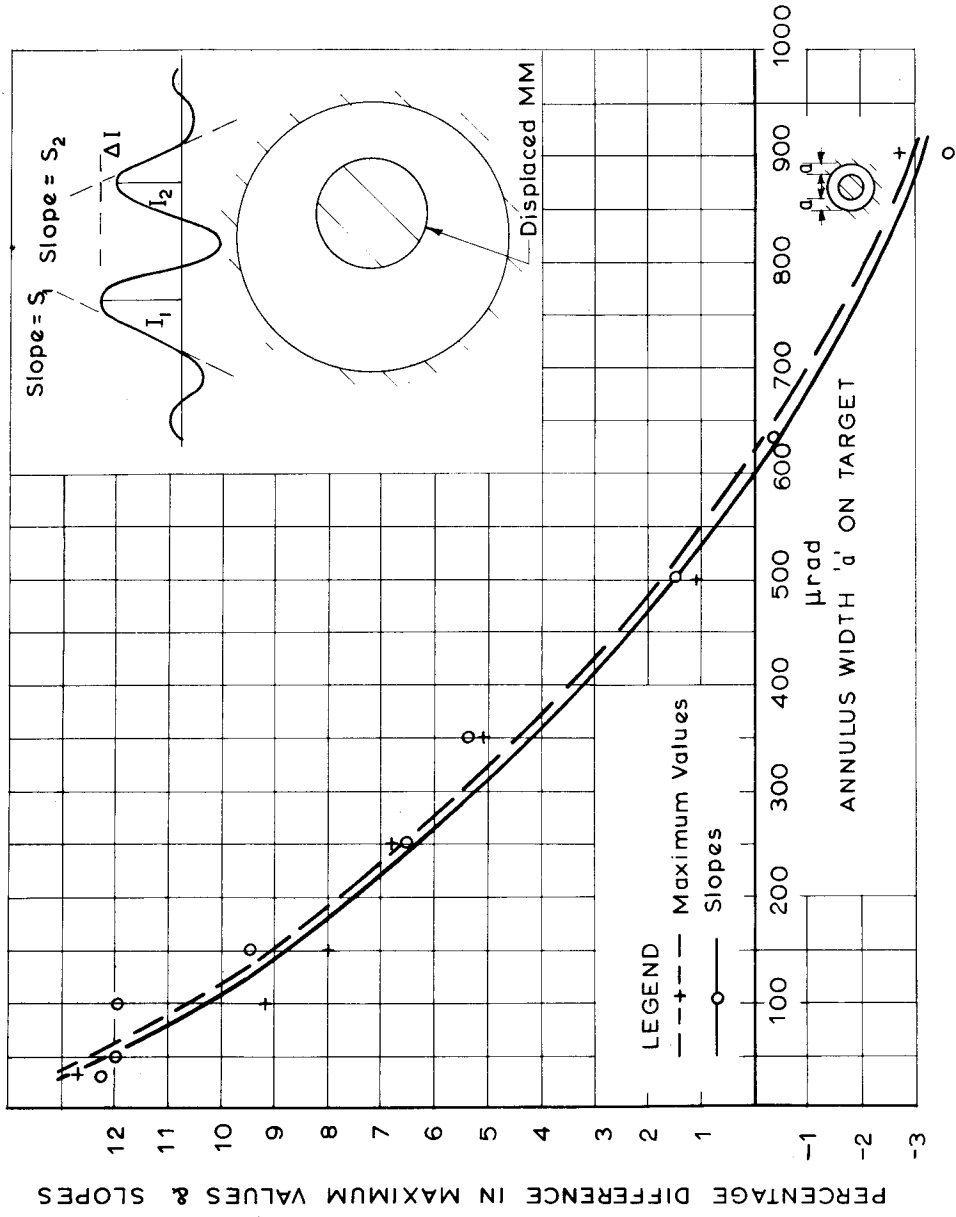


FIG. 3.72: Percentage differences in maximum values and slopes, caused by displacements of MM equal to curve I, fig 1.1, for profiles derived using the Sinc PSF in fig. 2.2. Values on the ordinate are computed from  $\Delta I / \frac{1}{2}(I_1 + I_2)$  and  $(S_1 - S_2) / \frac{1}{2}(S_1 + S_2)$  for maximum values and slopes respectively.

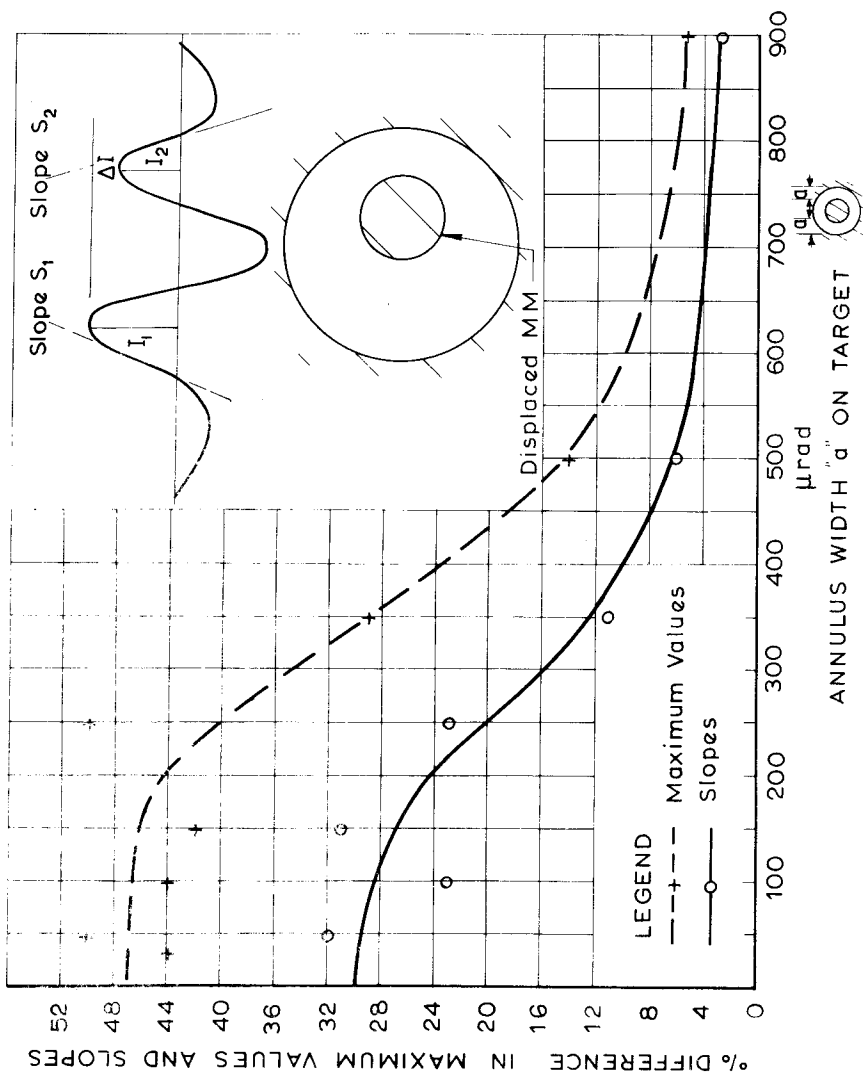


FIG. 3.73: Percentage differences in maximum values and slopes, caused by displacements of MM equal to curve I, fig. 1.1, for profiles derived using the Patel function in fig. 2.3. Values on the ordinate are computed from  $\Delta I / \frac{1}{2}(I_1 + I_2)$  and  $(S_1 - S_2) / \frac{1}{2}(S_1 + S_2)$  for maximum values and slopes respectively.



The pattern of results for the three gaussian SF's are almost identical. When comparing figure 3.71 with figures 3.4 and 3.5 of the previous study (*Trinder, 1968*), it is noticed that the curves do not remain at a constant value for annulus widths less than 250  $\mu$ rad. This tendency was not evident previously because only one SF was used. Apart from this factor, the curves behave in a similar manner to those in figures 3.4 and 3.5. Small variations in the results are caused firstly by small inaccuracies in the computational techniques, and secondly by experimental variations in the pointing results determined by *O'Connor (1967)*.

Maxima and slope differences for the sinc function follow a similar pattern to those of the gaussian functions. They are smaller for the small annuli, and become negative for annulus widths greater than approximately 500  $\mu$ rad. These negative values seem to be temporary, and it appears that the curves would return to zero for larger annulus widths. Annulus widths of 900  $\mu$ rad and less are the main object of investigation in these convolutions, since for these annulus widths, pointing accuracies apparently deviated significantly from Weber's Law, in figure 1.1

The Patel function gives a slightly different pattern of results for small annuli, but a similar pattern for larger annuli. For annuli less than 200  $\mu$ rad, the curves for the differences in slope and maxima are at a constant value of approximately 30% and 50% respectively. These values are considerably larger than the corresponding values derived for the other SF's.

Despite small variations between the figures 3.71 to 3.73, and figures 3.4 and 3.5, however, the patterns for differences in slopes and maxima of the profiles are similar to those derived previously (*Trinder, 1968*).

### 3.11 Widths of the Profiles.

The widths at five intensity levels on profiles, derived using the three gaussian functions, have been plotted in figures 3.81 to 3.83. For the larger SF's, some of the widths cannot be determined because of the high intensity values at the MM. Generally, widths of the sections of the profile on each side of the MM for annuli less than 250  $\mu$ rad approach a constant value which depends on the SF and the height at which the profile is measured.

Widths computed on profiles derived using the sinc function are shown in figure 3.84. This figure shows a sharp drop in profile widths for annulus widths from 900  $\mu$ rad to 500  $\mu$ rad and a gradual decrease thereafter. No constant value was reached, as obtained with the gaussian functions.

Difficulties encountered with the Patel function were mentioned previously. Since the widths of the profiles are taken at levels above an arbitrarily chosen background level, they have not been presented.

A full list of the percentage differences in profile widths measured at the five intensity levels above background is shown in table 3.1. The means of the five values for each SF are plotted in figure 3.9, against annulus width on the target.

The pattern of percentage differences in width is generally the same as in figure 3.62. For annulus widths less than approximately 250  $\mu$ rad, the percentage differences are less than 1%, while above 250  $\mu$ rad they are generally approximately 1 - 2%. The sinc function gives values marginally less than 1% for two annulus widths greater than 300  $\mu$ rad, and shows values greater than 1% for annulus widths of 33 and 50  $\mu$ rad. However, widths were difficult to determine on profiles for those annuli, since the profiles were so small. Results derived using the gaussian SF's generally agree with the relationship determined previously, except for the SF with  $\sigma = 250$   $\mu$ rad which shows erratic

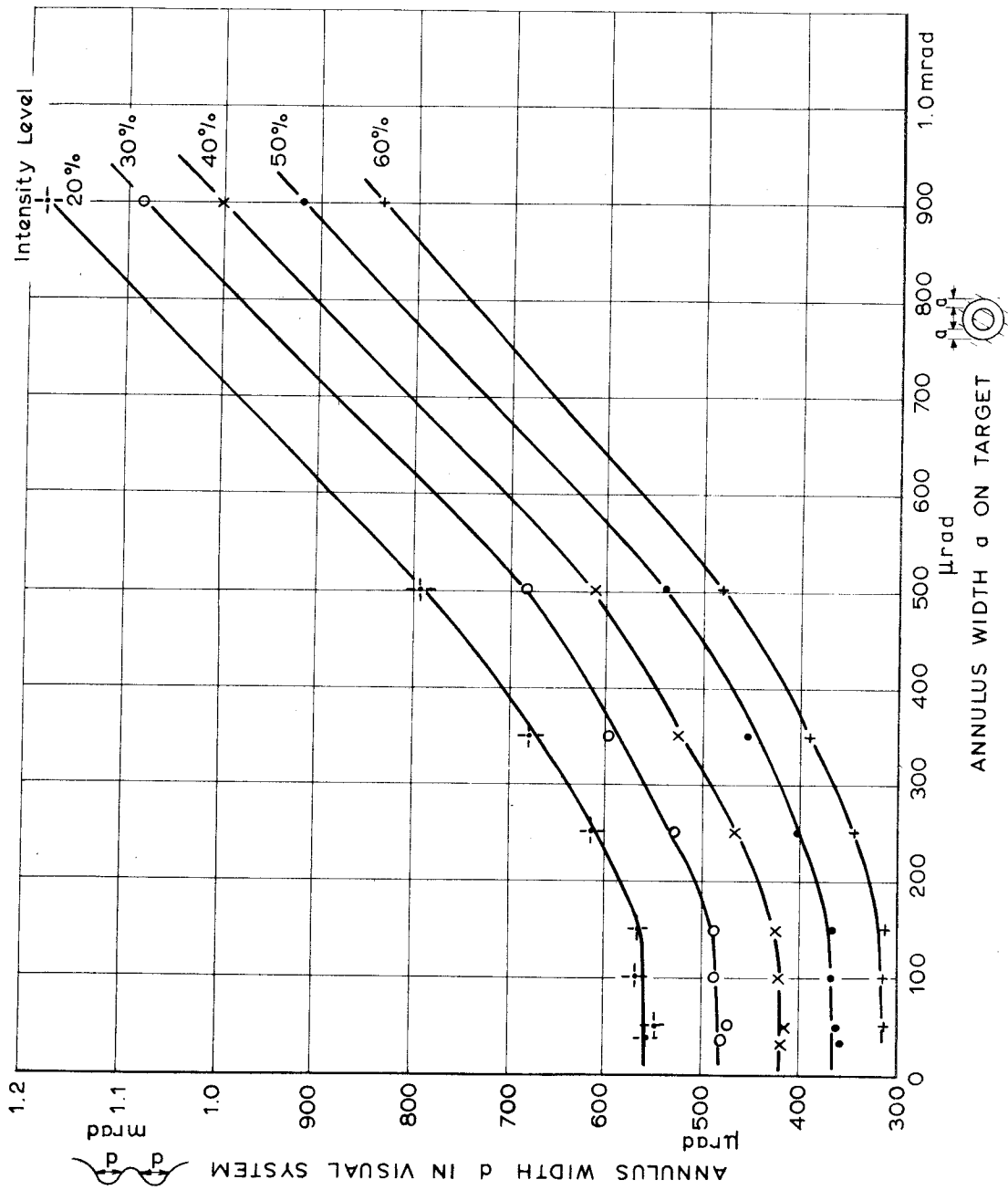


FIG.3.81: Relationship between width of annulus  $d$  seen by the visual system, at five levels on the intensity profile, and the width of annulus  $a$  on the target. The P.S.F. used for the convolution is the gaussian function with  $\sigma = 150 \mu\text{rad}$ . The MM is centrally located.

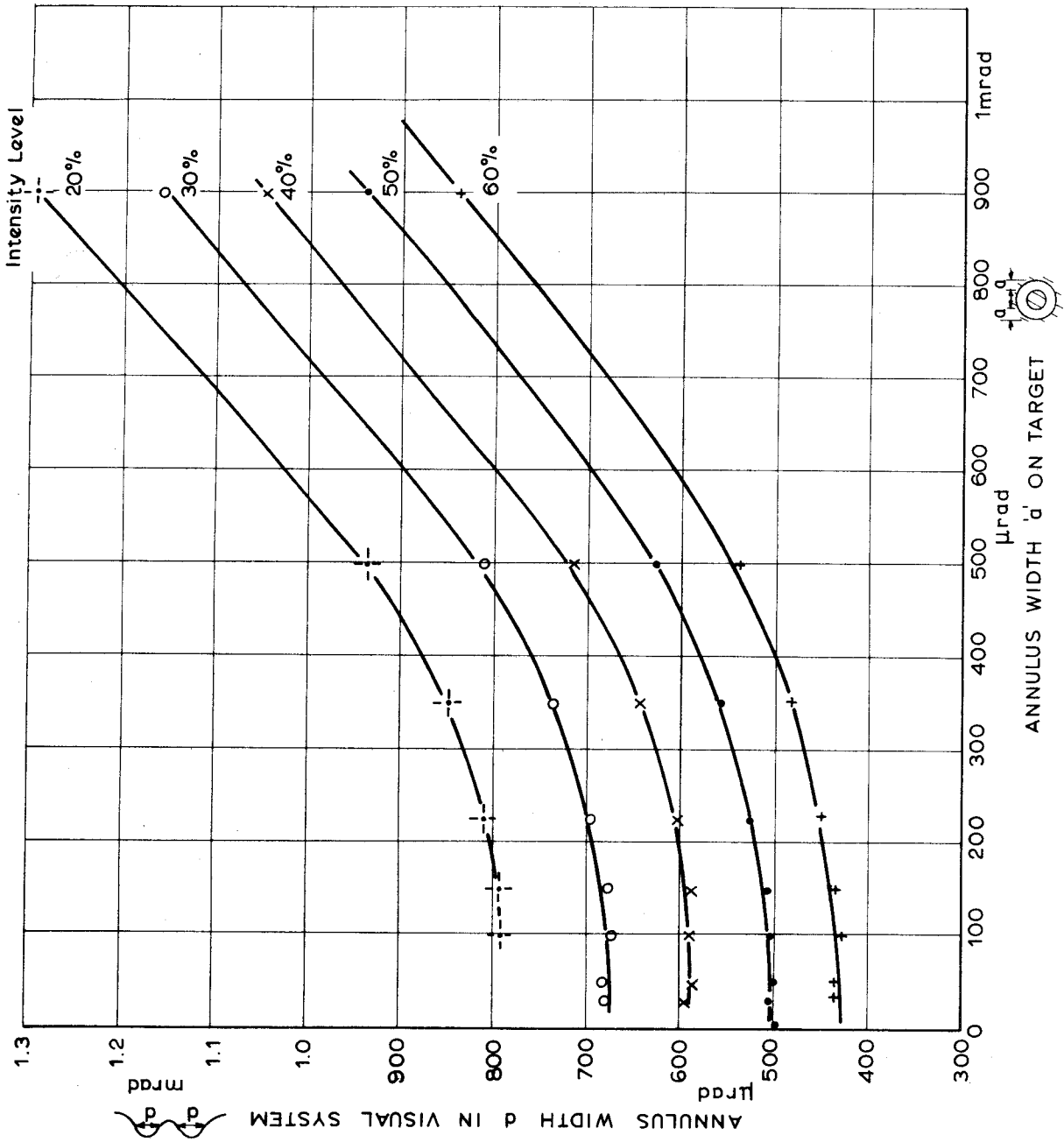


FIG. 3.82: Relationship between width of annulus  $d$  seen by the visual system, at five levels on the intensity profile, and the width of annulus  $a$  on the target. The P.S.F. used for the convolution is the gaussian function with  $\sigma = 200 \mu\text{rad}$ . The MM is centrally located.

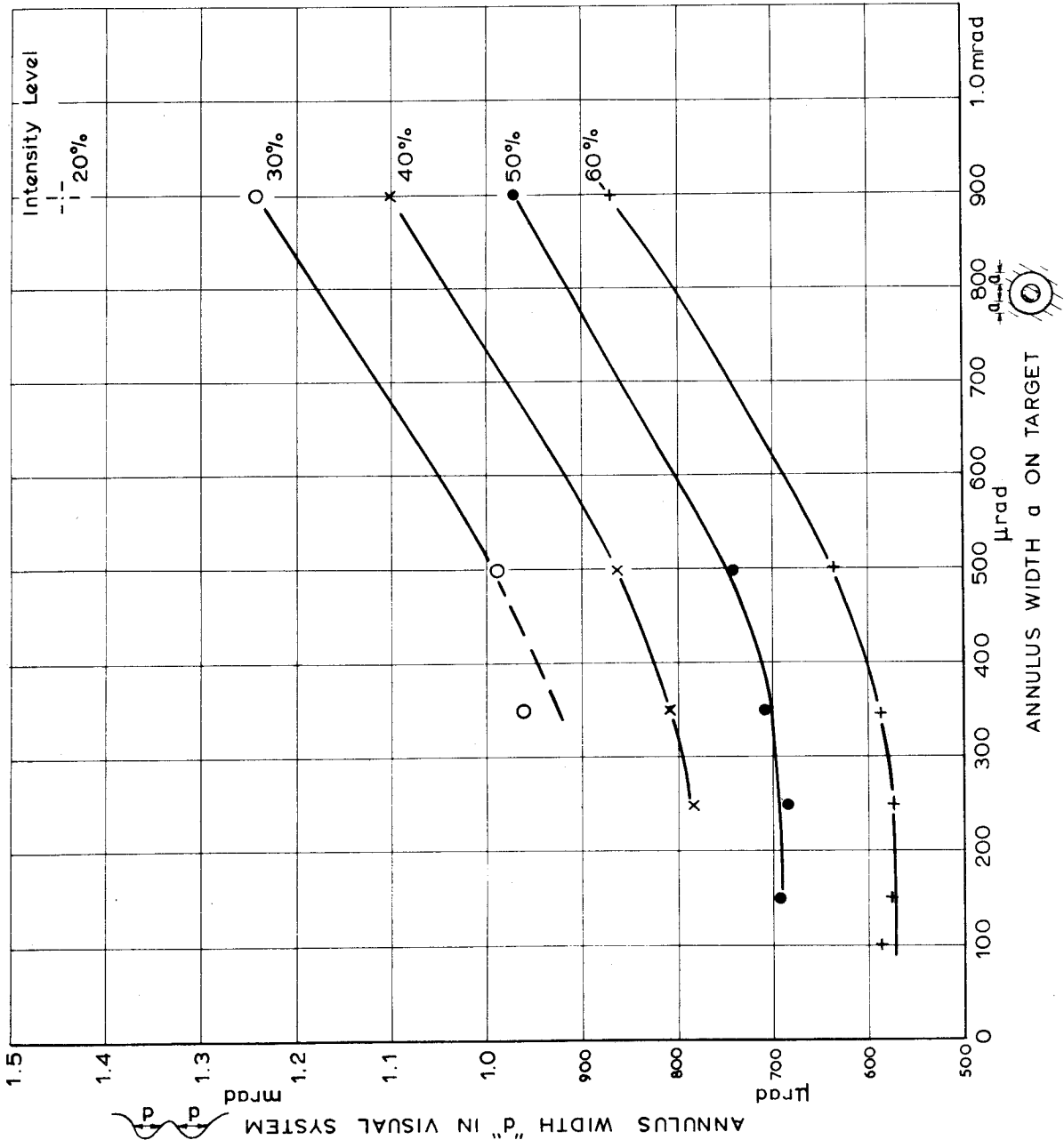


FIG. 3.83: Relationship between width of annulus "d" seen by the visual system, at five levels on the intensity profile, and the width of annulus a on the target. The P.S.F. used for the convolution is the gaussian function with  $\sigma = 250 \mu\text{rad}$ . The MM is centrally located.

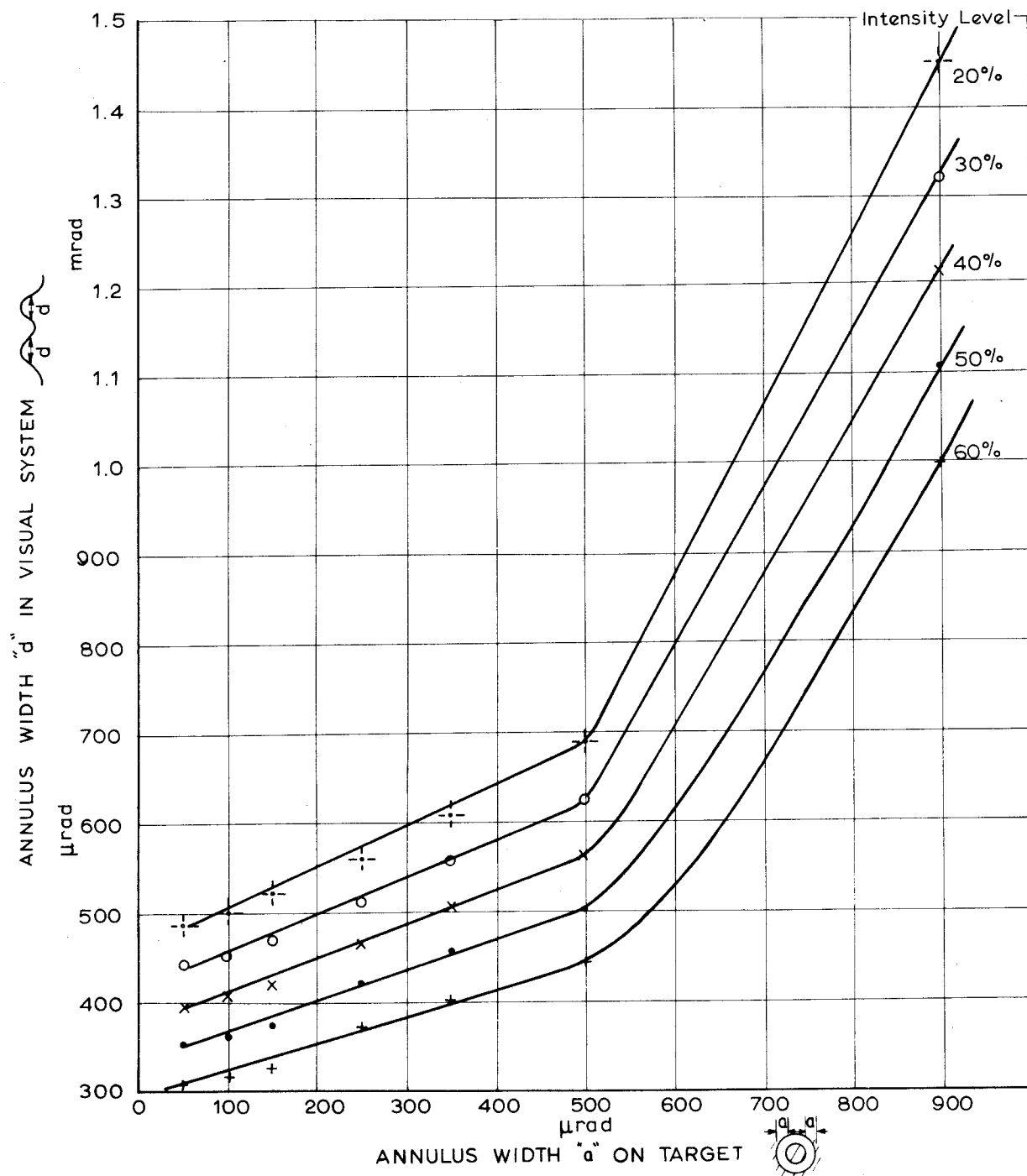


FIG. 3.84: Relationship between width of annulus  $\hat{d}$  seen by the visual system, at five intensity levels on the profile and the width of annulus "a" on the target. The P.S.F. used for the convolution is the sinc function. The MM is centrally located.

Table 3.1

Percentage differences in widths at five intensity levels, on profiles derived using five PSF's.

Annulus Widths on target Intensity Level % $\mu\text{rad}$	33	50	100	150	250	350	500	900
Gauss function, $\sigma = 150 \mu\text{rad}$								
60	0	0.6	0.3	1.6	1.1	1.9	3.0	2.0
50	0	0.6	0.6	0.3	1.6	2.1	1.4	1.7
40	0	0.3	-1.0	1.0	1.9	2.3	1.1	1.5
30	0	0.3	0.6	0.7	1.1	2.1	2.0	1.7
20	0	1.0	0	0.7	1.3	1.7	1.6	1.7
Mean	0	0.6	0.3	0.9	1.4	2.0	1.8	1.7
Gauss function, $\sigma = 200 \mu\text{rad}$								
60	0	0.2	0.3	0.3	0.6	2.3	1.9	2.1
50	0	0.2	0.9	0	0.6	1.2	1.7	1.6
40	0	0.2	0.2	0	0.8	1.0	1.7	1.2
30	0	0.3	0.6	0.4	0.4	1.5	2.6	0.8
20	-	-	-0.6	0.4	-0.7	1.8	2.3	1.5
Mean	0	0.2	0.3	0.2	0.3	1.6	2.0	1.4
Gauss function, $\sigma = 250 \mu\text{rad}$								
60	-	-	1.2	-1.5	-1.7	0.9	0.5	1.9
50	-	-	-	-1.9	-1.0	3.6	1.0	2.3
40	-	-	-	-	2.0	3.2	0.9	0
30	-	-	-	-	-	3.0	1.6	0
20	-	-	-	-	-	-	-	1.1
Mean	-	-	1.2	-1.7	-0.2	2.6	1.0	1.1
Sinc function								
60	1.4	2.2	0.9	0.9	1.6	0.5	1.0	2.8
40	1.5	3.0	0.7	1.0	1.1	0.5	0.7	2.3
40	1.1	2.8	0.5	0.9	1.2	1.2	0.9	1.2
30	1.1	2.3	0.3	0.9	0.5	1.1	0.7	1.2
20	1.4	1.8	0.8	0.9	0.5	0.8	0.6	1.0
Mean	1.5	2.6	0.6	0.9	1.0	0.8	0.8	1.8
Patel function								
60	-	-	-	1.0	1.3	1.5	1.2	-3.3
50	-	-	-	0	1.1	1.2	1.3	-3.7
40	-	-	-	0	0.9	1.1	0.8	-1.8
30	-	-	-	0	1.0	2.7	0.7	0
20	-	-	-	0.6	0.6	3.0	0.7	0.8
Mean	-	-	-	0.3	1.0	1.9	1.0	-1.6

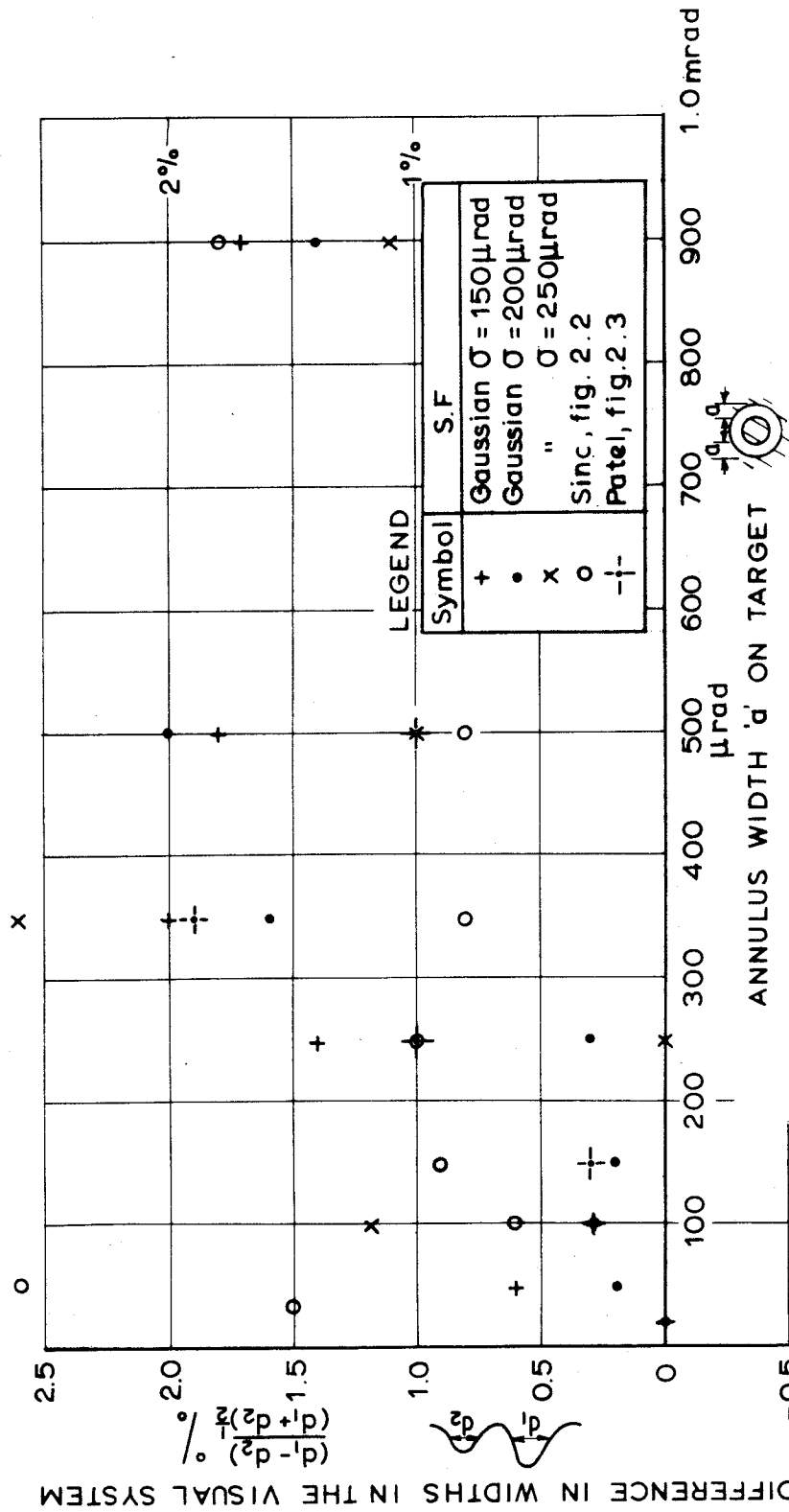


FIG. 3.9: Percentage differences in widths of profiles on each side of the MM, caused by a displacement of the MM equal to accuracies in curve 1 fig. 1.1, derived as a mean of values determined at 5 intensity levels. Separate points have been plotted for results derived for the 5 SF'S.

x

-+



variations for annuli less than 250  $\mu$ rad. This is because of the tendency for the profiles of each annulus to overlap. The Patel function also shows erratic values but generally fits into the range of 1 - 2%.

### 3.12 Discussion of Results of Convolutions.

The two separate criteria given in section 3.7 still appear to be valid after the additional convolutions presented in the previous sections. For the annulus widths greater than approximately 250  $\mu$ rad, the differences in slope and maximum values are considerably less than the corresponding values for annulus widths less than 250  $\mu$ rad. Meanwhile, the differences in widths of profiles are greater than approximately 1%, and therefore agree with Weber's Law, as formulated in section 3.6. Differences in slopes and maxima are too small to be visible, and therefore differences in widths of the annuli seen by the visual system are used as the criterion for pointing to targets with annulus widths greater than 250  $\mu$ rad.

For annulus widths smaller than 250  $\mu$ rad, differences in widths of the profiles approach zero in most cases, while differences in slopes and maxima increase. In line with the previous conclusions therefore, apparently luminance discrimination rather than width discrimination should be the criterion used for pointing. This conclusion is substantiated by the results of all five convolutions. The Patel PSF convolution results have not been added to figure 3.9 for annulus widths below 150  $\mu$ rad because the profiles on each side of the MM are so different. It is quite apparent when viewing the profiles, however, that luminance discrimination is the dominant factor.

The exact differences in slope and intensity used by the visual system for pointing seem unimportant, since the exact shape of the PSF is unknown. *Hempenius'* (1968) estimate of the PSF of the eye itself as a gaussian function with  $\sigma = 150$   $\mu$ rad, indicates that these differences on the retina would be represented in figure 3.71. If the PSF of the whole visual

system is similar to the sinc function, which appears to be more valid than Patel function, at least for small annuli, the differences used by the visual system would be similar to those in figure 3.74.

The unknown features of the visual system and also the uncertainties as to the linearity of the visual system, throw doubt on the rigid application of this technique. But the importance of these computations lies in the fact that for all five functions, the same general conclusions can be drawn as (*Trinder, 1965*). This fact shows very clearly that the complex pattern of pointing accuracies is primarily due to blurring effects of the visual system on the shape of the luminance pattern of the target seen by the observer. In particular, for annulus widths 250  $\mu$ rad to 1 mrad, the visual system adopts the same criterion for pointing as for the larger targets. The only targets which require a different criterion by the visual system apparently are those with annulus widths less than 250  $\mu$ rad.

Luminance discrimination of maxima and slopes is identical to flux discrimination as mentioned in section 2.6, since changes in maxima and slopes of the profile also mean changes in areas under the profile, and therefore the apparent luminance flux of the annuli. No attempt has been made to compute the areas under the profiles, since they are strongly dependent on the level at which the edge of the target is seen. In *O'Connor's (1967)* experiments, this level is unknown.

Though areas under the profiles for annulus widths greater than 250  $\mu$ rad will also differ, the associated differences in widths will be the most apparent feature. For annulus widths less than 250  $\mu$ rad, there is very little difference in profile width, but a significant difference in the overall luminance flux, as seen in the areas under the profiles. It seems likely therefore that flux discrimination is a more general expression for the criterion used for pointing over this range. This conclusion broadly agrees with *Blackwell's (1963)* theory used to predict detectability of targets, though the relationship between

minimum detectable flux and target size is extremely complex. Since tasks of detection e.g. the fine line targets used by *Byram (1944)*, and discrimination of the difference between very small annuli on each side of the MM seem to be similar in nature, it is likely that similar mechanisms will be involved in both cases.

### 3.13 Conclusions.

Since linearity of the visual system and constancy of its SF are in doubt, it is dangerous to make rigid conclusions from the computational techniques used. In addition, psychological factors are involved which may influence the observations, and for instance introduce large systematic errors, as shown in figure 1.2. Nevertheless, it is significant that the two general criteria in section 3.7 apply to curve 1, figure 1.1 for all SF's. This is sufficient proof that the blurring effects of the visual image are the dominant factors affecting the pointing accuracy curve for small annuli. The simple criteria (3) and (4) given in section 3.7 may therefore be derived to relate the geometry of the visual image to pointing accuracies.

#### 4. PSYCHOPHYSICAL TESTING.

##### 4.1 Introduction.

The field of psychology which deals with the determination of a relationship between a physical stimulus and the subsequent response, is called psychophysics (*Candland, 1968, 83*). Since an individual's behaviour may be measured by his response to stimuli, an understanding of the way in which responses may occur is fundamental to the prediction of behaviour to different stimulus conditions.

Psychophysics has an important bearing on everyday life, and in particular on occupations which require fine judgment by one or more of our senses. Metrology, for instance, may require the careful visual reading of linear scales. Detection of details on radar screens, reading of aircraft dials, detection of radio signals are other examples of psychophysical tasks in various occupations. Pointing to photogrammetric targets, stereoscopic height measurement, and point transfer are all examples of psychophysical judgments made by photogrammetrists. For an understanding of behaviour to stimuli and the associated judgment capabilities in each of these tasks, testing must be carried out over a wide range of conditions. Tasks particularly related to photogrammetry, as described above, however, have not been investigated in detail, despite the fact that many psychophysical aspects of vision have been investigated very extensively. Considerable research is therefore still necessary on psychophysical tasks undertaken in photogrammetry.

Investigations in the field of psychophysics were initially directed towards the determination of stimulus thresholds using classical psychophysical methods, and the description of these thresholds by a general psychophysical law. Fechner in the nineteenth century, aimed at establishing a relationship between *physical stimulus* or physical energy, and the subsequent *response* by the individual. For instance,

the question asked was - "Does a doubling of physical energy result in a doubling of the individual's perception of that energy?" Fechner's Law of 1882 (section 4.22) was for sometime, considered to be a suitable psychophysical law to describe this relationship. However, it has subsequently proved an incomplete law, particularly in the field of hearing. Some modifications to Fechner's Law which attempt to describe the relationship between physical stimulus and response more completely, will be discussed in section 4.7. In modern psychophysics, many aspects of human behaviour are investigated by psychophysical techniques, which determine the psychological response more efficiently than do the classical methods. Though it is unnecessary to describe these techniques, the aspects of modern psychophysics which influence experimentation on pointing will be given in this Chapter.

#### 4.2. Classical Psychophysical Theory.

The classical concept of psychophysics describes the relationship between the physical scale  $S$  and the response or psychological scale  $R$  as shown in figure 4.1 (after Guilford, 1954, 21).

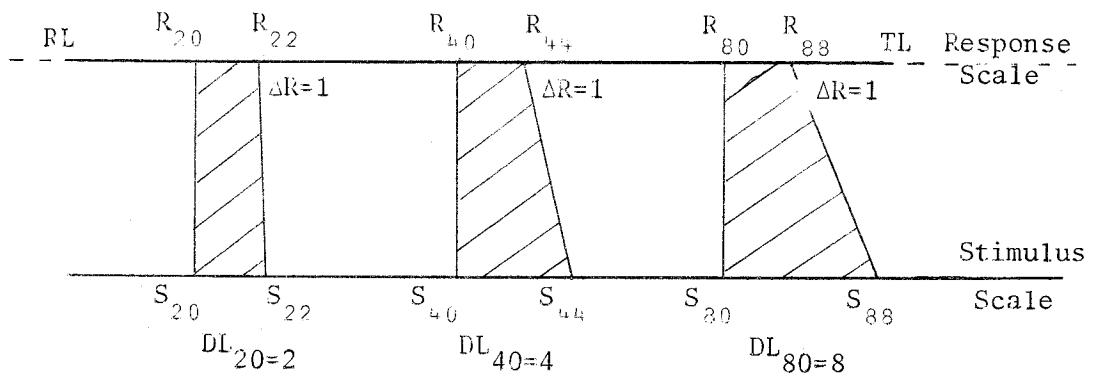


Fig. 4.1 The relationship between physical and psychophysical scales in classical psychophysics.

The Stimulus scale extends from zero to a very high value beyond the range of the human senses. The Response scale extends from the RL - the *Response Threshold* or *Limen* - to the TL - the *Terminal Threshold* or *Terminal*. Beyond these two points, the scale is marked by broken lines because the RL and TL cannot be well defined. They have a statistical variation depending on the task involved (*Swets, 1961*), and are generally fixed as points at which a positive response results 50% of the time. Although the TL and RL are thresholds on the response scale, they are expressed in terms of measurements on the physical scale.

Differential thresholds or *Difference Limens* - DL - are shown in figure 4.1 by the pairs of lines marked by hachuring. At the stimulus value of  $S_{20}$  a second stimulus  $S_i$  must reach the value  $S_{22}$  before it is judged different 50% of the time. At  $S_{40}$ ,  $S_i$  must reach  $S_{44}$  before it is judged different, and so on. The differences between  $S_{20}$  and  $S_{22}$ , and  $S_{40}$  and  $S_{44}$  are described as DL's. On the response scale these differences are shown as unity. That is, these differences give the same impression to the observer, in relation to the level of stimulation, though the magnitudes of the DL's increase as the level of stimulation increases. The results of *O'Connor (1962, 1967)* are examples of DL's expressed on the stimulus scale.

#### 4.21 Weber's Law.

The relationship between DL's and level of stimulation, expressed on the stimulus scale, is known as Weber's Ratio or Law:-

$$\frac{\Delta S}{S} = K$$

where

- $\Delta S$  = DL on the stimulus scale corresponding to a change on the R scale of unity.
- $S$  = the point on the physical scale.
- $K$  = constant depending on the observer and the modality of the sense.

K is approximately constant at  $1/100$  for the discrimination of distances (O'Connor, 1962),  $1/30$  to  $1/40$  for lifting of weights and varies for sounds with frequency and intensity. As shown in section 1.4, Weber's Law holds for pointing observations to targets with large annulus widths, but not for observations to targets with small annuli.

#### 4.22 Fechner's Law.

Weber's Law only describes behaviour in terms of the stimulus scale, with no reference to the response scale. Fechner's Law on the other hand expresses a relationship between the stimulus and response scales. The basis of this law is a logarithmic relationship between stimulus and response as follows:

$$R = K \log S$$

where

- R is the response;
- S the stimulus above threshold,
- K is a constant.

In words this law may be stated as:- R increases in *equal steps* as S increases in *equal ratio steps*, (Candland, 1968, 89) (ref. figure 4.1)  
This law makes two assumptions -

- (i) The DL is a function of all DL's which have occurred previously.
- (ii) that all DL's are subjectively equal.

As stated in section 4.1, Fechner's Law has proved to be an incomplete psychophysical law, although it is satisfactory for some aspects of psychophysics. A completely general law has yet to be found, but more adequate laws than Fechner's Law have been developed (Stevens, 1962).

Before describing the methods used in classical psychophysics, an introduction to some concepts of modern psychophysics will be given.

4.3 Some Aspects of Modern Psychophysics - The Response Matrix.

Modern psychophysics describes the behaviour on the response scale of an observer, in terms of the many variables which may be involved. This results in a general behavioural equation.

The response of an organism to a stimulus, is a function of factors in the stimulus, the internal conditions, number of stimulations and time itself (*Graham, 1950*), i.e. -

$$R = f(a, b, c, d)$$

where

- a = aspects of the stimulus
- b = number of times the stimulus is presented.
- c = time
- d = internal conditions of the observer, e.g. motivation, psychological attitude etc.

Generally in psychophysical investigations, the effects of factor "a" on the psychological response only are considered. In the research on pointing described in this work, stimulus conditions which have been considered are the size of target, degree of blur and the background density of the target. The effects of the remaining factors in the behavioural equation were expected to remain constant during the experiment, although it is impossible to say precisely that this was the case. In the course of pointing experiments, the factor "b" for instance, may affect the results if an excessive number of observations cause fatigue. It is not anticipated that the actual time of day would appreciably affect the results, but observations on each target have extended throughout the day and therefore the effect of time tends to be included in the overall results. Internal conditions may perhaps affect the results of observations under certain circumstances. Indeed some psychologists have claimed that even a strategically timed coffee break can improve psychophysical results. The particular purpose of these experiments



was to investigate pointing accuracies obtainable in photogrammetric practice. While the observations have been made with considerable care and concentration, the external laboratory conditions were similar to those which may be expected in photogrammetric practice. In addition, it is anticipated that with a large sample of targets, and a large sample of observations on each target, a representative pattern of results has been obtained.

From  $S_i$  ( $i = 1$  to  $n$ ) stimuli presented to the observer on  $O_j$  ( $j = 1$  to  $m$ ) occasions, a response matrix  $R$  is derived for each observer, where each single response element is  $R_{ij}$ . For more than one observer  $P_k$  ( $k = 1$  to  $l$ ), an additional dimension is added to the matrix, giving single response elements  $R_{ijk}$ . The response  $R_{jk}$  by each observer to stimulus  $S_i$  has a mean  $R_k$  derived from  $N$  observations:-

$$R_{jk} = R_k + e_{jk}$$

where  $e_{jk}$  is the variability of the discrimination of the observer for each single observation. The shape of dispersions,  $e_{jk}$  for psychophysical testing may or may not follow a symmetric pattern.

Over a restricted range on the S-scale, S and R are approximately linearly related. This can be seen by reference, for instance, to Fechner's logarithmic law, which is approximately linear over a restricted range of the S and R scales. It may therefore be assumed that the small dispersions of both S and R follow approximately the same frequency distribution (Guilford, 1954, 28). Guilford states that there is considerable evidence that discriminial dispersions follow the symmetrical normal distribution, particularly for tasks similar to those studied in this work. O'Connor (1962, 1967) has assumed normality of dispersions on the stimulus scale throughout. There seems ample justification, therefore, for assuming that the observations in this study also follow a normal distribution. Sample tests of normality, however, have been carried out in Appendix B.

The three classical methods of psychophysical testing which determine the RL and DL on the stimulus scale will be outlined in the next section. This will be followed by a brief description of some aspects of the more recently developed scaling procedures, which aim at determining the response matrix R.

#### 4.4 Classical Methods of Psychophysics.

##### 4.41. Method of Limits.

The method of limits is normally used for the determination of response thresholds of stimuli. The test object is presented to the subject in a series of steps in either ascending or descending order. For instance, in determining the luminance intensity threshold, the experimenter would commence with a stimulus brighter than the threshold. In a series of trials where the intensity of the stimulus is decreased in equal steps, the subject must judge whether or not the stimulus is above threshold. The point at which the stimulus is no longer visible is a measure of the threshold for decreasing stimuli. A similar set of observations must also be carried out for increasing stimuli. This method, which is covered thoroughly by *Guilford (1954)*, *Candland (1968)* and *Sidowski (1966)* has not been used in this research, because it is unsuitable for testing photogrammetric pointing accuracies.

##### 4.42. Method of Average Error.

The average error method has been described as a "free gift to psychophysics from the exact sciences of physics and astronomy" (*Guilford, 1954, 86*). Indeed, many fields of metrology, including surveying use this method as a basis for their measurements. The observer is required to produce *equal stimuli* by adjustment of the stimuli himself, e.g. photogrammetric pointing, where the annulus on one side of the MM must be equated to the annulus on the other. The central position of the MM can be approached from two mutually

opposite directions along each coordinate axis. The mean of the results obtained from each direction along each axis may be used to find the *Point of Subjective Equality* (PSE) (Candland, 1968, 95), (Guilford, 1954, 93), although there does seem to be some doubt over this point. The statistical testing of results obtained by this method is relatively straightforward but because of the observational technique it does not allow a direct estimation of a difference limen. Candland (1968, 95) states vaguely that the DL can be estimated "from some assumptions about the PSE." Guilford (1954, 93) suggests that the DL can be estimated from the mean of the combined data, if the means from both directions are not statistically different, or alternatively from the standard deviations of the individual directions. The DL in this study has been estimated from the standard deviation from only one direction of approach of the MM, because the means from opposite directions prove to be significantly different. Such a value is convenient when referred to photogrammetric practice however, since generally error estimations are made using standard deviations of such observations.

#### 4.43 Analysis of Errors in Average Error Method.

Guilford (1954, 93) defines the occasional variable error of each observation as  $e_m + e_r$ , where  $e_r$  represents the statistical fluctuation in observations, and  $e_m$  the "error of movement" inherent in the method. The extent to which the error of movement,  $e_m$ , is significant must be tested statistically;  $e_r$  is most conveniently described by the standard deviation. O'Connor (1967) has shown, figure 1.2, that the so-called movement errors (termed systematic errors in this work) are indeed significant, and may be of the order of 3 to 4 times the standard deviation of a single observation. Observations in this study agree with this finding, and in addition prove that such errors may vary if separate sets of observations are carried out several months apart. It therefore becomes necessary to use the standard deviation of one direction of approach as an estimate of the DL, as stated in the previous section. While it cannot be held that such estimates of difference limens would

agree with DL's determined by other psychophysical methods, they are suitable for comparing observations of different targets, all observed by the same method. As will be shown in section 4.5, the method of average error can also be treated as a psychophysical scaling method if certain assumptions are made.

#### 4.44. Suitability of the Method of Average Error to Psychophysical Testing.

The average error method is considered to be an accepted procedure for psychophysical testing. The active participation by the observer in the experiments increases interest and motivation in the observations, particularly for long series of experiments. However, activation of the equipment (e.g. by handwheels or switch) during observations depends on the transmission of response R through the body muscles to the equipment. The instrument readings are therefore an indirect measure of the observer's response. This leads to the so-called "motor errors" caused for instance, by the observer's inability to stop the instrument at the precise moment when the MM is subjectively central. Motor errors may also be due to the distracting influence of muscular effort, which reduce the accuracy of the visual task. Conversely, muscular activity may act as a form of irrelevant information, leading to accuracies higher than can be obtained by the visual system alone. *Guilford (1954, 96)*, quoting *Müller*, speaks of "uncertainties of the hand" reducing the accuracy of experimental results. However, she, maintains that suitable design of equipment should keep such inaccuracies to a minimum.

The method allows the observer to check the observation after stopping the movement of the instrument, and to make a further adjustment in the same direction if he sees fit. Because of the movement error, which is apparently dependent on the direction of movement of the equipment, setting must always be carried out in one direction. If checking shows an overshoot, the observation must be completely repeated. Strong evidence supporting this point will be given in Chapters 5, 6 and 7.

An advantage of this method is that statistical testing is straightforward, particularly if a normal distribution of observations is assumed. A further important advantage is that the method of observation is similar to that used in photogrammetric observations and though it may include some small inaccuracies due to motor errors, such errors may also be included in any photogrammetric observation. The statistical estimate of the DL derived by these observations is therefore applicable to photogrammetric practice.

#### 4.45. Constant Stimulus Methods.

*Guilford (1954, Ch. 6)* describes the constant stimulus method, or constant method, as the most accurate of the classical psychophysical methods. Referred to the problem of pointing, it is carried out as follows. Five or seven equally spaced MM positions are selected and the observer must reply whether the MM is "left" or "right" of the centre of the target. The two extreme positions are chosen such that replies will be correct about 95% of times, and the middle position will be very close to the centre of the target. Generally, psychologists prefer the subject to reply "left" or "right" despite the fact that the MM may be very nearly central. Replies to the middle position should be guesses, and therefore approximately equally distributed between "left" and "right".

Despite the fact that this method is considered as the most accurate of psychophysical methods, procedures proposed for the treatment of data, and particularly for statistical estimation of the accuracy, have varied. The most accurate method of computation of the limen and DL involves a least squares fit to a theoretical curve, using suitable weights for the observations. As mentioned in section 4.3, psychophysical tasks of the type involved in these investigations follow closely a normal distribution. If the observations are expressed as percentages of correct replies, (see Table 4.1), the "right" replies

will increase from nearly 0% to nearly 100%, as the MM position is moved from left to right across the target. The percentages of the "left" replies will be the complement of the "right" replies.

Table 4.1.

Micrometer Setting (MM) (S)	No. of "Right" replies	Proportion of Correct replies (p)
20.00	78	.975
20.40	60	.750
20.80	45	.563
21.20	19	.238
21.60	2	.025

No. of observations to each setting = 80

The relationship between S (stimulus or MM position) and p, the probability of "right" replies, will follow a cumulative normal distribution curve or normal ogive. The proportions p can therefore be transformed into the variable z by the formula -

$$p = \int_{-\infty}^z \frac{1}{\sqrt{2\pi}} \exp\left(-\frac{z^2}{2}\right) dz$$

Since p is normally distributed with respect to z, and also with respect to S (or MM position), z may be expressed as

$$z = a + bS \text{ where } a, b \text{ are constants.}$$

The relationship between a, b and the elements of the normal distribution of the observations is as follows:-

$$p = \int_{-\infty}^z \frac{1}{\sqrt{2\pi}} \exp\left(-\frac{z^2}{2}\right) dz$$

Changing the formula, where  $z = a + bS$  and  $dz = b.dS$ ,

$$p = \int_{-\infty}^{a+bS} \frac{b}{\sqrt{2\pi}} \exp \left\{ - \left[ S - \left( -\frac{a}{b} \right) \right]^2 / 2 \left( \frac{1}{b} \right)^2 \right\} ds$$

The cumulative normal curve is of the general form:

$$q = \int_{-\infty}^x \frac{1}{\sqrt{2\pi}\sigma} \exp \left\{ - \frac{(x - \bar{x})^2}{2\sigma^2} \right\} dx$$

where  $\bar{x}$  is the mean, and  $\sigma$  is the standard deviation. The mean of the observations is therefore  $-\frac{a}{b}$ , and the standard deviation,  $\frac{1}{b}$ , expressed in units of the stimulus S.

Five or seven points are determined for the straight line relationship between stimulus S, and the transformed proportions z. Since the observations may not be exactly normal, they may not fall exactly on a straight line. The recommended method for determining a best fit straight line is the least squares technique. A further refinement recommended by *Guilford* is the assignment of weights to the observations according to the proportions of correct observations. These weights are based on the work of *Müller and Urban*. *Müller* believed that observations near the central position, i.e. the proportions of approximately 0.50, were more significant than those which almost always result in a correct answer. The *Müller* weights are proportional to the squared ordinate of the normal probability curve at the distance z from the mean. This is to take account of the fact that a small error in p results in a small error in z at z values of nearly zero, but a large error in z for extreme z values, or z values at the extremes of the normal curve. *Urban* believed that for a least squares technique, the observations should be weighted in proportion to their reliabilities. The standard deviation of a proportion p is  $\sigma_p = \sqrt{pq/N}$  where p = (1-q) and N = number of observations, from the binomial distribution. *Urban's* weights are therefore proportional to  $\frac{1}{\sigma^2}$  or  $\frac{1}{pq}$ .

Combined weights of *Müller and Urban* (which are a product of both effects) are generally adopted. They vary from 0.11 for proportions of 99% to 1.0 for proportions of 50%. A least squares fit, with *Urban-Müller* weights, has been used to compute the PSE and DL from observations in the study. The derivation of formulae for the least squares adjustment is given in Appendix A.

The DL by the constant method is taken as the standard deviation of the normal distribution,  $(\frac{1}{\sigma})$ , and the subjective centre, PSE, the mean of the observations or the position of the MM when  $p = 50\%$ . *Guilford (1954, 131)* gives proposals put forward by some psychologists for estimating the standard deviation of the PSE. After the work of *Culler and Linder*, *Guilford* uses an estimate of the standard deviation, referred to as the Modified Culler Formula, as

$$\sigma_{\text{PSE}} = \text{DL} / \sqrt{N(\sum Wp)}$$

where DL is the difference limen of the observations  
N is the number of observations on each setting  
W is the *Urban - Müller* weight  
p is the proportion of "right" or "left" replies.

The computed results in Appendix B show an estimate of the standard deviation computed by the Modified Culler Formula, and also from the least squares adjustment based on the Law of Combination of Variances. In most cases they are substantially the same.

#### 4.46. Suitability of the Method.

The constant stimulus method measures the ability to discriminate the position of a motionless MM against the target, and the task is different from that involved in the average error method. It is, therefore, reasonable to assume, and this has also been supported by the experimental evidence in Chapter 6, that the DL from this method is significantly different from that determined by the average error method. Since the task of photogrammetric pointing is one of centrally



locating a moving MM on a target, rather than of discriminating a stationary MM, it appears that the constant stimulus method is unsuitable for testing photogrammetric pointing. (see section 4.6) From an experimental point of view however, both the constant stimulus and average error methods are useful and worthy of comparison.

#### 4.5 Modern Psychophysical Methods - Scaling Methods.

In modern psychophysical methods, judgments or observations are referred to the response or psychological scale, shown in figure 4.1. In all scaling methods, a particular value on a linear scale is assigned to each response. This linear scale may be graduated such that the actual numbers are arbitrarily derived, but each number is correct in relation to the others. Alternatively, the scale may be the stimulus scale itself, and graduations on this scale referred to only as labels.

Scaling methods, involving comparative judgments, may be related to Thurstone's Law of Comparative Judgment which defines the psychological distance or separation on the response scale, between two stimuli as:

$$R_j - R_k = z_{jk} \sqrt{\sigma_j^2 + \sigma_k^2 - 2r_{jk} \sigma_j \sigma_k}$$

where  $R_j$  and  $R_k$  are the mean values of responses to stimuli  $S_j$  and  $S_k$ ;  $z_{jk}$  is the deviate from the mean of the unit normal distribution,  $\sigma_j$  and  $\sigma_k$  are the standard deviations of each response  $R_j$  and  $R_k$  to  $S_j$  and  $S_k$ ; and  $r_{jk}$  is the coefficient of correlation between  $R_j$  and  $R_k$ .

Each of the elements in the above formula must be determined to find  $R_j - R_k$ . Since some of these terms are difficult to derive, Thurstone's Law may take on a number of approximate forms, depending on the assumptions made on  $\sigma_j$ ,  $\sigma_k$  and  $r_{jk}$ . Approximation referred to as Case V (*Guilford, 1954, 156*) assumes that  $R_j - R_k = z_{jk} \cdot \sigma_j \cdot \sqrt{2}$ .

(i.e.  $\sigma_j = \sigma_k$  and  $r_{jk} = 0$ )

The methods of average error or constant stimulus may be considered as scaling methods for pointing observations based on Case V above. Each pointing observation by the average error method requires the discrimination of the annulus on each side of the MM, and a decision as to whether the annuli are equal. The response to each annulus on each occasion is  $R_{ij}$  and  $R_{ik}$ . When  $R_{ij} = R_{ik}$  the annuli are subjectively equal, despite the fact that the annuli may actually be unequal, i.e.  $S_{ij}$  may not equal  $S_{ik}$ .  $R_{ij}$  and  $R_{ik}$  will have dispersions  $\sigma_j$  and  $\sigma_k$ . Any single observation  $i$  will therefore result in responses

$R_{ij} = R_j + e_{ij}$  and  $R_{ik} = R_k + e_{ik}$ , where  $e_{ij}$  and  $e_{ik}$  are the occasional variability in response. Each pointing observation requires that  $R_{ik} = R_{ij}$ . If the means  $R_j$  and  $R_k$  must also be equal, then statistically  $e_j$  must equal  $e_k$  or  $\sigma_j = \sigma_k$ .

A further assumption made is that  $r_{jk} = 0$ , i.e. the response to the area of the annulus around  $j$  figure 4.2, must be uncorrelated with the response to the area of the annulus around  $k$ . It is difficult to say positively whether this is indeed the case. However, the significant sections of the target to the observer if the MM is moving from left to right, are the areas of the annulus centred around  $j$  and  $k$  in figure 4.2, on opposite sides of the MM. These areas are separated by the MM diameter, and should cause separate stimulation at\*, and response by the observer. It therefore seems reasonable to assume that responses  $R_{ij}$  and  $R_{ik}$  are uncorrelated.

---

\* This condition is satisfied if the MM is sufficiently large. The convolutions in Chapter 3 indicate that a MM of 0.8 to 1 mrad should be satisfactory.

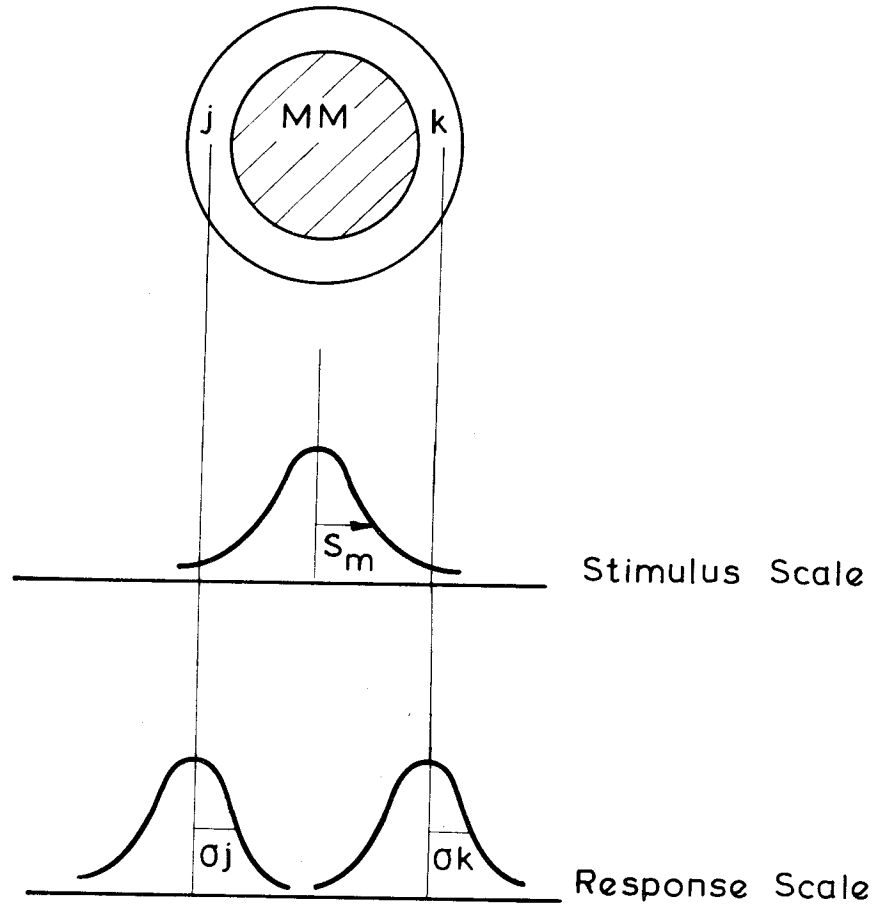


FIG. 4.2: THE RELATION BETWEEN STIMULUS AND RESPONSE SCALES FOR THE TASK OF POINTING.

Based on case V of Thurstone's Law, provided the above assumptions are valid, the psychological distance is thus

$$R_j - R_k = z_{jk} \cdot \sqrt{2} \cdot \sigma_j.$$

The execution of pointing by the average error method, requires the observer to evaluate  $R_{ij} - R_{ik}$  continually as the MM approaches the subjective central position. At the instant when  $R_{ij} = R_{ik}$  (i.e.  $R_{ij} - R_{ik} = 0$ ), movement of the MM ceases. The assessment of  $R_{ij} - R_{ik}$  as seen by the above formula, is dependent on the dispersion  $\sigma_j$  ( $= \sigma_k$ ).  $R_{ij} - R_{ik}$  for each observation, which is equivalent to the DL for pointing, is therefore a statistical quantity, proportional to  $\sigma_j$ . (Expressing  $R_j - R_k$  in terms of the standard deviation  $\sigma_j$  results in a  $z_{jk}$  value of unity). The measured value,  $S_m$  on the stimulus scale, which represents  $\sigma_j$ , hence may be used to derive  $R_{ij} - R_{ik}$  if the effects of muscular activity are ignored. That is,  $S_m$  on the stimulus scale, will be a scaling factor for the DL on the response scale. Each individual target, which involves its own task of comparative judgment, will give one scale value against which the scale values of other targets can be judged.

The inclusion of the classical psychophysical methods as scaling methods, is supported by *Guilford (1954, 260) and Candland (1968, 115)*. Similar reasoning would also apply to the constant stimulus method. It is important to realize however, that since different types of observations are involved for the average error and constant stimulus methods, the dispersions may not be the same, resulting in different scale numbers for the two types of observations.

The classical psychophysical methods can therefore be considered as scaling methods provided the necessary assumptions are made on the behaviour of  $\sigma_j$  and  $\sigma_k$ . There are no indications in the literature that these assumptions are invalid for this type of psychophysical task, though very little research has been carried out on such work. Measurements on the stimulus scale are important for this work, since results are required for reference to photogrammetric practice. The fact that observations are determined by a valid psychophysical method perhaps allows a direct comparison with psychophysical results and laws derived by other scientists. While it is agreed that results may depend on the method of observation, and to some extent the method of data processing, relative comparisons should still be possible.

Having discussed the various psychophysical methods, the reliability and validity of these methods will be defined. This will be followed by a brief outline of some recently developed psychophysical laws.

#### 4.6 Reliability and Validity of Results Obtained by Psychophysical Methods.

*Blackwell (1953, 4)* defines reliability and validity of psychophysical methods as follows:-

*Reliability within a session* is analysed by statistical processes, which test the goodness-of-fit of the measurements to a theoretical curve, e.g. normal frequency curve.

*Reliability between sessions* is inversely proportional to the variance obtained with repetitions of measurements by a given procedure.

The reliability of a method may also depend on the variation of means obtained in different sessions. Means have sometimes been found to be unreliable in observations in this study. Full statistical tests have been carried out to check the reliability of both means and standard deviations. Discussion of the statistical methods used can be found in the Appendix A.

A method is *valid* if it indeed measures the quantity it purports to measure. Regarding psychophysical methods used to determine photogrammetric pointing accuracies, it appears that the method of average error is a more valid procedure than the constant stimulus method since the observation in the average error method is very similar to that employed in photogrammetric pointing. This factor has already been discussed in section 4.46. Further, the standard deviation derived by the average error method is suitable for use in studying propagation of errors in the photogrammetric system, but it may prove to be unsuitable or even invalid if a true estimate of the DL is required. The constant stimulus method, on the other hand, may well prove to be the most suitable method for investigating the true DL and the PSE, unbiased by any movement error.

#### 4.7 Recently Developed Psychophysical Laws.

*Guilford* (1954, 41) has quoted variations of Weber's Law in the form of  $\Delta S = KS^{\frac{1}{2}}$  after *Fullerton and Cattell*. A more general form of this equation however is  $\Delta S = KS^n$ . This is similar to the form of psychophysical equation proposed by *Stevens* (1962, 30), which refers to the response scale. *Stevens'* formula is  $\psi = K(\phi - \phi_0)^n$

where K is a constant depending on the choice of axis;  
n is the exponent which depends on the modality or sense investigated, and also external parameters of the experiment, e.g. adaptation level;  
 $\psi$  is the psychological response or magnitude to the stimulus  $\phi$ ; and  
 $\phi_0$  is the effective threshold measured on the stimulus scale.

Evidence put forward by Stevens includes work based on a number of modalities and even cross-modalities, but this evidence cannot be considered as conclusive. The experimental procedure used by Stevens was the so-called magnitude estimation method, where the observer must

numerically estimate his subjective impression of the stimuli. This technique is another example of psychophysical scaling methods.

The above formula can be readily represented by a linear relationship if plotted on logarithmic scales. The curves in figure 1.1 representing pointing accuracies are linear on logarithmic scales over a wide range. Since the experimental method used to derive these curves is a psychophysical scaling method, as shown in section 4.5, it is valid to relate Stevens' law to these results. Attempts have been made in this work to relate further experimental results to this law.

While the determination of a general psychophysical law is not the main aim of this study, it is felt that a favourable comparison with existing laws gives a check on the validity of the data derived from the experiments. In addition, the data may well be one more contribution to the substantiation or otherwise of existing laws. Such a comparison has been made in Chapter 6.

#### 4.8 Conclusion.

The average error method may be assumed to be a valid psychophysical scaling method, suitable for the experimentation of photogrammetric pointing accuracies. Though the constant stimulus method may also be a psychophysical scaling method, it is doubtful if it is suitable for photogrammetric pointing investigation, considering the different type of task involved. Since both are psychophysical scaling methods, the results obtained from them may be compared with existing psychophysical laws.

5. EXPERIMENTAL PROCEDURES.

5.1 Introduction.

The pointing experiments to be carried out in this work entailed the design of an instrument which could make precise measurements on blurred and sharp targets. It was proposed to construct an instrument, as simply as possible, keeping in mind the limited finance available, which would give measuring accuracies of 1 sec. of arc (5  $\mu$ rad) or better. To simplify the design it was decided to investigate movements of the MM parallel to the eye-base only (approximately parallel to the x-direction in a photogrammetric instrument). *O'Connor's (1967)* results indicate that for annulus widths greater than 300  $\mu$ rad and sharp targets, accuracies in the x and y-directions for several observers, prove to be statistically the same. In some cases they prove to be different for annulus widths smaller than 300  $\mu$ rad, but there is no conclusive evidence for this finding. In any investigations on visual tasks, it is reasonable to assume that the pattern of results obtained by one or two experienced observers is indicative of the pattern which would occur for all experienced observers. Results of standard deviations of pointing to blurred targets obtained in these investigations may therefore be assumed to indicate the form of the relationship between pointing accuracies and blurred targets, although small variations will be expected from these results, for different observers. It is proposed that the results obtained in these experiments will be applicable to observations in both the x and y-direction, keeping in mind that sizes of annuli of targets being observed are larger than 300  $\mu$ rad. *O'Connor (1968)* has also shown that pointing errors in the x and y-directions are uncorrelated. The separation of observations in the x and y-directions in this study is also based on this finding.



## 5.2 Psychophysical Methods Used.

In Chapter 4, the conclusion reached was that the average error method of observing represented the most valid method for investigating pointing accuracies, particularly because of its similarity to observational techniques in photogrammetry. As a means of comparison with other psychophysical methods, the constant stimulus method has also been used, since it has been adopted by some experimenters in photogrammetry (*e.g.* Zorn, 1965).

## 5.3 Design of Experiments - Statistical Approach.

The variables to be investigated in these experiments, were the size of the annulus, the degree of blur of the target and its background density. An efficient approach to the investigation of these variables is to carry out an analysis of variance based on a factorial design of experiment (*Moroney, 1951, Ch. 19*). This would mean the selection of a number of discrete values for each of the above variables, and the observation of targets containing all possible combinations of these values. For instance, if 3 different annulus widths, 3 background intensities, and 5 degrees of blur of the target are chosen, 45 different targets would be observed. Applying a factorial design however, to psychophysical investigations is difficult for the following reasons. Firstly the exact width of the target as seen by the observer is impossible to predict before observations commence. This is deduced from the fact that different observers determine the target edge by psychophysical observations at different positions on the target (*Trinder, 1965*), (see section 5.53). The use of a set of targets of specific widths for a number of observers is therefore impossible. The accuracy of width measurements of blurred targets is however very low, and hence some range in the widths may be allowed. Secondly, small targets become invisible after a relatively small amount of blurring while large targets can be blurred considerably before they become invisible. It is therefore impossible to use all combinations of

degree of target blur, and target width for the observations.

An analysis of variance has been carried out in this research in two groups, involving two variables each, as follows. Three levels of background density were chosen - 0.25, 0.40 and 0.70 - which cover the normal range of density levels on aerial photographs. Targets were printed for each of these densities, to give an annulus width of approximately 2 mrad, at different grades of blur. It was not known at the commencement of the experiments, which characteristic of the blurred target was significant in determining pointing accuracies. As the observations progressed, it became apparent that the slope of the density profile of the target expressed as  $\Delta D/\text{mrad}$ , is a significant factor affecting pointing and therefore this was used as the parameter to describe the blur of the targets. By selecting suitable targets from the total observed, a variance analysis was carried out between the slopes of the target density profile and the background densities for annulus sizes of 2 mrad. Five levels of target blur were chosen at each of the three background density levels, *Test No. 1*. The actual levels of blur and background density of each target may vary slightly from the nominal values. Effects of these differences are minor and merely introduce a small amount of "noise" into the analysis.

Three separate analyses, testing the effect of width of annulus against grade of blur for targets of 0.25 background density, were necessary. The first involved 0.8 mrad and 2.0 mrad annuli at four levels of blur, *Test No. 2*. The second tested targets with 2.0 and 5.0 mrad annulus widths against three levels of blur of the target profile, *Test No. 3*. *Test No. 4* analysed annuli of 2.0 mrad and 5.0 mrad against two levels of blur at a higher adaptation level. Since *Test No. 1* indicated that background densities have only a minor effect on pointing accuracies, they were not included in the remaining tests. Following the completion of the analysis of variance, a linear regression of logarithm (slope) against logarithm (pointing standard deviation) has been carried out as described in section 6.3.

The analysis of variance adopted in these experiments required more observations than were necessary, for a purely factorial design of experiment. This was so because of the difficulties encountered in deriving the widths of the targets, and the significant characteristic of blurred targets, which affects pointing accuracies.

#### 5.4 Instrumentation.

In the design of the instrument for the research, it was decided to use direct viewing with no optical elements between the observer and the target. While this may not be of the utmost importance for sharp targets, optical elements may well influence results for blurred targets. Results in Chapter 6 tend to substantiate this point. The target in the instrument as shown in figures 5.1 and 5.2 is set in a vertical plane, such that the horizontal viewing line is at right angles to the plane of the target. The MM is attached to a clear perspex sheet which slides along a rail located 1 mm. in front of the target and parallel to it. A small spherical bearing attached to the perspex screen is the point of contact with a micrometer screw 25 mm. long. The micrometer is driven by a  $\frac{1}{25}$ th horse power electric motor with rotation speeds ranging from 60 RPM to zero (30 mm. per minute to zero). Speed is controlled by means of an electronic switching device manipulated by the observer at the viewing stand 10 meters away. Least count of the micrometer drum is .001 mm. or 0.1  $\mu$ rad. (0.02 sec. of arc). However, it is believed that the accuracy of the instrument is approximately 0.5  $\mu$ rad. (.005 mm. on the micrometer drum). Repeatability tests on well defined targets using theodolite telescopes have given standard deviations of better than 1  $\mu$ rad. The accuracy of the instrument is therefore more than 10 times higher than the pointing accuracies being investigated in this research. Observations have been carried out under controlled temperature and humidity conditions, and therefore no corrections were necessary for atmospheric conditions to either micrometer or target. Movements of the MM can be made in either direction because the MM slide bears on to the micrometer spindle with the

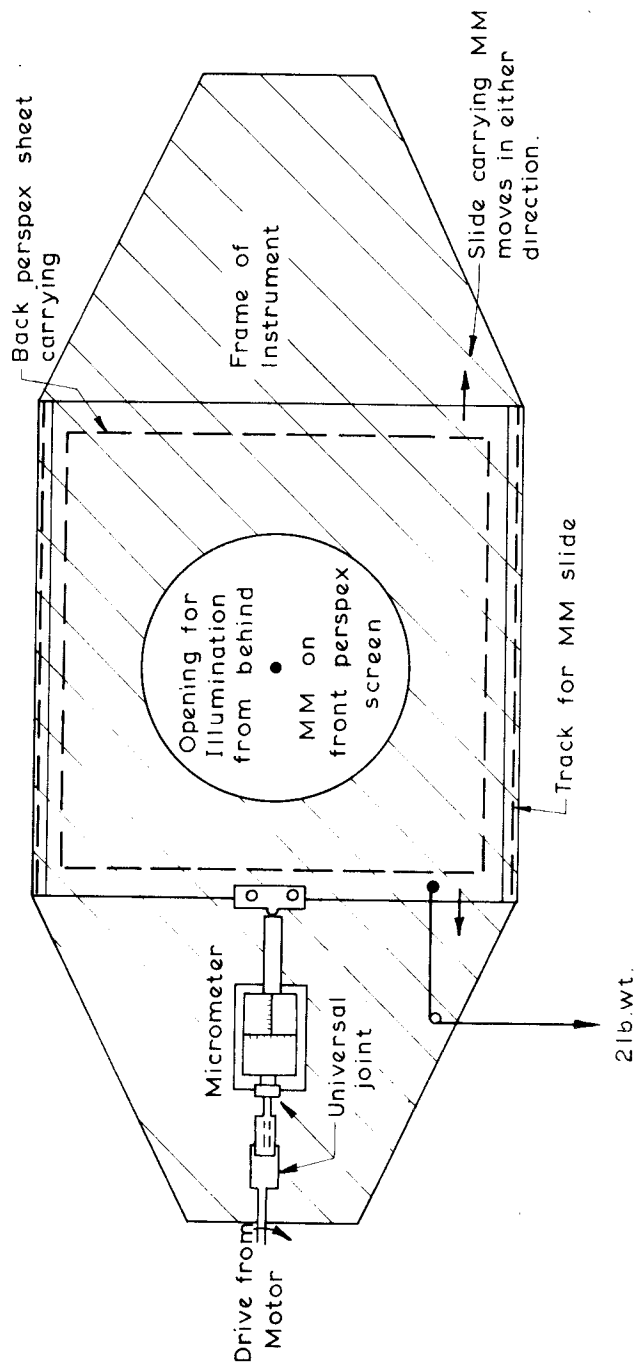


FIG. 5.1: INSTRUMENT USED IN POINTING OBSERVATION

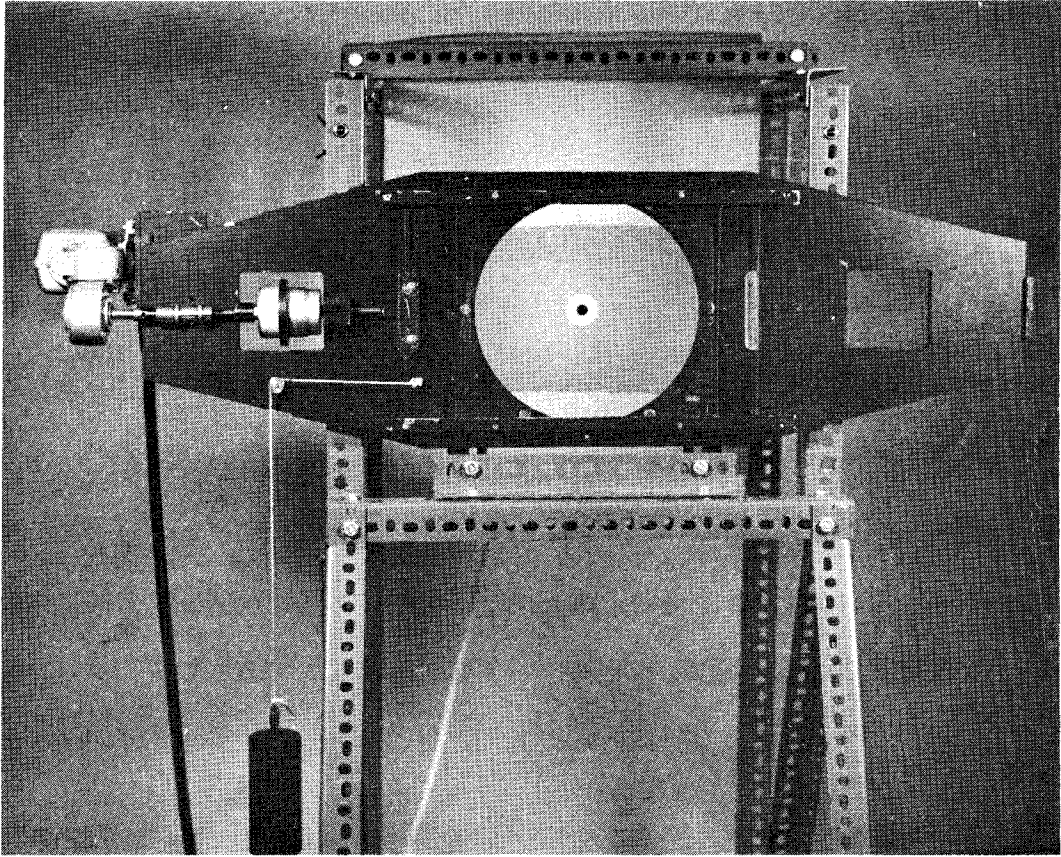


Fig. 5.2 Pointing Instrument.

force of a 2 lb. weight which is attached to the slide by a cord, via a small pulley. Since there were no linkages between the micrometer spindle and the MM slide, no backlash existed in the instrument. Backlash in the micrometer drum itself was also negligible.

Illumination of the target was by a tungsten filament lamp set 2 feet behind the target, and diffused by a diffusing screen 6" behind the target. This screen was the commercially known product Polacoat, which is claimed to be 80 - 90% efficient. Luminance of the target area, approximately 10 inches in diameter, was found to be constant at 12 mL, based on measurements on an SEI Photometer. Pointing observations were carried out in a laboratory, the lighting of which was used to illuminate an adaptation screen, 5' by 7', 2' in front of the target. The luminance of this screen was 15 mL. The whole instrument was obscured from the observer by the screen except for the target area and the micrometer, which was read using a theodolite telescope. Observations were carried out from a stand with a head rest, 10 meters from the target. The left eye was used by the observers because it was the eye normally used by them for monocular viewing; the right eye was restricted from seeing the target by a small screen on the viewing stand, but otherwise could see the area round the target, thus providing for equal adaptation of both eyes.

## 5.5 Observational Technique.

### 5.51 Average Error Method.

At the commencement of taking readings by observer No. 1, JCT, with the MM approaching the target from the left hand side, large systematic errors were noted when the subjective centre was compared with the true centre. This was particularly noticeable during the early part of the two weeks' practice period by JCT. The systematic

error decreased with experience, but was still significant. In an attempt to eliminate systematic errors the early targets were approached from both the left and the right hand sides with the belief that the mean of the two directions could give the true centre. This appeared to be justified considering the statements of *Candland (1968)* and *Guilford (1954)*, mentioned in section 4.42. The mean values of observations to target numbers 26, 18, 19, 21 clearly indicate that this approach would not give reliable estimates of the centre. Further discussion will be given on this point in section 5.52. For the purposes of investigating the standard deviation therefore, approach from the left only was used. This gave consistent mean values and enabled estimation of the systematic error.

It was found that the MM could be reset to a given position with a standard deviation of approximately 200  $\mu$ rad, by mentally recording the movement time of the MM, without reference to the target. The maximum standard deviation that could be investigated, unbiased by this time effect, was therefore considered to be approximately 1 mm. on the micrometer drum (100  $\mu$ rad. at 10 m.). For the investigation of the larger annuli of 5 mrad, the observation distance was reduced to 5 m., giving standard deviations on the micrometer drum of 0.7 mm. or less. Observations on sharp targets at both 5 m. and 10 m. viewing distance indicated that observation distance did not affect pointing accuracies to targets viewed under similar illumination conditions (Table 6.1).

The adaptation level for several targets observed at 5 m. was higher than planned, because the laboratory illumination close to the observer had not been controlled. In this case it was difficult to estimate the actual adaptation level, but it was clearly well in excess of the 15 mL luminance of the adaptation screen. The results at the higher adaptation level have been presented firstly to indicate the fact that adaptation level will alter the results, but particularly to give further data for testing the effects of widths of the targets in section 6.2.

Before commencing an observation, the MM was moved well off to the edge of the target. In the process of centering, the target was approached with care and at a slow speed of the motor. If an overshoot was suspected, the whole operation was repeated. Initially 4 sets of 25 observations were taken; the 100 observations resulting were considered to be sufficient to obtain reliable estimates of both the mean and standard deviation. The standard deviation of the mean is then (standard deviation of a single observation) /  $\sqrt{99}$ , and the 95% confidence interval of the estimate of the population standard deviation,  $S$ , derived from the  $\chi^2$ -distribution was 0.88  $S$  to 1.16  $S$ . After some experience however with very blurred targets, 10 sets of 10 observations were found to avoid fatigue more effectively, and therefore the majority of targets were observed in 10 sets of 10. *O'Connor (1967)* indicated that there was statistically no difference between results of 5 sets of 50 observations, and 10 sets of 10 in his experiments. Similar results were noted in these investigations where both 4 x 25 and 10 x 10 observations were taken, (targets 18, 19, 21 ). The number of observations to each target is shown with the results in Appendix B.

In addition to the blurred targets observed in this research, a number of sharp targets were also observed. This was done firstly to compare the two observers in these investigations with *O'Connor's (1967)* observers, and secondly to give a basis for judging the effects of blur on pointing accuracies.

#### 5.52 Elimination of Systematic Error.

The difficulties which arose in attempting to eliminate the systematic errors by observing in each direction may perhaps have been predicted, especially since conflicting conditions were imposed on the viewer. On the basis of these results the evidence is very clear that once a fixed observational technique has been established, observations can be consistent, provided the same technique continues. In the case of



pointing, a constant direction of approach is very important for reliable results. (see Chapter 7)

For the elimination of systematic errors, an observational technique has been devised, whereby the observer "sees" the MM to move always in the same direction in relation to the target. This is effected by a dove prism which can rotate the image of the target and MM through any required angle. The prism was used in two positions:

- (i) So that the MM appeared to move, as in the instrument, from the left - in this case the whole instrument was inverted.
- (ii) So that the MM appeared to travel from the left when in actual fact it travelled from the right - in this case the instrument was upright, but mirror reversed.

The procedure used in observing was to centre the MM, moving from the left with the dove prism in position (i). After recording, the MM was moved off to the right, the dove prism rotated to position (ii), and the MM recentered. It was proposed that this procedure of alternate observations would eliminate any variation in the systematic error. While this was not necessary for experienced observers, it was thought advisable for inexperienced observers whose systematic error tends to vary during sets.

Sharp targets only were observed in this series, because the correct target centre could be determined more accurately for sharp targets than for blurred targets. To eliminate any influence on the results, caused by the observer's recording his own measurements, readings were taken by an assistant. The whole instrument was arranged completely symmetrically with the adaptation screen symmetrical with the target, such that the external conditions did not affect the centering result. The exact location of the central position of the MM was found by taking theodolite observations of the widths of the annuli on each side of the MM for an approximately correct MM position, and subsequently adjusting the MM by half the difference in widths of the annuli. A Wild T3 was used for these

observations having a least count of 0.2 sec. (0.01 mm. on the target). The observations were taken twice each on 10 horizontal cross-sections over the target, giving standard deviations for the location of the central position of the MM of 0.03 mm. or 3  $\mu$ rad.

#### 5.53 Constant Stimulus Method.

The operation of the constant stimulus method is explained in section 4.45. Five settings were chosen and each presented to the observer 20 times in one sitting, lasting approximately 30 minutes. The order of presentations was random, according to numbers chosen from random number tables. Difficulty was encountered in obtaining suitable settings for the observations, and in some cases one or even two full sets had to be taken to find the values. Since different means and standard deviations result from this method, than from the average error method, readings obtained from the latter method could not be used as a guide for determining settings for the constant stimulus method. Each setting was presented to the observer by raising a shutter built into the adaptation screen. Replies were either "left" or "right" as advised by *Guilford (1954)*. In addition, replies of "doubtful left" and "doubtful right" were also allowed. These replies were included in the respective left and right categories when collecting the results, but gave a more acceptable reply to near central MM positions. Results of these observations and associated computations are given in Chapter 6 and Appendix B.

#### 5.54 Determination of Widths of Targets.

Since widths are an important factor in determining pointing accuracy, it was necessary to locate the edge of the target as part of the observational procedure. Edge location is a subjective determination (*Hempenius, 1968, 18*), depending on the illumination, observation distance and particularly the observer. Although a detailed study of the characteristics of edge location was not intended in this work, an estimate of widths was

necessary to relate pointing accuracies to characteristics of the target.

The measuring mark used for these observations was as shown in figure 5.3.

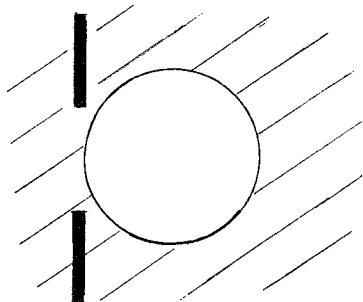


Fig. 5.3. Measuring mark used for edge location experiments.

The gap between the two sections gave the observer an unobstructed view of the whole target edge. Though it was necessary to visually interpolate the line across the edge of the target, it was felt that this arrangement was preferable to an unbroken line which tends to bias the observations. The width of the line was 1 mm. or 100  $\mu$ rad at the viewing distance of 10 m.

The first target observed for centering experiments was a 0.5 mrad annulus sharp target with 0.3 density background. Initial average error method pointing observations by JCT indicated a significant undershooting of the MM of 80  $\mu$ rad, though a standard deviation of 17  $\mu$ rad for a single observation could be obtained. To check that the observer perceived both edges of the target symmetrically with respect to the actual edges of the target, constant stimulus observations were carried out on both edges of the target without a black circular MM placed in the centre of the target. Further observations were taken with a black MM placed in the centre, on the left hand edge of the target and on the right hand edge of the MM. The full series of observations taken on this target are shown schemetically in figure 5.4, together with the results.

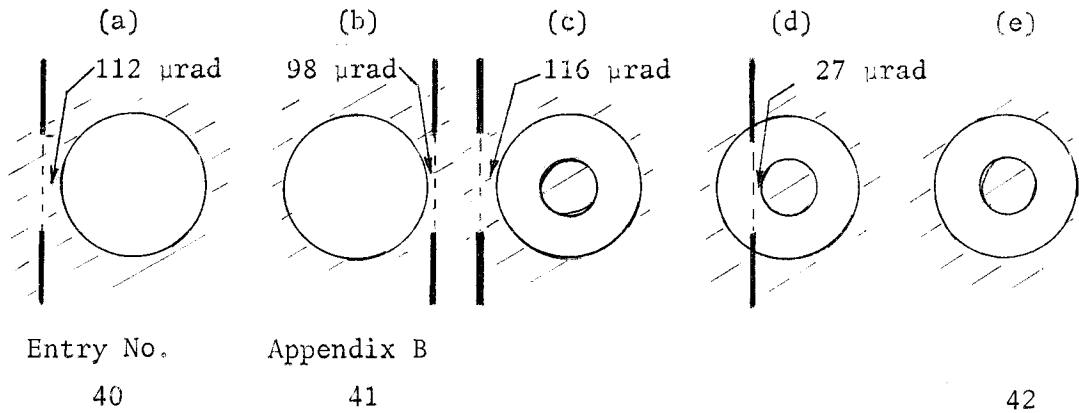


Fig. 5.4. Constant stimulus observations taken on 0.5 mrad target

As can be seen, no significant difference was observed between edge locations in (a) and (b), see Appendix B.3, or (a) and (c) and therefore the subjective locations of the edges of the targets were symmetrical with respect to true edges: the MM also did not alter the subjective location of the edge of the target. The location of the MM edge was particularly difficult, and little can be drawn from the above measurement, other than that the subjective edge of the MM is close to the true edge.

The widths of blurred targets were also initially observed by the constant stimulus method using 40 observations on each setting. However, it became clear when considering the low degree of accuracy of these determinations (the standard deviation was between 50 and 100  $\mu$ rad), and the relative unimportance of the width of blurred targets, in determining pointing accuracies, that a large number of observations was unwarranted. The bulk of the widths were therefore determined using the average error method, by approaching the edge from both directions. An extended rest period (usually overnight) was taken between each set. The location of the edge was then taken as the mean of the two sets. Several tests showed that edges determined by the above method and the constant stimulus method were not substantially different.

Both JCT and AHC observed the widths of the targets. This was necessary because each observer "saw" the edges of the target at different positions, AHC usually appearing to see the target wider than JCT. The widths of the targets observed are shown along with the data on each target in Tables 6.2 and 6.3. In the cases where density profiles of targets have been presented in Appendix C, location of edges are shown superimposed on these profiles.

Subjective width determinations of sharp targets of different background densities were not carried out as was thought necessary by *Trinder (1968)*. Since edge locations on blurred targets according to JCT and AHC were significantly different, it was clear that similar observations on sharp targets would be unwarranted. Different observers may see the width at quite widely distributed positions on the profile. For this reason the widths of the convolved curves in Chapter 3 were computed at a number of different levels of intensity. The fact that almost the same proportional difference in widths is obtained at the different intensity levels on the profiles (Table 3.1), is further evidence for not carrying out width determinations on sharp targets.

#### 5.6 Observers.

O'Connor's experiments indicated the possible variations in standard deviations for sharp targets with different observers. In addition to JCT a second observer, AHC, was therefore used for the investigations in this work. Considering the large amount of time necessary for each target (approximately half a day excluding the necessary rest breaks), it was impossible for AHC to observe every target. However, the targets observed by him are representative of the whole series. Occular and visual characteristics of both JCT and AHC may be found in Appendix E.

A number of additional observers were contracted to test the technique of eliminating the systematic errors. They were all young men in their final year at University, and there was no reason to suspect

that any of them should have serious defects in their vision. None of them had had experience in pointing other than in their training of 4 years at University. They may be classed as unskilled, but generally observations by such students with theodolites might be termed fair. Each observer made 30 observations from each direction alternately.

#### 5.7 Production of Targets.

##### 5.71 Sharp Targets and MM.

The sharp targets were cut from photographic film of a specific density using a sharp compass. Background density of the targets was chosen as 0.30 D, though pointing accuracies are not influenced by background density (*O'Connor, 1967*) for the range of annulus widths being investigated. The MM, 1.0 mrad in diameter was made of aluminium sheeting and adhered to the MM slide with black paint.

##### 5.72 Blurred Targets.

*Trinder (1965)* developed an optical analogue computer (termed "Umbrascope") for the purpose of carrying out convolutions of annuli and point spread functions. It was intended to use targets with gaussian blur characteristics in this research because the general blurring characteristics of photographic systems closely approach a gaussian function, i.e. the spread functions of photographic systems are approximately gaussian (*Hempenius, 1965*) (*Wolfe and Tuccio, 1960*). The Umbrascope equipment was used to carry out similar convolutions of sharp circular targets, and gaussian spread functions to produce blurred targets for this research.

In figure 5.5, the variable transmittance pattern on shelf A transmits illumination according to a gaussian function. The circular pattern which is graded in discrete steps of 10%, is made up of layers of film of different densities, such that the curve joining the centres of the steps is a gaussian curve of transmittance. This pattern represents the point spread function to be used for the convolution.

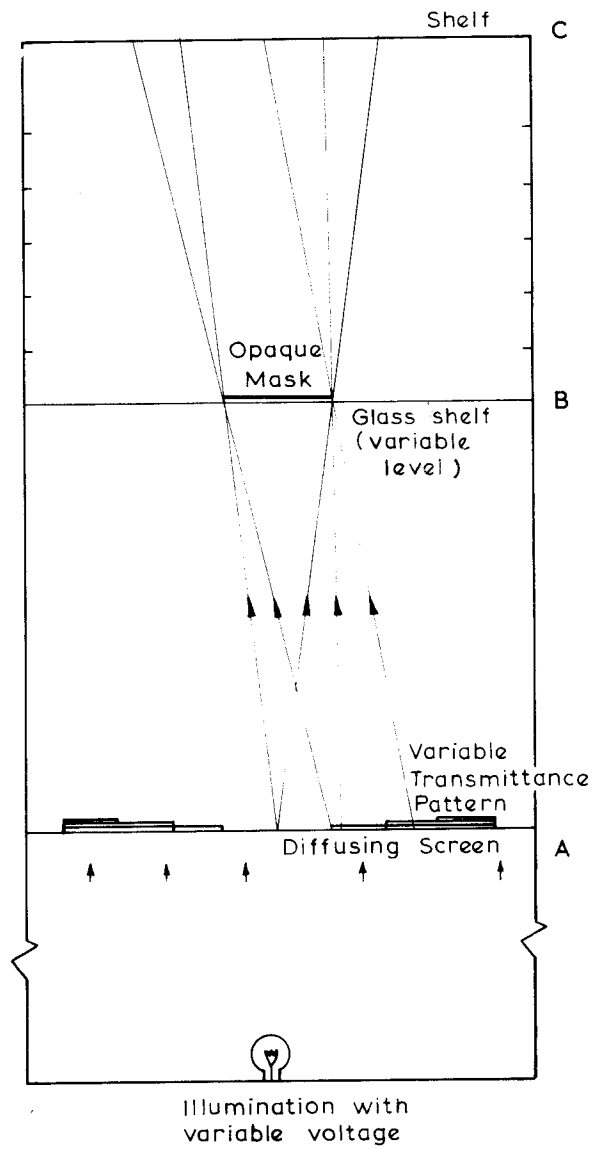


FIG: 5.5: ANALOGUE COMPUTER "UMBRASCOPE" USED FOR PRINTING BLURRED TARGETS

The steps are not apparent in the pattern after convolution on shelf C, because diffused light is used.

The opaque area on the intermediate glass shelf B, the circular sharp target, masks out the central area on the top shelf C from the projected light. However, since the illumination is diffused, light from the edges of the transmittance pattern will partially illuminate the masked area, as shown in figure 5.5. The extent to which the masked area is illuminated depends on the level of the intermediate shelf B, and the size of the target on shelf B. When the shelf B is close to shelf C, the pattern on C, the blurred target, is dark in the centre and grades sharply to light at the edges. If the shelf B is close to A, the illumination from both sides of the transmittance pattern overlaps, giving a pattern on C which is grey in the centre and graded to light on the edges. Because a significant amount of blur is necessary before pointing accuracies are affected, most targets were printed with the blur patterns overlapping, giving only small changes in density on the target from background to centre.

The accuracy of this technique has been discussed before (*Trinder, 1965*). It was conceded that the two main limitations are firstly in the efficiency of the diffusing screen below the pattern, and secondly in the increasing inefficiency of the illumination of inclined rays from the edges of the transmittance pattern. The diffusing screen in the instrument was Polacote referred to in section 5.4. The second factor depends on  $\text{Cos}^4$  (angle of inclination of ray) and becomes particularly significant for greatly inclined rays. However, the inclination of rays generally was  $10^\circ$  or less and therefore this effect is only small. Background densities around the targets did not vary more than .02 to .04, for a distance of 4 cm. from the edges of the photographed target.

Tests with this equipment (*Trinder, 1965*) and in the present work show close comparisons between a theoretical gaussian curve and the



profiles actually obtained. Examples of the comparison are shown in figure 5.6. The  $\sigma$ -values of the effective spread function for six levels in the Umbrascope, and two different gaussian patterns are shown in Table 5.1.

Table 5.1.

$\sigma$  - values of spread functions for six levels of the Umbrascope expressed as mrad for a viewing distance of 10 m.

<u>Level</u>	<u>Pattern</u>	
	1	2
1	.95	1.4
2	.73	1.1
3	.55	0.82
4	.36	0.58
5	.20	0.37
6	.04	0.10

Although small discrepancies exist in the comparisons in figure 5.6, these did not affect the assessment of results, since all targets were measured on a Joyce Lobel Automatic Recording Microdensitometer and therefore the exact profile of the target was obtained. The approximation to a gaussian function however is sufficiently close for comparison with photographic systems in Chapter 8.

Targets were printed on photographic film (Gevaert N31P) with a  $\gamma$  of approximately 1. Three different background densities of 0.25, 0.4 and 0.7 were chosen, covering the normal range of densities occurring in photogrammetry. The sizes of the targets were also those normally found in photogrammetry, giving annuli ranging from 0.3 mrad to 5.0 mrad, equivalent to annulus widths of 7.5  $\mu$  to 160  $\mu$  at 10x magnification in a photogrammetric instrument, or target sizes of 55  $\mu$  to 360  $\mu$ , using a MM of 40  $\mu$ . Printing the targets onto film gave a light central area with a dark background.

The profiles of the targets were recorded at a linear magnification of 5x on the microdensitometer. Fine reference scratches on the targets,

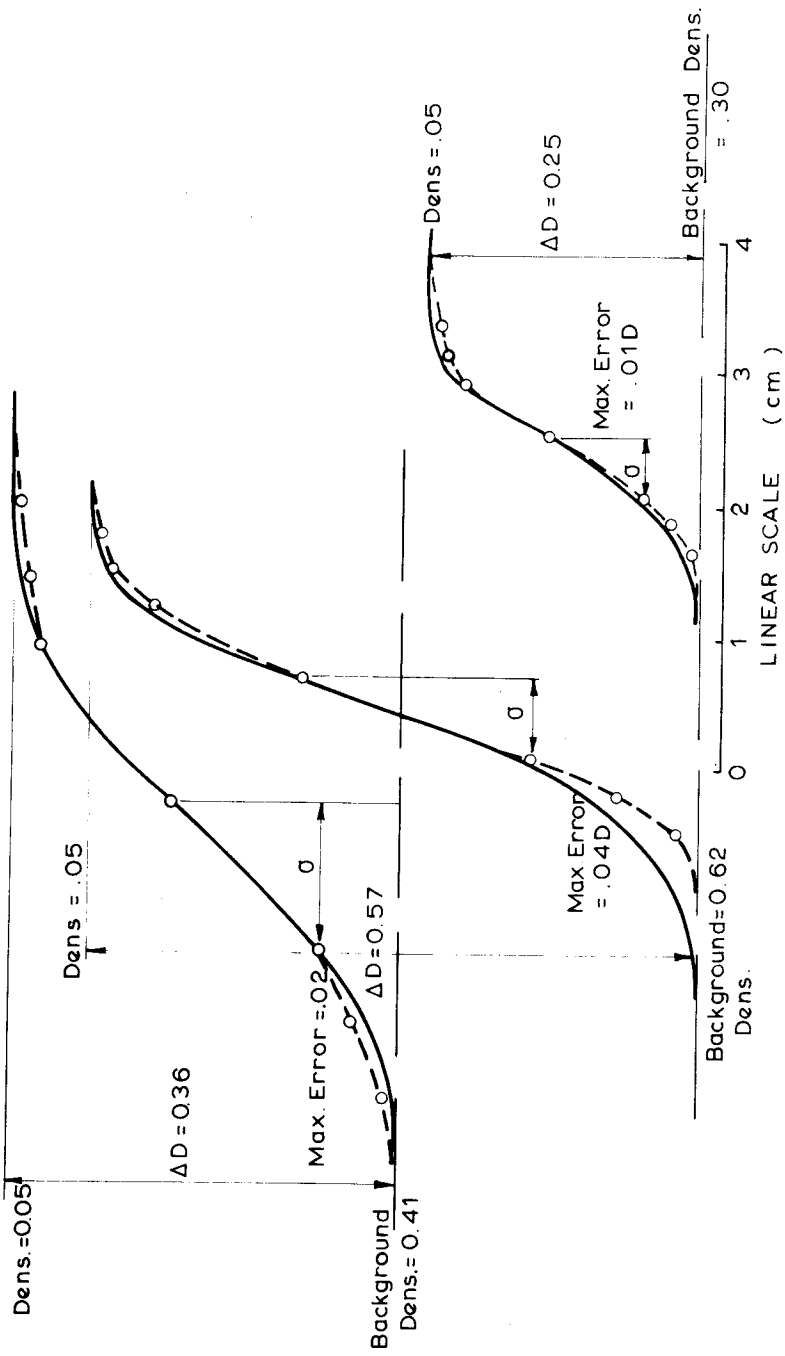


FIG. 5.6: Comparison between microdensitometer traces of blurred targets and gaussian integral curves (shown by broken line). In all cases the curves represent "edge" profiles, since the blur patterns on each side of the target do not overlap.

also recorded on the trace, were used to calibrate the target for finding the systematic error. Though the magnitude of systematic errors was not considered a significant part of this research, it was thought that an impression of the way in which systematic errors behave could be gained from the observations. The centre of the target was derived from the symmetrical density trace of the profile, and referred to the micrometer readings via the reference scratches.

To describe the target, the trace was analysed in terms of 3 elements - background density, the grade of the blur of the target in  $\Delta D/\text{mrad}$ , and the width of the annulus derived from observations in section 5.53. The flanks of the profiles of the targets were sufficiently long to allow accurate estimation of the grade of blur. Results of the observations will be presented in Chapters 6 and 7.

6. STANDARD DEVIATIONS OF OBSERVATIONS TO SHARP AND BLURRED TARGETS - PRESENTATION OF RESULTS.

6.1 Introduction.

The results of the observations to blurred and sharp targets are summarized in Tables 6.1 to 6.4. Examples of statistical tests which have been carried out on all targets may be found in Appendix B. Table 6.1 contains results of observations by both JCT and AHC on sharp targets. Since the blurred targets have been investigated in terms of three variables, i.e. target blur, width and background density, pointing accuracies for blurred targets using the average error method have been presented under the heading of background densities, and under separate sub-headings of grade of blur, and target width in Tables 6.2 and 6.3. In cases where a viewing distance of 5 m. was used, observations have been appropriately marked; the remainder were observed at a distance of 10 m. Observations carried out by JCT at the higher adaptation level are also included in Table 6.2. The systematic errors presented in Tables 6.2 and 6.3 are for the MM moving from the left. A discussion on systematic errors may be found in Chapter 7. Results of centering observations by the constant stimulus method are summarized in Table 6.4, while examples of associated computations are given in Appendix B.3.

With regard to the use of statistics in psychophysical research, the large number of possible variables entering into the investigations must be kept in mind. *Graham's (1951)* statement given in section 4.3 shows that the psychophysical response to stimuli may depend on many factors such as motivation, attitude, time etc. as well as the stimulus conditions being investigated. Statistics require the treatment of homogeneous data of the same statistical registration. If additional variables enter into the investigations, then theoretically the application of statistics is invalid, unless these variables are included in the statistical tests.

In this study, statistical testing has been used as a guide in Appendix B, and in the following analysis of variance. The analysis

Table 6.1.

Summary of Standard Deviations and Systematic Errors of Pointing to Sharp Targets.

Width mrad	Viewing Dist. (m)	S μrad	System. Error μrad	Target No.
Observer - JCT				
0.5	10 m	16.7	Undershoot 75*	1
1.0	10	13.9	Overshoot 30	2
2.0	10	22.3	" 16	3
5.0	10	43.5	" 18	4
1.0	5	16.0	Undershoot 58*	2a
2.0	5	22.8	0*	3a
4.0	5	38.0	-	4a
Observer - AHC				
0.5	10	16.0	Undershoot 40	1b
1.0	10	17.1	0	2b
2.0	10	29.3	Overshoot 176	3b
5.0	10	53.8	" 211	4b
2.0	5	26.2	-	3c

\* Systematic Errors not plotted in Figs. 7.1 and 7.2

Table 6.2.

Summary of Standard Deviations and Systematic  
Errors of Pointing to Blurred Targets

Observer: JCT

Background Density = 0.25 : Argument - Grade of Blur

Blur $\Delta D/mrad$	Width mrad	Back. Dens.	Stand. Dev. $\mu rad$	System. Error $\mu rad$	No.
0.012	2.2	0.24	104.0	u'shoot 280*	5
0.015	5.5 (5m)	0.20	114.0	o'shoot 720	6
0.017	2.2	0.17	81.6	" 720	7
0.024	5.5 (5m)	0.20	84.0	" 460	8
0.025	2.0	0.20	67.9	" 60	9
0.031	2.4	0.25	56.5	" 160	10
0.035	2.0	0.30	50.7	" 160	11
0.037	2.0	0.26	58.5	" 320	12
0.040	0.6	0.19	56.3	" 370	13
0.042	1.9	0.20	41.0	" 450	14
0.043	4.6 (5m)	0.25	60.6	" 370	15
0.072	0.4	0.22	33.7	0*	16
0.077	0.9	0.20	29.9	" 50	17
0.082	1.7	0.30	30.0	-	18
0.10	2.7	0.26	25.6	-	19
0.10	0.9	0.23	28.9	" 100	20
0.12	1.5	0.24	24.7	0*	21
0.125	0.8	0.23	23.8	" 40	22
0.15	0.3	0.22	34.0	u'shoot 80*	23
0.195	0.9	0.25	21.6	o'shoot 20	24
0.50	1.4	0.30	17.1	" 20	25
1.0	0.6	0.30	15.6	" 49	26

\* Systematic Errors not plotted in Figs. 7.1 and 7.2

Table 6.2. (Contd.)

Observer: JCT

Background Density = 0.25 : Argument - Annulus Width.

Width mrad	Blur $\Delta D/mrad$	Back. Dens.	Stand. Dev. $\mu rad$	System. Error $\mu rad$	No.
0.3	0.15	0.22	34.0	u'shoot 80*	23
0.4	0.072	0.22	33.7	0*	16
0.6	0.040	0.19	56.3	o'shoot 370	13
0.6	1.0	0.30	15.6	" 49	26
0.8	0.125	0.23	23.8	" 40	22
0.9	0.10	0.23	28.9	" 20	20
0.9	0.195	0.25	21.6	" 20	24
0.9	0.077	0.20	29.9	" 50	17
1.4	0.50	0.30	17.1	" 20	25
1.5	0.12	0.24	24.6	0*	21
1.7	0.082	0.30	29.5	-	18
1.9	0.042	0.20	41.0	" 450	14
2.0	0.037	0.26	58.5	" 320	12
2.0	0.035	0.30	50.7	" 160	11
2.0	0.025	0.20	67.9	" 60	9
2.2	0.012	0.24	104.0	u'shoot 280*	5
2.2	0.017	0.17	81.6	o'shoot 720	7
2.4	0.031	0.25	56.5	" 160	10
2.7	0.10	0.26	26.5	-	19
4.6 (5m)	0.043	0.25	60.6	" 370	15
5.5 (5m)	0.024	0.20	84.0	" 460	8
5.5 (5m)	0.015	0.20	114.0	" 720	6

\* Systematic Errors not plotted in Figs. 7.1 and 7.2

Table 6.2. (Contd.)

Observer: JCT

Background Density = 0.40 : Argument - Grade of blur.

Blur $\Delta D/\text{mrad}$	Width mrad	Back. Dens.	Stand. Dev. $\mu\text{rad}$	System. Error $\mu\text{rad}$	No.
0.024	2.3	0.40	69.8	o'shoot 380	27
0.032	2.0	0.44	51.0	" 280	28
0.050	1.8	0.45	46.0	" 150	29
0.053	1.8	0.40	36.2	" 220	30
0.065	2.0	0.40	37.0	" 50	31
0.09	1.2	0.40	30.6	" 100	32
0.12	1.7	0.44	26.2	" 80	33

Background Density = 0.40 : Argument Annulus width

Width mrad	Slope $\Delta D/\text{mrad}$	Back. Dens.	Stand. Dev. $\mu\text{rad}$	System. Error $\mu\text{rad}$	No.
1.2	0.09	0.40	30.6	o'shoot 100	32
1.7	0.12	0.44	26.2	" 80	33
1.8	0.053	0.40	36.2	" 220	30
1.8	0.05	0.45	46.0	" 150	29
2.0	0.065	0.40	37.0	" 50	31
2.0	0.032	0.44	51.0	" 280	28
2.3	0.024	0.40	69.8	" 380	27



Table 6.2 (Contd.)

Observer: JCT

Background Density = 0.70 : Argument - Grade of Blur

Blur $\Delta D/\text{mrad}$	Width mrad	Back. Dens.	Stand. Dev. $\mu\text{rad}$	System. Error $\mu\text{rad}$	No.
0.021	2.5	0.71	80.3	o'shoot 240	34
0.043	1.9	0.75	37.6	" 250	35
0.046	2.5	0.62	45.8	" 280	36
0.085	2.2	0.69	33.7	" 330	37
0.089	1.6	0.69	31.3	" 490	38
0.15	1.1	0.69	25.5	" 80	39

Background Density = 0.70 : Argument - Annulus Width.

Width mrad	Slope $\Delta D/\text{mrad}$	Back. Dens.	Stand. Dev. $\mu\text{rad}$	System. Error $\mu\text{rad}$	No.
1.1	0.15	0.69	25.5	o'shoot 80	39
1.6	0.089	0.69	31.3	" 490	38
1.9	0.043	0.75	37.6	" 250	35
2.2	0.085	0.69	33.7	" 330	37
2.5	0.046	0.62	45.8	" 280	36
2.5	0.021	0.71	80.3	" 240	34

Higher Adaptation Level - Observer JCT.

Blur $\Delta D/\text{mrad}$	Width mrad	Back. Dens.	Stand. Dev. $\mu\text{rad}$	System. Error $\mu\text{rad}$	No.
0.015	5.5	0.20	149.0	o'shoot 800	6a
0.024	5.5	0.20	113.0	" 720	8a
0.043	5.3	0.25	77.2	" 180	15a
0.018	2.2	0.26	104.0	" 400	12a
0.032	2.0	0.44	76.2	" 400	31a

Table 6.3.

Summary of Standard Deviations and Systematic  
Errors of Pointing to Blurred Targets

Observer: AHC

Background Density = 0.25 : Argument - Grade of Blur.

Blur $\Delta D/\text{mrad}$	Width mrad	Back. Dens.	Stand. Dev. $\mu\text{rad}$	System. Error $\mu\text{rad}$	No.
0.015	5.5	0.20	126.8	-	6b
0.042	2.3	0.20	40.5	-	14b
0.043	5.0	0.25	73.6		15b
0.077	0.80	0.20	28.1	0	17b
0.082	2.4	0.30	27.5	-	18b
0.10	2.7	0.30	23.1	-	19b
0.12	1.5	0.24	22.7	u'shoot 110	21b
0.125	1.0	0.23	25.9	" 40	22b
0.15	0.3	0.22	48.1	" 210	23b
0.195	1.2	0.25	23.5	-	24b
0.50	1.2	0.30	16.0	" 52	25b
1.0	0.6	0.30	17.3	o'shoot 20	26b

Background Density = 0.25 : Argument - Annulus Width

Width mrad	Blur $\Delta D/\text{mrad}$	Back. Dens.	Stand. Dev. $\mu\text{rad}$	System. Error $\mu\text{rad}$	No.
0.3	0.15	0.22	48.1	u'shoot 210	23b
0.6	1.0	0.30	17.3	o'shoot 20	26b
0.8	0.077	0.20	28.1	0	17b
1.0	0.125	0.23	25.9	u'shoot 40	22b
1.2	0.195	0.25	23.5	-	24b
1.2	0.50	0.30	16.0	-	25b
1.5	0.12	0.24	22.7	" 110	21b
2.3	0.042	0.20	40.5	-	14b
2.4	0.082	0.30	29.5	-	18b
2.7	0.10	0.30	23.1	-	19b
5.0	0.043	0.25	73.6		15b
5.5	0.015	0.20	126.8		6b

Table 6.3. (Contd.)

Observer: AHC

Background Density = 0.40 : Argument - Grade of Blur

Blur $\Delta D/\text{mrad}$	Width mrad	Back. Dens.	Stand. Dev. $\mu\text{rad}$	System. Error $\mu\text{rad}$	No.
0.024	2.9	0.40	83.3	o'shoot 200	27b
0.032	2.3	0.44	64.4	" 50	28b
0.050	1.8	0.45	54.0	" 50	29b
0.090	1.6	0.40	24.2	" 30	32b
0.12	2.7	0.44	30.3	" 50	33b

Background Density = 0.40 : Argument - Annulus Width

Width mrad	Blur $\Delta D/\text{mrad}$	Back. Dens.	Stand. Dev. $\mu\text{rad}$	System. Error $\mu\text{rad}$	No.
1.6	0.09	0.40	24.2	u'shoot 30	32b
1.8	0.05	0.45	54.0	o'shoot 50	29b
2.3	0.032	0.44	64.4	" 50	28b
2.7	0.12	0.44	30.3	" 50	33b
2.9	0.024	0.40	83.3	" 200	27b

Background Density = 0.70

2.5	0.085	0.69	30.3	o'shoot 270	37b
-----	-------	------	------	-------------	-----

Table 6.4

Constant Stimulus Method Results

Observer: JCT

Blur $\Delta D/mrad$	Width mrad	Back. Dens.	Stand. Dev. $\mu rad$	System. Error $\mu rad$	No.
0.042	1.9	0.20	79.3	o'shoot 270	14
0.09	1.2	0.40	45.0	" 140	32
0.12	1.5	0.24	34.0	" 30	21
0.50	1.4	0.30	19.1	" 11	25
1.0	0.6	0.30	17.1	" 61	26
Sharp	0.5	0.30	18.9	0	1

Observer: AHC

Blur $\Delta D/mrad$	Width mrad	Back. Dens.	Stand. Dev. $\mu rad$	System. Error $\mu rad$	No.
0.042	2.3	0.20	132.5	o'shoot 191	14
0.09	1.5	0.40	83.7	u'shoot 138	32
0.12	1.5	0.24	40.0	" 38	21
0.50	1.2	0.30	28.4	" 46	25
1.0	0.6	0.30	29.5	o'shoot 21	26

indicates that target width and blur are significant while background density is only a marginally significant property of the target affecting pointing accuracies. Further work on regression in section 6.3 will indicate the small differences between pointing accuracies for different backgrounds. A very much larger sample of observations than is used in this research, taken over a very extended period would be necessary to investigate all possible factors affecting accuracies. Such an amount of work would be impractical considering the very limited advantages gained. Statistical theory is considered as a very useful tool in psychophysical testing, but one which must be used carefully.

The results in Table 6.2 were firstly tested by an analysis of variance according to the method outlined by *Moroney (1952, Ch. 19)*, in the following section.

## 6.2 Analysis of Variance.

In section 5.3 it was pointed out that four separate analyses were necessary to test the effects of the three variables. The values used for the tests were ten individual variances derived by sets of ten observations.

### *(i) Background density against Target blur - Test No. 1.*

Five categories of target blur and three background densities were used as shown in Table 6.51. The actual values of the grade of blur and background density agreed closely with nominal values given in the table. The width of all targets was approximately 2.0 mrad except target No. 39 which was 1.1 mrad wide. This target however did not disturb the observations, since the effect of widths as seen in the subsequent analyses is small.

Table 6.51.

Back D	0.25		0.40		0.70	
Grade of blur $\Delta D/mrad$	Target	Variance	Target	Variance	Target	Variance
0.12	21	622.7	33	687.1	39	651.3
0.09	19	590.3	32	936.8	38	983.0
0.08	18	960.1	31	1369.0	37	1132.2
0.045	14	1685.6	30	1310.4	35	1413.5
0.023	9	4609.0	27	4872.0	34	6446.0

Table 6.52.

Source	Sum of Squares	Degrees of Freedom	Variance Est.	Test
Blur	42164	4	$10541 = S^2_4$	$\frac{S^2_4}{S^2_1} = 83^*$
Black Dens.	996	2	$498 = S^2_3$	$\frac{S^2_3}{S^2_1} = 3.95$
Interaction	3198	8	$400 = S^2_2$	$\frac{S^2_2}{S^2_1} = 3.15^*$
Residual	17035	135	$126 = S^2_1$	
Total	63393	149		

There are 10 determinations of each variance in Table 6.51, giving 149 degrees of freedom in the test. Tests carried out on the variance estimates are shown in Table 6.52. Blur, clearly, is the dominant factor in the test, being significant at all levels, while background density proves to be significant at the 95% level. Interaction between the two effects, blur and background density is significant at the 99% level. In view of the very significant effect of the blur of the target compared with the background density, and also the fact that the background density effect itself is significant only at 95% level, the interaction effect will be neglected. This effect is only just significant at the levels tested, and considering the variable nature of the performance of observers, as is indicated by the spread of results about the regression lines in figures 6.1 and 6.2, it is considered that this action is warranted. The conclusion that background density does not affect pointing accuracies of blurred targets is identical with *O'Connor's (1967)* conclusions on pointing accuracies of sharp targets for annuli greater than 0.3 mrad.

(ii) *Target Blur against annulus sizes.*

One test was carried out for annulus sizes of 0.8 and 2.0 mrad, against target blur, and two separate tests were carried out for annulus sizes of 2.0 mrad and 5.0 mrad, one at 15 mL adaptation level, and the other at a higher adaptation level. It was mentioned in section 5.51 that a number of observations were carried out a higher adaptation level. These results which were presented in Table 6.2 to provide further testing material for the influence of annulus sizes, have not been used for a quantitative estimate of the influence of adaptation level on accuracies, because the exact value of the higher adaptation was unknown.

(a) Target Annulus sizes 0.8 and 2.0 mrad - Test No. 2.

Table 6.61.

Size Target Blur $\Delta D/\text{mrad}$	0.8 mrad		2.0 mrad	
	Target	Variance	Target	Variance
0.12	22	557.6	21	610.4
0.10	20	847.4	19	654.9
0.08	17	895.4	18	895.9
0.04	13	3165.3	14	1685.6

Table 6.62.

Source	Sum of Squares	Degrees of Freedom	Variance Est.	Tests
Target blur	4361	3	1450 = $S_4^2$	$\frac{S_4^2}{S_1^2} = 450^*$
Size	432	1	432 = $S_3^2$	$\frac{S_3^2}{S_1^2} = 13^*$
Inter.	982	3	328 = $S_2^2$	$\frac{S_2^2}{S_1^2} = 93^*$
Residual	2300	72	32 = $S_1^2$	
Total	8075	79		



(b) Target Annulus sizes 2.0 mrad and 5.0 mrad.  
Adaptation Level = 15 mL - Test No. 3.

Table 6.71.

Size mrad  Target Blur $\Delta D/mrad$	2.0		5.0	
	Target	Variance	Target	Variance
0.043	14	1685.6	15	3674
0.024	9	4609.0	8	7017
0.015	7	6658.0	6	12972

Table 6.72.

Source	Sum of Squares	Degrees of Freedom	Variance Est.	Test
Target blur	48381	2	$24000 = S^2_4$	$\frac{S^2_4}{S^2_1} = 46^*$
Size	24762	1	$24000 = S^2_3$	$\frac{S^2_3}{S^2_1} = 46^*$
Interaction	9128	2	$4563 = S^2_2$	$\frac{S^2_2}{S^2_1} = 8.6^*$
Residual	28387	54	$525 = S^2_1$	
Total	110657	59		

(c) *Targets Annulus sizes 2.0 and 5.0 mrad at Higher Adaptation Level - Test No. 4.*

Table 6.81.

Size mrad Target blur $\Delta D/mrad$	2.0		5.0	
	Target	Variance	Target	Variance
0.038	31a	5813	8a	12748
0.020	12a	10918	6a	22458

Table 6.82.

Source	Sum of Squares	Degree of Freedom	Variance Est.	Test
Target Blur	1184	1	$1184 = S_4^2$	$\frac{S_4^2}{S_1^2} = 22^*$
Sizes	721	1	$721 = S_3^2$	$\frac{S_3^2}{S_1^2} = 13^*$
Interaction	43	1	$43 = S_2^2$	$\frac{S_2^2}{S_1^2} = 0.8^*$
Residual	1920	36	$53 = S_1^2$	
Total	3869	39		

In all tests, the blur of the target is clearly the most significant factor. The widths of targets in the three tests also proved to be significant, while two tests indicated that the interaction between widths and blur is significant.

Conclusions based on the tests in this section may be stated as follows. The most significant effect on pointing accuracies over the ranges tested is the blur of the target. Widths of the annulus are a secondary effect, while the interaction between these factors is also marginally significant. There may be some interaction between background density and grade of the blur, though this effect is very small. It is possible that further minor interactions may exist between all three elements, but these effects are not worthy of investigation. When considering the practical applications of this research only the most significant features need be investigated, since one may expect variations from one observer to the next for the same target. This is clearly indicated by the results of *O'Connor (1967)* as well as the present research. In addition, other observers may indicate different characteristics with respect to the interactions mentioned above. *O'Connor* for instance, found that pointing accuracies in the x and y-directions were significantly different for himself for annuli smaller than 0.3 mrad, but not for other observers. The visual system, and the psychophysical aspects involved in visual tasks are very complex and over simplification of the processes involved are unwarranted. The two aspects of blur and width only will therefore be investigated in the following section, by regression analysis.

### 6.3 Regression Analysis.

Based on the work in the previous section, it was found necessary to carry out separate regression analyses for the three widths of 0.8, 2.0 and 5.0 mrad. Plots of the results on logarithm scales indicated a linear relationship between the logarithms of pointing accuracy and target blur. Regression analyses were carried out according to the formulae derived in

Appendix A, i.e.  $y = ax + b$ , where  $y =$  logarithm of pointing standard deviation,  $x =$  logarithm of grade of blur, and  $a$  and  $b$  are parameters. Details of the computed parameters, and targets used are given in Table 6.9. Regression lines for annulus sizes of 2 mrad for three background densities are given in figure 6.1. Since these lines did not differ significantly and the analysis of variance indicated a very marginal influence of the background densities, the regression lines for the three annulus widths given in figure 6.2 are based on the combined results of all densities. The regression lines in figures 6.1 and 6.2, plus the 99% confidence limits as shown in figure 6.2 were computed based on weights inversely proportional to the (standard deviations)<sup>2</sup>. The same regression lines were also computed using equal weights. Results of AHC given in figure 6.3 were initially computed using weights inversely proportional to the variance. However, because of uneven distribution of points along the regression line, and significantly larger weights for points on the lower end of the line, weighted values gave a poor location of the regression line. The regression line in figure 6.3 was therefore computed using equal weights. Regression lines computed in figure 6.2 using weights as above, and equal weights showed no significant difference. Weights were therefore excluded from subsequent regression analyses.

The regression lines for the 0.8 mrad and 2.0 mrad annuli are very close in figure 6.2, indicating the very small effect of the size of the annulus of the target over this range. The regression line for the 5.0 mrad annulus on the other hand, indicates a marked increase in the standard deviations. Since a greater variation is evident in the results of AHC as seen in figure 6.3, only one regression line was computed for the range of annulus widths 0.8 to 2.0 mrad. Regression lines for 5.0 mrad were derived from three targets by JCT and two targets by AHC. There is good agreement between the line and individual plotted points in figure 6.2 for observations by JCT, and therefore the regression line appears acceptable. The line computed from two targets observed (each derived by  $6 \times 10$  observations) by AHC would converge on the 2.0 mrad line. Since this

Table 6.9.

No.	Widths	Target Nos.	Parameters		Weights	Observer
			a	b		
1	2.0, D=0.25	5,7,9,10,11,12	-0.617	0.815	equal	JCT
		14,18,19,21	-0.617	0.809	unequal	
2	2.0, D=0.4	27,28,29,30,31	-0.576	0.878	equal	JCT
		32,33,	-0.539	0.919	unequal	
3	2.0, D=0.7	34-39	-0.548	0.926	equal	JCT
			-0.443	1.037	unequal	
4	0.8	13,16,17,20,22,24,	-0.495	0.993	equal	JCT
			-0.532	0.938	unequal	
5	2.0	5,7,9,10,11,12,14,	-0.583	0.867	equal	JCT
		18,19,21,27-39	-0.543	0.904	unequal	
6	5.0	6,8,15	-0.598	0.962	equal	JCT
7	0.8-2.0	14,17,18,19,21-29	-0.654	0.791	equal	AHC
		32,33,37				
8	5.0	6b,15b	-0.710	0.838	equal	AHC
9	2.0	49,51,53	-0.794	0.810	equal	JCT const. stim.meth.
10	2.0	50,52,54	-0.802	0.957	equal	AHC const. stim.meth.

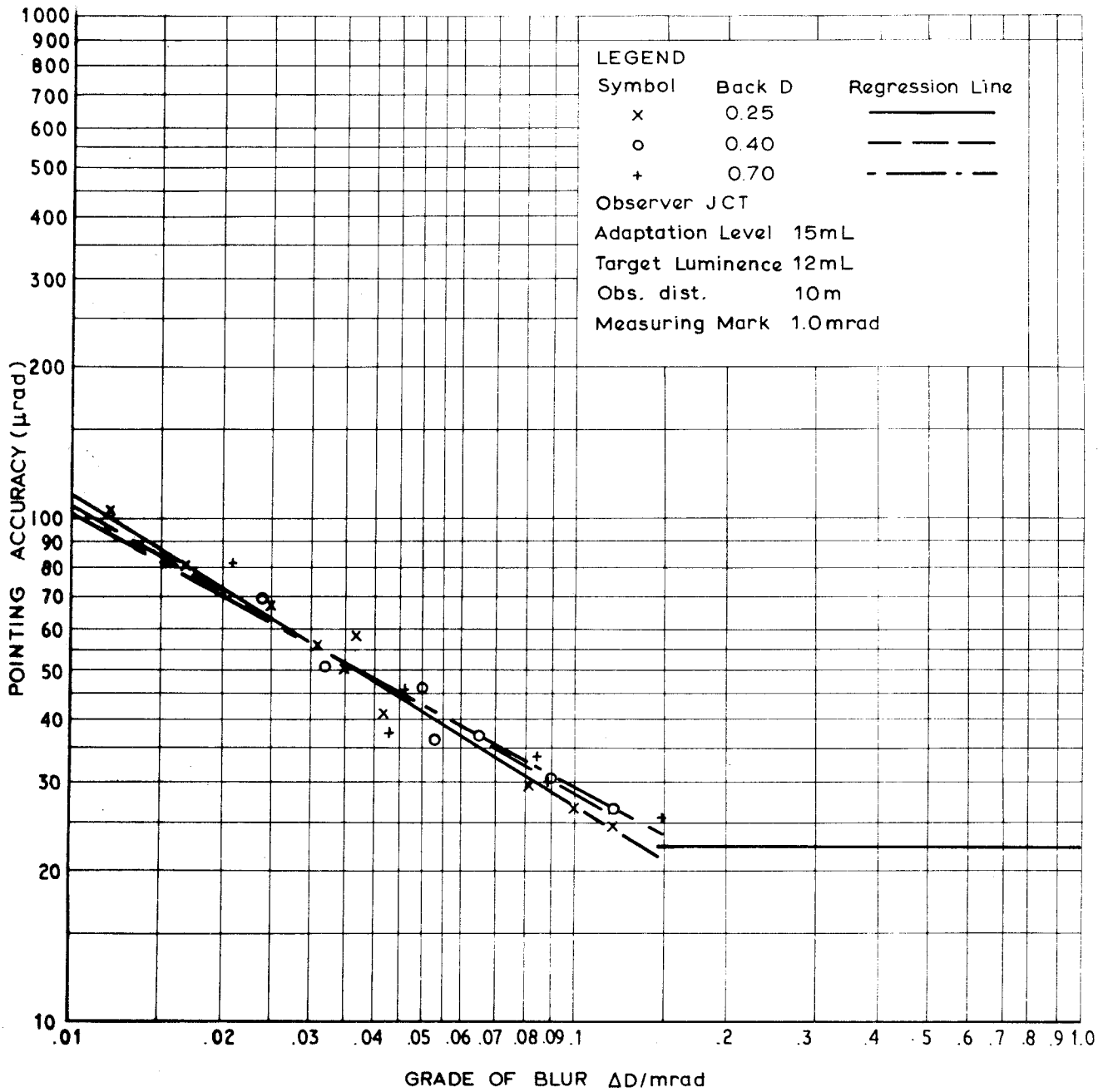
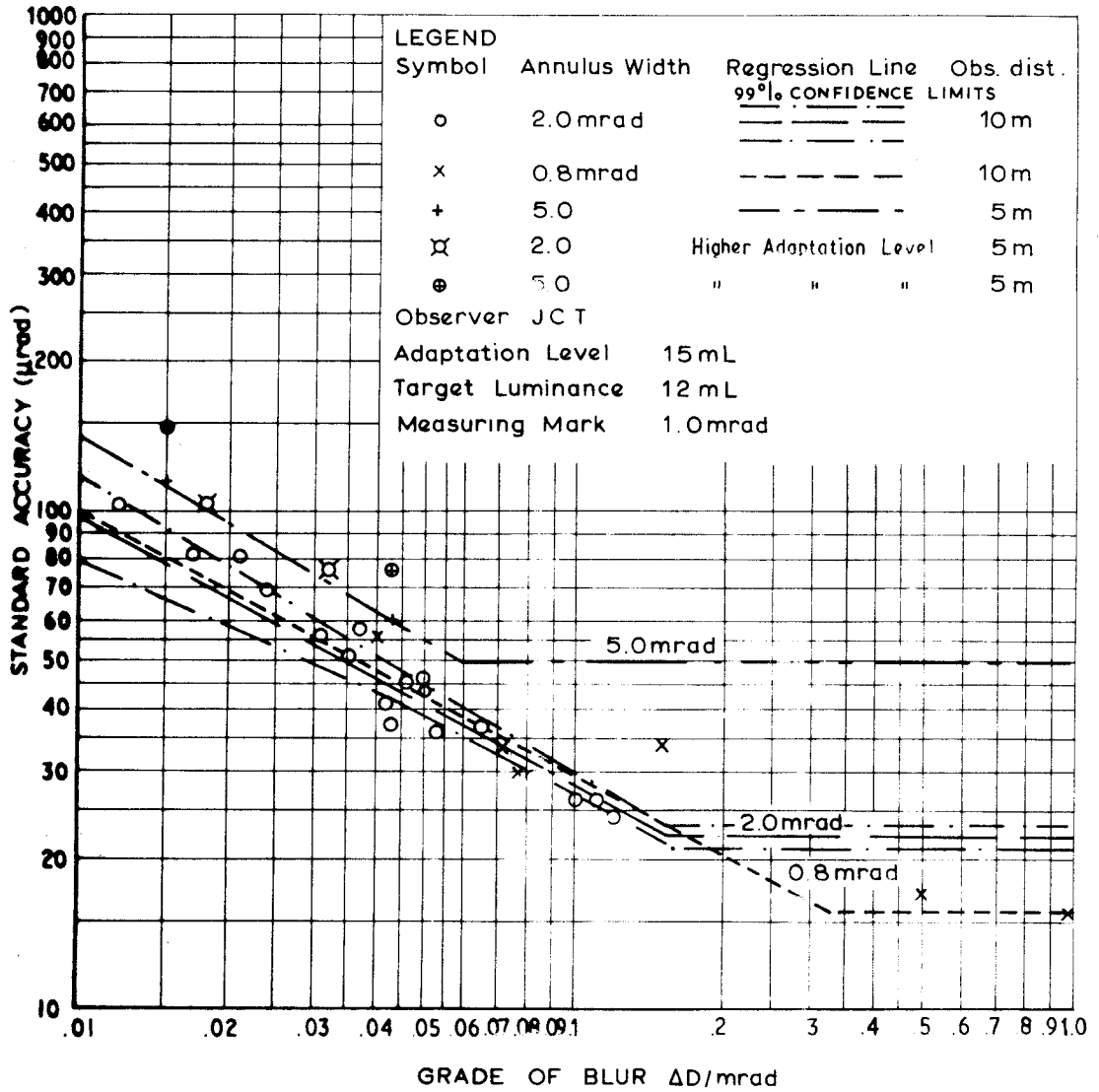


FIG. 6.1: POINTING STANDARD DEVIATIONS AGAINST TARGET BLUR FOR 3 DIFFERENT BACKGROUND DENSITIES, AND ANNULUS SIZES OF 2mrad. REGRESSION LINES HAVE BEEN COMPUTED USING WEIGHTS PROPORTIONAL TO THE (STANDARD DEVIATIONS)<sup>2</sup>



**FIG. 6.2: POINTING STANDARD DEVIATIONS AGAINST TARGET BLUR, FOR 3 TARGET ANNULUS WIDTHS. REGRESSION LINES HAVE BEEN COMPUTED USING WEIGHTS INVERSELY PROPORTIONAL TO THE (STANDARD DEVIATIONS.)<sup>2</sup>**

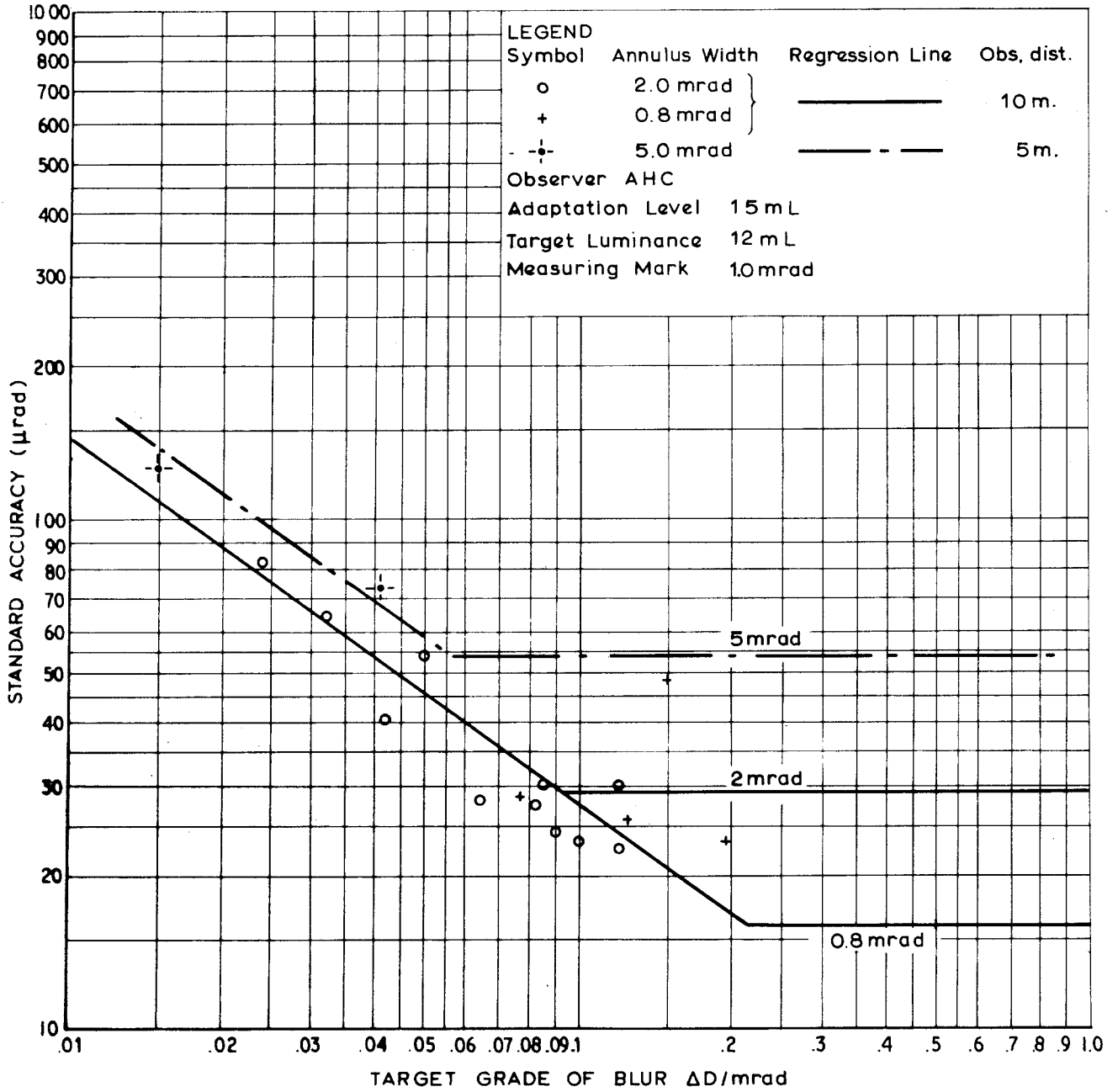


FIG. 6.3: POINTING STANDARD DEVIATIONS, AGAINST TARGET BLUR, FOR 3 TARGET ANNULUS WIDTHS. REGRESSION LINES HAVE BEEN COMPUTED USING EQUAL WEIGHTS.



seemed unlikely, after the results of JCT, the regression line has been located approximately parallel to the 2.0 mrad line, and equidistant between the two points.

Figure 6.4 shows the DL's derived by the constant stimulus method (CSM) plotted against target blur characteristics for annulus widths of 2.0 mrad. For comparison, the regression lines for 2.0 mrad in figures 6.2 and 6.3 have been superimposed.

The regression lines clearly indicate a linear relationship between the logarithm of pointing accuracy and logarithm of target blur, except perhaps for grades of blur of 0.01  $\Delta D$ /mrad. to 0.02  $\Delta D$ /mrad. Such grades, as far as pointing is concerned, are close to the visibility threshold. The derivation of a relationship between target width and blur and standard deviation, will be investigated in the next section.

Constant stimulus method (CSM) results indicate that a different mechanism is apparently involved in discriminating a stationary MM than centering a moving MM. The accuracies are not only larger, but the differences become proportionally greater as the blur increases, leading to the steeper slope in the relationship in figure 6.4. The computational techniques used to derive the standard deviations and DL's in the two methods are different and a direct comparison therefore cannot be made. Normal distributions are assumed for both types of observations, but there is more involved than simply a difference in computation technique. A comparison of the results from the average error method and constant stimulus method is shown in Table 6.10. The ratio of DL/S (the DL from the constant stimulus method, and S, the standard deviation derived by the average error method) indicates an increase in DL with respect to S, for increasing blur. The constant stimulus method results have been plotted on normal probability paper and S superimposed on them in Appendix B. The figures show, that the point derived using S, approaches the PSE as the blur characteristics increase. Equating this point from normal probability tables to a proportion of the DL gives the last column in Table 6.10.

The conclusion may be reached on the basis of observations carried out in

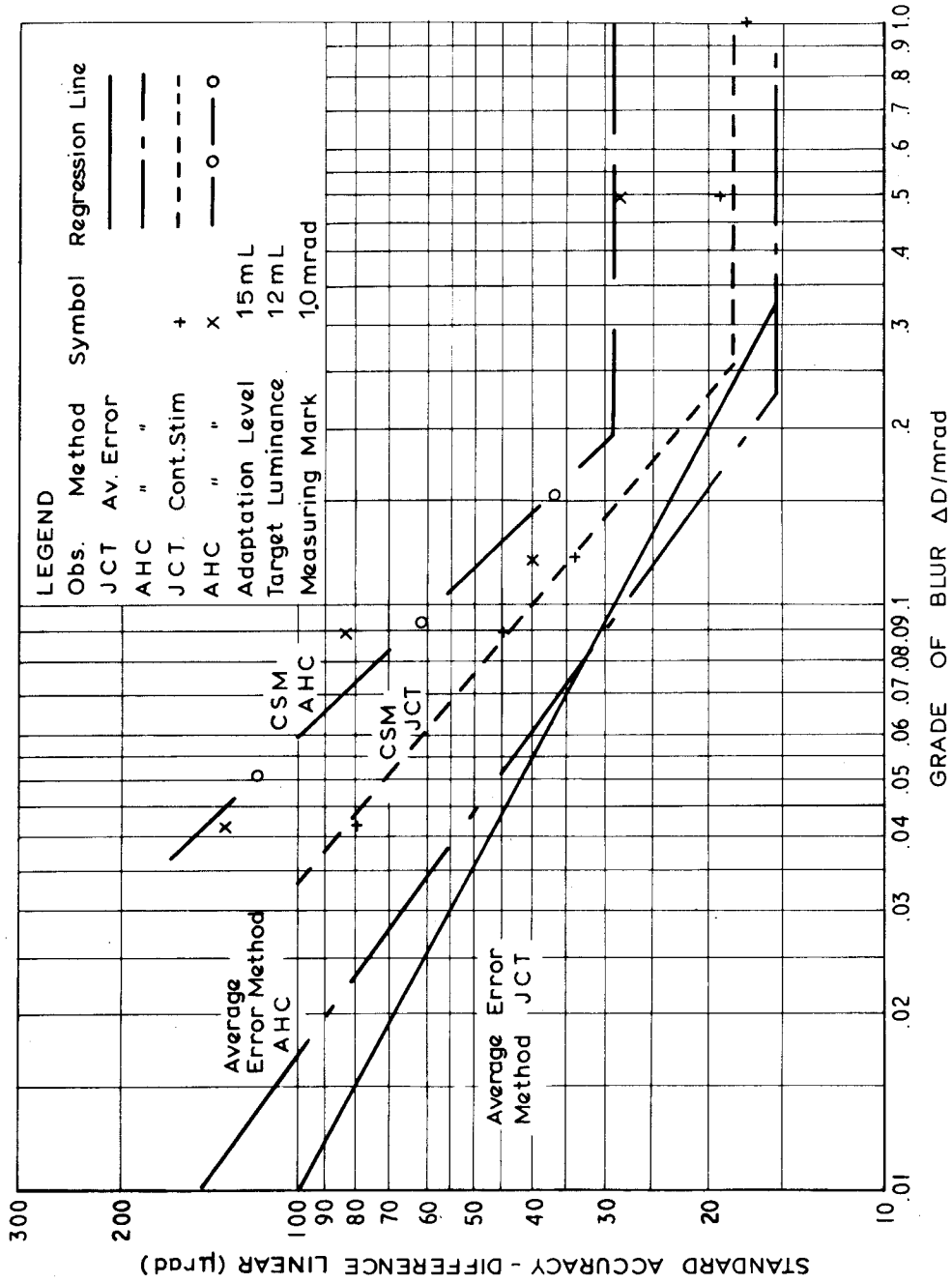


FIG. 6.4: POINTING STANDARD DEVIATIONS DERIVED BY THE AVERAGE ERROR METHOD AND DL'S DERIVED BY THE CONSTANT STIMULUS METHOD FOR 2 OBSERVERS ANNULUS WIDTH IS 2 mrad.

this research, that in respect of the standard deviation of observations (or DL), an instrument based on the average error method of observation will give superior results to an instrument based on the constant stimulus method. This is particularly the case with blurred targets, though for sharp targets a smaller, significant difference in accuracies is still present.

Table 6.10.

Target No.	Grade of Blur $\Delta D/mrad$	DL Const. Stim. Meth. ( $\mu rad$ )		S ( $\mu rad$ )		$\frac{DL}{S}$		S equivalent on (CSM) graph	
		JCT	AHC	JCT	AHC	JCT	AHC	JCT	AHC
14	0.042	79.3	132.5	41.0	40.5	1.94	3.28	0.52	0.31
32	0.09	45.0	83.7	30.6	24.2	1.47	3.33	0.69	0.28
21	0.12	34.0	40.0	24.7	22.7	1.37	1.75	0.71	0.58
25	0.50	19.1	28.4	17.1	16.0	1.11	1.77	0.88	0.56
26	1.0	17.1	29.5	15.6	17.3	1.10	1.89	0.91	0.59

6.4 The Relationship Between Experimental Results and Psychophysical Formulae.

The results of pointing to sharp targets, as given in figure 1.1, clearly indicate the relationship between width and pointing accuracies of 1-2%, which follows Weber's Law. The section of the curve where annulus widths are between 250  $\mu rad$  and 1 mrad as shown in Chapter 3, also follows Weber's Law provided the widths are considered as those seen by the visual system. For annulus widths less than 250  $\mu rad$ , luminance discrimination appears to be the criterion used for pointing.

In referring to blurred target results, the significant features derived from the analysis of variance are the degree of blur and the width of the target, the former being the more significant. Since the average error method may be considered as a psychophysical scaling method (Chapter 4), it is valid to apply the results of pointing to existing psychophysical laws. This has in fact already been done in the case of

Weber's Law in section 1.4. Stevens' law given in section 4.7 is a suitable psychophysical law which may be applied to blurred target results.

The general form of Stevens' psychophysical law is  $\psi = K(\phi - \phi_0)^n$ ; where K is a constant depending on the choice of axes;

n is the exponent depending on the modality or sense investigated, and also the parameters of the experiment;

$\psi$  is the psychophysical reaction to the stimulus  $\phi$ , and

$\phi_0$  is the effective threshold measured on the stimulus scale.

The linear regression computed in section 6.3 is based simply on the grade of blur of the target. To compute the regression based on Stevens' formula, the equations must read:

$$S = K(\Delta D - \Delta D_0)^n \dots\dots\dots (6.1)$$

where

S = Accuracy in  $\mu$ rad

$\Delta D$  = grade of blur ( $\Delta D$ /mrad)

$\Delta D_0$  = visibility threshold grade of blur for pointing for a particular annulus width

K and n are constants.

A new linear regression must be computed using  $\Delta D - \Delta D_0$  as the argument. The parameters a and b from this regression can be introduced into the above formula since  $n = a$  and  $K = \text{antilog}(b)$ . The  $\Delta D_0$  term must be estimated before the above regression can be computed. Table 6.11 gives the visibility thresholds  $\Delta D_0$  for the three annulus sizes for JCT and AHC.

Table 6.11.

Width	JCT $\Delta D$ /mrad	AHC $\Delta D$ /mrad
0.8	0.03	0.04
2.0	0.01	0.015
5.0	0.0035	0.005
2.0 CSM	0.015	0.025

These thresholds have been estimated from experience gained during the observations and from values given by *Hempenius (Trinder, 1965, 60)* who states that the necessary density changes for visibility range from 0.004 to .01  $\Delta D/\text{mrad}$ , with no reference to size of object. The smaller annulus widths however, definitely required a greater change in density to be visible. According to Stevens' formula, pointing accuracies become infinite as the threshold is approached, since the exponent  $n$  is less than zero. In figures 6.2 and 6.3 it is noted that accuracies tended to rise above the regression line for near threshold targets. Thresholds may therefore also be estimated from the pattern of the near threshold targets for annulus sizes of 0.8 and 2.0 mrad. A plot of the thresholds in Table 6.11 against annulus width on logarithm scales gives approximately a linear relationship.

The computed regression lines using the values of  $(\Delta D - \Delta D_0)$  led to the following versions of formula 6.1, as plotted in figures 6.5 and 6.6.

<u>Width</u>	<u>Obs.</u>	<u>Equation</u>
0.8 mrad	JCT	$13.5(\Delta D - .03)^{-.297}$
2.0 mrad	JCT	$11.2(\Delta D - .01)^{-.403}$
5.0 mrad	JCT	$12.0(\Delta D - .0035)^{-.499}$
0.8 mrad	AHC	$18.8(\Delta D - 0.04)^{-0.123}$
2.0 mrad	AHC	$7.3(\Delta D - .015)^{-0.52}$
5.0 mrad	AHC	$12.3(\Delta D - .005)^{-0.52}$
2.0 mrad	JCT CSM	$9.0(\Delta D - 0.015)^{-0.607}$
2.0 mrad	AHC CSM	$13.7(\Delta D - .025)^{-.555}$

The exponents in the above equations for JCT decrease for increasing annulus width, while the coefficients of the equations are approximately constant. The relationship between width and exponent is linear on logarithmic scales, giving an equation for the exponent for JCT, viz.:-

$$\text{exponent} = 0.322 (\text{width})^{0.282}$$

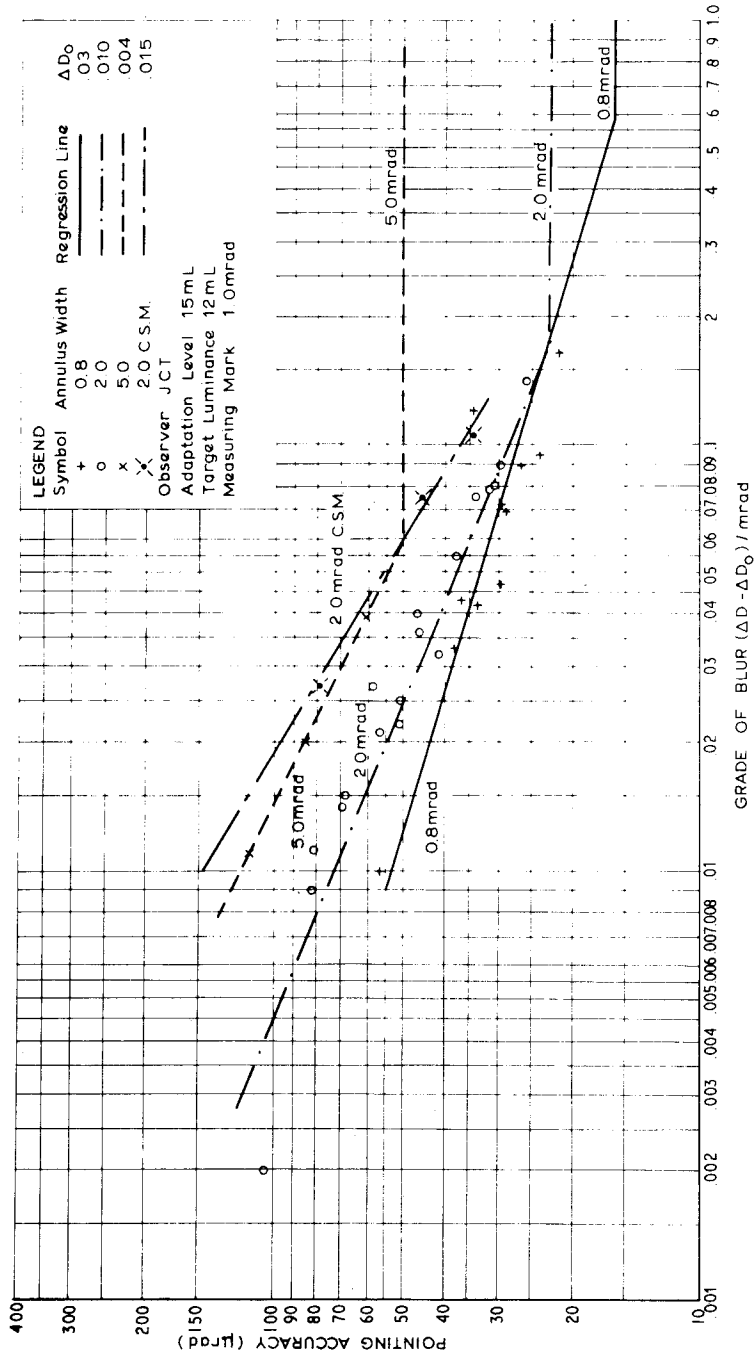


FIG. 6.5. POINTING STANDARD DEVIATIONS (FROM AVERAGE ERROR METHOD) AND DL (FROM CONSTANT STIMULUS METHOD) AGAINST GRADE OF BLUR - THRESHOLD  $\Delta D_0$  VALUES OF  $\Delta D$ /μrad ARE SHOWN IN LEGEND

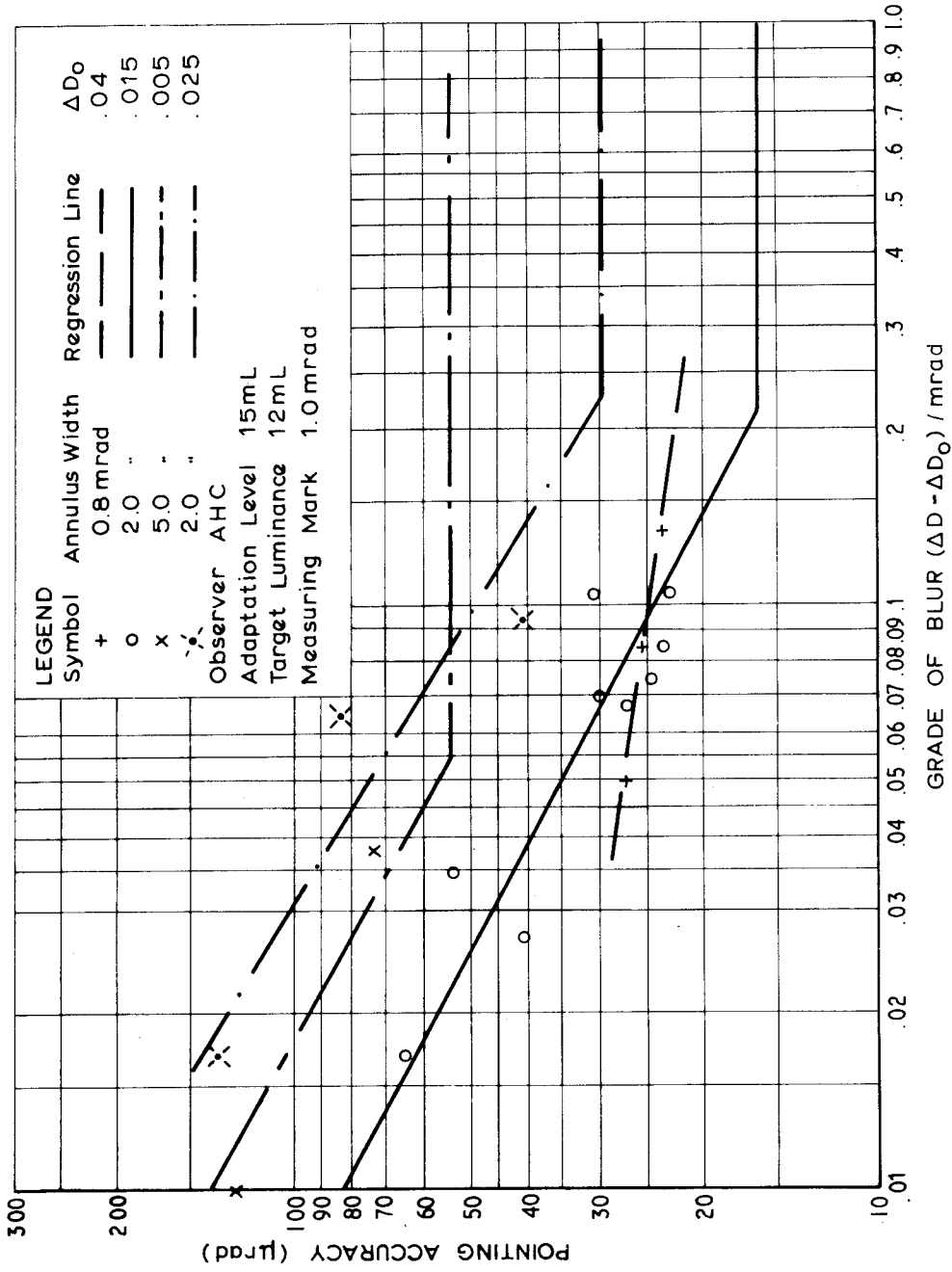


FIG. 6.6: POINTING STANDARD DEVIATIONS (FROM AVERAGE ERROR METHOD) AND DL (FROM CONSTANT STIMULUS METHOD) AGAINST GRADE OF BLUR - THRESHOLD  $\Delta D_0$  VALUES OF  $\Delta D$ /mrad ARE SHOWN IN LEGEND.

A general expression of the equation for pointing accuracy by JCT based on equation 6.1 therefore may be written as

$$S = \{12(\Delta D - \Delta D_0)\}^{-0.322} [(width)]^{0.282} \dots (6.2)$$

This formula though complicated indicates the general form of the equation which describes pointing accuracies in terms of grade of blur and width of the annulus. The thresholds in the above results are clearly an important factor, particularly for the smaller annuli. In referring back to the analysis of variance, the above formula follows the general conclusions reached in the tests, including the interaction effect.

The formula for AHC cannot be derived accurately. Observations by AHC were always more erratic than those of JCT, and therefore considerably more observations would be necessary to derive an accurate formula. This was not possible because of AHC's limited time. It is possible however, that the regression lines for 0.8 mrad and 5.0 mrad in figure 6.6, could produce an equation similar to 6.2, though the actual lines between the points are erratic. The determination of a formula similar to 6.2 for AHC is not considered to be of prime importance. Figure 6.3 nevertheless, is sufficiently accurate for deriving the graphical presentation of equation 6.2 as shown in figure 6.7.

Though the results of the constant stimulus method are unimportant for photogrammetric purposes, it is worth noting that the coefficients of the equations are substantially the same but the exponents are smaller. This appears to reflect the greater difficulty experienced by the observer in the discrimination of annulus width, since the exponent "n" in Stevens' Law is the parameter dependent of the type of task and the sense being investigated. One of the difficulties associated with constant stimulus method observations, particularly with blurred targets, is that the target is always partially obscured by the MM. With the average error method on the other hand, the MM is moved away from the target centre before observations commence, and therefore a better impression of the true centre can be gained.



From a psychophysical point of view, the transition between the two straight lines in figures 6.2 and 6.3 probably should be gradual rather than abrupt. Figures 6.2 and 6.3 indicate that Stevens' formula is only an approximate description of pointing accuracies. A more complete formula embracing both straight line sections, together with the transition, would appear to be more appropriate. Formula 6.2 however, does indicate the significance of the visibility thresholds on pointing accuracies of targets of given sizes.

A more practical method of presenting the above formula, is in graphical form in figure 6.7. The accuracies for the annulus widths of 0.8, 2.0 and 5.0 mrad have been derived from figure 6.2. Values for 10 mrad have been extrapolated using the above formula. Further extrapolation of the curves indicates that they would approach the 1 - 2% lines of Weber's Law, although the curve for  $.01 \Delta D/\text{mrad}$  appears to be parallel to the 2% line, but at a slightly larger value than 2%. At their lower levels, the curves terminate approximately at the visibility threshold values. Accuracies over the range of annulus widths less than 1 mrad tend to rise for the  $.10$  and  $.15 \Delta D/\text{mrad}$  curves, as the visibility threshold is approached. From a practical point of view, pointing accuracies of targets near thresholds are not particularly useful. Ground target sizes should not be designed so that they produce photographic images which are almost invisible. Only the approximate behaviour near threshold therefore is shown in figure 6.7. The SF of the visual system may have a small influence on the subjective impression of targets with annulus widths between 0.3 mrad and 1.0 mrad. A convolution of the SF of the visual system and the target profile may show a slight decrease in the grade of target blur. The effect of the SF of the visual system however would be very marginal indeed, since the target profile is very much shallower than the SF. The significant factor in pointing to smaller blurred targets is the increased visibility threshold which raises the level of the curves in figure 6.7. Because of the almost insignificant effect of the SF of the visual system on grades of blur of  $0.10 \Delta D/\text{mrad}$

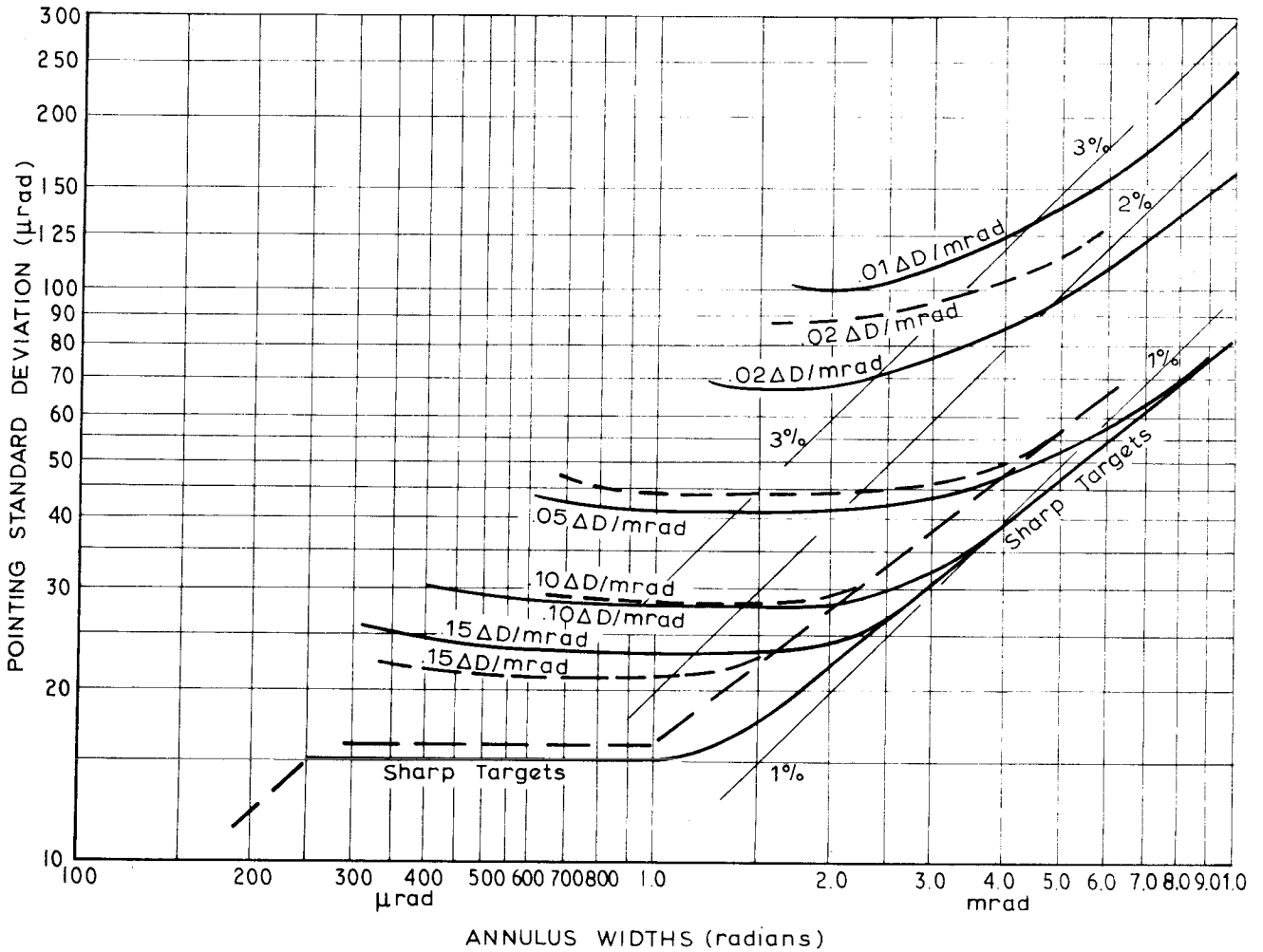


FIG. 6.7: POINTING STANDARD DEVIATIONS FOR JCT (full lines) and AHC (broken lines) USING SHARP AND BLURRED CIRCULAR TARGETS. THE GRADE OF BLUR (in  $\Delta D/mrad$ ) CORRESPONDING TO EACH LINE IS SHOWN (MEASURING MARK = 1.0 mrad)

or less, convolutions of blurred target profiles and SF of the visual system have not been carried out.

Points where the curves join the sharp target straight lines in figure 6.7 correspond with the points of discontinuity in figures 6.2 and 6.3. These points indicate the approximate grade of blur below which pointing accuracies will deteriorate for a given annulus width. The points of discontinuity in figures 6.2 and 6.3 are given approximately in Table 6.12, based on mean values for JCT and AHC.

Table 6.12.

<u>Annulus Width</u>	<u>Limit</u>
mrad	$\Delta D/\text{mrad}$
0.8	0.30
2.0	0.12
5.0	0.06

For degrees of blur greater than those in Table 6.12, pointing standard deviations are approximately 1% of the annulus width for annulus widths greater than 1 mrad, and approximately constant at 16  $\mu\text{rad}$  for annulus widths between 0.3 and 1.0 mrad.

Results of AHC have been plotted on figure 6.7 using broken lines. In comparing the results of AHC and JCT, pointing standard deviations do not differ significantly for target blurs of 0.05  $\Delta D/\text{mrad}$  or greater, but because of AHC's higher visibility thresholds, the line for 0.02  $\Delta D/\text{mrad}$  is much higher than that of JCT. As visibility threshold is approached pointing accuracies deteriorate rapidly.

### 6.5 Discussion.

Figure 6.8 contains data in figure 1.1 plus the results in figure 6.7. The curves for sharp targets by JCT and AHC clearly follow the same pattern as the results of *O'Connor (1962)* and *O'Connor (1967)* as presented in figure 6.8. Significant variations were detected by O'Connor in results for different observers, though the general patterns were still the same.

Such differences are clearly due to the many factors, both physiological and psychological, involved in psychophysical tasks. The very good agreement by JCT and AHC with the results presented by O'Connor is an indication that pointing accuracies obtained in this research are indicative of the trend of results by average observers, though variations of 10 - 20% may be expected. Further variations in standard deviations may occur due to changes in adaptation level. Increases by a factor of 1.3 were noted in the higher adaptation results presented in Table 6.2. This higher adaptation level was caused by side illumination entering the observer's eye, a situation which could occur during normal photogrammetric observations. The observer's ability to discriminate luminance differences in blurred targets is apparently reduced when the eye is adapted to a higher luminance level.

Curve II in figure 6.8 derived by *O'Connor (1962)* follows almost exactly the same line as the .05  $\Delta D/mrad$  curve derived in these experiments. The curves of *O'Connor (1962)* were derived using a Zeiss Pulfrich Stereocomparator. *O'Connor (1967)* stated that inaccuracies in this instrument obscured the true pattern of results which could be obtained by the observer's visual system. The similarity between the two curves is however quite significant. The experiments carried out by *O'Connor (1962)* involved sets of ten observations only, on a large number of targets. This led to a significantly lower confidence interval than for results obtained by *O'Connor (1967)* or those carried out in this work. Curves III and IV are difficult to define accurately, but there is some tendency for them to follow shapes similar to the curves in figure 6.7. This is particularly the case for curve IV, which also may follow a line closer to the 2% line than is actually shown. It is impossible to compare directly the two sets of experiments, especially considering the completely different experimental conditions of the two sets of data. The relative agreement between the shapes of the curves is nevertheless very good.

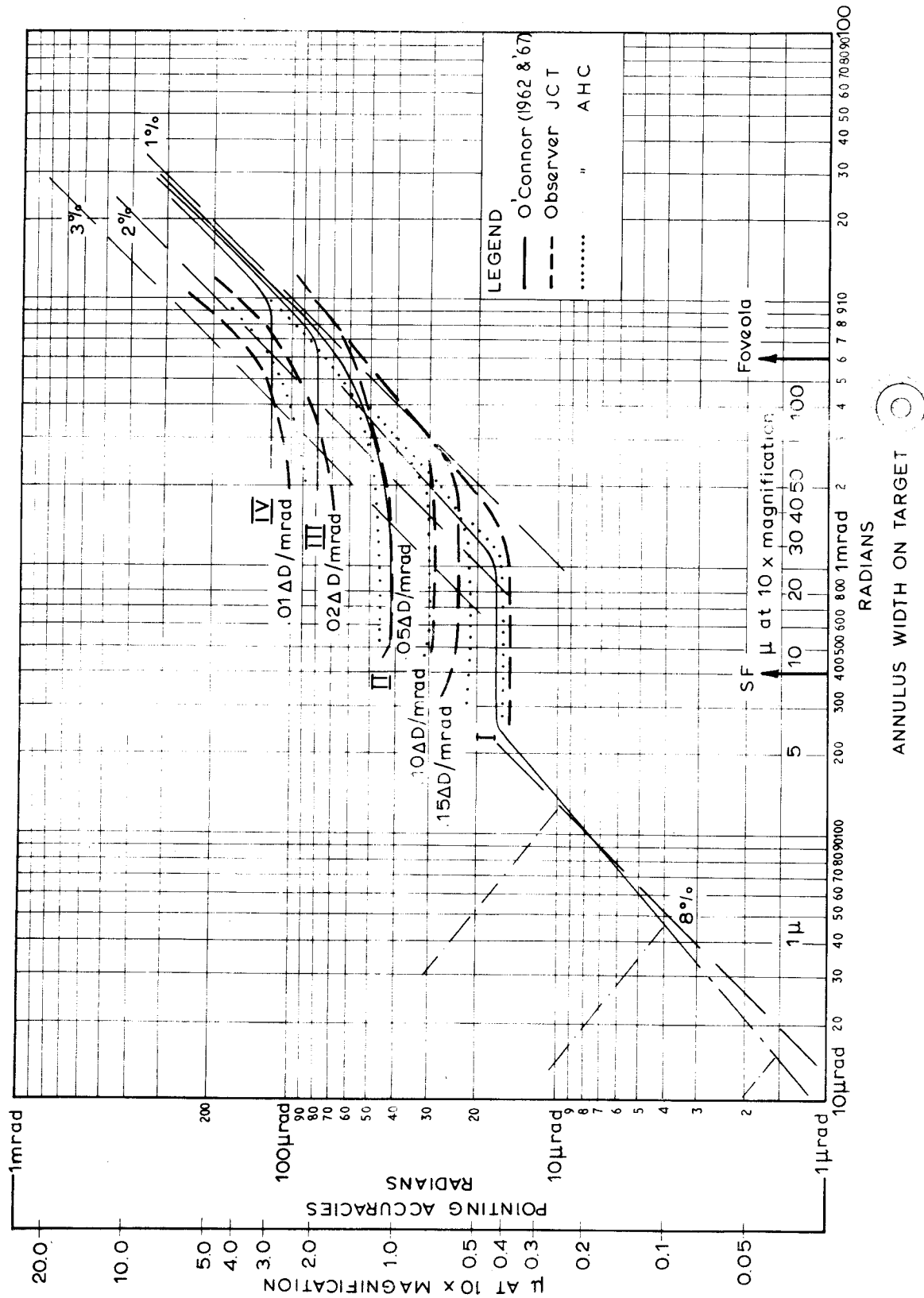


FIG. 6.8: Results from Fig. 6.7 superimposed onto curves of Fig. 1.1. Curves derived by J.C.T. and A.H.C. have been marked according to the legend. The grade of blur (in  $\Delta D/mrad$ ) corresponding to each line is shown.

The three straight lines plotted for the sharp, low and medium contrast curves derived by *O'Connor (1967)* for annulus widths less than 250  $\mu$ rad, which apparently represent near threshold results, agree with the pattern of reduced accuracies in figure 6.7, obtained for near visibility threshold blurred targets. In both situations luminance discrimination seems an important criterion for pointing, and therefore a similar pattern of results for near threshold targets would be expected.

Composite curves in figure 6.8 clearly indicate the very complex non-linear behaviour of the visual system in respect to pointing. Various criteria are apparently adopted by the visual system for pointing, depending on the size and luminance profile of the target. Equation 6.2, derived for the pointing results to blurred targets indicates that a simple criterion of flux as proposed in section 2.6 is not involved. The relationship, on the contrary, is based primarily on width discrimination, the accuracy of which is reduced by increased blurring of the target, with perhaps some assistance from the luminance levels of the target.

With regard to contour sharpening mechanisms referred to in section 2.7, Mach bands were not consciously observed on any of the targets, though the edges of the targets always appeared to be moderately well defined. The accuracy of location of target edges by the average error method varied from 50  $\mu$ rad to 200  $\mu$ rad. Subjective positions of the edges on the density profiles were not at an abrupt change, as might have been expected by the subjective impression of the targets (See Appendix C). The main influence of the contour sharpening mechanisms therefore seems to be in aiding the definition of the target edges, and hence the width of the annulus. This, however, seems to be only a secondary effect as is indicated by the fact that the ability to discriminate width is substantially reduced by large degrees of blur.

The basic explanation for pointing accuracies appears to lie in the proposals put forward by *Andersen and Weymouth (1923)* as described in section 2.4, together with the minor influences of neutral processing effects

such as inhibition and contour sharpening mechanisms, in locating the target edge. Luminance patterns projected onto the retinal mosaic lead to the discrimination of a mean local sign according to Anderson and Weymouth, such that the MM is located centrally, despite the fact that edges of the targets can only be located with an accuracy of 50 - 200  $\mu$ rad. No explanation is available as to how the mean local sign is resolved from the stimulated cones, particularly for blurred patterns. The neural processing in the retina and higher centres of the visual system are expected to influence the manner in which this mean local sign is resolved, since these functions are basic to the visual system. Though contour sharpening mechanisms are significant it appears they should not be given undue importance. These were also the general findings of the convolutions carried out in Chapter 3. Further descriptions of the complex manner in which the visual system carries out pointing tasks are impossible at this stage, but it is important to indicate the possible factors which may influence accuracies.

The equation 6.2 is a simplified representation of pointing standard deviations in terms of two variables. It seems possible that curves in figure 6.8 could be represented by the one complex equation embracing all variables and the subsequent interactions between these variables. This equation would describe the effect of each variable on pointing accuracies. Such an equation would no doubt vary for different observers in magnitude, and with respect to the interactions. The description of the equation is not necessary for photogrammetry, if indeed it could ever be formulated. Figure 6.8 is sufficient and far more useful for practical application of the results. It is nonetheless worth noting that a modern psychophysical law, Stevens' law, with a great deal of evidence behind it, can be applied to the results of pointing to blurred targets, at least over a limited range of target blur.

6.6 Conclusions.

- (i) The standard deviations of pointing to blurred targets follow the pattern of results derived by other experiments.
- (ii) These results can be conveniently represented in graphical form as shown in figure 6.8. The significant variables are annulus width, and the grade of blur expressed as  $\Delta D/mrad$ .
- (iii) Pointing standard deviations derived represent the pattern for particular observation conditions, observer and observational method. The results may vary by as much as 30% for different observers and adaptation levels, or perhaps even more if the constant stimulus method of observation is used.
- (iv) The results obtained in this research represent ideal results indicative of the pattern which may be obtained with the unaided eye.
- (v) Stevens' psychophysical law can be applied to pointing accuracies over a limited range of blur of the target. This law indicates the significance of the visibility thresholds in pointing to blurred targets.



## 7. SYSTEMATIC ERRORS.

### 7.1 Presentation and Discussion of Results.

A full list of the systematic errors derived with the MM approaching the target from the left hand side is presented in Tables 6.1 to 6.4. The pattern of systematic errors in terms of the two variables, grade of blur and annulus width has been plotted separately for JCT and AHC in figures 7.1 to 7.4. Overshoot errors by JCT were plotted on logarithmic scales, while errors of AHC were either overshoots or undershoots and have therefore been presented on natural scales. Several values by JCT marked thus\* in Tables 6.1 and 6.2, were not plotted since they were either zero or undershoots.

There is generally a regular pattern in the systematic errors of both JCT and AHC though there are wide variations in the actual values, and occasionally an extremely "wild" value occurs. There seems little purpose in investigating the relationship between the two variables and the systematic errors because of their unpredictable nature. Statements put forward in section 4.3, after *Graham (1950)* indicate that the variables involved in such investigations may not only include those of the stimulus, but also external conditions, and psychological factors etc. External conditions and psychological factors appear to have influenced the systematic errors very significantly in these studies. It is particularly noticeable that variations in the systematic errors are much larger than variations in the standard deviations of the observations. The fact that these errors cannot be predicted or controlled is clearly a very weak point in an observational technique based simply on one direction of approach of the MM.

In the first attempt to eliminate systematic errors the target was approached from both directions. This was done on targets listed in Table 7.1 which shows errors arising from each direction of approach, the mean of these errors, and the pattern in which the sets of observations were taken. Various patterns of observations were used. Some targets were observed with sets from each direction alternately, while for other

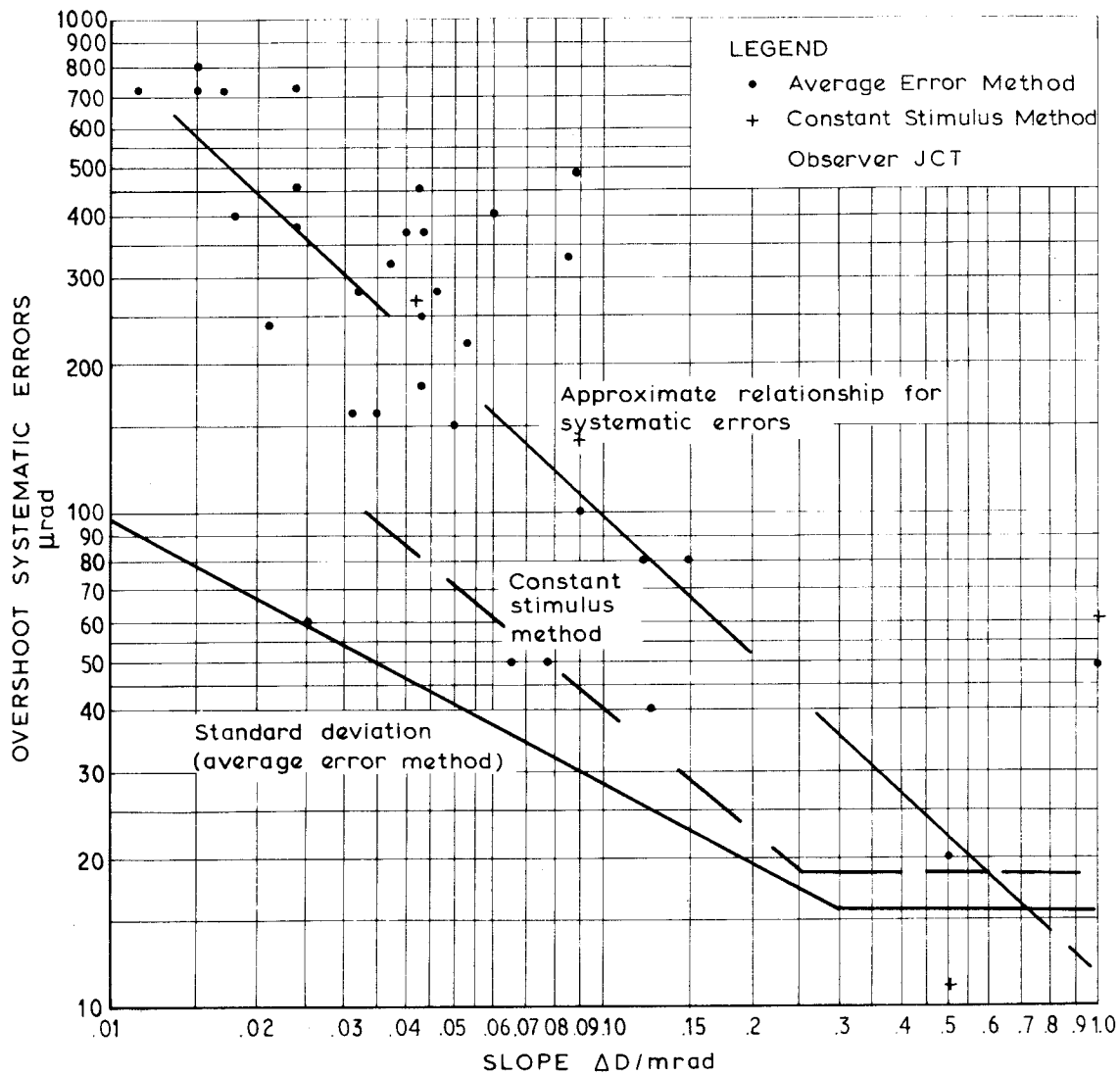


FIG. 7.1: OVERSHOOT SYSTEMATIC ERRORS DERIVED FOR THE MM APPROACHING THE TARGET FROM THE LEFT HAND SIDE IN TERMS OF GRADE OF BLUR

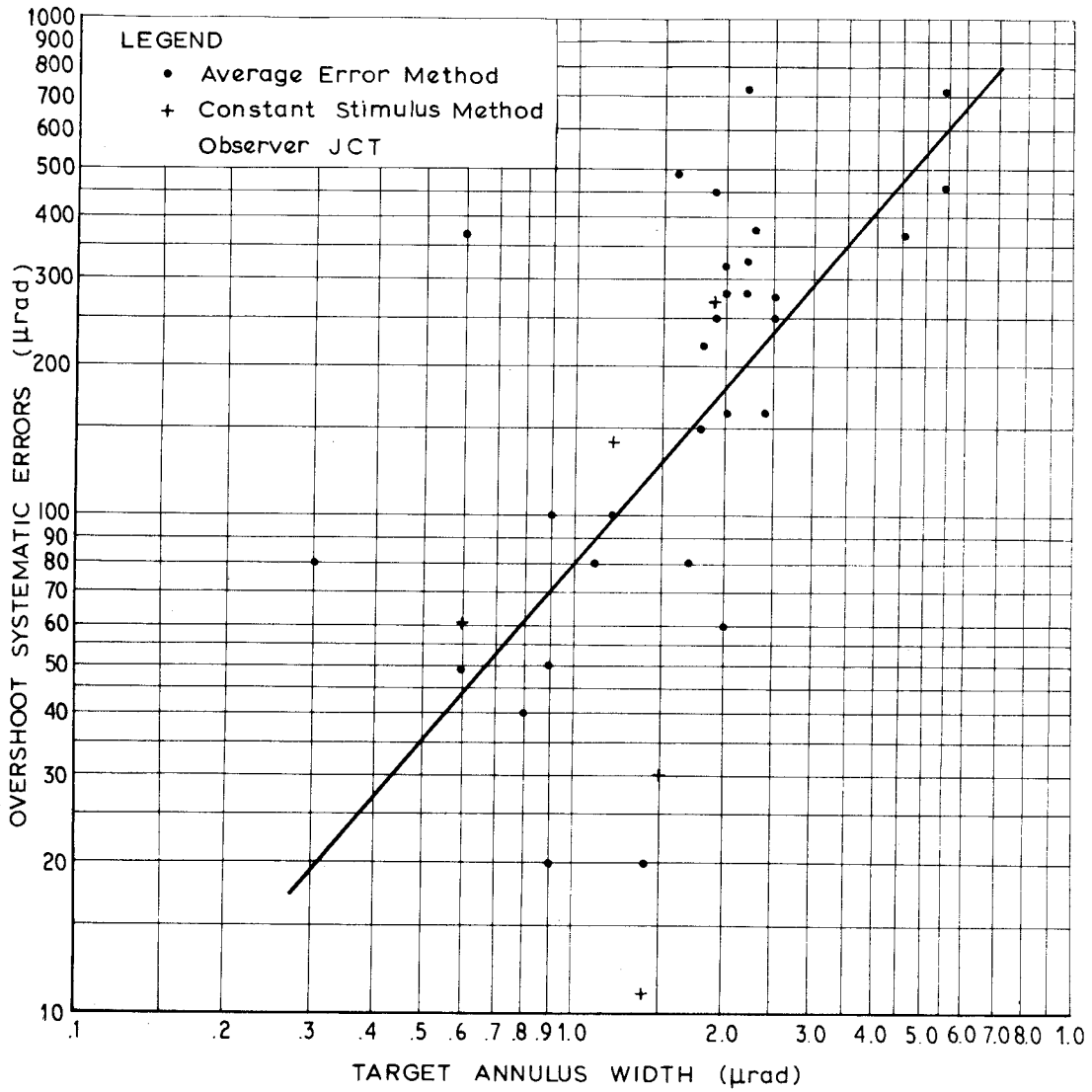


FIG. 7.2: OVERSHOOT SYSTEMATIC ERRORS DERIVED FOR THE MM APPROACHING THE TARGET FROM THE LEFT HAND SIDE IN TERMS OF TARGET ANNULUS WIDTH.

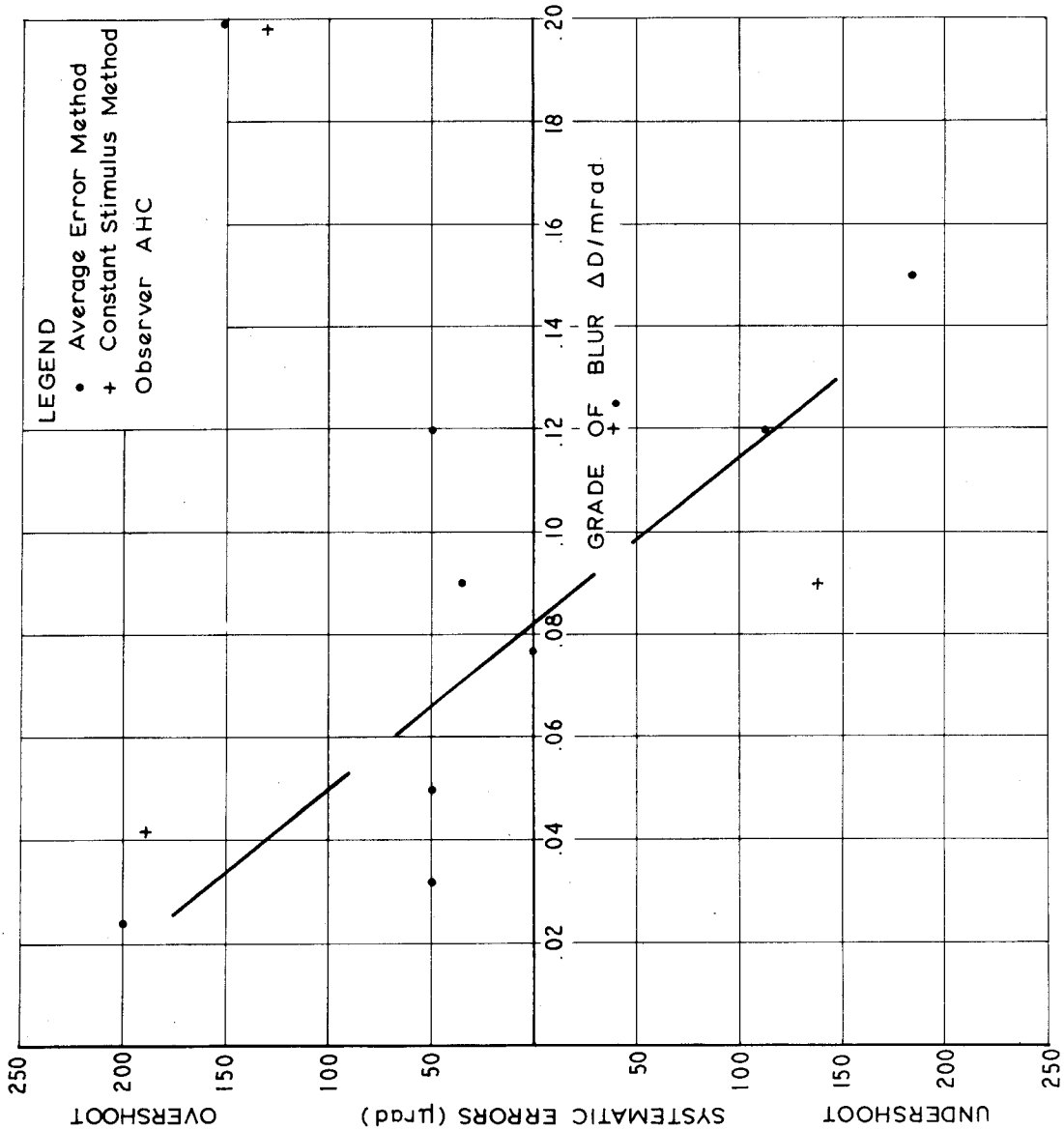


FIG. 7.3: SYSTEMATIC ERRORS DERIVED FOR THE MM APPROACHING THE TARGET FROM THE LEFT HAND SIDE IN TERMS OF GRADE OF BLUR.

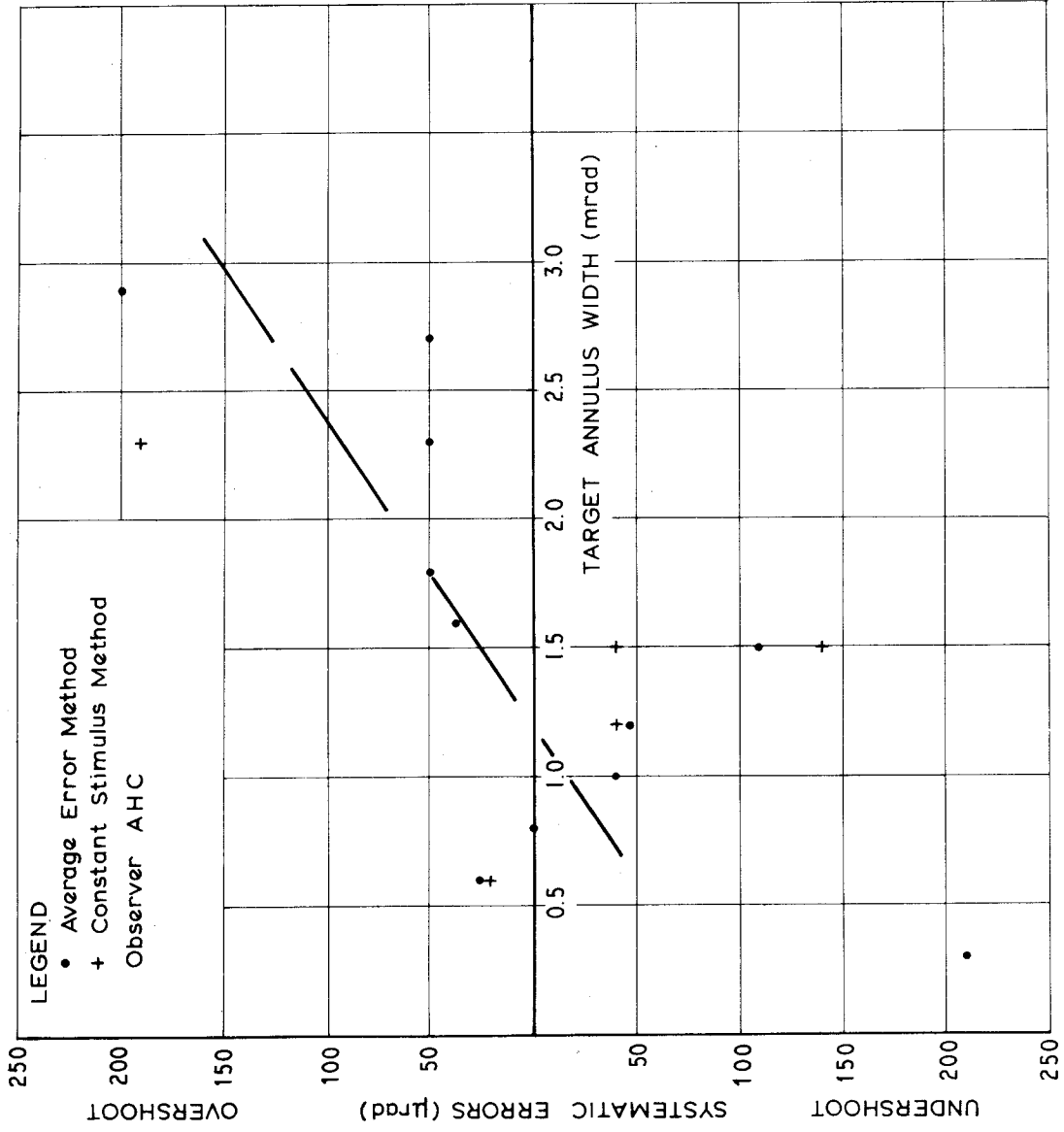


FIG.7.4: SYSTEMATIC ERRORS DERIVED FOR THE MM APPROACHING THE TARGET FROM THE LEFT HAND SIDE IN TERMS OF TARGET ANNULUS WIDTH.

Table 7.1.

-ve = undershoot

+ve = overshoot

Target No.	Obs.	System Error $\mu\text{rad}$		Mean Error $\mu\text{rad}$	$\sigma$ -Syst. Error $\mu\text{rad}$	Pattern of Obs.
		→	←			
18	JCT	-288	+140	214 to left	6	Alternate sets
18b	AHC	Tests not satisfied		-	-	" "
19a	JCT	-92	0	46 to left	5	" "
20	"	+58	-180	119 to left	5	Left hand approach then right hand approach
21	"	Tests	failed			Alternately 2 sets
21a	"	"	"			" " "
21b	AHC	"	"			Alternate sets
24	JCT	+20	0	10 to right	3	Left hand approach then right hand approach
24b	AHC	Tests	failed			" " "
25	JCT	+20	-35	28 to right	5	" " "
25b	AHC	-52	Tests failed	-		Alternately
26	JCT	+53	"	-		Left hand approach then right hand approach
26b	AHC	+25	-104	65 to right	5	" " "

targets a full series of left approach was taken and then a full series of approach from the right. The observations taken alternately gave very poor results, since on all but two occasions out of seven, the variance tests described in Appendix A failed. In most cases where each direction was observed separately, the variance tests were satisfactory, but large residual errors still remained. The technique of two directions of approach therefore clearly failed to eliminate the systematic error.

A further significant factor was that the systematic errors derived by the constant stimulus method followed approximately the same pattern as results derived by the average error method. Remembering that there were large variations in the systematic errors in figures 7.1 to 7.4, and also that a limited number of results were determined by the constant stimulus method, the systematic errors derived by that method nevertheless do appear to follow the same general pattern. Systematic errors therefore, do not seem to be a function of the method of observation but rather appear to depend on the observer himself.

Results of investigations by *Brown (1953) and Brown (1955)* on the task of partitioning (bisecting) horizontal and vertical lines can be compared with pointing experiments carried out in this study. To investigate systematic errors (defined as "half-meridional differences"), Brown used the average error method of testing. Ten observations were made in each set, in which the measuring mark was moved from each side of the correct centre, an equal number of times. *Brown's (1953)* investigations on six subjects, revealed large negative systematic errors (i.e. the subjective centre was located to the right of the correct centre) for horizontal lines, and smaller positive and negative errors (for positive errors the measuring mark was lower than the correct centre) for vertical lines. Over an extended series of daily observations, these errors followed a definite trend. This trend appeared to be due to measuring effects since the direction of the trend altered when the frequency of observations was reduced (*Brown, 1955*).

Brown also found that systematic errors followed the same pattern for both eyes. Even after long periods of testing only one eye, the other eye was found to have followed the same trend when subsequently tested. He maintained that the systematic errors were partly due to ocular effects, but the instability of the errors, affecting both eyes concomitantly as a function of time, appeared to be due to influences at least at the cortical level of the visual system. No further explanations were given for the instability of the errors.

The results of investigations in this study agree with findings of *Brown (1953) and Brown (1955)*. The variable nature of the systematic errors of JCT and the fact that most were overshoots - equivalent to negative errors in *Brown(1953)* - are consistent with Brown's results. The smaller range in AHC's errors may be due to the fact that AHC took fewer observations at less frequent intervals.

The necessity for using only one direction of approach of the MM in this study appears to be due to movement after-effects, which become substantially reinforced when the observations are taken in one direction for an extended period. This conclusion seems to be strengthened by the fact that reliable results can be obtained from observations when the MM is moved from opposite directions, provided an extended rest period is taken between observations in each direction. The movement after-effects appear to be related to the phenomenon of apparent motion, which results from a steady gaze on a moving field, e.g. a waterfall (*Davson, 1962a, 242*). Though no apparent motion was observed in this study, the effects may have been present subliminally, thus influencing the discrimination of the MM and target when the MM was moved from the opposite direction. Figural effects described by *Gregory (1966, 212)*, e.g. *Köhler et al. (1944)*, appear to be similar to the after-effects due to motion experienced in this study. Köhler wore glasses coloured half red (on left) and green (on right). When he had become adapted to the glasses, he removed them and found that objects were red, when his eyes were directed to the right, and green when directed to the left. After-effects may also



be related to factors causing trends in systematic errors derived by *Brown (1953)*. It appears that these effects are due to influences at the cortical level, and therefore cannot be explained simply (*Brown, 1955*) (*Gregory, 1966*).

On the basis of Table 7.1 it was clearly necessary to develop some auxiliary equipment to eliminate systematic errors.

## 7.2 Elimination of Systematic Error.

Three significant points arose from the previous section:

*Firstly*, observations from opposite directions will not eliminate the systematic error even if observations in each direction are taken separately.

*Secondly*, reliable results can be obtained provided one direction of approach of the MM is constantly maintained.

*Thirdly*, systematic errors rather than being a function of the method of observing, seem to be a characteristic dependent on the observer.

These points led to the development of the method of observing, described in section 5.52, whereby a dove prism was used to rotate the image of the MM and target, such that the MM moved in the same apparent direction (from the left hand side in these investigations) relative to the retinal mosaic, whether in fact the MM moved from the left or right. This enabled an effective elimination of the systematic error to be made without appreciably disturbing the image quality of the target, or the accuracy of the observations. In Tables 6.1 to 6.3 the systematic errors for a given target remained constant for the left hand direction of approach. It should therefore be constant for both directions of approach of the MM, provided these two directions always appear unchanged to the observer.

The results using the dove prism are shown in Table 7.2. Two sharp targets were observed by JCT and AHC and a number of inexperienced student

Table 7.2.

Observations for Elimination of Systematic Errors.

Each entry for each direction has been determined by 10 observations. MM direction is indicated by arrows, +ve residual error = MM to right of correct centre.

Target No. 2 - Annulus = 1 mrad.

Observer: JCT			Observer: BL		
→	←	Means	→	←	Means
12.73	12.80	12.77	13.21	12.36	12.78
12.79	12.68	12.73	13.28	12.29	12.79
12.84	12.73	12.78	13.27	12.35	12.81
	Mean	12.76		Mean	12.79
S		= 21.0 μrad	S		= 28.2 μrad
Residual Error		= +11 μrad	Residual Error		= + 5 μrad
99% C.I.		= ±12 μrad	99% C.I.		= ±17 μrad
-----			-----		
Observer: JCT			Observer: JN		
→	←	Means	→	←	Means
9.87	10.32	10.10	12.70	12.07	12.39*
10.04	10.32	10.18	13.08	12.40	12.74
9.92	10.33	10.12	12.91	12.35	12.63
	Mean	10.13		Mean	12.68
S		= 21.0 μrad	S		= 30.0 μrad
Residual Error		= + 5 μrad	Residual Error		= +19 μrad
99% C.I.		= ±14 μrad	99% C.I.		= ± 20 μrad
-----			-----		
Observer: AHC			Observer: GD		
→	←	Means	→	←	Means
13.08	12.72	12.90	13.63	11.93	12.78
12.67	12.78	12.72	13.14	12.88	13.01
12.74	12.85	12.79	12.99	12.55	12.77
12.73	12.84	12.78			
	Mean	12.80		Mean	12.85
S		= 17.0 μrad	S		= 24.8 μrad
Residual Error		= + 7 μrad	Residual Error		= + 2 μrad
99% C.I.		= ±12 μrad	99% C.I.		= ±17 μrad

Table 7.2. (Contd.)

Observer: RP

→	←	Means
13.35	12.30	12.83
13.06	12.14	12.60
13.13	12.11	12.62
Mean		12.68

S = 20.5  $\mu$ rad  
 Residual Error = +19  $\mu$ rad  
 99% C.I. =  $\pm 15$   $\mu$ rad

Observer: FH

→	←	Means
13.76	12.32	13.04
13.61	12.56	13.08
13.46	12.53	13.00
Mean		13.04

S = 23.7  $\mu$ rad  
 Residual Error = -17  $\mu$ rad  
 99% C.I. =  $\pm 15$   $\mu$ rad

Target No.5 - Annulus=2mrad

Observer: AHC

→	←	Means	
12.32	12.07	12.20	} Right Eye } Dark } Adapted
12.58	11.72	12.15	
12.67	11.47	12.07	
Mean		12.14	

S = 27.8  $\mu$ rad  
 Residual Error = +14  $\mu$ rad  
 99% C.I. =  $\pm 17$   $\mu$ rad

Observer: IW

→	←	Means
12.85	11.58	12.22
12.40	12.08	12.24
12.62	11.82	12.22
Mean		12.23

S = 24.7  $\mu$ rad  
 Residual Error = + 5  $\mu$ rad  
 99% C.I. =  $\pm 17$   $\mu$ rad

Target No.5 - Annulus=2 mrad (Contd.)

Observer: IS

→	←	Means
12.89	11.44	12.17
13.29	11.23	12.26
13.28	11.35	12.32
Mean		12.25

S = 27.8  $\mu$ rad  
 Residual Error = + 3  $\mu$ rad  
 99% C.I. =  $\pm 17$   $\mu$ rad

Observer: GT

→	←	Means
13.81	10.14	11.97
14.39	9.71	12.05
14.12	9.82	11.97
Mean		12.00

S = 27.6  $\mu$ rad  
 Residual Error = +28  $\mu$ rad\*  
 99% C.I. =  $\pm 17$   $\mu$ rad

Observer: PF

→	←	Means
12.63	10.74	11.69
12.75	11.20	11.97
12.07	11.71	11.89
Mean		11.85

S = 33.7  $\mu$ rad  
 Residual Error = +43  $\mu$ rad\*  
 99% C.I. =  $\pm 19$   $\mu$ rad

Observer: AR

→	←	Means
13.74	10.58	12.16
13.09	11.28	12.19
13.07	10.79	11.93
12.93	11.07	12.00
Mean		12.07

S = 37.1  $\mu$ rad  
 Residual Error = +21  $\mu$ rad  
 99% C.I. =  $\pm 20$   $\mu$ rad

Target No.3 - Annulus=2 mrad (Contd.)

Observer: JCT

→	←	Means	
12.37	11.83	12.10	
12.30	11.88	12.09	
12.57	11.91	12.24	
12.39	11.98	12.18	
12.33	12.08	12.20	
12.52	12.02	12.27	
12.40	12.10	12.25	
12.44	11.88	12.16	} Right Eye Dark Adapted
12.40	12.13	12.27	
12.48	12.07	12.28	
12.34	12.12	12.23	
12.27	12.18	12.23	
	Mean	12.21	

S = 19.0  $\mu$ rad  
 Residual Error = + 7  $\mu$ rad  
 99% C.I. =  $\pm 10$   $\mu$ rad

---

Observer: AHC

→	←	Means	
11.72	11.13	11.43	} Right Eye Light Adapted
11.46	11.36	11.41	
11.84	11.07	11.46	
11.71	11.44	11.58	
	Mean	11.47	

S = 25.9  $\mu$ rad  
 Residual Error = + 9  $\mu$ rad  
 99% C.I. =  $\pm 14$   $\mu$ rad

---

Observer: JCT

→	←	Means	
11.46	11.49	11.48	Right
11.48	11.47	11.48	
11.54	11.55	11.55	Eye
11.47	11.53	11.50	
11.51	11.59	11.55	Light
11.40	11.59	11.50	
11.31	11.76	11.54	} Adapted
11.36	11.75	11.56	
	Mean	11.52	

S = 16.5  $\mu$ rad  
 Residual Error = + 4  $\mu$ rad  
 99% C.I. =  $\pm 10$   $\mu$ rad

---

Observer: JCT

→	←	Right Eye Mean
11.37	13.00	12.18
11.53	12.73	12.13
11.54	12.70	12.12
11.53	12.86	12.20
		12.16

S = 15.4  $\mu$ rad  
 Residual Error = +10  $\mu$ rad  
 99% C.I. =  $\pm 10$   $\mu$ rad

---

Dove Prism No. 2 - Target 2 mrad.

Observer: JCT

→	←	Means
14.45	14.83	14.64
14.33	14.70	14.52
14.40	14.48	14.44
14.16	14.91	14.56

Mean 14.55

S = 15.0  $\mu$ rad  
Residual Error = + 4  $\mu$ rad  
99% C.I. =  $\pm 10$   $\mu$ rad

---

Observer: WK

→	←	Means
15.34	13.51	14.42
14.54	14.17	14.36
14.55	14.49	14.52

Mean 14.43

S = 32.7  $\mu$ rad  
Residual Error = +16  $\mu$ rad  
99% C.I. =  $\pm 19$   $\mu$ rad

---

Observer: AHC

→	←	Means
14.60	14.74	14.67
14.33	14.50	14.41
14.42	14.44	14.43

Mean 14.50

S = 32.6  $\mu$ rad  
Residual Error = +9  $\mu$ rad  
99% C.I. =  $\pm 19$   $\mu$ rad

---

Observer: AR

→	←	Means
14.74	13.48	14.10
15.37	13.80	14.59
14.62	13.35	13.99

Mean 14.22

S = 31.3  $\mu$ rad  
Residual Error = +37  $\mu$ rad\*

Results erratic - unsatisfactory  
for estimation of centre.

---

observers. Observations in each direction were taken alternately, the mean of these two readings giving an estimate of the central position of the target. The three columns in Table 7.2 are the means of sets taken in each direction, and the composite mean of these two means. The first two columns have been presented to give an estimate of the systematic errors of the observers. Since observations in each set for the inexperienced observers tended to drift, means of these sets are not considered to be important. *The means of the two observations taken alternately from left and right directions* of approach, however, gave reliable results and therefore estimates of the target centre and the standard deviations were based on these values.

Computing means of observations taken alternately in each direction was necessary for the inexperienced observers, since this procedure eliminated the variations in systematic errors which occurred. In Table 7.2, the accuracies derived from the means of inexperienced observers, were only marginally lower than accuracies of observations by JCT and AHC, though the students had had no prior training. A tentative conclusion which can be drawn from the results of inexperienced observers, therefore, is that the apparently large variations in pointing errors of inexperienced observers when approaching the target from one direction are due more to a change in the observers' interpretation of the centre, rather than a large standard deviation. Once the variation in systematic error is controlled by training, reliable results should be obtained. Training may also be expected to improve the standard deviation slightly but from results in this work, the instability of observations in each individual direction was mainly due to variations in the systematic error.

Contributions to the composite means in Table 7.2 are considered to be derived from ten observations (i.e. one from left, and one from right is equivalent to one observation). An estimate of the standard deviation of a single observation as defined above, the error of the mean against the correct centre and an estimate of the 99% confidence interval of the

difference between the subjectively determined centre and correct centre, derived from the t-distribution are shown. The confidence interval was derived from standard deviations of the mean pointing position, and the standard deviation of location of the true centre, which was 3  $\mu$ rad in section 5.52.

On three occasions, i.e. when PF, AR and GT observed to the 2 mrad target (marked with asterisk), the means proved to be significantly different from the exact centre. Several other sets of observations gave residual errors marginally outside the confidence interval. The observations of JCT and AHC proved to be a satisfactory estimate of the centre, although the systematic errors inherent in these observations were not large. Slight variations occurred when observations were taken several weeks apart (e.g. JCT - 1 mrad observations - 2 sets). With regard to the inexperienced observers, the results are considered satisfactory in view of their lack of experience.

The one significant feature noticeable in the results is that all but one of the residual errors were positive. Though each error in itself was not significant, a very strong tendency towards positive errors existed. It is not known why this tendency should occur. The instrument which was tested repeatedly, gave negligible backlash. Observations were taken by JCT and AHC with the adaptation level of the right eye, the same as that of the left eye, and also with the right eye dark adapted. Further observations were taken by JCT with the right eye, to test whether the use of the other eye had any effect. No significant differences were noted as is seen in Table 7.2. As stated in section 5.52, elaborate precautions were taken to ensure that the screen and target were completely symmetrical so that they would not affect the subjective impression of the centre. Readings were recorded by a separate individual so that no bias would enter the observations on this point.

Referring to the dove prism, it is essential that rays projected through it should be parallel. The maximum angle between rays projected from

opposite sides of the target for the 2 mrad target was 5 mrad or approximately 17 mins. of arc. No aberrations were detected with the naked eye or through a telescope with a 40x magnification eye-piece. The angle of 5 mrad was therefore considered to be insufficient to affect the viewer. Additional observations (marked dove prism No. 2) were taken with a second dove prism, but no alteration in the sign of the residual error was noted.

An inverted image of the target and surrounding area was seen for one position of the prism and an upright image for the other position. This condition could not be controlled during the observations and it is not known whether it may have influenced the results. The only way this condition could have been controlled was to enclose the sighting line in a tunnel such that the surrounding area was completely obscured. This would make it impossible to detect whether the circular target was inverted. It was impractical to do this in the laboratory in which the observations were carried out.

Some experiments on the inversion of visual images are described by *Gregory (1966, 208)*. These experiments involved wearing inverting prisms for long periods. Adaptation to the inverted image took considerable time, while on removal of the prisms, adaptation was usually much quicker. Conditions in this study are different from those in experiments described by *Gregory (1966)*. Images were viewed alternately inverted and upright, each situation lasting only about 1 minute. Difficulties encountered in adapting to the inverted image in the above experiments, however, indicate that unless the surrounding area of the target is completely obscured, such that the observer is unaware that the image is inverted, small residual effects of image inversion as in this study may still exist. The influence of inverted images on the residual errors may be a subject for future research.

It must be emphasised, however, that the residual errors derived by these observations are in the order of 5 - 10  $\mu$ rad (1 - 2 secs. of arc) for experienced observers, and slightly larger for inexperienced observers.



These values are approximately  $1/10$ th of the interconal distance on the retina and are also approximately equal to the smallest visual acuity values obtained, as given in section 2.25. The residual errors derived by this technique therefore appear to be acceptable considering the capabilities of the visual system.

Based on the standard deviations of one direction of approach given in figure 6.8, and the fact that the centre of the target is derived by taking means of both directions of approach of the MM, the standard deviation of the estimated central position is simply  $\sqrt{2}$  times the standard deviation given in figure 6.8.

### 7.3 Conclusion.

The technique of eliminating systematic errors by the dove prism attachment proved to be successful for both experienced and inexperienced observers. This leads to a significant improvement in accuracies of location of targets, since the systematic errors of observations in which one direction of approach only was used, proved to be large and very unreliable. It is suggested that observations be taken alternately from each direction to eliminate variations in systematic errors, particularly for inexperienced observers. With regard to its application in photogrammetric equipment, since many instruments are equipped with dove prisms, there seems to be no reason why this technique could not be applied immediately to precise coordinate measurements, provided sufficient range of rotation of the dove prism is available.

## 8. PRACTICAL APPLICATION OF RESEARCH.

### 8.1 Introduction.

The results in Chapter 6 outline monocular pointing accuracies which can be obtained by the visual system using blurred targets of low and medium contrast. For binocular viewing, improvements in pointing accuracies may be expected, particularly for very blurred targets. *O'Connor (1962)* indicated that there was not a marked difference between monocular and binocular pointing results, for the targets observed in his investigations. From experiences in this study, the use of binocular vision lowers the threshold and therefore should improve pointing accuracies at least for very blurred targets. The exact relationship however is unknown. The following discussion will therefore relate to monocular pointing results. Such a discussion may be applied directly to observations on monocomparators. Since the relationship between monocular and binocular observations is likely to be simple, except perhaps for near threshold targets, the conclusions reached in the following discussion should also be applicable to binocular pointing results.

If sufficient information is known on the image quality of the target being viewed by the observer in the photogrammetric instrument, pointing accuracies may be predicted. The many steps which may be involved in predicting pointing accuracies based on figure 6.8, are given by *Hempenius (1964, 310)*. A more useful approach to the practical problem is to be able to choose a target size which, when viewed in the photogrammetric instrument, will give a predictable maximum pointing accuracy. This approach requires a knowledge of the luminance characteristics of the target and its background, details of the imaging characteristics of the photographic and photogrammetric systems, and also the results given in Chapter 6. Since there are many unknown variables involved in such a problem, it is impossible to treat it in detail in this work. However, examples of targets artificially produced by the Umbrascope described in section 5.72 will be discussed. This discussion will indicate the manner in which the problem can be treated, and also estimate

a formula for optimum target sizes. Another application of pointing results may be in the choice of an economic scale of photography to give maximum pointing accuracy for certain specific ground objects, e.g. manhole covers. The effects of granularity on pointing accuracies are outside the scope of this work and therefore cannot be included in this investigation.

Before proceeding with investigations on target size a brief résumé of existing literature on signalized targets will be given.

## 8.2 Signalized Targets.

*Eekhout (1963)* carried out a comprehensive investigation on signalized targets with the purpose of finding the most suitable and economic types of targets for local conditions. He recommends a white square target with a black surround approximately the same width as the target. To aid in identification, four bars should form a cross through the target centre, with their length about 5 times their width. The whole target should be surrounded further by a dark background, produced artificially if necessary. *Ackerl and Neumaier (1969)* recommend a yellow centered target with a black border with no cross bars for identification. The border of their target is narrower than that recommended by Eekhout above, but the two targets are basically similar. A high contrast between the target and its background should give the steepest target density profile, and therefore the best pointing accuracy, provided target width is also controlled.

Very few recommendations are available for the size of targets. *Pastorelli (1959)* recommends that the minimum size of target in meters should be -

Scale No. of Photograph / 40,000.

*Hempenius (1964, 314)* suggests that the target size should equal the scale No. of photograph times the  $2\sigma$ -width of the combined spread function of the photographic and photogrammetric systems. Since the quality of the image of the target is dependent on the spread function of the total system, and pointing accuracies are dependent on the grade of the blur, this criterion is clearly more acceptable than that of Pastorelli. Pastorelli's formula

would normally prescribe smaller targets than Hempenius' rule.

Target profiles given by *Hempenius (1964, 311)* are not directly applicable to figures 6.2 and 6.7 since the spread functions of the optical systems of photogrammetric instruments are unknown. No actual pointing results however were reported. Pointing observations to such targets carried out on a photogrammetric instrument would include the inaccuracies of the instrument, e.g. *Visser (1964)*. *O'Connor (1967)* commenting on results of his earlier work, indicated that the stereocomparators obscured the true capabilities of the visual system, particularly for small targets. The grades of the density profiles of the signalized targets presented by *Hempenius (1964, 311)* range from 0.15 to 0.32  $\Delta D/mrad$ , if viewed in an instrument at 10x magnification with perfect optics. Since such grades of the density profile are larger than at the points of discontinuity in figure 6.2, neglecting instrumental errors, pointing accuracies would be determined by size rather than blur characteristics.

In the following section an attempt will be made to relate the size of the target on the ground to the target blur, and therefore predict the accuracy for different ground target sizes.

### 8.3 Prediction of Pointing Accuracies.

Table 5.1 gives  $\sigma$ -widths of the SF's for six levels of shelf B in the Umbrascope, derived from some 50 targets at different contrasts. By varying the level of shelf B and the size of the opaque mark on that shelf, different target sizes and grades of blur could be obtained. Various background densities were obtained by altering the exposure time when the targets were photographed (see section 5.72).

The circular opaque mark on the central shelf was considered to be the ground signalized target and the image of this target on an aerial photograph

equivalent to the pattern obtained on the top shelf after the convolution. Because of the design of the Umbrascope, it was impossible to produce images of targets which would be obtained from ground targets with different background luminance characteristics. The situation reproduced artificially is that of a white target on a dark background at different exposures. Since this is similar to the recommended situation described in the previous section, the treatment in this section may be applied to practical cases.

It must be pointed out that some inaccuracies do exist in the Umbrascope, as mentioned in section 5.72. These inaccuracies were not important in the printing of the targets themselves, since each target was accurately measured on a microdensitometer. They may, however, influence the results in figures 8.1 and 8.2 for the larger targets, and therefore these figures are only an approximate representation of the relation between ground target size and target blur.

Figures 8.1 and 8.2 show the grades of blur for targets of 0.3 and 0.6 background density produced in the Umbrascope, with different spread functions and five ground target sizes. These figures have been derived from microdensitometer traces of approximately 120 blurred targets. Based on these figures, the grades of blur for 5 spread functions have been deduced. Transferring these grades of the density profile to figure 6.2, with the appropriate annulus sizes, pointing accuracies have been determined as presented in Table 8.1.

Annulus sizes are approximately equal to the targets which were used to produce them, for grades of the density profiles less than  $0.1 \Delta D/\text{mrad}$ , assuming a MM of 1 mrad. For grades of blur greater than  $0.3 \Delta D/\text{mrad}$ , annulus widths equal approximately half the size of targets which were used to produce them. There is a gradual transition between these two extremes, the transition being more rapid for the larger targets. Annulus sizes can be estimated sufficiently accurately to enable the estimation of pointing accuracies from figure 6.2, keeping in mind the fact that the subjective width of the annulus will depend on the observer.

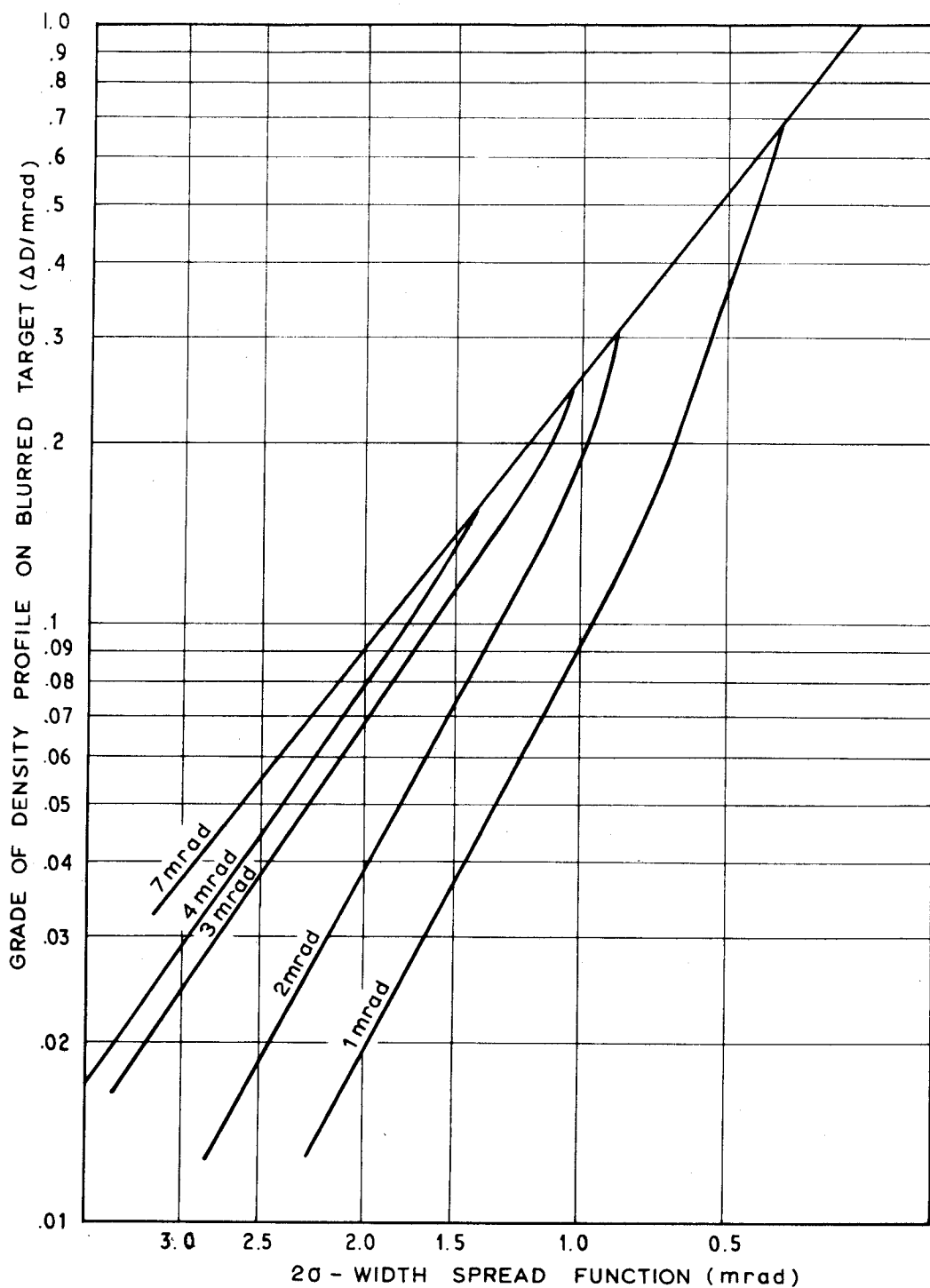


FIG. B.1: RELATIONSHIP BETWEEN GRADE OF DENSITY PROFILE ON BLURRED TARGET, AND 2σ-WIDTH OF THE SPREAD FUNCTION USED IN THE CONVOLUTION, FOR DIFFERENT GROUND TARGET SIZES. BACKGROUND DENSITY OF TARGET IS 0.3

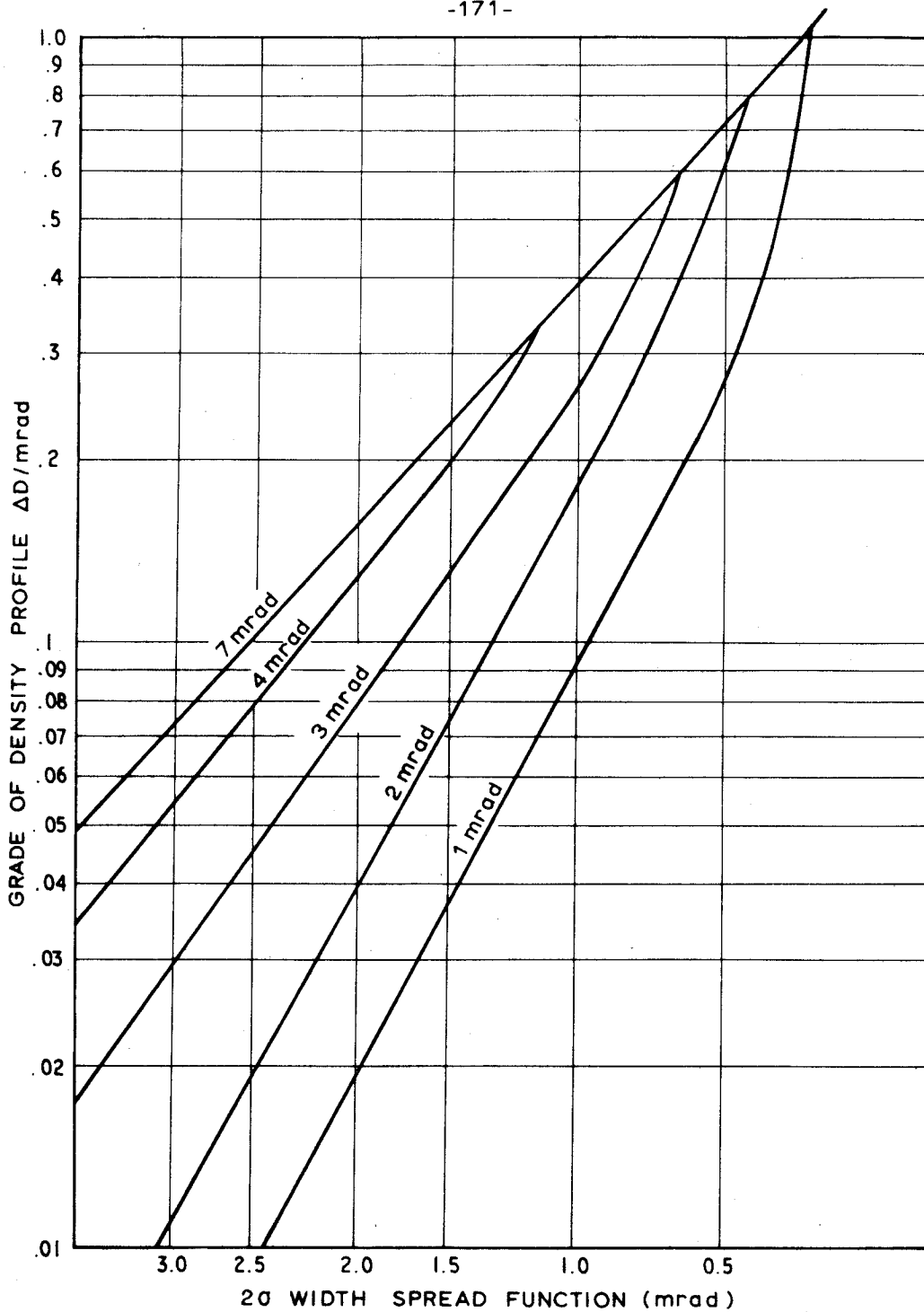


FIG. 8.2: RELATIONSHIP BETWEEN GRADE OF DENSITY PROFILE OF BLURRED TARGET AND THE  $2\sigma$ -WIDTH OF THE SPREAD FUNCTION USED IN THE CONVOLUTION FOR DIFFERENT GROUND TARGET SIZES. BACKGROUND DENSITY OF TARGET IS 0.6.

Table 8.1.

2 $\sigma$ -value of SF	3.0 mrad		2.4 mrad		1.8 mrad		0.7 mrad		0.2 mrad	
	Blur $\Delta D/mrad$	St.Dev. $\mu rad$	Blur $\Delta D/mrad$	St.Dev. $\mu rad$	Blur $\Delta D/mrad$	St.Dev. $\mu rad$	Blur $\Delta D/mrad$	St.Dev. $\mu rad$	Blur $\Delta D/mrad$	St.Dev. $\mu rad$
Density of Background = 0.3										
7 mrad	0.037	84	0.060	65	0.12	45	0.18	38	0.8	35
4 "	0.029	71	0.050	51	0.095	35	0.40	22	0.8	22
3 "	0.024	70	0.042	53	0.035	28	0.40	22	0.8	20
2 "	0.01	>100	0.021	68	0.05	34	0.40	16	0.8	16
1 "	<.01	-	0.012	-	0.025	51	0.40	16	0.8	16
Density of Background = 0.6										
7 mrad	0.070	58	0.12	45	0.18	38	0.57	35	>1.0	35
4 "	0.051	50	0.085	39	0.15	35	0.57	22	>1.0	22
3 "	0.027	61	0.049	42	0.095	33	0.50	22	>1.0	20
2 "	<.01	-	0.021	65	0.05	41	0.35	16	>1.0	16
1 "	-	-	0.01	-	0.024	61	0.17	16	>0.9	16



Three factors enter into the determination of pointing accuracy:

- (i) The size of the signalized ground target,
- (ii) The grade of blur for the different target sizes in (i),
- (iii) The width of the annulus.

For large  $2\sigma$ -widths of the SF, factor (i) is clearly important in determining the grade of blur and therefore the pointing accuracy. In contrast, for small SF's, ground target size has no effect on the grade blur, and therefore pointing accuracies are determined by annulus size only. The optimum size of ground target for the three SF's of 3.0, 2.4 and 1.8 mrad is between 2 and 3 times the  $\sigma$ -value of SF. This agrees approximately with Hempenius' rule (1964, 314) mentioned in the previous section. Adopting an average value of  $60 \mu$  (2.4 mrad at 10x magnification) as the  $2\sigma$ -width of the SF of a photogrammetric system, the recommended ground target size is approximately 3.0 mrad or  $75 \mu$  at the scale of the negative, assuming a MM of  $25 \mu$ rad.

If the system SF has a  $2\sigma$ -width less than 1 mrad, adoption of a target smaller than 1 mrad will not improve pointing results, since accuracies reach a constant value of approximately  $16 \mu$ rad for annulus widths between 0.25 and 1.0 mrad (figure 1.1). If annulus widths can be decreased to less than .25 mrad an improvement in accuracies may result provided the targets are of very high contrast and very sharp. The intention to use annuli smaller than  $250 \mu$ rad would have to be studied very carefully since pointing accuracies may decrease rapidly if the ideal conditions are not satisfied (refer figure 6.8).

For a given ground target size and spread function, pointing accuracies are dependent on the blur of the target. This varies according to the background density of the photographed target, and therefore the exposure and characteristics of photographic emulsion. From the results in Table 8.1, maximum accuracies are obtained when the targets are photographed at high contrast. Further work on specific practical problems, however, must be carried out to confirm this statement.

#### 8.4 Conclusions.

Though figures 8.1 and 8.2 are only approximate, good agreement has been obtained between different spread functions and the derived empirical formula for optimum ground target size, neglecting the effects of granularity of photography. This formula, for practical photogrammetry is as follows:-

*Optimum target size = photograph scale number times 2.5 times the  $\sigma$ -width of the SF of the photogrammetric system.  
A minimum target size should be chosen such that annulus widths are not less than 1 mrad subtended at the eye.  
Targets should be photographed at high contrast, for maximum accuracy.*

The above rule has been derived for the particular case of a theoretically bright target on a black background and a gaussian SF. Different target configurations and SF's may produce a slightly different relationship. Since SF's are normally approximately gaussian, and targets high contrast, the above work gives a reliable estimate of a rule for optimum ground target size.

9. FINAL CONCLUSIONS.

- 9.1 The overall pattern of pointing accuracies to sharp and blurred targets is very complex.
- 9.2 The complex pattern for sharp targets with annulus widths less than 1 mrad is due to the blurring effects of the visual system. Convolutions of approximate SF's for the visual system, which include effects of inhibition, with the luminance profile of the target substantiate this finding. Based on these convolutions, simple criteria used by the visual system for pointing to sharp targets can be determined.
- 9.3 Pointing accuracies for blurred targets of low and medium contrast are dependent primarily on the grade of the density profile of the target, and secondly on the annulus width, for grades of the density profile less than  $0.3 \Delta D/\text{mrad}$  for 0.8 mrad annulus width,  $0.12 \Delta D/\text{mrad}$  for 2.0 mrad annulus width, and  $0.06 \Delta D/\text{mrad}$  for 5.0 mrad annulus width. For target density profiles greater than those values, pointing accuracies equal those for sharp targets.
- 9.4 Stevens' psychophysical law may be related to pointing to blurred targets, and indicates the significance of target visibility thresholds in determining pointing accuracies.
- 9.5 Systematic errors can be eliminated using a dove prism in the optical system of an instrument. This technique allows movement of the MM from mutually opposite directions, while it appears to the observer always to move in the same direction. The mean of the measurements from mutually opposite directions gives a true estimate of the actual centre of the target.

- 9.6 Based on the pointing accuracies derived from blurred targets, an empirical rule prescribing the size of targets for pointing accuracies is as follows:-

*Target size = scale No. of the photograph times 2.5 times the  $\sigma$ -width of the spread function of the photogrammetric system. Target sizes should be chosen such that the annulus width is not smaller than 1 mrad or 25  $\mu$  at 10x magnification and should be photographed at high contrast.*

This law is related to targets produced artificially and must be checked when applied to specific photogrammetric problems.

REFERENCES.

- ACKERL, F. and  
K. NEUMAIER  
1959 "Über die Signalisierung der Passpunkte für  
Infrarot Aufnahmen ", *Photogrammetria*,  
Vol. XVI, No. 1, 17-28.
- ANDERSEN, E.E. and  
F.W. WEYMOUTH  
1923 "Visual Perception and Retinal Mosaic ",  
*Amer. J. Physiol.*, 64, 561-594.
- BLACKWELL, H.R.  
1953 "Psychophysical Thresholds : Experimental Studies of  
Methods of Measurement", *Univ. of Michigan Eng.*  
*Research, Bull. No. 36.*
- BLACKWELL, H.R.  
1963 "Neural Theories of Simple Visual Discrimination",  
*J. Opt. Soc. Am.*, 53, 129-160.
- BROWN, K.T.  
1953 "Factors Affecting Differences in Apparent Size  
Between Opposite Halves of a Visual Medium",  
*J. Opt. Soc. Am.*, 43, 464-472.
- BROWN, K.T.  
1955 "An Experiment Demonstrating Instability of  
Retinal Directional Values", *J. Opt. Soc. Am.*,  
45, 301-307.
- BYRAM, G.M.  
1944 "The Physical and Photochemical Basis of Visual  
Resolving Power". I. The Distribution of  
Illumination in Retinal Images " , *J. Opt. Soc. Am.*,  
34, 571-591.
- CANDLAND, D.K.  
1968 "*Psychology: The Experimental Approach*", McGraw-  
Hill Book Co., N.Y. 1968.
- CHARMAN, W.W. and  
B.M. WATRASIEWICZ  
1964 "Mach Effect Associated with Microscopic Images",  
*J. Opt. Soc. Am.*, 54, 791-795.
- DAVSON, H.  
1962 "*The Eye*", Vol. 2, ed. H. Davson, Academic Press,  
London.
- DAVSON, H.  
1962a "*The Eye*", Vol. 4, ed. H. Davson, Academic Press,  
London.
- DAVSON, H.  
1963 "*The Physiology of the Eye.*" J. and A. Churchill  
Ltd., London.

- DePALMA, J. and  
E.M. LOWRY  
1962 "Sine-Wave Response of the Visual System. II. Sine-Wave and Square-Wave Contrast Sensitivity", *J. Opt. Soc. Am.*, 52, 328-335.
- EEKHOUT, L.  
1963 "Experiments on Point Signalization", *Technical Publication No. 3*, Ministry of Lands and Natural Resources, Rhodesia.
- ENSLEY, H.H.  
1955 "*Visual Optics*, Vol. 1, Hatton Press, London.
- FLOM, M.C.,  
F.W. WEYMOUTH,  
D. KAHNEMAN  
1963 "Visual Resolution and Contour Interaction", *J. Opt. Soc. Am.*, 53, 1026-1032.
- FRY, G.A.  
1947 "The Relation of a Brightness Contrast Border to its Visibility", *J. Opt. Soc. Am.*, 37, 166-175.
- FRY, G.A.  
1955 "*Blur of the Retinal Image*", Ohio State University Press, Columbus, Ohio.
- FRY, G.A.  
1963 "Retinal Image Formation, Review, Summary and Discussion," *J. Opt. Soc. of Am.*, 53, 94-97.
- GRAHAM, C.H.  
1950 "Behaviour, Perception and the Psychophysical Methods", *Psychological Rev.*, 57, 108-118.
- GREGORY, R.L.  
1966 "*Eye and Brain*," World University Library, London.
- GUBISCH, R.W.  
1967 "Optical Performance of the Human Eye," *J. Opt. Soc. Am.*, 57, 407-415.
- GUILFORD, J.P.  
1954 "*Psychometric Methods*", McGraw-Hill, New York.
- HALD, A.  
1952 "*Statistical Theory with Engineering Applications*," John Wiley and Son, Inc., New York.
- HEMPENIUS, S.A.  
1962 "Aspects of Photographic Systems Engineering", *Applied Optics*, 3, 45-53.
- HEMPENIUS, S.A.  
1964 "Physical Investigations on Pricked Points Used in Aerial Triangulation", *Photogrammetria*, 19, 301-328.

- HEMPENIUS, S.A.  
1965 "Spread Functions and Transfer Functions in Image, Formation and Recording." *I.T.C. Lecture Notes*.
- HEMPENIUS, S.A.  
1968 "Physiological and Psychological Aspects of Photo-Interpretation," *Invited Paper, Commission VII, 11th Congress ISP, Lausanne*.
- HERING, E.  
1865 *Arch. f. Anat., Physiol. und Wissench. Med.*, 152
- HILDEBRAND, R.  
1956 "*Introduction to Numerical Analysis*". McGraw Hill, New York.
- JENNISON, R.C.  
1961 "*Fourier Transforms and Convolutions for the Experimentalist*", Pergamon Press, London.
- KEESEY, V.T.  
1960 "Effects of Involuntary Eye Movements on Visual Acuity." *J. Opt. Soc. Am.*, 50, 769-774.
- KINCAID, W.M.  
H.R. BLACKWELL and  
A.B. KRISTOFFERSON,  
1960 "Neural Formulations of the Effects of Target Size and Shape on Visual Detection." *J. Opt. Soc. Am.*, 50, 143-148.
- KOHLER, W. and  
H. WALLACH,  
1944 "Figural after-effects." *Proc. Am. Phil. Soc.*, 88, 269.
- KRAUSKOFF, J.  
1962 "Light Distribution in Human Retinal Images." *J. Opt. Soc. Am.*, 52, 1046.
- LAMAR, E.,  
S. HECHT,  
S. STEER and  
C. HENLEY,  
1947 "Size, Shape and Contrast in Detection of Targets by Daylight Vision," *J. Opt. Soc. Am.*, 37, 531-545.
- LINFOOT, E.H.  
1965 "*Fourier Methods in Optical Image Evaluation*", Focal Press, London.
- LOWRY, E.M. and  
J.J. DePALMA,  
1961 "Sine-Wave Response of the Visual System. I. The Mach Phenomenon," *J. Opt. Soc. of Am.*, 51, 740-746.

- MARIMOT, R.B.  
1963 "Linearity and the Mach Phenomenon,"  
*J. Opt. Soc. Am.*, 53, 400-401.
- MENSEL, E.  
1959 Der Gesichtssinn als linearer Übertragungskanal und  
die Machschen Streifen," *Die Naturwissenschaften*,  
46, 316-317.
- MORONEY, M.S.  
1951 "*Facts from Figures*", Penguin Books Ltd.,  
Middlesex.
- O'CONNOR, D.C.  
1962 "On Pointing and Viewing to Photogrammetric  
Signals," *I.T.C. Publication A 14/15*.
- O'CONNOR, D.C.  
1967 "Visual Factors Affecting the Precision of  
Coordinates Measurements in Aerotriangulation,"  
*University of Illinois, Photogrammetry Series No. 6*.
- O'CONNOR, D.C.  
1968 "X - Y - Correlation in Coordinate Measurement,"  
*Phot. Eng.*, 34, 682-687.
- PASTORELLI, A.  
1959 "Die Signalisierung der Fix - und Grenzpunkte im  
Gelände als Massnahme der Praxis - Photogrammetrie"  
*Photogrammetria*, Vol. XVI, No. 2, 106-108.
- PATEL, A.S.  
1966 "Spatial Resolution by Human Visual System. The  
Effect of Mean Retinal Illuminance,"  
*J. Opt. Soc. Am.*, 56, 689-694.
- POLYAK, S.  
1948 "*The Retina*," University of Chicago Press.
- RATLIFF, F.  
1965 "*Mach Bands: Quantitative Studies on Neural Networks  
in the Retina*," Holden-Day Inc., San Francisco.
- RIGGS, L.A.  
1965 "*Vision and Visual Perception*," Ed. C.H. Graham,  
John Wiley and Son, New York.
- RIGGS, L.A.  
F. RATLIFF,  
J.C. CORNSWEET and  
T.N. CORNSWEET  
1953 "The Disappearance of Steadily Fixated Visual  
Test Objects." *J. Opt. Soc. Am.*, 43, 495-501.
- SCHMID, H.H.  
1964 "Analytical Photogrammetric Instruments,"  
*Photogrammetric Engineering*, XXX, 559-567.



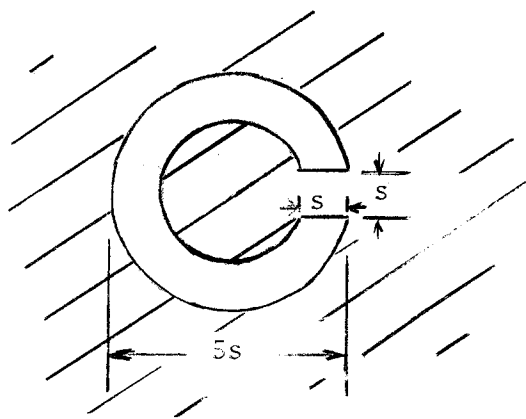
- SENDERS, V.L.  
1948 "The Physiological Basis of Visual Acuity,"  
*Psychol. Bull.*, 45, 465-490.
- SHLAER, S.  
E.L. SMITH and  
A.M. CHASE,  
1942 "Visual Acuity and Illumination in Different  
Spectral Regions," *J. Gen. Physiol.*,  
25, 553-569.
- SIDOWSKI, J.B.  
1966 "*Experimental Methods and Instrumentation in  
Psychology*," McGraw-Hill, New York.
- STEVENS, S.S.  
1962 "The Surprising Simplicity of Sensory Metrics,"  
*American Psychologist*, Vol. 17, 29-39.
- SWETS, J.A.  
1961 "Is there a sensory threshold?" *Science*,  
134, 168-177.
- TRINDER, J.C.  
1965 "Retinal Image Criteria in Photogrammetric  
Pointing," *M.Sc. Thesis, I.T.C. Delft*.  
Chap. 7 "On the Subjective Location of Edges  
and Pointing to Edges," by J.C. Trinder and  
S.A. Hempenius.
- TRINDER, J.C.  
1968 "Photogrammetric Pointing Accuracy as a Function  
of Properties of the Visual Image."  
*UNISURV Report No. 9, University of N.S.W.*
- VISSER, J.  
1964 "Tests of the Precision of Observing Plate  
Coordinates and Parallaxes in a Stereocomparator,"  
*Photogrammetria*, XIX, No. 7, 297-300.
- WALSH, J.W.T.  
1953 "*Photometry*," Constable and Co. Ltd., London.
- WATRASIEWIEZ, B.M.  
1966 "Some Factors Affecting the Appearance of Mach  
Bands," *J. Opt. Soc. Am.*, 56, 499-503.
- WESTHEIMER, G. and  
F.W. CAMPBELL,  
1962 "Light Distribution in the Image Formed by the  
Living Human Eye," *J. Opt. Soc. Am.*,  
52, 1040-1045.
- WOLFE, R.N. and  
S.A. TUCCIO  
1960 "The Effect of the Variables of a Photographic  
System on Detail Rendition, with Special Reference to  
Camera Motion," *Photographic Science and Engineering*,  
4, 330-340.
- ZORN, H.C.  
1965 "An Instrument for Testing Stereoscopic Acuity,"  
*Photogrammetria*, 20, 229-238.

GLOSSARY OF TERMS.

*Convolution.* (p.10) (Jennison, 1961, 6) is "the operation whereby a structure under observation is smeared or spread out by the response or resolution of an instrument or mathematical operation." In Optics, convolution is used to derive the image of an object which is "smeared" by an optical system. In terms of the above definition, the "structure" is the intensity profile of the object, while the "instrument" is the optical system.

*Inhibition.* (p.15) The depression of the response to illumination of a given receptor by the stimulation of neighbouring receptors.

*Landolt C* (p.16). The accompanying figure shows the form of the Landolt C. The width  $s$  of the gap is  $1/5$ th of the overall diameter of the circle (Ensley, 1955, 63).



*Luminance Profile (p.10)*. If the pattern of luminance over an object either reflected or transmitted, e.g. a line, is measured by a light sensing instrument, the profile resulting is termed a luminance or intensity profile. The abscissa scale refers to the position on the object, while the ordinate scale, the intensity readings either in relative or absolute units (see fig. 3.1).

*Retinal illuminance (p.10)* is defined as L.S. trolands, where L is the luminance of the stimulus in candelas/sq. m.<sup>2</sup> (3.1 candelas/sq.m = 1 mL), and S is the area of the pupil in mm<sup>2</sup>. A number of difficulties arise in the use of retinal illuminances:-

- (i) amount of light at the retina is not constant with wavelength;
- (ii) area of pupil can vary for different observers;
- (iii) light entering the marginal areas of the pupil is less effective to retinal stimulation than light entering the centre of the pupil.

This last point is known as the *Stiles-Crawford (p.10)* effect. The loss in effective illuminance for a 3 mm diameter pupil is about 5% (Walsh, 1953, 60). Because of the indefinite nature of the retinal illuminance, no attempt is made to correct for this difference.

*Luminance (p.10)*. A perfectly reflecting and diffusing surface, normal to incident light from a source of 1 candela, 1 centimetre away, has a luminance of 1 Lambert. Since this unit is usually too large the millilambert (mL) is used. A perfect reflecting and diffusing surface reflects all light it receives, and moreover appears equally bright from all directions.

*Micro-nystagmus (p.21)*. The small involuntary movements of the eye during fixation. They are divided into three (3) types (Davson, 1963, 250):-

- (a) Irregular high frequency movements and small excursions over about 20 sec. of arc.

- (b) Flicks or saccades of several minutes of arc occurring at irregular intervals of the order of 1 sec.
- (c) Between saccades there are slow drifts extending up to 6 mins. of arc.

*Spread Function (SF) (p.10)* describes the blurring or spreading of fine details in an image formed by an optical system. It is the resulting intensity or luminance profile across the image formed by the optical system, of a very small detail, either a point or a line. The resulting functions are the line spread function (LSF) and the point spread function (PSF).

APPENDIX A.

Statistical Analysis of Pointing Observations.

A.1 Analysis of Variance for Average Error Method.

Observations by the average error method were carried out in 4 or 8 sets of 25, or 10 sets of 10; the majority of targets were observed in 10 sets of 10 observations to reduce fatigue. For each set  $i$  with  $N_i$  observations,  $\bar{x}_i$  is the sample mean, being an estimate of the population mean  $\xi_i$ , and the variance  $S_{i1}^2$  is an estimate of the population variance  $\sigma^2$ . Within each group, observations are assumed to be normally distributed, based on findings of psychophysical tests, and also tests in Appendix B.

Firstly, an analysis of variance is necessary to investigate whether  $S_{i1}^2$  ( $i = 1, K$ ) are estimates of the same population variance. Because the population variance is unknown, the analysis will test whether  $S_{i1}^2$  ( $i = 1, K$ ) are all estimates of the same variance  $S_1^2$ , which itself is an estimate of the population variance  $\sigma^2$ . Secondly, a further analysis is necessary to test the hypothesis that the individual population means of each set  $\xi_1, \dots, \xi_i$  are equal, and are represented by the same sample mean  $\bar{x}$ . This test renders a further estimate of  $\sigma^2$ ,  $S_2^2$ , which can be tested against  $S_1^2$ .

A.11 Tests of Variance.

*Hald (1962, 291)* quotes the formulae attributed to Bartlett, in which a set of estimates of variance  $S_{11}^2, S_{21}^2, \dots, S_{i1}^2$  with degrees of freedom  $f_1, f_2, f_i$ , may be tested as to whether they are estimates of the same variance  $\sigma^2$ . The following function  $E$  has approximately a  $\chi^2$ -distribution with  $K-1$  degrees of freedom:-

$$E = \frac{2.3026}{c} (f \log S_1^2 - \sum_{i=1}^K f_i \log S_{i1}^2) \dots\dots\dots (A1)$$

where  $S_1^2$  is the pooled variance estimate of  $\sigma^2$  derived from

$$S_1^2 = \frac{\sum_{i=1}^K f_i S_{i1}^2}{\sum_{i=1}^K f_i} \dots\dots\dots (A2)$$

$$f = \sum_{i=1}^K f_i \dots\dots\dots (A3)$$

$$\text{and } c = 1 + \frac{1}{3(K-1)} \left( \sum_{i=1}^K \frac{1}{f_i} - \frac{1}{f} \right) \dots\dots\dots (A4)$$

(The approximation is poor for  $f_i \leq 2$ .)

In the case of the investigations in this study,  $f_i$  was generally either 7 or 9. For observations in which  $f_i = f_o = \text{constant}$ , the formula becomes

$$E = \frac{2.3026}{c} K f_o (\log S_1^2 - \frac{1}{K} \sum_{i=1}^K \log S_{i1}^2) \dots\dots\dots (A5)$$

$$\text{where } c = 1 + \frac{K+1}{3 f_o K} \dots\dots\dots (A6)$$

For 8 sets of 25 observations

$$E = 435.30 (\log S_1^2 - \frac{1}{8} \sum_{i=1}^K \log S_{i1}^2)$$

For 10 sets of 10 observations

$$E = 199.12 (\log S_1^2 - \frac{1}{10} \sum_{i=1}^K \log S_{i1}^2)$$

The pooled  $S_1^2$  may be computed from formula (A2), and tested as outlined in formula (A5). Provided the test is not significant,  $S_1^2$  may be considered as an estimate of the population variance  $\sigma^2$ .  $\chi^2$ -distribution values were computed for the observations carried out in this study, for the upper and lower 5% significance levels as shown in Appendix B. *Halđ (1962, 292)* recommends that the lower significance level tests whether the variances fit "too well." Such a result may mean that the individual variances are not statistically independent or some observations may perhaps have been incorrectly discarded.

A further check may be carried out on the individual variances by computing individual estimates of  $\chi^2$ , i.e.  $\chi'^2 = \frac{f_i S_{i1}^2}{S_1^2}$  which has  $f_i$  degrees of freedom. If  $f_i$  is large compared with  $f_0$ , the estimated value of  $\chi'^2$  is approximately equal to  $\chi^2$  as computed previously.  $\chi'^2$  should be within the lower and upper significance levels. On occasions when variances have been eliminated in Appendix B, they have been marked with an asterisk.

#### A.12 Tests of Means.

The sample means of each set of observations  $\bar{x}_i$  must be tested whether they are estimates of the same population mean  $\xi$ . Though this test is not necessary if only a variance or standard deviation is required, the means were tested in this study, for purposes of investigating the systematic error. This test can be carried out by a further analysis of variance.

Two estimates of the population variance can be made from the observations. The first is  $S_1^2$  as given in formula (A2), known as the variation *within sets of observations* and is independent of sample means  $\bar{x}_1, \bar{x}_2, \dots, \bar{x}_i$

The second may be computed from

$$S_2^2 = \frac{\sum_{i=1}^K N_i (\bar{x}_i - \bar{x})^2}{K - 1} \dots\dots\dots (A7)$$

where  $\bar{x}_i$  is the mean of  $N_i$  observations in set  $i$   
and  $\bar{x}$  is the total mean of observations in  $K$  sets of  $N_i$  observations.

This formula tests whether the hypothesis that  $\xi_1 = \xi_2 = \xi_3 = \dots = \xi_i$  is true, and consequently that  $S_2^2$  is an estimate of the population variance  $\sigma^2$ . This is termed the *between the sets* estimate and computes the variation of the sample means against the total mean. To test the hypothesis that  $S_1^2$  and  $S_2^2$  are both estimates of the same variance  $\sigma^2$ , the ratio  $\frac{S_2^2}{S_1^2}$  must follow the  $v^2$ -distribution or Fisher distribution with

$(k - 1, \sum_{i=1}^K N_i - K)$  degrees of freedom.

i.e.  $\frac{S_2^2}{S_1^2} = v^2_{(K-1), \sum_{i=1}^K N_i - K}$

The  $v^2$ -distribution values at the 5% significant level are shown in the results.

A further check on the individual means may be made by the t-test:-  
 $\frac{\bar{x}_i - \bar{x}}{S/\sqrt{N_i}}$  must follow a t-distribution with  $N_i - 1$  degrees of freedom.



Summary of test as outlined by Hald are:-

Variations	Sum of Squares	Degrees of Freedom	$S^2$	Test
Between sets	$\sum_{i=1}^K N_i (\bar{x}_i - \bar{x})^2$	$K - 1$	$S_2^2$	$v^2 = \frac{S_2^2}{S_1^2}$
Within sets	$\sum_{i=1}^K \sum_{v=1}^{N_i} (x_{iv} - \bar{x}_i)^2$	$\sum_{i=1}^K N_i - K$	$S_1^2$	
Total	$\sum_{i=1}^K \sum_{v=1}^{N_i} (x_{iv} - \bar{x})^2$	$\sum_{i=1}^K N_i - 1$	$S_0^2$	

Provided  $v^2$  is not significant, a pooled estimate of variance may be computed from the formula for  $S_0^2$  as shown in the above table. In the tests in this study  $S_0^2$  has been accepted as the estimate of population variance  $\sigma^2$  provided  $v^2$  is not significant, while  $S_1^2$  has been taken if  $v^2$  is significant.

A.13 Confidence Limits of  $\sigma^2$ .

The confidence limits of  $\sigma^2$  are:-

$$P \left( S^2 \frac{f}{\chi^2_{P_2}} < \sigma^2 < S^2 \frac{f}{\chi^2_{P_1}} \right) = P_2 - P_1 \dots \dots \dots (A8)$$

where  $S^2$  is the estimate of the population variance  $\sigma^2$ , either  $S_1^2$  or  $S_0^2$ .

## A.2 Regression Analysis.

A straight line regression analysis was computed for two purposes in this study.

- (i) The computation of a best fit line from the constant stimulus observations as outlined in section 4.45. The observed frequencies were transformed into equivalent ordinates on the standard cumulative normal curve, and regression was computed for the transformed frequencies against the MM position.
- (ii) The location of a best-fit line between the standard deviations determined by the average error method and the grade of the blur on the blurred targets. Since the curve was linear on a log-log scales, logarithms of both the standard deviations and the grade of blur were used in the regression computation.

## A.21 Formulation of Least Square Regression Analysis.

The general form of the straight line is:-

$$y = ax + b$$

where  $y$  refers to transformed observed frequencies, case (i) above; and logarithm of standard deviations of pointing, case (ii) above; and  $x$  refers to MM position, case (i); while it refers to logarithm of grade in density, case (ii).

There are only two unknowns, so if more than two points are known along the line, a least square technique must be used to compute  $a$ ,  $b$ .

Since the values of  $y$  in each case have different standard deviations, relative weights may be assigned to individual values.

In case (i) the Urban-Müller weights are used as specified in section 4.45. For case (ii) suitable weights may be chosen for the standard deviations  $S_o$ , in terms of their reliabilities or variances.

The distribution of a standard deviation derived from the variance of normally distributed observations is approximately normal with mean of  $\sigma$  (population standard deviation) and variance  $\frac{2\sigma^2}{f}$  for large  $f$  (Hald, 1962, 300). No correlation is assumed between the values of  $S_o$  because each target was observed completely independently of the others.

The variance-covariance matrix for the observed  $S_o$  of  $i$  targets is therefore

$$G = \begin{bmatrix} g_{11} & & \\ & g_{22} & \\ & & \dots \\ & & & g_{ii} \end{bmatrix}$$

where  $g_{ii} = \frac{2S_{io}^2}{f\sigma_o^2}$

and  $\sigma_o^2$  is a convenient constant and  $f$  is the number of degrees of freedom.

°. Matrix of weights =  $W = G^{-1}$ .

General equation for solution is

$$v_i = ax_i + b - y_i \quad (i = 1, \dots, K) \quad \dots \dots \dots \quad (A9)$$

where  $v_i$  is the discrepancy between the observed value of  $y$  and the computed regression line.

In matrix notation

$$v = Ax - f \quad \dots\dots\dots (A10)$$

$$\text{Normal equations are } Nx = F \quad \dots\dots\dots (A11)$$

where  $N = A'WA$

$$F = A'Wf$$

$$\text{Solution is } x = N^{-1} F \quad \dots\dots\dots (A12)$$

giving  $a, b$  parameters.  $v_i$  values may then be solved.

Variance-covariance matrix of the unknown parameters is therefore

$$Q = N^{-1} \quad \dots\dots\dots (A13)$$

$$\text{The standard error of unit weight, } \sigma_o = \sqrt{\frac{[v'Wv]}{K-2}}$$

which is equivalent to

$$\sqrt{\frac{K}{\sum_{i=1} w_i} \frac{(y_i - \bar{y})^2}{K-2}} \quad \text{where } y_i \text{ is the observed value with weight } w_i,$$

$\bar{y}$  is the corresponding point on the regression line, and  $K$  is the number of points. (Hald, 1962)

A.22 Confidence Interval of Regression Line.

By the Law of Combination of Variances

$$Q^{yy} = x^2 Q^{aa} + Q^{bb} + 2Q^{ab} x$$

and  $\sigma_y^2 = Q^{yy} \sigma_o^2$ , giving the standard deviation of  $y$  along the regression line. The 99% confidence limits of the regression line can be determined as  $\pm t_{(0.995, f)} \sigma_y$  from the computed regression lines, where  $t$  refers to the  $t$ -distribution. Based on the confidence limits, the observed points plotted graphically can be compared with the computed regression line. In general plotted points in figure 6.2 agreed with the 99% confidence limits of the regression line.

Separate computer programmes were written for the two cases where linear regression was necessary, but each programme contained the same nucleus for the formation and solution of the normal equations.

A.3 Tests of Goodness - of - Fit.

It was stated in Chapter 4 that observations in psychophysical tasks similar to those carried out in this study, follow a normal distribution. Several pilot tests were carried out to check the normality of observations determined by the average error method. The test is that:-

$$\sum_{i=1}^K \frac{(a_i - \hat{\theta}_i)^2}{\hat{\theta}_i} \text{ will approximate to a } \chi^2 \text{-distribution of } K-c-1 \text{ degrees}$$

of freedom,

where  $c$  is the number of linear constants.

$a_i$  is the observed frequencies in a given interval,

$\hat{\theta}$  are the theoretical frequencies computed from the theoretical normal curve over that interval,

$K$  is the number of intervals.

The above statement is true, provided the theoretical computed frequencies  $\hat{\theta} : 5$ . (Hald, 1962, 742)

A similar test can be carried out for the goodness -of-fit of the constant stimulus observations as

$$N \sum_{i=1}^K \frac{(p_i - p'_i)^2}{p'_i q'_i} = \chi^2 \text{-distribution with } K-2 \text{ degrees of freedom,}$$

where  $K$  = number of setting positions,  
 $p_i$  = observed frequency,  
 $p_i^!$  = computed frequency,  
 $q_i^!$  =  $1 - p_i^!$ ,  
 $N$  = number of observations on each MM position in the  
constant stimulus observations.

A check on normality of observations by the average error method and goodness-of-fit tests computed for the constant stimulus methods may be found in Appendix B.

APPENDIX B.

Experimental Results and Associated Computations.

B.1 Results of Observations by Average Error Method -  
Sample Presentation.

The results have been presented with the entry number as the target number given in the body of the study. For observations by JCT, the entry number is either, for instance, 6 or 6a while for observations by AHC, the entry number is either, for instance, 3b or 3c. The number of observations taken on each target have been indicated. Where sets of 25 and 10 observations have been taken on the same target, the two variances obtained have been tested against each other. Statistical methods for testing each group of observations on each target, are according to those in Appendix A. Unless otherwise stated the direction of approach of the MM is from the left hand side.

Target No. 1

Observer: JCT.

No. of Observations - 10 x 10

Annulus Width - 0.5 mrad

Obser. Dist. - 10 m.

Microm. Read (mm)	S <sup>2</sup> (μrad <sup>2</sup> )
11.08	221.67
11.04	337.70
11.04	280.84
11.01	293.27
11.02	257.09
11.06	226.23
11.09	268.78
11.05	115.14
11.01	115.14
11.01	452.76
11.12	476.58
Mean 11.05	293.01

E = 6.2

$$\chi^2_{(.975,9)} = 19.0 \quad \chi^2_{(.025,9)} = 2.7$$

Variance	f	Test
S <sub>2</sub> <sup>2</sup> = 131.11	9	$\frac{S_2^2}{S_1^2} = 0.5$
S <sub>1</sub> <sup>2</sup> = 293.01	90	
		$v^2_{(0.975,9,90)} = 2.25$

S<sub>0</sub><sup>2</sup> = 278.3

S<sub>0</sub> = 16.7 μrad

Syst. Error = u'shoot 75 μrad



Target No. 1b

Observer: AHC

No. of Observations - 10 x 10

Annulus Width - 0.5 mrad

Obser. Dist. - 10 m.

Microm. Read (mm)	S <sup>2</sup> (μrad <sup>2</sup> )
9.30	415.6
9.26	254.0
9.34	237.3
9.25	349.4
9.21	153.0
9.27	213.8
9.23	404.0
9.32	202.4
9.28	236.0
9.29	192.0
<hr/>	<hr/>
Mean 9.28	265.8

E = 4.4

$\chi^2_{(.975, 9)} = 19.0$        $\chi^2_{(.025, 9)} = 2.70$

Variance	f	Test
S <sub>2</sub> <sup>2</sup> = 161.0	9	$\frac{S_2^2}{S_1^2} = 0.6$ $\nu^2_{(0.975, 9, 90)} = 2.25$
S <sub>1</sub> <sup>2</sup> = 265.8	90	

S<sub>0</sub><sup>2</sup> = 256.24

S<sub>0</sub> = 16.0 μrad

Syst. Error = u'shoot 44 μrad

Target No. 18.

Observer: JCT.

No. of Observations - 5 x 10 in each direction

Annulus Width - 1.7 mrad

Obser. Dist. - 10 m.

Microm. Read (mm)	S <sup>2</sup> (μrad <sup>2</sup> )
→ MM direction	
13.81	920.8
13.67	384.2
13.62	1751.4
13.54	589.7
13.62	776.4
<hr/>	
Mean 13.65	
← MM direction	
12.62	669.4
12.83	1177.1
12.60	925.1
12.61	807.9
12.71	1599.0
<hr/>	
Mean 960.10	

E = 7.9

$\chi^2_{(0.975,9)} = 19.0$

$\chi^2_{(0.025,9)} = 2.7$

→ MM direction

← MM direction

Variance	f	Test	Variance	f	Test
S <sub>2</sub> <sup>2</sup> =997.5	4	$\frac{S_2^2}{S_1^2} = 1.0$	S <sub>2</sub> <sup>2</sup> =955.0	4	$\frac{S_2^2}{S_1^2} = 1.0$
S <sub>2</sub> <sup>2</sup> =960.1	90	$\nu^2_{(0.975,4,90)} = 2.94$	S <sub>2</sub> <sup>2</sup> =960.1	90	$\nu^2_{(0.975,4,90)} = 2.94$

S<sub>1</sub><sup>2</sup> = 960.10

S<sub>1</sub> = 31.1 μrad

Syst. Error → = u'shoot 288 μrad

Syst. Error ← = o'shoot 140 μrad

Mean = 214 μrad left of centre

Target No. 18a

Observer: JCT

No. of Observations - 4 x 25 in each direction

Annulus Width - 1.7 mrad

Obser. Dist. - 10 m.

Microm. Read (mm)	S <sup>2</sup> (μrad <sup>2</sup> )
→ MM direction	
13.71	595.4
13.66	1183.4
13.39	1317.7
13.52	660.5
<hr/>	
Mean 13.57	
← MM direction	
12.51	449.4
12.66	835.2
12.52	729.0
12.55	1156.0
<hr/>	
Mean 12.57	865.8

E = 11.5

$\chi^2_{(0.975,7)} = 16.0$

$\chi^2_{(0.025,7)} = 1.69$

→ MM direction

← MM direction

Variance	f	Test
S <sub>2</sub> <sup>2</sup> = 4,950	3	$\frac{S_2^2}{S_1^2} = 5.7^*$
S <sub>1</sub> <sup>2</sup> = 865.8	192	

Variance	f	Test
S <sub>2</sub> <sup>2</sup> = 3,387	3	$\frac{S_1^2}{S_2^2} = 3.9^*$
S <sub>1</sub> <sup>2</sup> = 865.8	192	

$S_1^2 = 865.8$        $S_1 = 29.5 \mu\text{rad}$

Syst. Error Not Estimated due to

Failure of Tests.

Test of targets 18, 18a for Variances  $\frac{960.1}{868.8}$  using Fisher

Test .90, 192 degrees of freedom - acceptable

Combined Variance  $S_1^2 = 895.9$

$S_1 = 30.0 \mu\text{rad}$

Target No. 18b.

Observer: AHC.

No. of Observations - 4 x 25 in each direction

Annulus Width - 2.4 mrad

Obser. Dist. - 10 m.

Microm. Read (mm)	S <sup>2</sup> (urad <sup>2</sup> )
→ MM direction	
15.18	492.8
14.45	428.5
14.71	691.7
14.77	734.4
<hr/>	
Mean 14.78	
← MM direction	
15.10	1056.3
14.74	1288.8
14.88	519.8
15.16	841.0
<hr/>	
Mean 14.97	756.7
E = 12.3	

$$\chi^2_{(0.05, 7)} = 16.0$$

$$\chi^2_{(0.025, 7)} = 1.69$$

→ MM direction

← MM direction

Variance	f	Test	Variance	f	Test
S <sub>2</sub> <sup>2</sup> = 22,734	3	$\frac{S_2^2}{S_1^2} = 300^*$ $\nu^2_{(0.05, 2, 192)} = 3.2$	S <sub>2</sub> <sup>2</sup> = 10,259	3	$\frac{S_2^2}{S_1^2} = 135^*$
S <sub>1</sub> <sup>2</sup> = 756.7	192				

$$S_1^2 = 756.7$$

$$S = 27.5 \text{ urad}$$

Syst. Error not Estimated due to failure of Tests.

Target No. 22

Observer: JCT

No. of Observations - 10 x 10

Annulus Width - 0.8 mrad

Obser. Dist. - 10 m.

Microm. Read (mm)	S <sup>2</sup> (μrad <sup>2</sup> )
11.33	358.3
11.32	482.0
11.30	560.0
11.34	344.4
11.39	811.0
11.28	484.0
11.31	590.4
11.42	858.8
11.52	261.3
11.25	825.7
Mean 11.35	557.6

E = 6.1

$\chi^2_{(0.975,9)} = 19.0$

$\chi^2_{(0.975,9)} = 2.7$

Variance	f	Test
S <sub>2</sub> <sup>2</sup> = 630.0	9	$\frac{S_2^2}{S_1^2} = 1.1$
S <sub>1</sub> <sup>2</sup> = 557.6	90	
		$\nu^2_{(0.975,9,90)} = 2.25$

S<sub>0</sub><sup>2</sup> = 557.6

S<sub>0</sub> = 23.8 μrad

Syst. Error = o'shoot 40 μrad

Target No. 22b

Observer: AHC

No. of Observations - 10 x 10

Annulus Width - 1.0 mrad

Obser. Dist. - 10 m.

Microm. Read (mm)	S <sup>2</sup> (μrad <sup>2</sup> )
17.07	501.6
17.04	617.5
17.02	933.7
17.20	433.2
17.00	930.3
17.03	744.5
17.16	368.6
17.23	129.0*
17.21	480.0
17.10	967.8
17.02	735.6
Mean 17.09	674.5

E = 4.60

$\chi^2_{(0.975,9)} = 19.0$

$\chi^2_{(0.025,9)} = 2.7$

Variance	f	Test
S <sub>2</sub> <sup>2</sup> = 621.1	9	$\frac{S_2^2}{S_1^2} = 0.9$
S <sub>1</sub> <sup>2</sup> = 674.5	90	
		$\nu^2_{(.975,9,90)} = 2.25$

S<sub>0</sub><sup>2</sup> = 669.6

S<sub>0</sub> = 25.9 μrad

Syst. Error = o'shoot 40 μrad

B.2 Tests of Normality of Observations, Average Error Method.

A number of tests were carried out to check the normality of the observations taken in these investigations. The observations were divided into 10 - 15 equal intervals. Theoretical frequencies  $\hat{\theta}$  over this interval were then compared with the observed frequencies  $a_i$ . The hypothesis tested was that  $\sum_{i=1}^K \frac{(a_i - \hat{\theta}_i)^2}{\hat{\theta}_i}$  was distributed as a  $\chi^2$  distribution.

In the six (6) randomly chosen cases in these experiments, the hypothesis proved to be true. Based on this evidence, and also previous experience in psychophysics, there seems to be no reason to doubt the normality of the observations.

Three of these tests have been presented in the following.

1. Target No. 2. - Mean = 10.94 mm -  $S_o = 13.9 \mu\text{rad}$

Class Interval = 0.05 mm Obs. JCT.

Microm. Reading at Class Midpoint	Frequency $a_i$	Calcul. Freq. $\hat{\theta}_i$	Diff. $(a_i - \hat{\theta}_i)$
> 11.27	0	0.8	
11.24	1	1.4	1.0
11.19	3	2.8	
11.14	4	5.1	1.1
11.09	14	8.0	6.0
11.04	9	11.0	2.1
10.99	13	13.4	0.4
10.94	13	14.3	1.3
10.89	11	13.4	2.4
10.84	15	11.1	3.9
10.79	7	8.0	1.0
10.74	6	5.1	0.9
10.69	1	2.8	
10.64	2	1.4	1.6
10.59	1	0.6	
< 10.56	0	0.8	

$$\sum_{i=1}^K \frac{(a_i - \hat{\theta}_i)^2}{\hat{\theta}_i} = 12.8$$

$$= \chi^2_{(10, 0.75)}$$

i.e. Observations  
Normal



2. Target No. 1b - Mean = 9.28  $S_o = 16.0 \mu\text{rad}$

Class Interval = 0.5 mm Obs. AHC

Microm. Reading at Class Midpoint	Frequency $a_i$	Calcul.Freq. $\hat{\theta}_i$	Diff. $(a_i - \hat{\theta}_i)$
> 9.605	0	2.0	
9.58	4	2.1	1.2
9.53	5	3.7	
9.48	12	5.7	6.3
9.43	4	8.0	4.0
9.38	8	10.3	2.3
9.33	10	11.9	1.9
9.28	7	12.5	5.5
9.23	12	11.9	0.1
9.18	11	10.3	0.7
9.13	12	8.0	4.0
9.08	6	5.7	0.3
9.03	6	3.7	
8.98	3	2.1	1.2
< 8.955	0	2.0	

$$\sum_{i=1}^K \frac{(a_i - \hat{\theta}_i)^2}{\hat{\theta}_i} = 14.6$$

$$= \chi^2_{(10, 0.8)}$$

i.e. Observations Normal

3. Blurred Target No. 22 - Mean = 11.35 -  $S_o = 23.8 \mu\text{rad}$

Class Interval = 0.5 mm Obs. JCT.


Microm. Reading at Class Midpoint	Frequency $a_i$	Calcul. Freq. $\hat{\theta}_i$	Diff. $(a_i - \hat{\theta}_i)$
> 11.755	5	5.3	0.3
11.73	2	2.4	1.5
11.68	5	3.1	
11.63	2	4.2	2.2
11.58	7	5.3	1.7
11.53	6	6.3	0.3
11.48	6	7.2	1.2
11.43	8	7.9	0.1
11.38	11	8.3	2.7
11.33	8	8.3	0.3
11.28	4	7.9	3.9
11.23	8	7.2	0.8
11.18	10	6.3	3.7
11.13	2	5.3	3.3
11.08	5	4.2	0.8
11.03	5	3.1	
10.98	4	2.4	3.5
< 10.95	2	5.3	3.3

$$\frac{\sum (a_i - \hat{\theta}_i)^2}{\hat{\theta}_i} = 16.1$$

$$= \chi^2_{(15, 0.6)}$$

i.e. Observations  
Normal

B.3 Sample Results of Observations by Constant Stimulus Method.

Entry No. 40. Target No. 1 (0.5 mrad, sharp)  Obs. JCT.  
 No. of Observations per setting 80

Micrometer Setting (mm)	Observed frequency	Weight
20.00	0.975	0.1504
20.40	0.750	0.8460
20.80	0.563	0.9911
21.20	0.238	0.8277
21.60	0.025	0.1504


PSE = 20.82 mm ;  $\sigma$  = 0.04 mm.

DL = 49  $\mu$ rad ;  $\sigma$  = 6  $\mu$ rad

Standard Deviation of PSE according to Culler's

Modified Formula = 0.04 mm

Edge Subjectivity Located 1.12 mm or 112  $\mu$ rad left of true edge position.

Entry No. 41. Target No. 1 (0.5 mrad, sharp)  Obs. JCT  
 No. of Observations per setting 80

Micrometer Setting (mm)	Observed frequency	Weight
17.70	0.838	0.6971
18.10	0.450	0.9943
18.50	0.100	0.5376
18.90	0.025	0.1504
19.30	0.013	0.1315

PSE = 18.06 mm ;  $\sigma$  = 0.06 mm

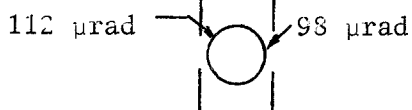
DL = 43  $\mu$ rad ;  $\sigma$  = 5  $\mu$ rad

Standard Deviation of PSE according to Culler's

Modified Formula = 0.05 mm.

Edge Subjectivity Located 98  $\mu$ rad to right of true edge position

Summary of Entries 40 and 41.



Since  $\sigma$  of each location is 5  $\mu$ rad, difference is insignificant

Entry No. 42. Target No. 1 (0.5 mrad - sharp) (MM centered) Obs. JCT

No. of Observations per setting 80

Micrometer Setting (mm)	Observed frequency	Weight
10.03	0.95	0.3519
10.19	0.60	0.9768
10.35	0.288	0.8801
10.51	0.075	0.4535
10.67	0.035	0.2892

$$\text{PSE} = 10.26 \text{ mm} ; \quad \sigma = .02 \text{ mm}$$

$$\text{DL} = 18.9 \text{ } \mu\text{rad} ; \quad \sigma = 2 \text{ } \mu\text{rad}$$

Standard Deviation of PSE according to Culler's

$$\text{Modified Formula} = .02 \text{ mm}$$

$$\text{System.Error} = 0.$$

---

Entry No. 43. Target No. 32 (MM centered) Obs. JCT

No. of Observations per setting 100

Micrometer Setting (mm)	Observed frequency	Weight
10.20	0.94	0.3954
10.60	0.70	0.9043
11.00	0.30	0.9043
11.40	0.10	0.5376
11.80	0.03	0.2499

$$\text{PSE} = 10.83 \text{ mm} ; \quad \sigma = 0.03 \text{ mm}$$

$$\text{DL} = 45.0 \text{ } \mu\text{rad} ; \quad \sigma = 0.03 \text{ } \mu\text{rad}$$

Standard Deviation of PSE according to Culler's

$$\text{Modified Formula} = 0.04 \text{ mm}$$

$$\text{System.Error} = 100 \text{ } \mu\text{rad to right of centre}$$

---

B.4 Sample Tests of Normality - Constant Stimulus Method Observations.

Entry No. 40.

Observed freq.	Computed freq.		
p	p'	p - p'	
0.975	0.952	0.023	$N \Sigma \frac{(p-p')}{p'q'} = 7.6$ $= \chi^2_{(3,0.95)}$ <p>∴ Observations normal</p>
0.750	0.803	0.053	
0.563	0.516	0.047	
0.236	0.220	0.018	
0.025	0.056	0.031	

---

Entry No. 42.

Observed freq.	Computed freq.		
p	p'	p-p'	
0.950	0.890	0.06	$N \Sigma \frac{(p-p')}{p'q'} = 5.5$ $= \chi^2_{(3,0.60)}$
0.600	0.698	0.048	
0.288	0.319	0.031	
0.075	0.094	0.001	
0.038	0.015	0.001	

---

Entry No. 43.

Observed freq.	Computed freq.		
p	p'	p-p'	
0.980	0.966	0.014	$N \Sigma \frac{(p-p')}{p'q'} = 5.5$ $= \chi^2_{(3,0.060)}$
0.810	0.867	0.057	
0.720	0.653	0.067	
0.380	0.373	0.007	
0.130	0.141	0.011	

---

B.5 Constant Stimulus observations by JCT and AHC have been plotted on normal probability paper, together with the computed regression lines. The PSE is located at the 0.50 probability level, while the DL is measured from the PSE to the 0.16 or 0.84 levels. The standard deviation determined by the average error method has been superimposed onto the graphs, measured from the PSE. Since different settings were used for AHC and JCT, the abscissa scale has been marked separately for each observer.

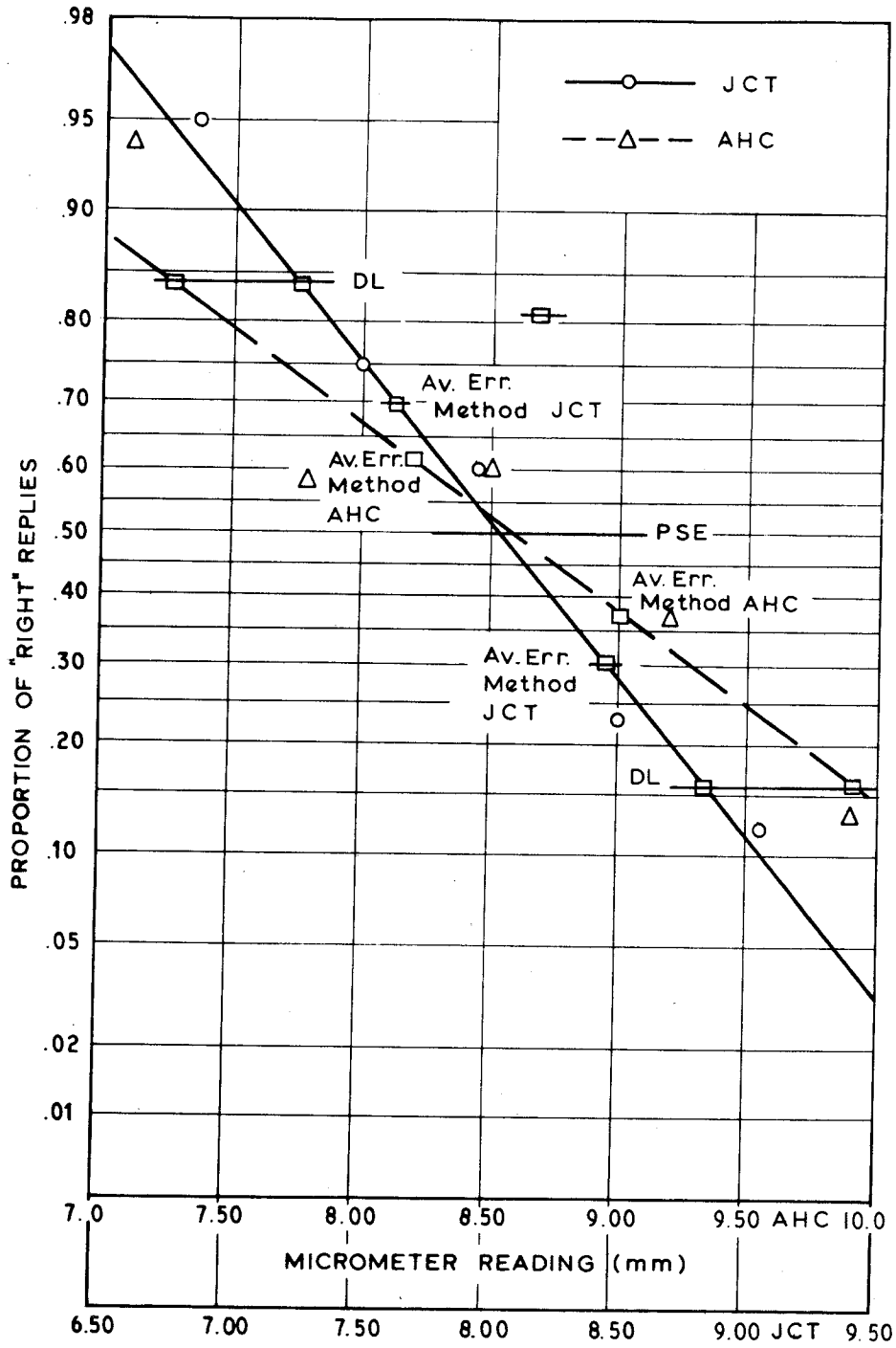


FIG. B1: CONSTANT STIMULUS METHOD OBSERVATIONS TARGET No. 14.

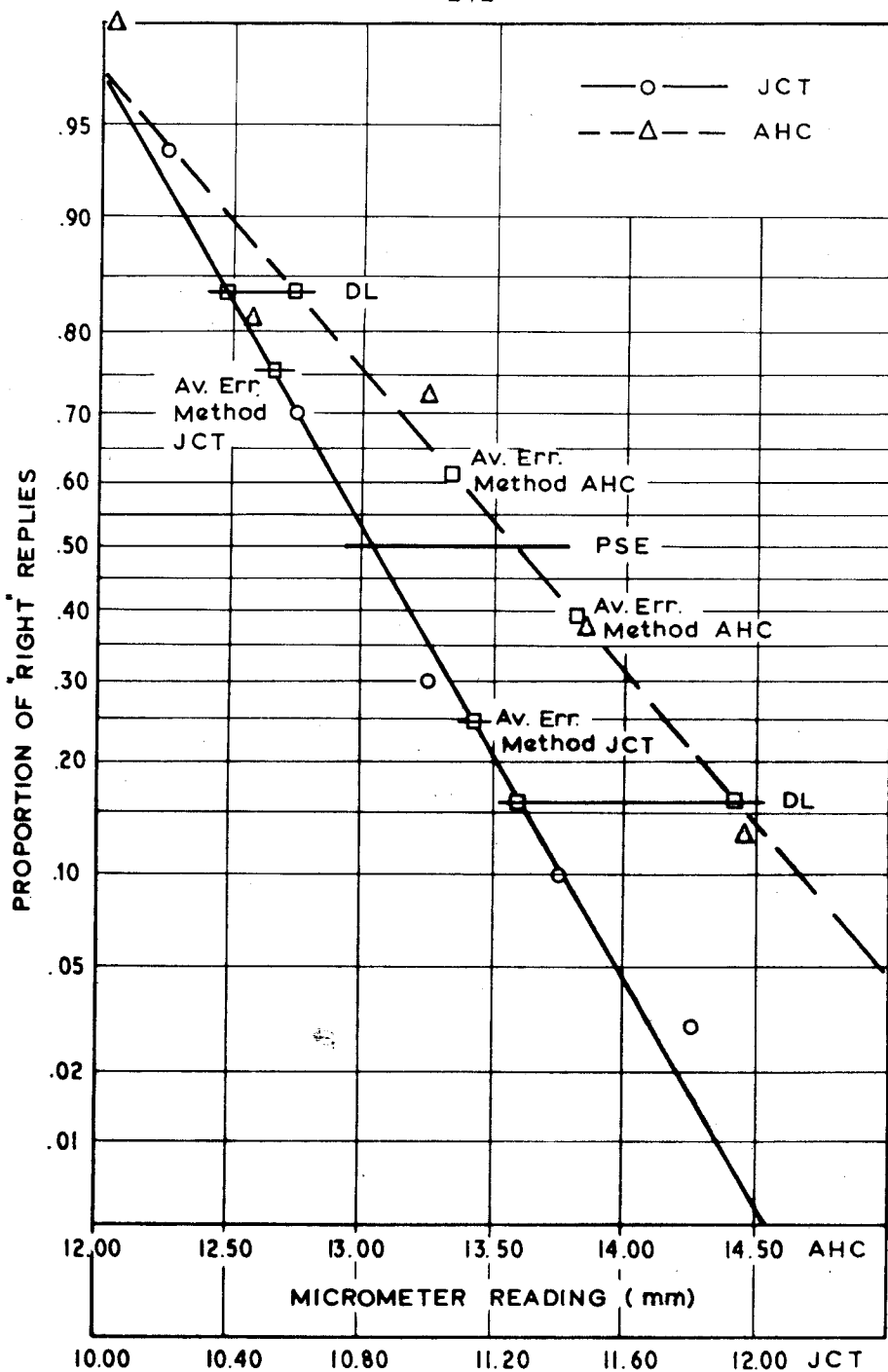


FIG. B2: CONSTANT STIMULUS METHOD OBSERVATIONS  
TARGET No. 32.



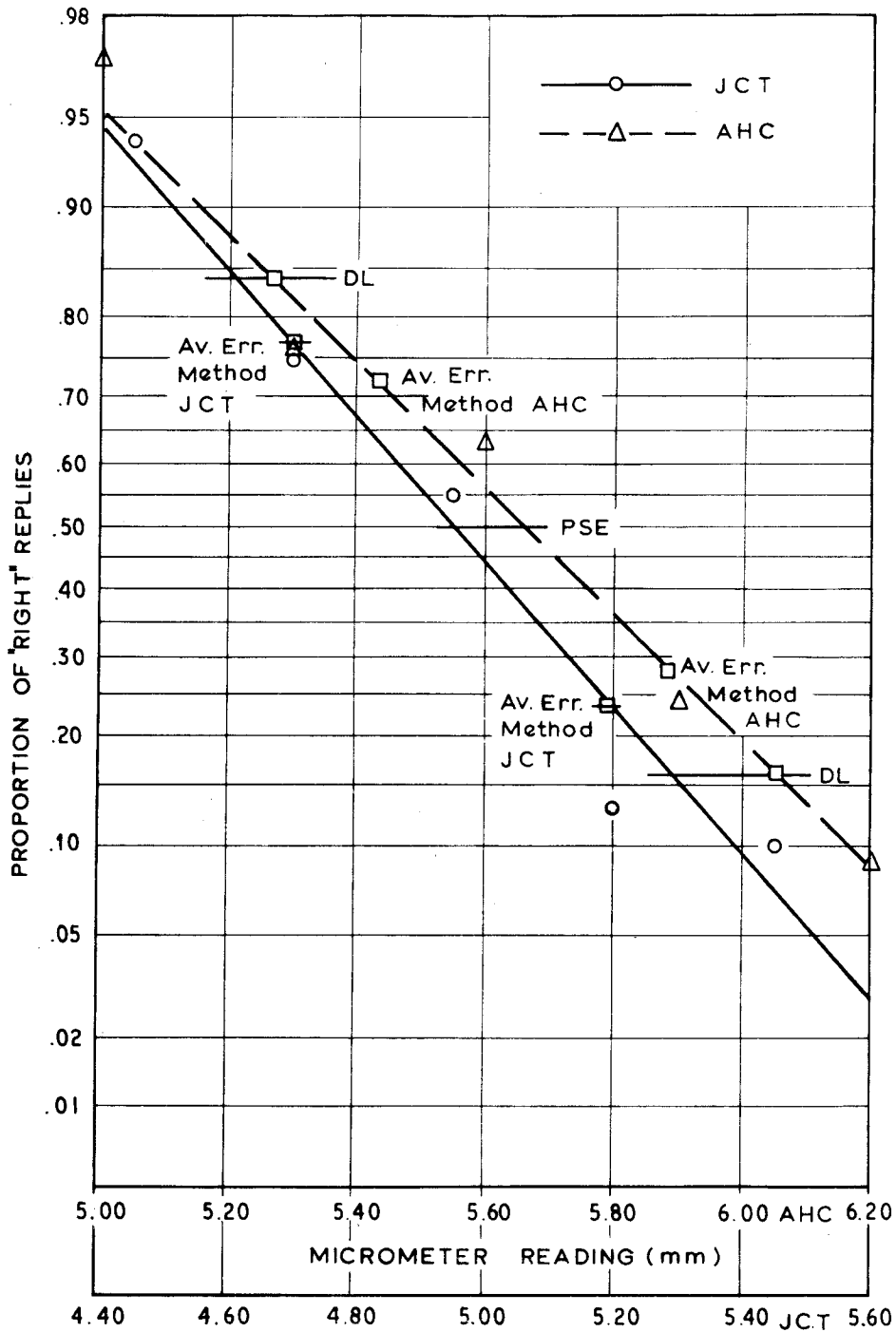


FIG. B3: CONSTANT STIMULUS METHOD OBSERVATIONS TARGET No. 21.

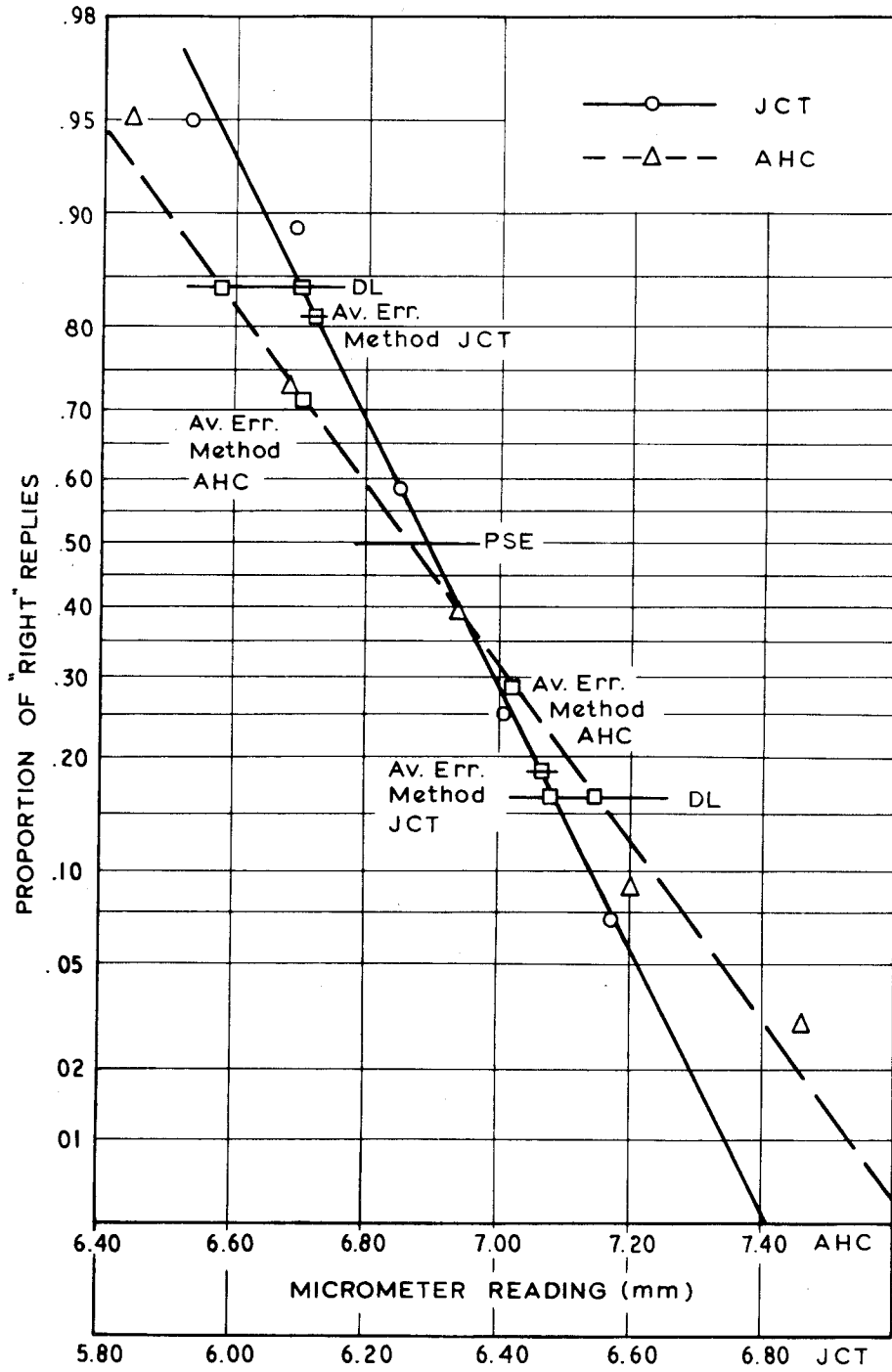


FIG. B4: CONSTANT STIMULUS METHOD OBSERVATIONS TARGET No. 25.

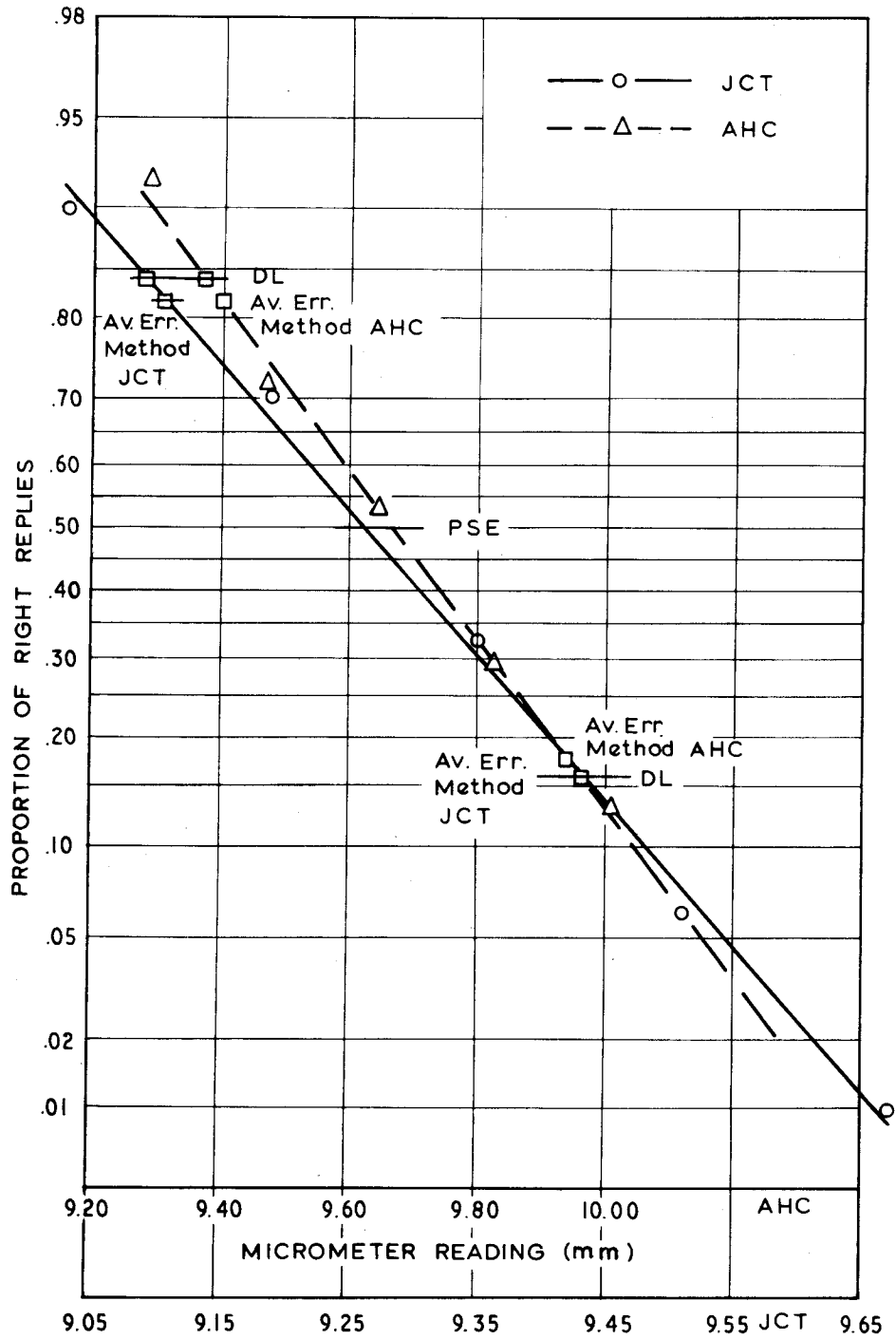


FIG. B5: CONSTANT STIMULUS METHOD OBSERVATIONS  
TARGET No. 26.

APPENDIX C.

Microdensitometer Traces of Blurred Targets.

Sample smoothed microdensitometer traces of blurred targets observed in investigations. Location of the edges determined by JCT (and AHC when observed) are shown on the traces. The position of scratches used as reference marks on the targets are also shown.

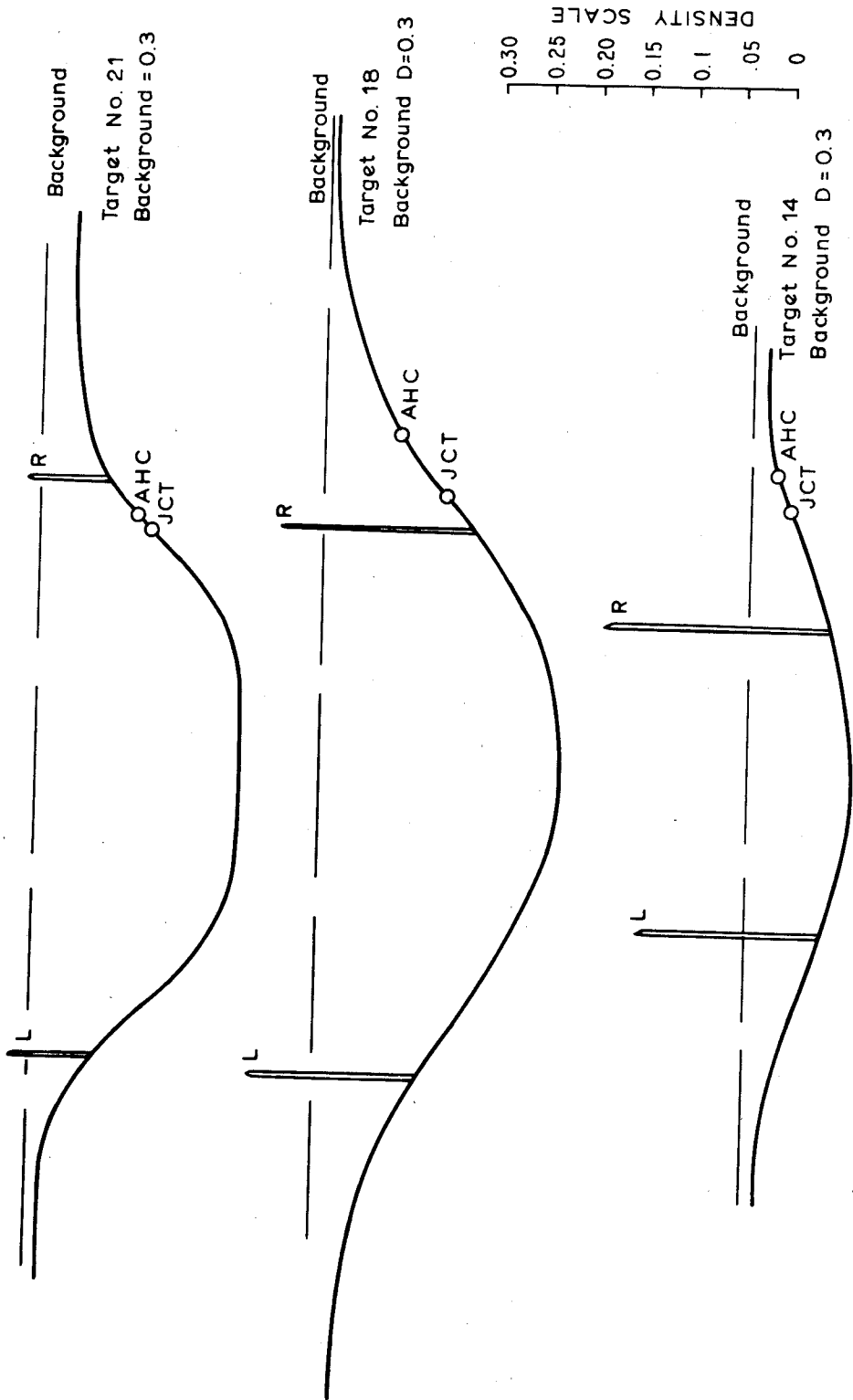


FIG. C1

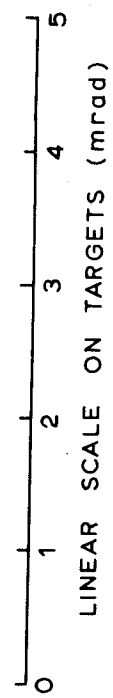
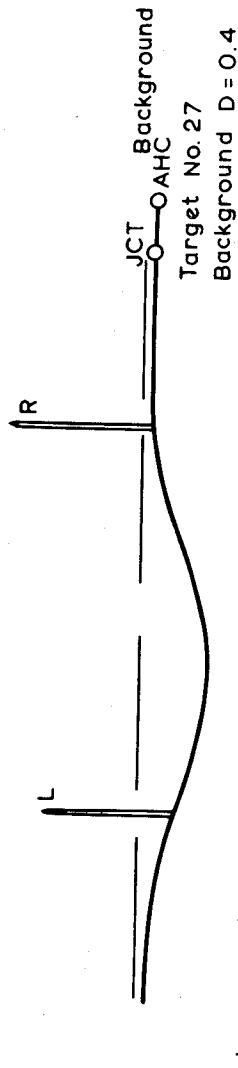
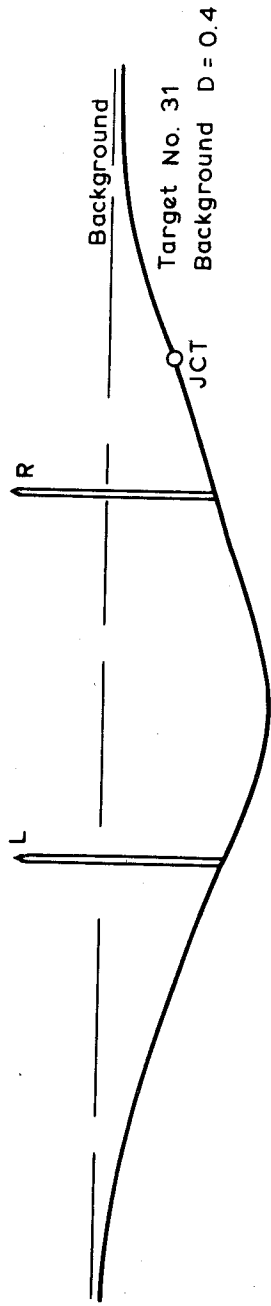
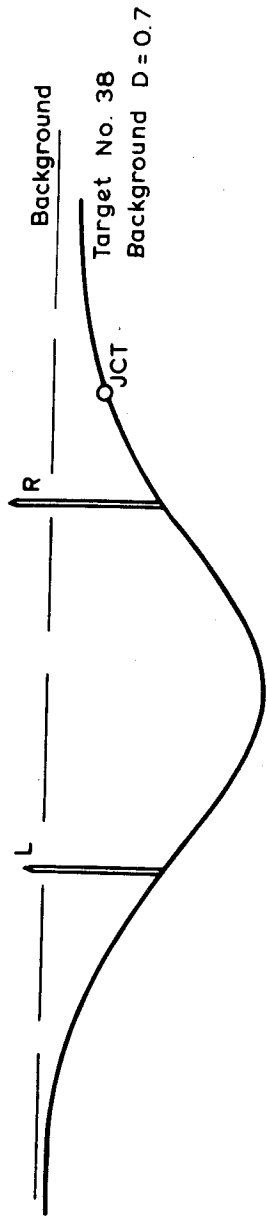
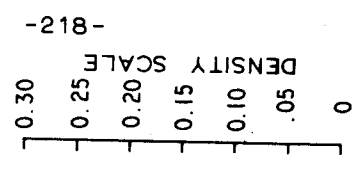


FIG. C2



- 812 -

APPENDIX D.

Profiles of Annuli derived by Convolution.

Luminance profiles determined by the PSF method (see Ch.3) using five PSF's, together with corresponding luminance profiles before convolution. The units for height of the profiles after convolution are arbitrary, but have been drawn to a consistent scale on each page. In the luminance profiles before convolution, the heights have been decreased for reasons of space.

The method of weighting the influence of MM for low and medium contrast targets is as follows.

The Density (D) of a material is given by the formula -

$$D = \log_{10} \left( \frac{I_0}{I} \right),$$

where  $I_0$  is the incident intensity, and  
 $I$  is the transmitted intensity.

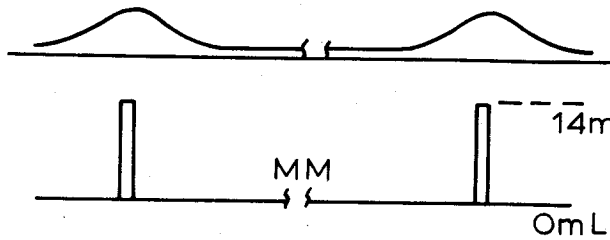
If  $D = 0.3$ , incident intensity is twice transmitted intensity, i.e., background intensity will be 18.5 mL, if the incident luminance is 37 mL. Similar computations can be carried out for the densities of 0.9 and 1.2.

In the convolution of these profiles, the influence of the section below the background level, i.e. MM, must be weighted against the annulus profile above background. For instance, the annulus and measuring

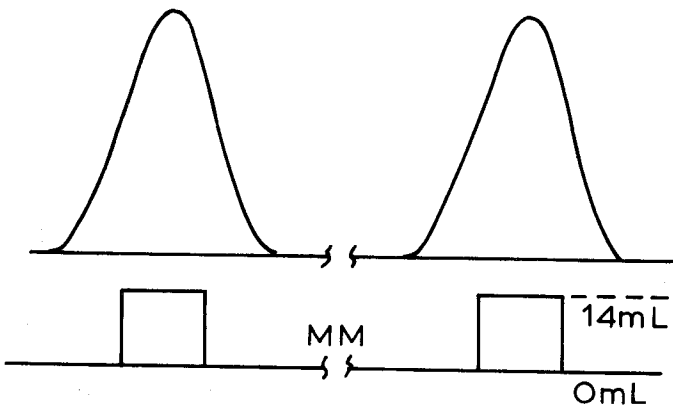
mark profiles were given equal weight for the density of 0.3, because the luminance intensities above and below background are equal. For the densities of 0.9 and 1.2, weighting was 7.15 to 1 and 14.9 to 1 respectively, for annulus and MM influences.



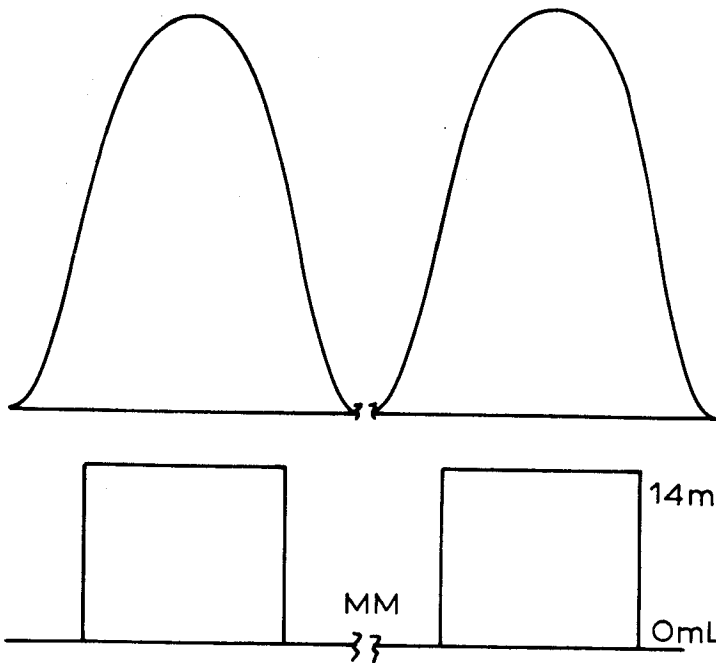
GAUSS PSF  $\sigma = 200 \mu\text{rad}$   
MM 5.1mrad  
HIGH CONTRAST



(a) Target diameter 5.2 mrad  
Annulus = 50  $\mu\text{rad}$



(b) Target 5.7 mrad  
Annulus 300  $\mu\text{rad}$



(c) Annulus 900  $\mu\text{rad}$   
Target 6.5 mrad

FIG. D1

GAUSS PSF  $\sigma = 200 \mu\text{rad}$   
MM 0.645 mrad  
HIGH CONTRAST

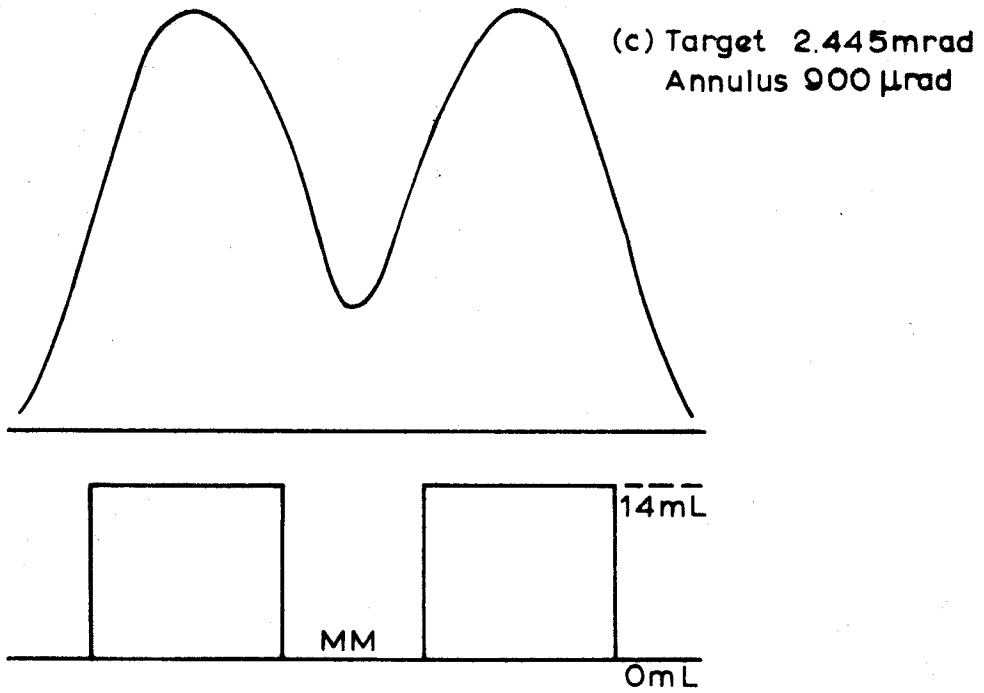
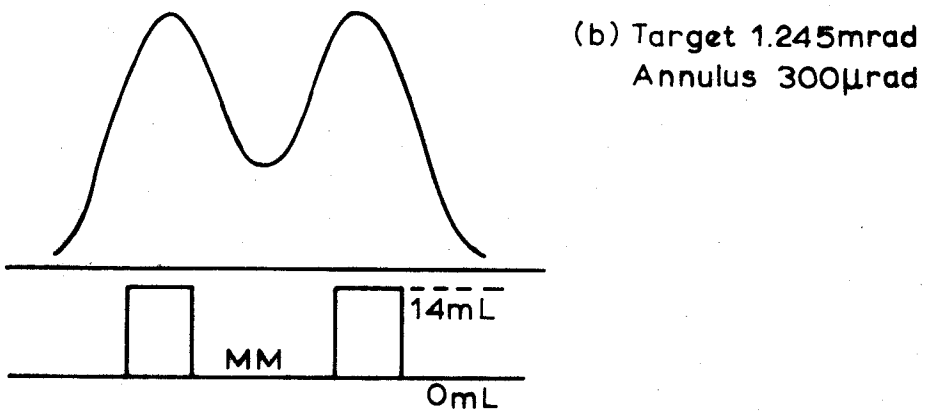
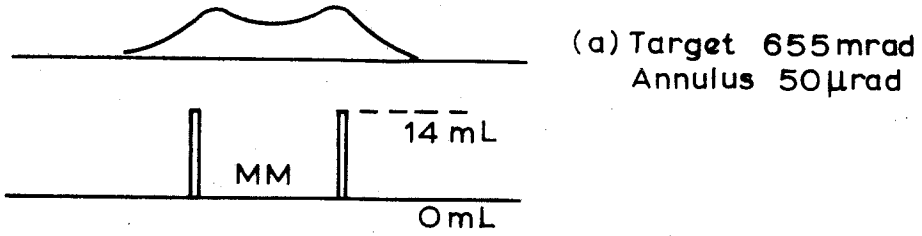


FIG. D2

GAUSS PSF  $\sigma = 200 \mu\text{rad}$   
MM 0.99 mrad  
HIGH CONTRAST

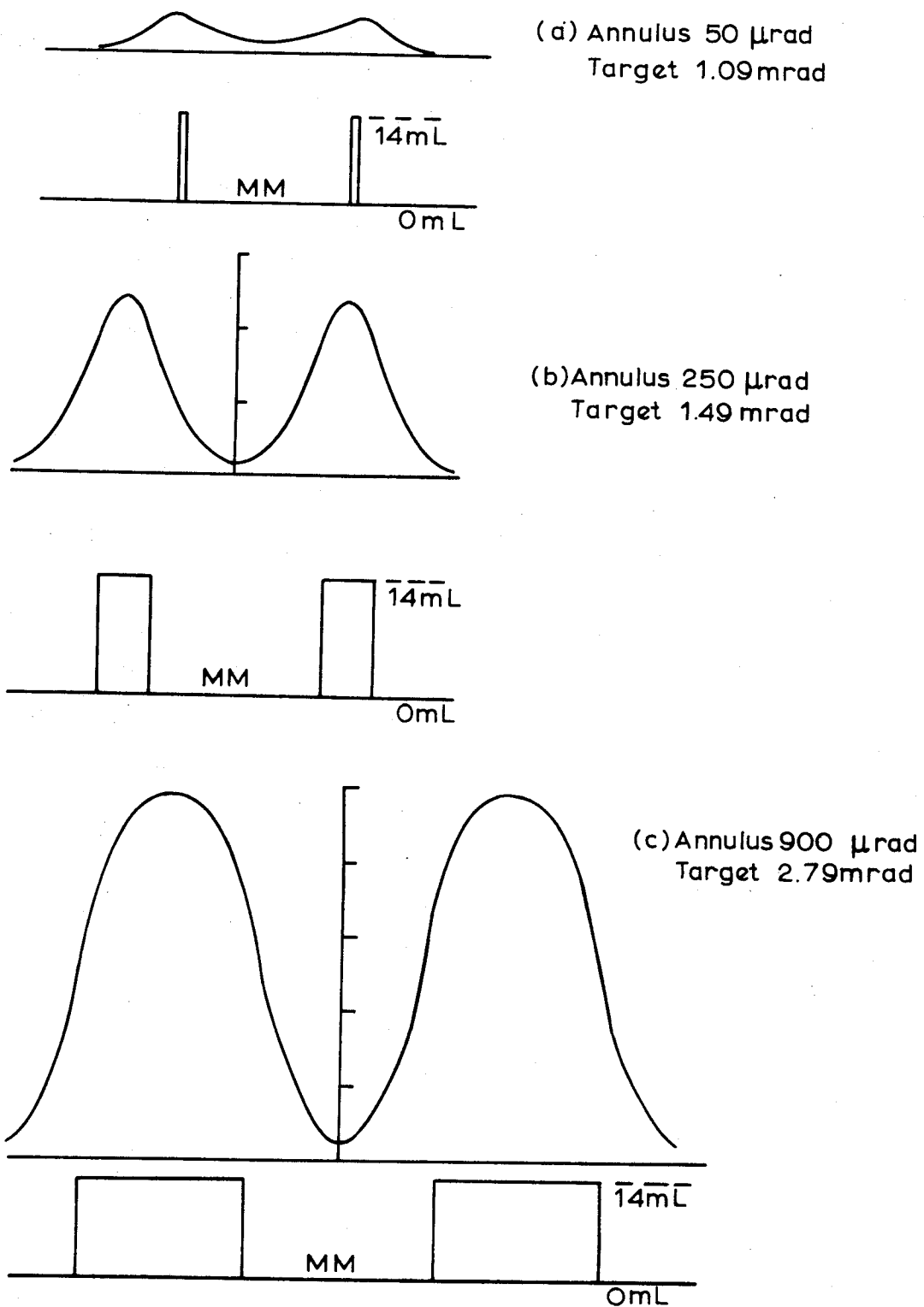


FIG. D3

GAUSS PSF  $\sigma = 200 \mu\text{rad}$   
MM 0.99 mrad  
MEDIUM CONTRAST

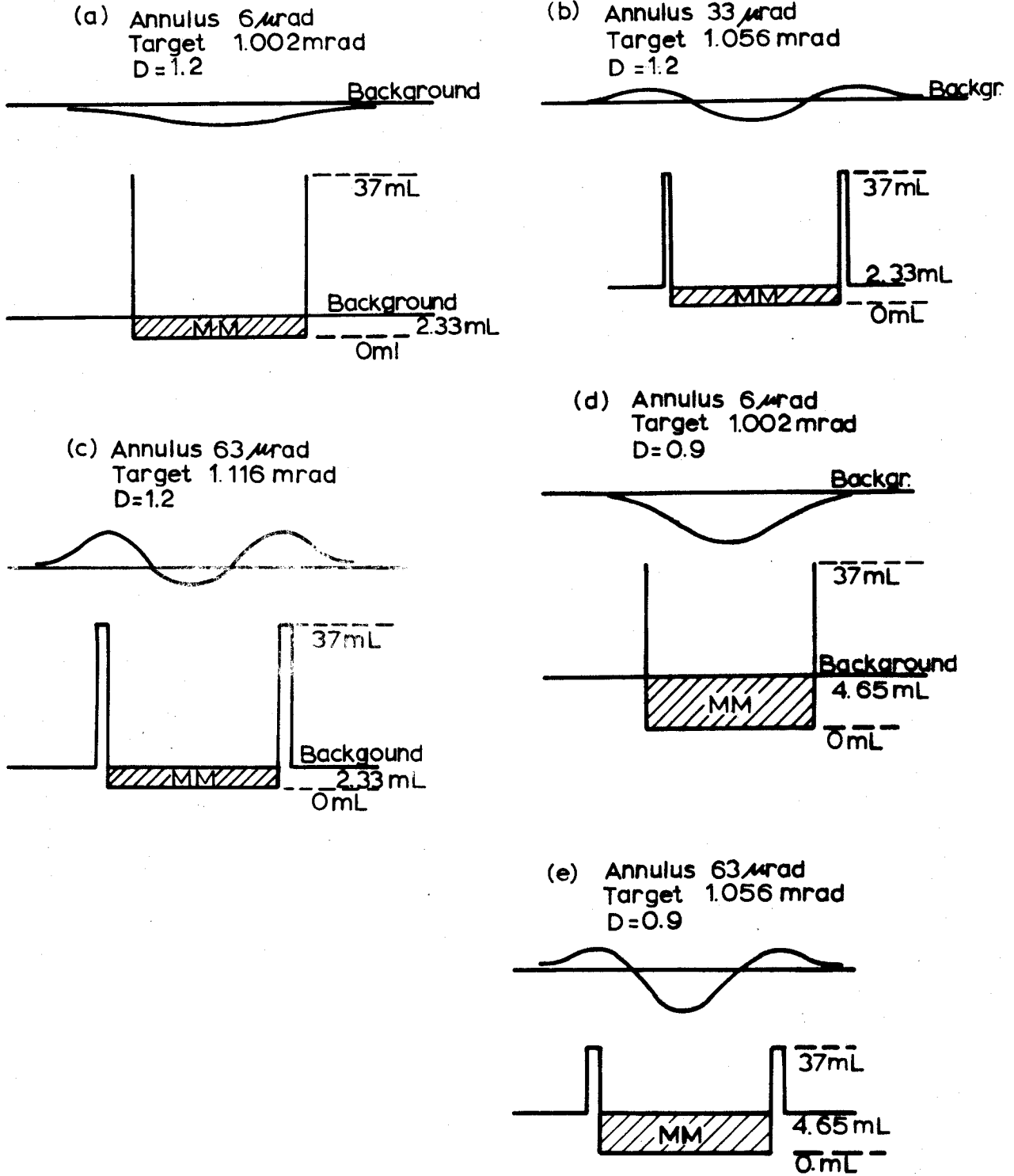


FIG. D 4

GAUSS PSF  $\sigma = 200 \mu\text{rad}$   
MM 0.99 mrad  
LOW CONTRAST

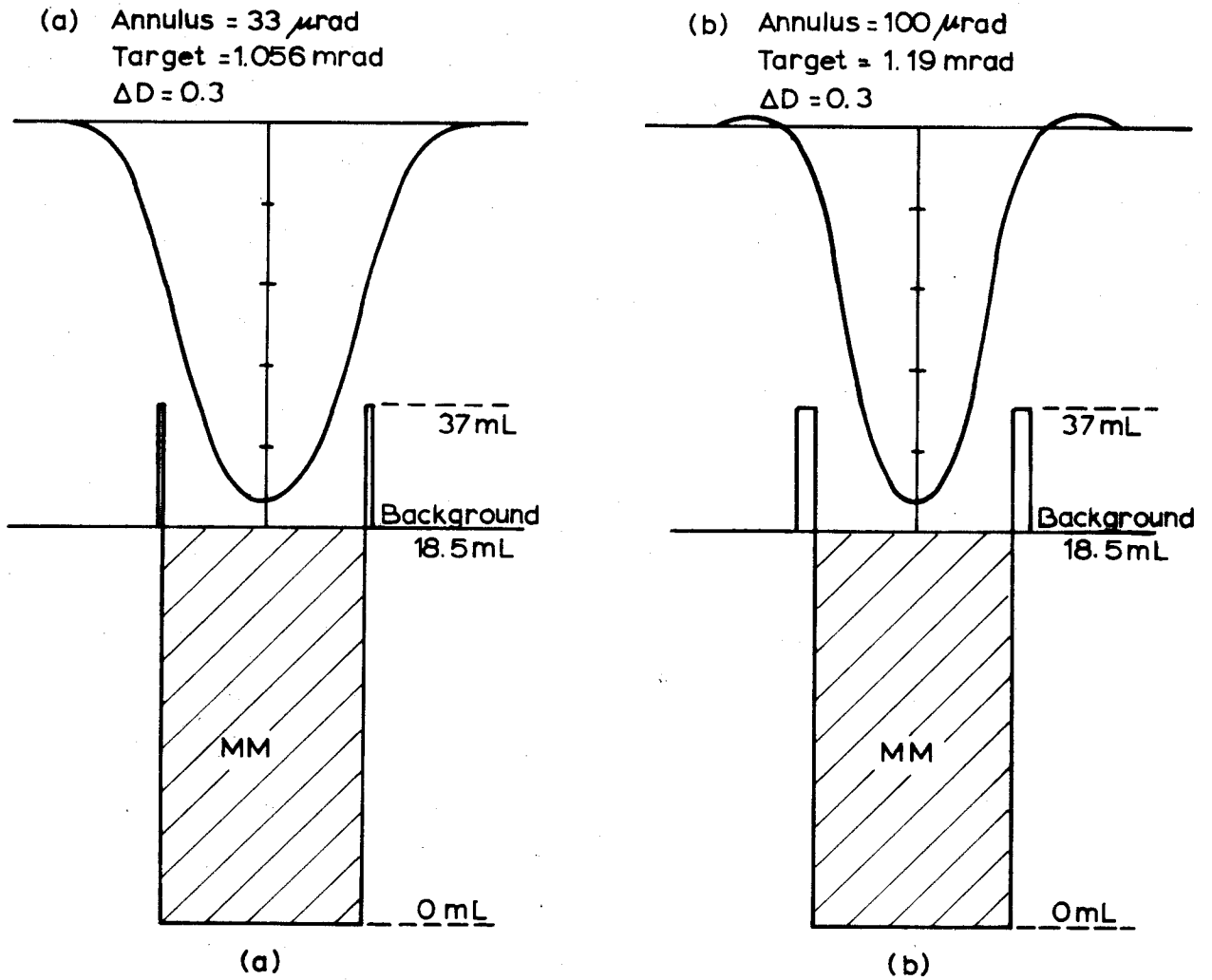


FIG. D5

GAUSS PSF  $\sigma = 200 \mu\text{rad}$   
 MM 0.99 mrad  
 LOW CONTRAST

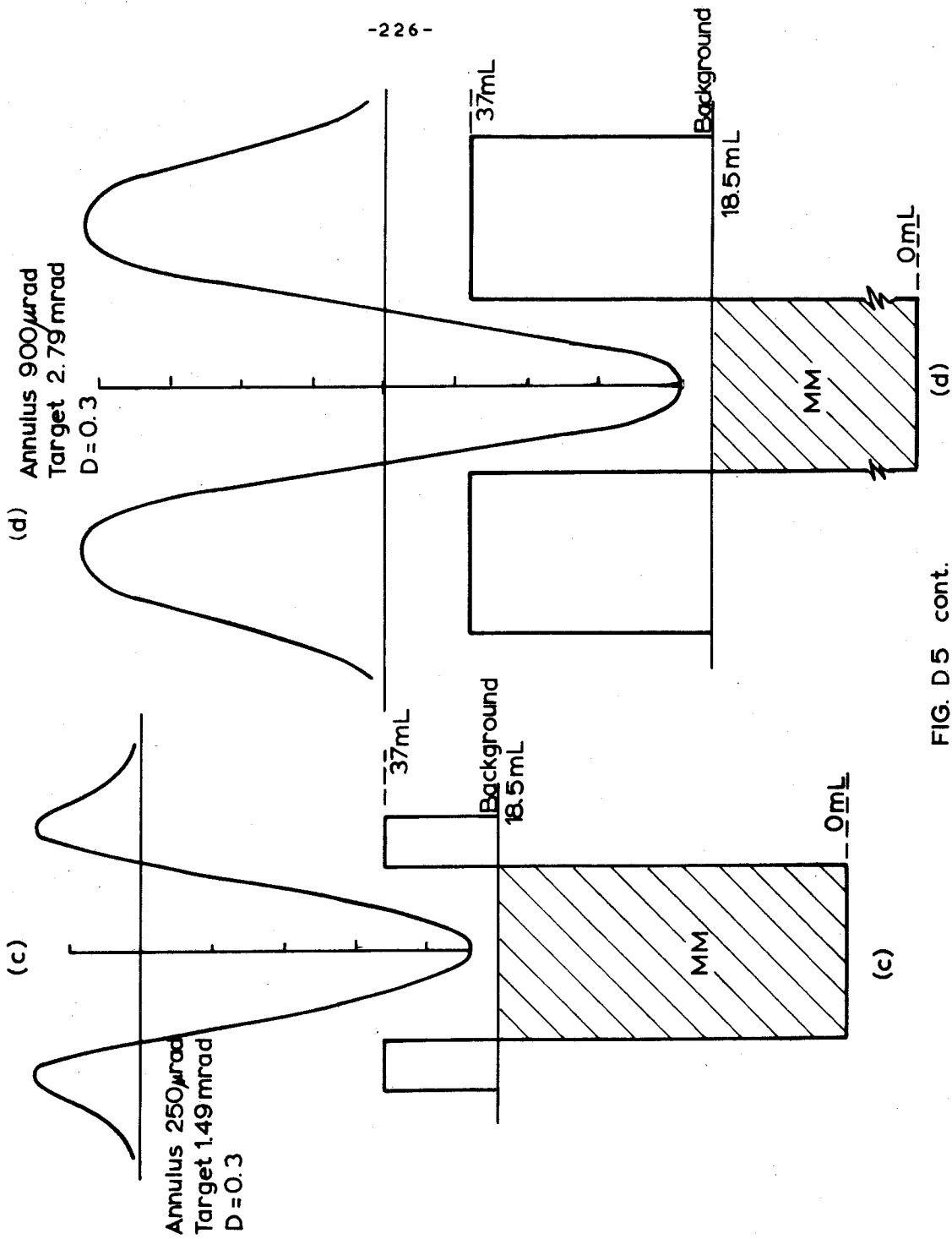


FIG. D.5 cont.

GAUSS PSF  $\sigma = 150 \mu\text{rad}$   
MM 0.99 mrad  
HIGH CONTRAST

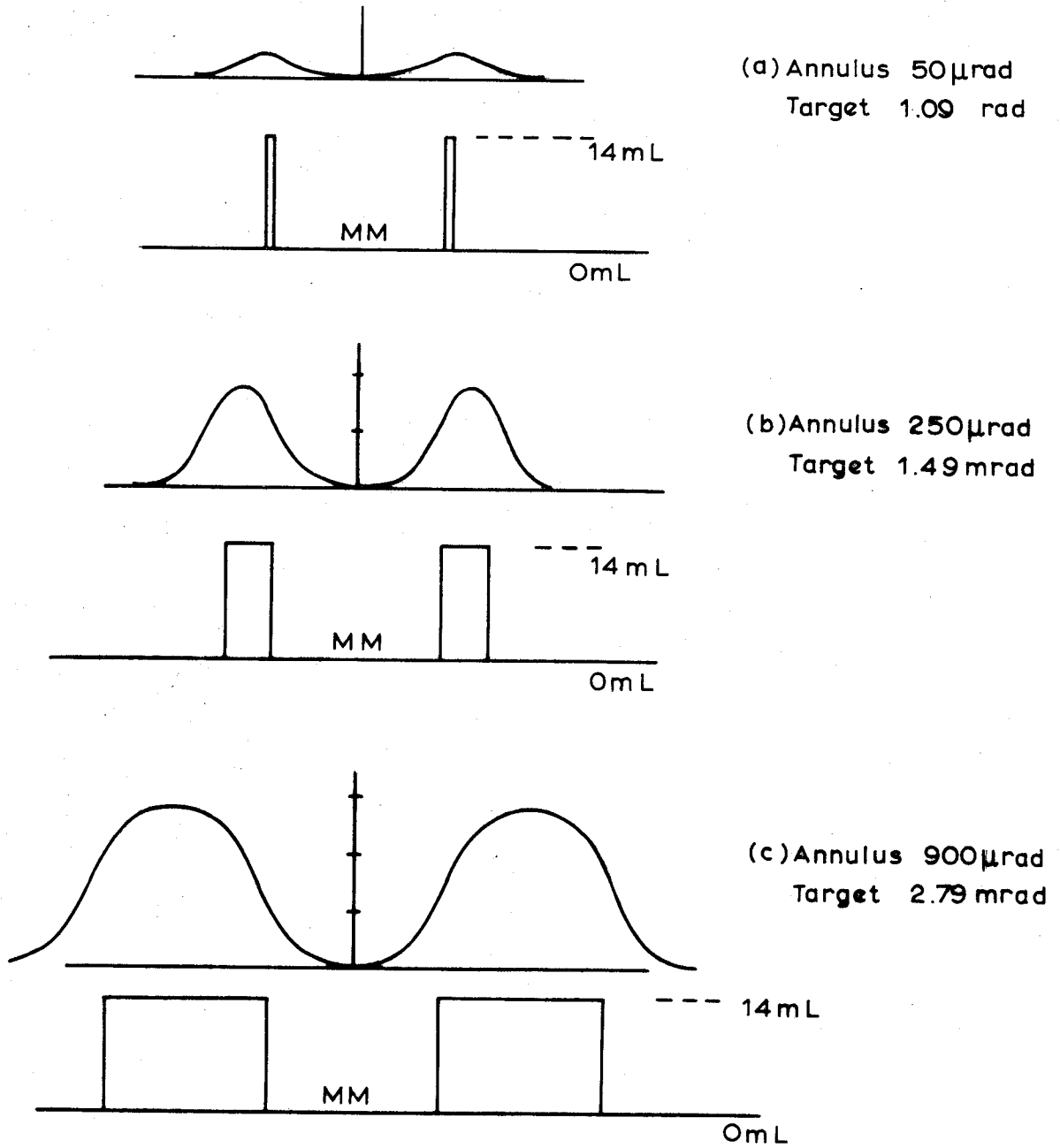


FIG. D6

GAUSS PSF  $\sigma = 250 \mu\text{rad}$   
MM 0.99 mrad  
HIGH CONTRAST

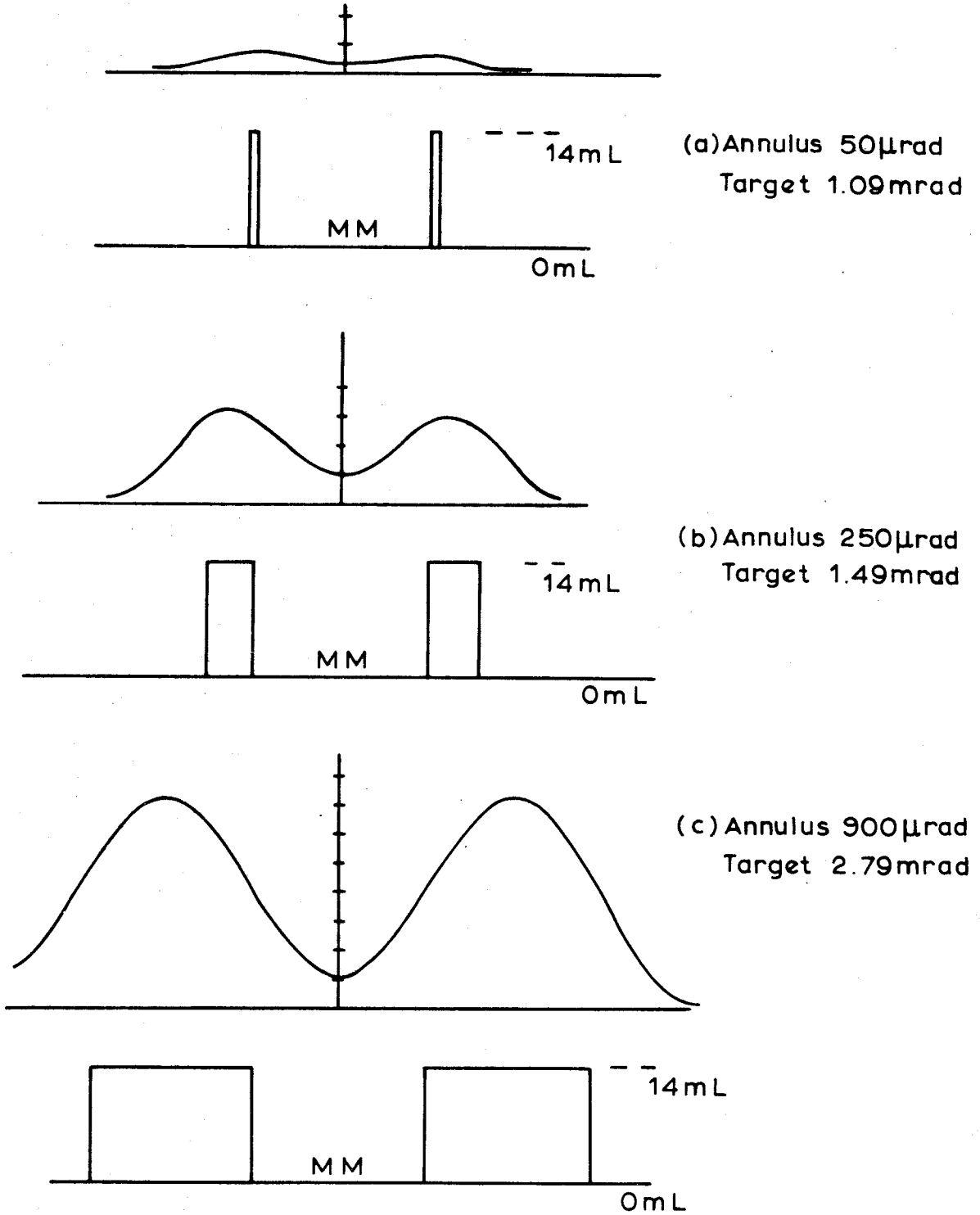


FIG. D7



PATEL P S F  
MM 0.99 mrad  
HIGH CONTRAST

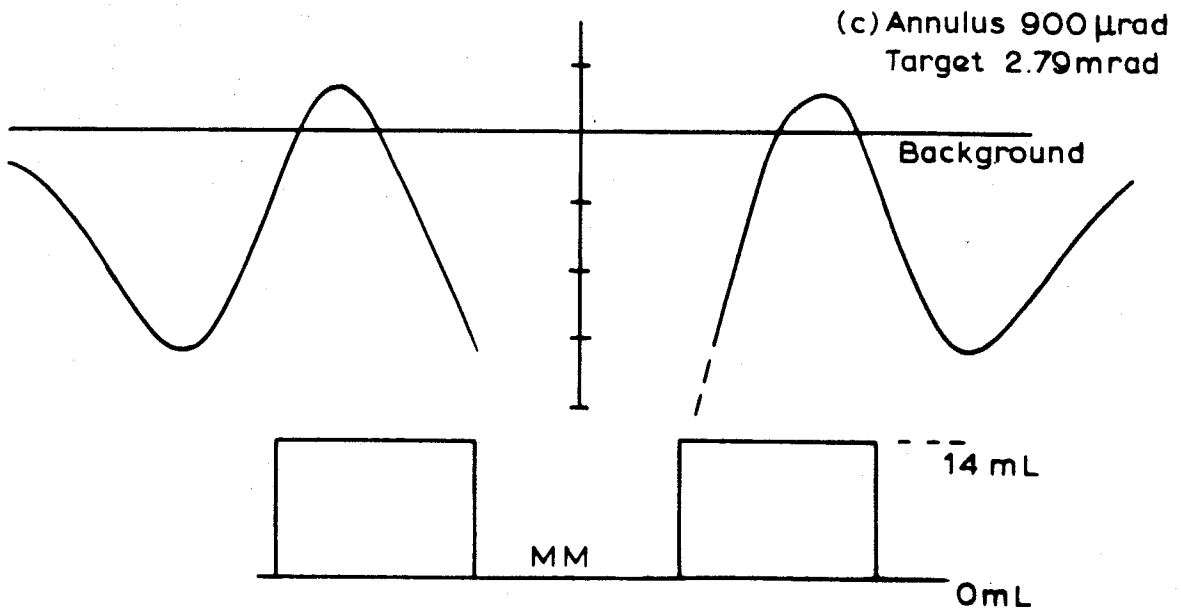
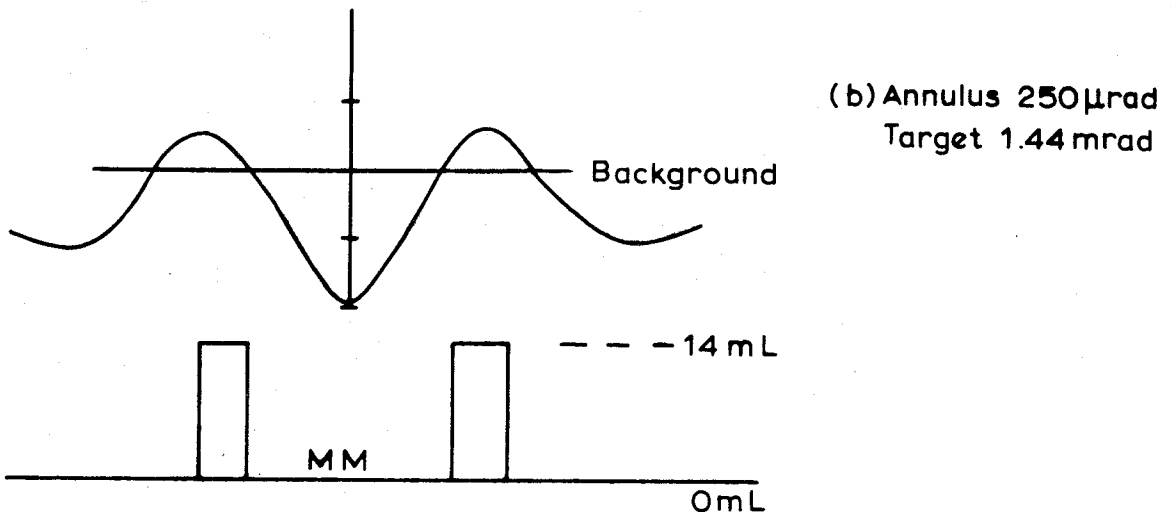
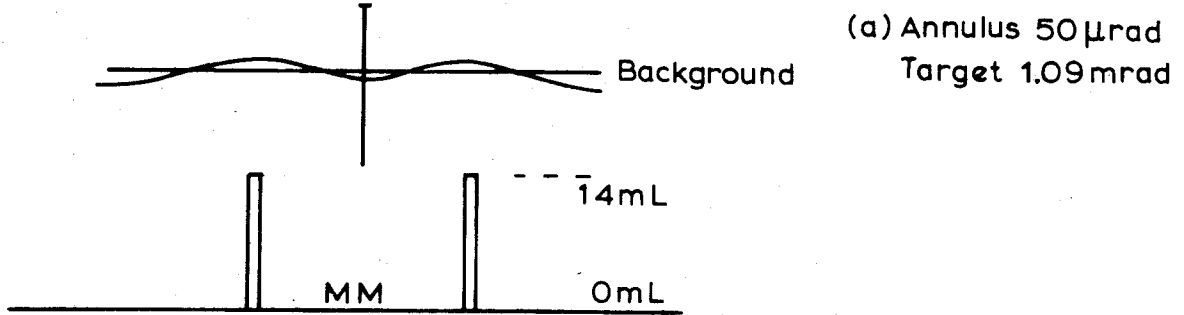


FIG. D8

SINC P.S.F.  
MM 0.99 mrad  
HIGH CONTRAST

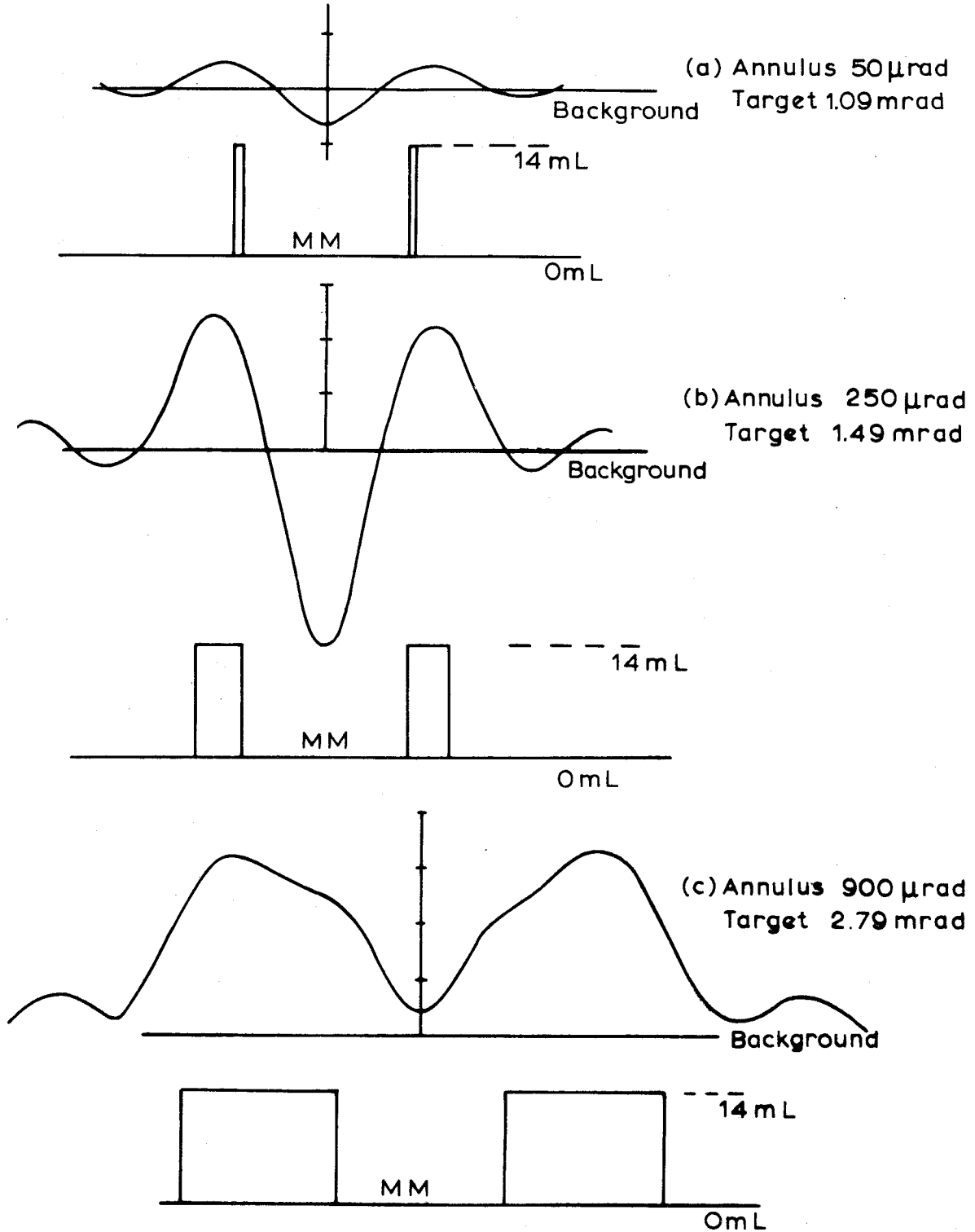


FIG. D9

APPENDIX E.

Visual and Ocular Characteristics of Eyes of Observers JCT and AHC.

JCT:

Unaided Visual Acuity - 6/4.5 both eyes  
Near phorias - ORTHO  
Distance phorias:  
    Horizontal - 2 EXO  
    Vertical - ORTHO  
Stereoscopic Acuity - better than 40 secs. of arc.  
Abduction - slightly low especially at break point  
Adduction - Normal  
Pupillary Distance - 62.5 mm

AHC:

Unaided Visual Acuity - 5/4.5 both eyes  
Near phorias:  
    Horizontal - 1 ESO  
    Vertical - ½ left HYPER  
Distance phorias:  
    Horizontal - 5 ESO  
    Vertical - ½ left HYPER  
Stereoscopic Acuity - 400 secs. of arc  
Abduction - low especially recovery point at distance  
Adduction - Normal  
Pupillary Distance - 64 mm

BIOGRAPHICAL NOTES.

*JOHN TRINDER* graduated from the University of New South Wales with a Bachelor's degree in Surveying in 1963. He then spent two years at the International Training Centre at Delft, Holland, where he specialised in Photogrammetric Engineering and received both a bachelor's and a master's degree. Mr. Trinder has practiced as a Surveyor in New South Wales from 1960 to 1963 and joined the staff of the University of New South Wales in 1965 where he now holds the position of Lecturer.

Mr. Trinder has carried out research into the determination of monocular pointing criteria as a function of the shape of the retinal image. His current research interests are the physiology of vision as applied to monocular and stereoscopic pointing in photogrammetry, and the assessment of image quality of aerial photography.

DEPARTMENT OF SURVEYING - UNIVERSITY OF NEW SOUTH WALES

Kensington. N.S.W. 2033.

Reports from the Department of Surveying, School of Civil Engineering.

- \* 1. The discrimination of radio time signals in Australia.  
*G.G. BENNETT* (UNICIV Report No. D-1)
- \* 2. A comparator for the accurate measurement of differential  
barometric pressure.  
*J.S. ALLMAN* (UNICIV Report No. D-3)
- \* 3. The establishment of geodetic gravity networks in South Australia.  
*R.S. MATHER* (UNICIV Report No. R-17)
- 4. The extension of the gravity field in South Australia.  
*R.S. MATHER* (UNICIV Report No. R-19)

UNISURV REPORTS.

- \* 5. An analysis of the reliability of barometric elevations  
*J.S. ALLMAN* (UNISURV Report No. 5)
- \* 6. The free air geoid in South Australia and its relation to the  
equipotential surfaces of the earth's gravitational field.  
*R.S. MATHER* (UNISURV Report No. 6)
- \* 7. Control for Mapping. (Proceedings of Conference, May 1967).  
*P.V. ANGUS-LEPPAN*, Editor. (UNISURV Report No. 7)
- \* 8. The teaching of field astronomy.  
*G.G. BENNETT and J.G. FREISLICH* (UNISURV Report No. 8)
- \* 9. Photogrammetric pointing accuracy as a function of properties  
of the visual image.  
*J.C. TRINDER* (UNISURV Report No. 9)
- \* 10. An experimental determination of refraction over an icefield.  
*P.V. ANGUS-LEPPAN* (UNISURV Report No. 10)
- 11. The non-regularised geoid and its relation to the telluroid and  
regularised geoids.  
*R.S. MATHER* (UNISURV Report No. 11)
- 12. The least squares adjustment of gyro-theodolite observations.  
*G.G. BENNETT* (UNISURV Report No. 12)
- 13. The free air geoid for Australia from gravity data available  
in 1968.  
*R.S. MATHER* (UNISURV Report No. 13)

\* Out of print

14. Verification of geoidal solutions by the adjustment of control networks using geocentric cartesian coordinate systems.  
*R.S. MATHER* (UNISURV Report No. 14)
15. New methods of observation with the Wild GAKI gyro-theodolite.  
*G.G. BENNETT* (UNISURV Report No. 15)
16. Theoretical and practical study of a gyroscopic attachment for a theodolite.  
*G.G. BENNETT* (UNISURV Report No. 16)
17. Accuracy of monocular pointing to blurred photogrammetric signals.  
*J.C. TRINDER* (UNISURV Report No. 17)
18. The computation of three-dimensional cartesian coordinates of terrestrial networks by the use of local astronomic vector systems  
*A. STOLZ* (UNISURV Report No. 18)
19. The Australian geodetic datum in earth space.  
*R.S. MATHER* (UNISURV Report No. 19)

